Beam Scanning Offset Cassegrain Reflector Antennas by Subreflector Movement

by

James William LaPean, Jr.

Thesis submitted to the Faculty of Virginia Polytechnic Institute and State University in partial fulfillment of the requirements for the degree of

Master of Science

in

Electrical Engineering

APPROVED:

Warren L Stutzman

Dr. Warren L. Stutzman, Chairman

Dr. Timothy Pratt

A. Safaai-Jazi

Dr. Ahmad Safaai-Jazi

November 1993

Blacksburg, Virginia

ABSTRACT

In 1987 a NASA panel recommended the creation of the Mission to Planet Earth. This mission was intended to apply to remote sensing experience of the space community to earth remote sensing to enhance the understanding of the climatalogical processes of our planet and to determine if, and to what extent, the hydrological cycle of Earth is being affected by human activity. One of the systems required for the mission was a wide scanning, high gain reflector antenna system for use in radiometric remote sensing from geostationary orbit.

This work describes research conducted at Virginia Tech into techniques for beam scanning offset Cassegrain reflector antennas by subreflector translation and rotation. Background material relevant to beam scanning antenna systems and offset Cassegrain reflector antenna system is presented. A test case is developed based on the background material. The test case is beam scanned using two geometrical optics methods of determining the optimum subreflector position for the desired scanned beam direction. Physical optics far-field results are given for the beam scanned systems. The test case system is found to be capable of beam scanning over a range of 35 half-power beamwidths while maintaining a 90% beam efficiency or 50 half-power beamwidths while maintaining less than 1 dB of gain loss during scanning.

For my grandfather, Samuel Wesley Causey (1920-1984), who never failed to fuel the fires of my imagination and taught me that memorized equations do not constitute knowledge.

ACKNOWLEDGMENT

I would like to express my appreciation for the assistance and guidance provided during the course of this research by my advisor Dr. Warren L. Stutzman. The breadth and depth of experience he provided proved invaluable. I would also like to thank Dr. Timothy Pratt and Dr. Ahmad Safaai-Jazi for serving on my committee.

I would like to thank Koichiro Takamizawa, Paul Werntz, Bing Shen, and Mike Barts for their friendship and assistance with this research. My thanks also go to my fellow graduate students who provided support and encouragement during the research process and the preparation of this thesis: Dennis Sweeney, Richard Allnut, Fatim Haidara, Marco Terada, John Musson, Brent Evers, and all the rest of the Satellite Communications Group. Many thanks also go to Cyndi Marshall for her assistance throughout this research with the preparation of presentations and this document.

I would also like to express my thanks for the continuing love and support of my parents Linda Joyce LaPean and James William LaPean, Sr. and my sister Amber Denise LaPean.

The work presented here was made possible by the support of the Antenna and Microwave Research Branch at the NASA Langley Research Center, Hampton, Virginia.

TABLE OF CONTENTS

LIST OF FIGURES

LIST OF TABLES

Chapter 1

INTRODUCTION

1.1 Overview

In 1987 a committee of the National Aeronautics and Space Administration chaired by Sally Ride proposed the Mission to Planet Earth [1]. The concept of this long-term experiment is to draw upon the space community's vast experience with remote sensing from unmanned inter-planetary probes to assess better the changing climate of Earth [1]. High resolution remote sensing is crucial to the success of this project [2]. It would be advantageous to place these remote sensing packages in geostationary orbits to allow real-time tracking of developing micro-scale weather systems such as convective cells and to decrease scene revisit time below what can be achieved with a reasonable constellation of low earth orbit platforms. Unlike infrared and visual light imaging, high resolution microwave radiometry has previously been performed from only low-earth orbits because very large antennas are required at geostationary orbit for good resolution. Additionally, a radiometric system must be able to repoint accurately its beam reasonably quickly to achieve the required tracking performance and scanning speed to minimize revisit time. This beam repointing speed requirement presents a further complication because the large antennas which are required generally cannot be slewed fast enough without disturbing both the antenna structure and its shared spacecraft bus. From 1987 through 1993 the Satellite Communications Group at Virginia Tech worked with the Antenna and Microwave Research Branch at NASA Langley Research Center to develop reflector antenna systems which achieve high gains, and therefore narrow beam widths, while being capable of wide angle beam scanning without main reflector motion.

1.2 Project Motivation

The original science objectives of the Mission to Planet Earth required a 100-meter class reflector antenna capable of operating with high beam efficiencies over a frequency range of 10 to 60 GHz to achieve the necessary resolution [2]. Revisions to the intended geophysical science applications of the radiometric experiment [3] and studies of the size/complexity characteristics of large space antennas [4] have since reduced the antenna size requirement to a 25 meter diameter projected aperture. This antenna size will produce a resolution of 20 km at the sub-satellite point at 18 GHz and still allow the spacecraft system to be launched by a single STS mission [4].

As mentioned above, beam scanning a reflector antenna of this size by main reflector slewing is impractical due to mechanical considerations. To avoid main reflector mechanical motion, beam scanning must be achieved by a combination of feed and/or sub-optic motions. Purely electrical beam scanning for a high gain, multi-band, wide scanning reflector antenna has been ruled out because of the immensely complex feed array which would be needed [5]. Also, scanning schemes which use feed motion are not feasible because even a single feed per band radiometer is quite heavy and extremely gain sensitive and so should not be moved. Because of these restrictions, the antenna must be capable of wide angle beam scanning by sub-optics motion. The simplest reflector antenna configurations which are capable of beam scanning by sub-optics motion are the dual reflector Cassegrain and Gregorian systems. From geometrical optics reflector antenna theory, comparable performing Cassegrain and Gregorian systems can be synthesized. Cassegrain reflector antenna systems are more compact than an equivalent

Gregorian system because the subreflector is located between the main reflector and the focal point in a Cassegrain system but beyond the focal point in a Gregorian system. For this reason, this work focuses on Cassegrain reflector antenna systems. The need for an offset main reflector is the final geometry restriction imposed by the mission requirements. This requirement is generated by the high beam efficiency (90%) needed for accurate radiometric measurements [3]. The desired characteristics of this wide scanning, high gain reflector system are shown in Table 1.2-1.

Krichevsky and DiFonzo [6] developed a method for designing offset Cassegrain reflector antenna systems for use on multi-beam communications satellites. Unfortunately, as shown in Section 3.3, their configuration scans by feed motion and does not place any limits on reflector size. In 1990, Peter Foldes proposed the Type 6 reflector antenna as a compromise system to meet these requirements [7]. This reflector antenna beam scans by tilting its small subreflector. Analysis of this system at Virginia Tech using the GRASP7 reflector antenna physical optics package suggested that its scan range would become extremely limited at higher operating frequencies as shown in Section 3.4. Virginia Tech began research into the scanning properties and optimum scanning of offset Cassegrain reflector antennas in cooperation with the Antenna and Microwave Research Branch at NASA Langley Research Center. This thesis presents the results of that research.

Table 1.2-1. Required characteristics of a wide scanning, high gain, geostationary radiometric reflector antenna system

Operating frequency	20 - 60 GHz
Maximum half-power beam width (HPBW)	0.04°
Beam efficiency (BE)	$> 90\%$
Scan range	$\pm 7^\circ$
Scanning mechanism	suboptic motion or simple array feed
Aperture efficiency (ε_{ap})	$> 70\%$
Main reflector diameter (D_M)	≤ 25 m.
Areal efficiency $\left(\frac{D_M^2}{D_M^2 + D_S^2}\right)$	as high as possible

References

[1] S. K. Ride, "Leadership and America's Future in Space - A Report to the Administrator," NASA, August 1987.

[2] A. J. Gasiewski and D. H. Staelin, "Science Requirements for Passive Microwave Sensors on Earth Science Geostationary Platforms," *Proceedings of the NASA Technology Workshop for Earth Science Geostationary Platforms*, NASA CP-3040, July 1989.

[3] W. L. Stutzman and G. S. Brown, "The Science Benefits of and the Antenna Requirements for Microwave Remote Sensing From Geostationary Orbit," NASA Contractor Report 4408, October 1991.

[4] C. A. Rogers and W. L. Stutzman, "Large Deployable Antenna Program, Phase 1: Technology Assesment and Mission Architecture," NASA Contractor Report 4410, October 1991.

[5] P. Foldes, "Preliminary Considerations for the Feed System of the Triple Reflector Scanning Radiometer," Foldes Inc., August 1991.

[6] V. Krichevsky and D. F. DiFonzo, "Optimum feed locus for beam scanning in the symmetry plane of offset Cassegrain antennas: Two dimensional case," *Comsat Technical Review*, Vol. 11, No. 1, pp. 131-157, Spring 1981.

[7] P. Foldes, "Some Characteristics of Six Alternative Multireflector Radiometers for 6-31 GHz GEO Operation," Foldes Inc., May 1990.

Chapter 2

REFLECTOR ANTENNA SYSTEM GEOMETRY

The electrical properties of reflector antenna systems depend primarily on the ratio of the focal length of the reflector to its diameter. This quantity, F/D, determines the level of edge taper due to geometrical effects, the required directivity of the feed antenna, and, for offset systems, the cross-polarization level. Further, of particular interest to this study of scan behavior, the scanning performance of reflector antenna systems degrades as F/D decreases for a given aperture size. F/D cannot be decreased to much less than unity because then the surface area of the reflector increases at a much greater rate than the projected aperture area. Since the feed must be placed at the focal point and supported by a boom, the constraints on the minimum F/D value require a deep structure which increases the mechanical complexity and weight. The mechanical depth of a reflector antenna system can be reduced by using a secondary reflector to form an image of the feed at the focal point of the main reflector paraboloidal surface. In addition, the use of folded optics allows the feed to be located in a more convenient position.

The two classical types of dual reflector antenna systems are the Gregorian system and the Cassegrain system. In a Gregorian reflector antenna system, an ellipsoidal subreflector is mounted farther from the main reflector surface than the focal point of the main reflector paraboloid. Although this method allows a longer electrical focal length for a given main reflector paraboloid, the system is still quite deep since the subreflector must be mounted beyond the focal point. The focal length, and therefore F/D of the main reflector surface, of this type of system is still limited by the requirement of mounting the subreflector beyond the focal point. The Cassegrain reflector antenna system, which is the system of interest here, consists of a hyperboloidal subreflector mounted between the main reflector surface and the focal point of the main reflector paraboloid. In this system, the length of the reflector antenna system is reduced compared to the Gregorian system since the subreflector is mounted closer to the main reflector surface. This difference allows the main reflector surface of a Cassegrain reflector antenna system to have a higher F/D value but still allows the antenna to be built with a relatively short support structure for the subreflector.

This chapter explains how the Cassegrain reflector antenna system evolves from the prime-focus paraboloidal reflector antenna system. The concept of the equivalent prime-focus paraboloid is introduced for the Cassegrain reflector antenna system. A method for determining the geometry of an offset Cassegrain reflector antenna system which has an axi-symmetric equivalent paraboloid is given. Finally, the test case which will be studied is specified.

2.1 The Prime-Focus Paraboloid Reflector Antenna System

The prime-focus paraboloid reflector antenna system consists of a paraboloidal main reflector and a feed located at the focal point of the main reflector. The equation that defines the main reflector surface, as shown in Figure 2.1-1, is

$$z_M = \frac{x_M^2 + y_M^2}{4\,F_M} \tag{2.1-1}$$

where

F_M = focal length of the paraboloid.

The focal point of the paraboloid is located on the z-axis and the vertex of the paraboloid is located at the origin. In general, the physical reflector is a section of the parent paraboloid and

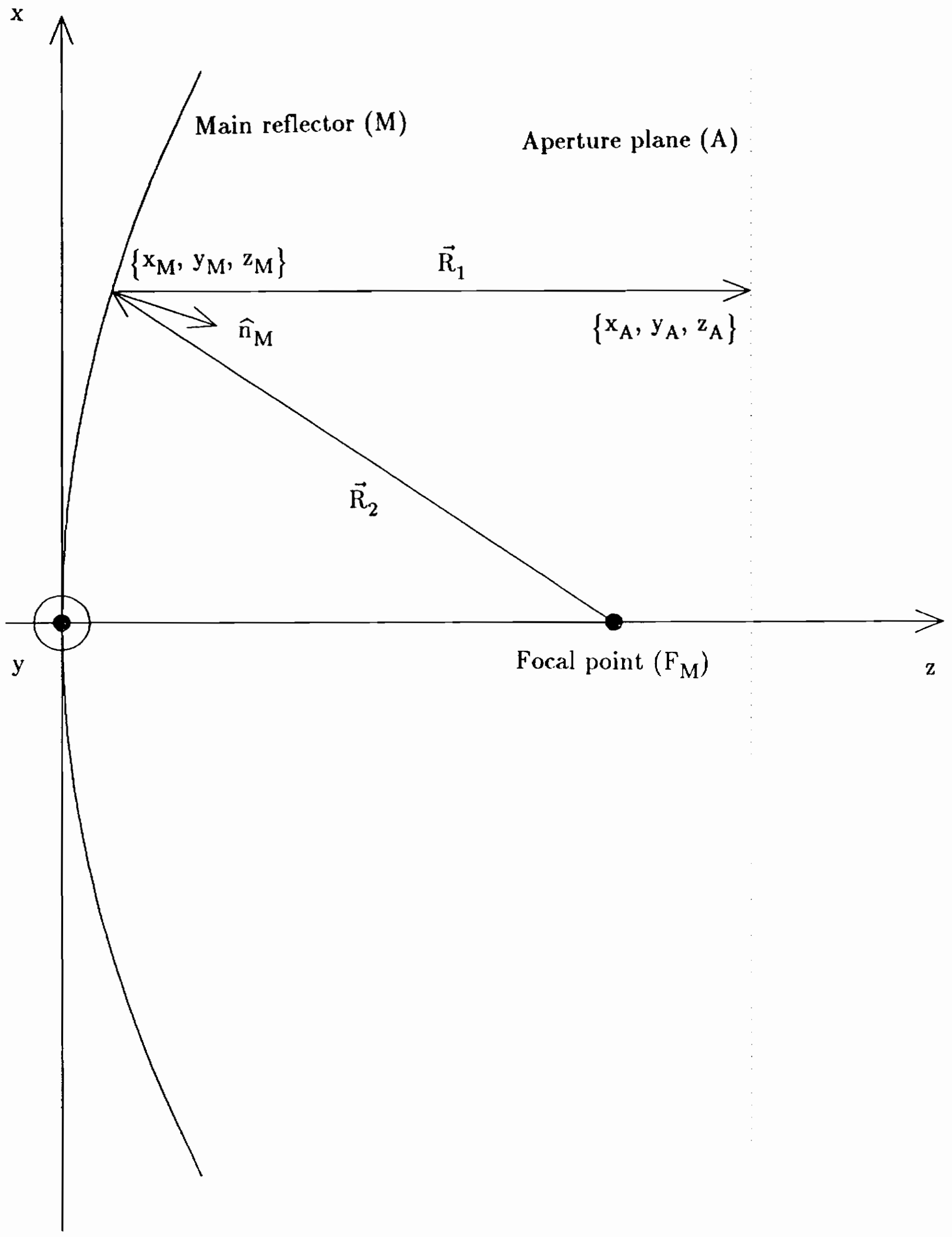

Figure 2.1-1. Prime-focus paraboloidal reflector antenna system geometry.

can be either axi-symmetric or offset. In the case that the physical reflector is offset, the feed is located at the focal point on the z-axis but is tilted to evenly illuminate the physical reflector. A paraboloidal main reflector is used because a spherical wave leaving a point source located at the focal point will be transformed into a planar wavefront exiting the aperture of the antenna. This requirement is equivalent, in a geometrical optics (GO) sense, to the requirement that all rays traced from the feed point exit the aperture of the antenna system perpendicular to the aperture plane after reflection from the paraboloidal surface [1]. The correct main reflector shape is verified by substituting the incident and reflected ray unit vectors, $\hat{r}_2$ and $\hat{r}_1$, at the main reflector and the unit normal of the surface, $\hat{n}_M$, into Snell's law.

For the prime-focus reflector antenna system shown in Figure 2.1-1, a ray from the feed point, $\{0,\ 0,\ F_M\}$, to any point on the reflector surface, $\{x_M,\ y_M,\ z_M\}$, is

$$\vec{r}_2 = \{\ x_M\,\hat{x},\ \ y_M\,\hat{y},\ \ (z_M - F_M)\,\hat{z}\ \}. \tag{2.1-2}$$

Since the length of this ray is

$$|\vec{r}_2| = \sqrt{x_M^{\,2} + y_M^{\,2} + (z_M - F_M)^2}\ , \tag{2.1-3}$$

the unit vector of a ray from the feed point to any point on the reflector surface is

$$\hat{r}_2 = \left(\sqrt{x_M^{\,2} + y_M^{\,2} + (z_M - F_M)^2}\,\right)^{-1} \{\ x_M\hat{x},\ \ y_M\hat{y},\ \ (z_M - F_M)\,\hat{z}\ \}. \tag{2.1-4}$$

The unit vector of a ray exiting the aperture in the z-direction is

$$\hat{r}_1 = \{0,\ 0,\ 1\}. \tag{2.1-5}$$

The required surface shape can be verified by substituting (2.1-4) and (2.1-5) into Snell's law. Snell's law, expressed in vector notation, is

$$\hat{r}_1 = \hat{r}_2 - 2\,(\,\hat{r}_2 \cdot \hat{n}_M\,)\hat{n}_M \tag{2.1-6}$$

where

$\hat{n}_M$ = the inward unit normal of the main reflector paraboloid at the point of reflection.

An inward normal vector at the paraboloidal main reflector surface is

$$\vec{n}_M = \left\{\frac{-\partial x_M}{\partial z}\hat{x},\ \frac{-\partial y_M}{\partial z}\hat{y},\ \frac{\partial z_M}{\partial z}\hat{z}\right\}. \qquad (2.1\text{-}7)$$

For the paraboloidal surface given by (2.1-1)

$$\frac{-\partial x_M}{\partial z} = \frac{-\,x_M}{2\,F_M} \qquad (2.1\text{-}8c)$$

$$\frac{-\partial y_M}{\partial z} = \frac{-\,y_M}{2\,F_M} \qquad (2.1\text{-}8c)$$

$$\frac{\partial z_M}{\partial z} = 1 \qquad (2.1\text{-}8c)$$

so

$$\vec{n}_M = \left\{\frac{-\,x_M}{2\,F_M}\hat{x},\ \frac{-\,y_M}{2\,F_M}\hat{y},\ \hat{z}\right\}. \qquad (2.1\text{-}9)$$

Since the length of this normal vector is

$$|\vec{n}_M| = \frac{\sqrt{x_M^{\,2} + y_M^{\,2} + 4\,F_M^{\,2}}}{2\,F_M}, \qquad (2.1\text{-}10)$$

the unit vector normal to the paraboloidal surface is

$$\hat{n}_M = \left(\sqrt{x_M^{\,2} + y_M^{\,2} + 4\,F_M^{\,2}}\right)^{-1} \{-\,x_M\hat{x},\ -\,y_M\hat{y},\ 2\,F_M\hat{z}\}. \qquad (2.1\text{-}11)$$

Substituting the incident ray unit vector (2.1-4), the reflected ray unit vector (2.1-5), and the inward normal unit vector at the point of reflection (2.1-11) into Snell's law (2.1-6) and expressing the result as equations for each of the x, y, z components gives:

$$0 = \frac{x_M}{\sqrt{x_M^{\,2} + y_M^{\,2} + (z_M - F_M)^2}} - 2\,(\hat{r}_2\cdot\hat{n}_M)\frac{-\,x_M}{\sqrt{x_M^{\,2} + y_M^{\,2} + 4\,F_M^{\,2}}} \qquad (2.1\text{-}12a)$$

$$0 = \frac{y_M}{\sqrt{x_M^{\,2} + y_M^{\,2} + (z_M - F_M)^2}} - 2\,(\hat{r}_2\cdot\hat{n}_M)\frac{-\,y_M}{\sqrt{x_M^{\,2} + y_M^{\,2} + 4\,F_M^{\,2}}} \qquad (2.1\text{-}12b)$$

$$1 = \frac{(F_M - z_M)}{\sqrt{x_M^{\,2} + y_M^{\,2} + (z_M - F_M)^2}} - 2\,(\hat{r}_2\cdot\hat{n}_M)\frac{2\,F_M}{\sqrt{x_M^{\,2} + y_M^{\,2} + 4\,F_M^{\,2}}} \qquad (2.1\text{-}12c)$$

where

$$(\hat{r}_2\cdot\hat{n}_M) = \left(\sqrt{x_M^{\,2} + y_M^{\,2} + (z_M - F_M)^2}\ \sqrt{x_M^{\,2} + y_M^{\,2} + 4\,F_M^{\,2}}\right)^{-1} \left[-\,x_M^{\,2} - y_M^{\,2} + 2\,F_M(z_M - F_M)\right]. \qquad (2.1\text{-}13)$$

Equation (2.1-12) is simplified by manipulating the radical in the denominator of the $\hat{r}_2$ terms into the form of the $\hat{n}_M$ terms. Expanding the radical in $\hat{r}_2$ and substituting (2.1-1) for z_M into

(2.1-12) leads to

$$\sqrt{x_M^2 + y_M^2 + (z_M - F_M)^2} = \sqrt{x_M^2 + y_M^2 + \left(\frac{x_M^2 + y_M^2}{4F_M} - F_M\right)^2} \tag{2.1-14}$$

$$= \frac{1}{4F_M}\sqrt{16F_M^2 x_M^2 + 16F_M^2 y_M^2 + \left(x_M^2 + y_M^2 - 4F_M^2\right)^2} \tag{2.1-15}$$

$$= \frac{1}{4F_M}\sqrt{16F_M^2 x_M^2 + 16F_M^2 y_M^2 + x_M^4 + 2x_M^2 y_M^2 - 8F_M^2 x_M^2 - 8F_M^2 y_M^2 + y_M^4 + 16F_M^4} \tag{2.1-16}$$

$$= \frac{1}{4F_M}\sqrt{8F_M^2 x_M^2 + 8F_M^2 y_M^2 + x_M^4 + 2x_M^2 y_M^2 + y_M^4 + 16F_M^4} \tag{2.1-17}$$

$$= \frac{1}{4F_M}\sqrt{\left(x_M^2 + y_M^2 + 4F_M^2\right)^2} \tag{2.1-18}$$

which is the form of the radical in the $\hat{n}$ terms of (2.1-12). Substituting (2.1-18) into (2.1-12) and (2.1-13) gives

$$0 = \frac{4F_M x_M}{x_M^2 + y_M^2 + 4F_M^2} - 2(\hat{r}_i \cdot \hat{n})\frac{-x_M}{\sqrt{x_M^2 + y_M^2 + 4F_M^2}} \tag{2.1-19a}$$

$$0 = \frac{4F_M y_M}{x_M^2 + y_M^2 + 4F_M^2} - 2(\hat{r}_i \cdot \hat{n})\frac{-y_M}{\sqrt{x_M^2 + y_M^2 + 4F_M^2}} \tag{2.1-19b}$$

$$1 = \frac{4F_M(F_M - z_M)}{x_M^2 + y_M^2 + 4F_M^2} - 2(\hat{r}_i \cdot \hat{n})\frac{2F_M}{\sqrt{x_M^2 + y_M^2 + 4F_M^2}} \tag{2.1-19c}$$

where

$$(\hat{r}_2 \cdot \hat{n}_M) = 4F_M \frac{-x_M^2 - y_M^2 + 2F_M(z_M - F_M)}{\left(x_M^2 + y_M^2 + 4F_M^2\right)\sqrt{x_M^2 + y_M^2 + 4F_M^2}}. \tag{2.1-20}$$

Defining

$$\zeta = x_M^2 + y_M^2 + 4F_M^2 \tag{2.1-21}$$

and using ζ in (2.1-19) with (2.1-20), yields the following equations that correspond to the Cartesian component equations of (2.1-12)

$$0 = \frac{4\,F_M x_M}{\zeta} + \frac{8\,F_M}{\zeta^2}\Big[-\,x_M^2 - y_M^2 + 2\,F_M(z_M - F_M)\Big]\,x_M \tag{2.1-22a}$$

$$0 = \frac{4\,F_M y_M}{\zeta} + \frac{8\,F_M}{\zeta^2}\Big[-\,x_M^2 - y_M^2 + 2\,F_M(z_M - F_M)\Big]\,y_M \tag{2.1-22a}$$

$$1 = \frac{4\,F_M(z_M - F_M)}{\zeta} + \frac{8\,F_M}{\zeta^2}\Big[-\,x_M^2 - y_M^2 + 2\,F_M(z_M - F_M)\Big]\,2\,F_M. \tag{2.1-22a}$$

Substituting (2.1-1) into the bracketed term common to (2.1-22a), (2.1-22b), and (2.1-22c) gives

$$\Big[-\,x_M^2 - y_M^2 + 2\,F_M(z_M - F_M)\Big] = \Big[-\,x_M^2 - y_M^2 + 2\,F_M z_M - 2\,F_M^2\Big] \tag{2.1-23}$$

$$= \frac{1}{2}\Big[-2\,x_M^2 - 2\,y_M^2 + x_M^2 + y_M^2 - 4\,F_M^2\Big] \tag{2.1-24}$$

$$= \frac{-1}{2}\Big[x_M^2 + y_M^2 + 4\,F_M^2\Big] = \frac{-\zeta}{2}. \tag{2.1-25}$$

The satisfaction of the x and y components of (2.1-12) by the paraboloidal main reflector shape is verified by substituting (2.1-25) back into (2.1-22)

$$0 = \frac{4\,F_M x_M}{\zeta} - \frac{4\,F_M x_M}{\zeta} \tag{2.1-26a}$$

$$0 = \frac{4\,F_M y_M}{\zeta} - \frac{4\,F_M y_M}{\zeta} \tag{2.1-26b}$$

$$1 = \frac{4\,F_M(z_M - F_M)}{\zeta} + \frac{8\,F_M^2}{\zeta}. \tag{2.1-26c}$$

The satisfaction of the z component of (2.1-12), shown in (2.1-26c), is verified by substituting (2.1-1) into (2.1-26c). This substitution and simplification gives

$$1 = \frac{4\,F_M}{\zeta}(z_M + F_M) = \frac{4\,F_M}{\zeta}\left(\frac{x_M^2 + y_M^2}{4\,F_M} + F_M\right) \tag{2.1-27}$$

$$= \frac{4\,F_M}{\zeta}\left(\frac{x_M^2 + y_M^2 + 4\,F_M^2}{4\,F_M}\right) = \frac{\zeta}{\zeta}. \tag{2.1-28}$$

The equalities of (2.1-26a), (2.1-26b), and (2.1-28), derived by enforcing Snell's law at the reflector surface, prove that the paraboloid focuses the rays from a point source feed at the focal point to infinity as a prime-focus reflector antenna system. Although this method of GO raytracing can be used for synthesis, it is desirable to have a simpler synthesis method that does not require taking derivatives at the surface.

2.2 The Levi-Civita Theorem

The proper reflector surface shape for a prime-focus antenna system can also be determined by imposing an equal path length constraint on each ray traced from a feed point at the focus to the reflector surface and leaving the reflector antenna system in a direction perpendicular to the aperture plane. The Levi-Civita theorem [1] states that, for a set of rays which exit a single reflector antenna system mutually parallel and strike a reference plane, the following two conditions are equivalent:

(1) The path length of every ray from the source to the reference plane must be equal.

(2) Snell's law is satisfied at the reflector surface.

Since the rays in a focused prime-focus reflector system exit the system mutually parallel, present a planar phase front in the aperture, and undergo a single reflection in the antenna system, this theorem can be used to determine the proper shape for its reflector surface [1].

The reflector shape of a prime-focus paraboloidal reflector antenna system can now be found by determining the path lengths for rays traced from the feed point to the aperture after reflection from the reflector surface. The reflector is assumed to have a feed point at z = F on the z-axis and to have a parent surface which passes through the coordinate system origin as shown in Figure 2.1.1. As in Section 2.1, where the shape was verified by enforcing Snell's law at the reflector surface, the desired direction of propagation is along the z-axis. Unlike in Section 2.1, the correct reflector shape will be found directly rather than verified. The length of any ray from any point on the reflector surface to the aperture plane is

$$\left|\overline{R}_1\right| = z_A - z_M \tag{2.2-1}$$

where

z_A = the location of a point in the aperture plane along the z-axis

$\{ x_M, y_M, z_M \}$ = a point on the reflector surface.

As shown in Figure 2.1-1, the distance from the point feed at the focus, $\{0, 0, F_M\}$, to any point on the reflector surface is

$$|\overline{R}_2| = \sqrt{x_M^2 + y_M^2 + (z_M - F_M)^2}\ . \tag{2.2-2}$$

To satisfy condition (1) of the Levi-Civita theorem

$$|\overline{R}_1| + |\overline{R}_2| = z_A - z_M + \sqrt{x_M^2 + y_M^2 + (z_M - F_M)^2} = L_p \tag{2.2-3}$$

where

L_p = the constant path length for all rays.

Rewriting (2.2-3) and squaring both sides

$$\sqrt{x_M^2 + y_M^2 + (z_M - F_M)^2} = L_p - z_A + z_M. \tag{2.2-4}$$

$$x_M^2 + y_M^2 + (z_M - F_M)^2 = (L_p - z_A + z_M)^2. \tag{2.2-5}$$

After expanding the squared terms, (2.2-5) results in

$$x_M^2 + y_M^2 + z_M^2 - 2F_M z_M + F_M^2 = L_p^2 - 2L_p z_A + 2L_p z_M + z_A^2 - 2z_A z_M + z_M^2 \tag{2.2-6}$$

Evaluating (2.2-5) at the coordinate origin $(0, 0, 0)$ gives

$$L_p = z_A + F_M. \tag{2.2-7}$$

Substituting this expression for the constant L_p into (2.2-6) gives

$$x_M^2 + y_M^2 + z_M^2 - 2F_M z_M + F_M^2 = z_A^2 + 2F_M z_A + F_M^2 - 2z_A^2 - 2F_M z_A + 2z_A z_M + 2F_M z_M + z_A^2 - 2z_A z_M + z_M^2. \tag{2.2-8}$$

After simplification, (2.2-8) becomes

$$\frac{x_M^2 + y_M^2}{4\,F_M} = z_M. \tag{2.2-9}$$

This is the equation for a paraboloid as given by (2.1-1). This establishes the paraboloid as the proper shape for the reflector of a prime-focus reflector antenna system and shows that this shape can be developed from either Snell's law or the equal path length constraint. The simplicity of the equal path length condition compared to the verification using Snell's law presented in Section 2.1 is striking and is of great value. It suggests that the equal path length should be used when examining the more complex dual reflector antenna system.

2.3 The Canonical Cassegrain Reflector Antenna System

The canonical Cassegrain reflector antenna system consists of a paraboloidal main reflector surface, a hyperboloidal subreflector surface mounted with one of its focal points coinciding with the focal point of the main reflector surface shape, and a feed located at the second focal point of the hyperboloidal subreflector. The equation which defines the paraboloid of revolution that forms the main reflector surface, as shown in Figure 2.3-1, is given by (2.1-1). The general second order equation which defines the subreflector surface, as shown in Figure 2.3-1, is

$$A x_S^2 + B x_S y_S + C y_S^2 + D x_S + E y_S + F = G z_S^2 + H z_S + I x_S z_S + J y_S z_S \qquad (2.3\text{-}1)$$

where

$$A = 4\left(\beta^2 - \alpha^2\right) \qquad F = \theta^2 - 4\alpha^2\left(x_{f2}^{\ 2} + y_{f2}^{\ 2} + {}_{f2}^{\ 2}\right)$$

$$B = 8\beta\gamma \qquad G = 4\left(\alpha^2 - \delta^2\right)$$

$$C = 4\left(\gamma^2 - \alpha^2\right) \qquad H = -4\left(\delta\theta + 2\alpha^2 z_{f2}\right)$$

$$D = 4\left(\beta\theta + 2\alpha^2 x_{f2}\right) \qquad I = -8\beta\delta$$

$$E = 4\left(\gamma\theta + 2\alpha^2 y_{f2}\right) \qquad J = -8\gamma\delta$$

$$\alpha = \frac{\sqrt{\left(x_{f1} - x_{f2}\right)^2 + \left(y_{f1} - y_{f2}\right)^2 + \left(z_{f1} - z_{f2}\right)^2}}{e}$$

$$\beta = \left(x_{f2} - x_{f1}\right) \qquad \gamma = \left(y_{f2} - y_{f1}\right) \qquad \delta = \left(z_{f2} - z_{f1}\right)$$

$$\theta = x_{f1}^{\ 2} + y_{f1}^{\ 2} + z_{f1}^{\ 2} - x_{f2}^{\ 2} - y_{f2}^{\ 2} - z_{f2}^{\ 2} - \alpha^2,$$

f1, f2 = the two focal points of the hyperboloid,

e = the eccentricity of the hyperboloid.

The details of the derivation of this equation have been omitted due to their length. In the Cassegrain reflector antenna system, the hyperboloidal subreflector surface is used because the

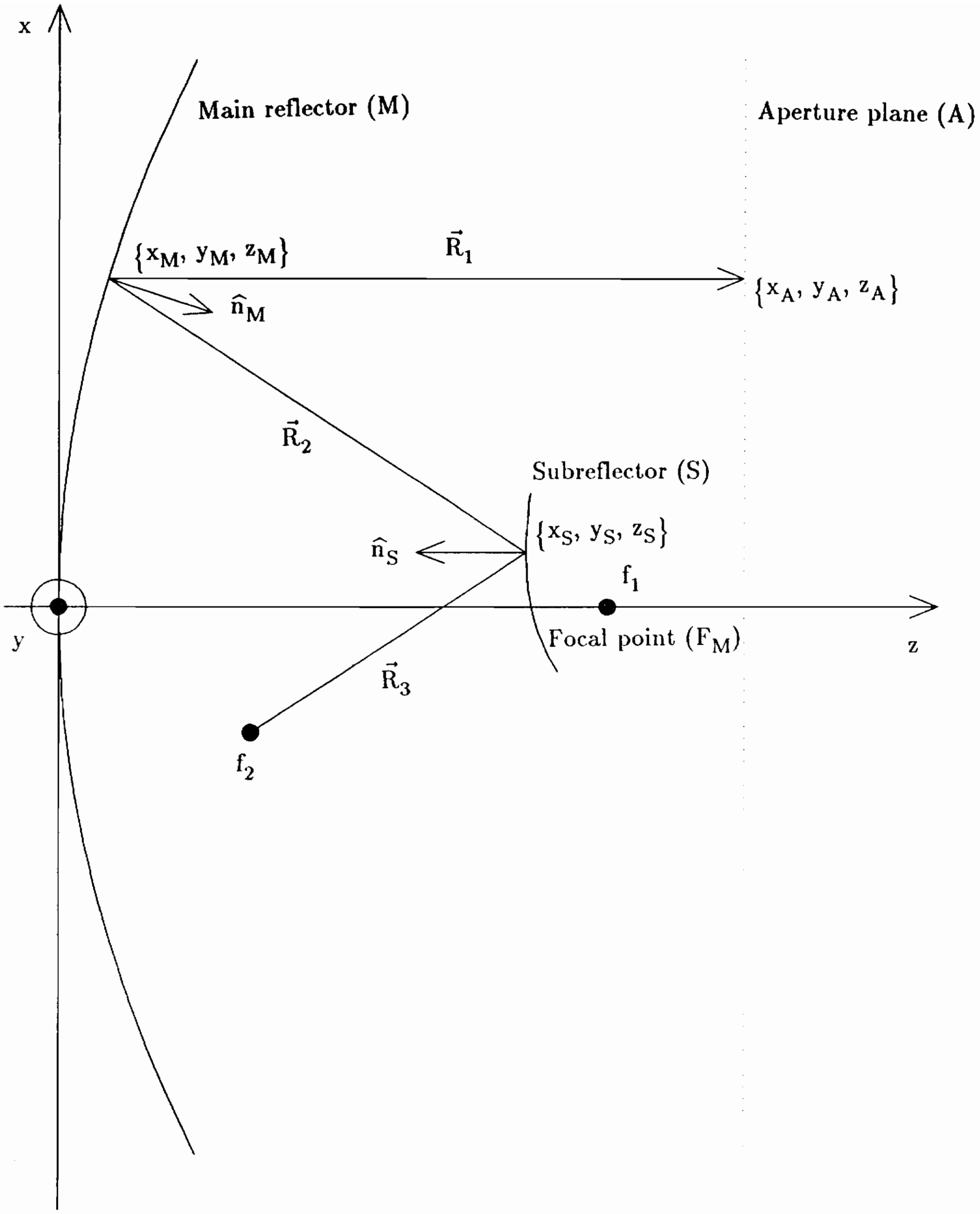

Figure 2.3-1. Cassegrain reflector antenna system geometry.

focal points of the hyperboloid are conjugate points. That is, an image of the feed placed at the second focal point of the hyperboloid is formed at the first focal point of the hyperboloid which is located at the focal point of the paraboloidal main reflector surface. The subreflector surface is chosen to be on the branch of the hyperboloid which is closer to the focal point of the main reflector. As with the prime-focus paraboloidal reflector antenna system, in general, the Cassegrain reflector antenna system can be either axi-symmetric or offset. In either case, the physical main reflector and subreflector are sections of the surface of the parent paraboloid and hyperboloid, respectively.

The imaging property of the hyperboloidal subreflector can be simply shown through the use of an extension of the Levi-Civita theorem discussed in Section 2.2. Xianzhong [3] has extended the Levi-Civita theorem to include arbitrary focused dual reflector antenna systems. Xianzhong starts by assuming a set of rays which emanate from a point source at the focal point and reflect through the dual reflector system shown in Figure 2.3-2 [3]. The rays exit the aperture mutually parallel and strike a perpendicular reference plane. Xianzhong considers three restrictions on the set of rays:

(1) The path length of every ray from the source to the reference plane must be equal.
(2) Snell's law is satisfied at the main reflector surface.
(3) Snell's law is satisfied at the subreflector surface.

If the rays satisfy any two of these conditions, then the remaining restriction is satisfied automatically [3]. The proof uses an arbitrary dual reflector system including an aperture plane, A, a main reflector, M, and a subreflector, S. The equations for these surfaces then are [3]

$$z_S = z_S(x_s, y_S) \tag{2.3-2}$$

$$z_M = z_M(x_M, y_M) \tag{2.3-3}$$

$$z_M = z_a \left(\text{where } z_a > [z_M]_{\max}\right). \tag{2.3-4}$$

where x, y, and z are the coordinates of the intersection of the ray with the surface indicated by

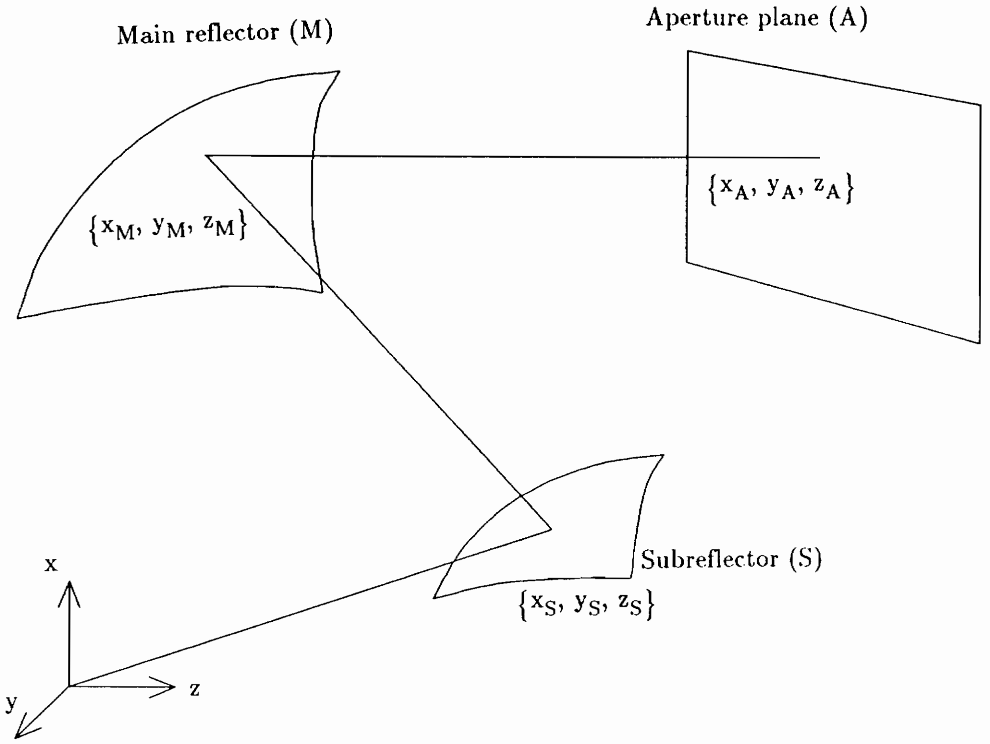

Figure 2.3-2. General doubly reflected ray geometry as used by Xianzhong [3].

the subscript and z_a is the z-coordinate of the intersection of the ray with the aperture plane. The z-axis is taken to be normal to the reference plane and the rays which strike the plane are parallel to the z-axis [3]. The unit vectors $\hat{r}_3$, $\hat{r}_2$, and $\hat{r}_1$ are the unit vectors of one of the rays which is reflected through the system as indicated in Figure 2.3-2 [3]. If Snell's law is enforced at the subreflector and main reflector, then

$$\left(\frac{\partial z_S}{\partial x_S}\right) = \frac{\left(\cos\alpha_x - \cos\beta_x\right)}{\left(\cos\beta_z - \cos\alpha_z\right)} \tag{2.3-5a}$$

$$\left(\frac{\partial z_S}{\partial y_S}\right) = \frac{\left(\cos\alpha_y - \cos\beta_y\right)}{\left(\cos\beta_z - \cos\alpha_z\right)} \tag{2.3-5b}$$

at the subreflector and

$$\left(\frac{\partial z_M}{\partial x_M}\right) = \frac{\cos\beta_x}{\left(1 - \cos\beta_z\right)} \tag{2.3-6a}$$

$$\left(\frac{\partial z_M}{\partial y_M}\right) = \frac{\cos\beta_y}{\left(1 - \cos\alpha_z\right)} \tag{2.3-6b}$$

at the main reflector [3]. The constant path length through the system, L_p, is

$$L_p = \sqrt{x_S^2 + y_S^2 + z_S^2} + \sqrt{\left(x_M - x_S\right)^2 + \left(y_M - y_S\right)^2 + \left(z_M - z_S\right)^2} + \left(z_a - z_M\right) . \tag{2.3-7}$$

Xianzhong solves the system by taking the partial derivatives of (2.3-7) considering either x_M and y_M or x_S and y_S to be the independent variables in the system. If the main reflector parameters, x_M and y_S, are considered independent, then

$$\begin{aligned}\left(\frac{\partial L_p}{\partial x_M}\right) = {} & \left(\frac{\partial x_S}{\partial x_M}\right)\left[\left(\cos\alpha_x - \cos\beta_x\right) - \left(\cos\beta_z - \cos\alpha_z\right)\left(\frac{\partial z_S}{\partial x_S}\right)\right] \\ & + \left(\frac{\partial y_S}{\partial y_M}\right)\left[\left(\cos\alpha_y - \cos\beta_y\right) - \left(\cos\beta_z - \cos\alpha_z\right)\left(\frac{\partial z_S}{\partial y_S}\right)\right] \\ & + \left[\cos\beta_x - \left(1 - \cos\beta_z\right)\left(\frac{\partial z_M}{\partial y_M}\right)\right]\end{aligned} \tag{2.3-8a}$$

$$\begin{aligned}\left(\frac{\partial L_p}{\partial y_M}\right) = {} & \left(\frac{\partial x_S}{\partial y_M}\right)\left[\left(\cos\alpha_x - \cos\beta_x\right) - \left(\cos\beta_z - \cos\alpha_z\right)\left(\frac{\partial z_S}{\partial x_S}\right)\right] \\ & + \left(\frac{\partial y_S}{\partial y_M}\right)\left[\left(\cos\alpha_y - \cos\beta_y\right) - \left(\cos\beta_z - \cos\alpha_z\right)\left(\frac{\partial z_S}{\partial y_S}\right)\right]\end{aligned}$$

$$+\left[\cos\beta_y - \left(1 - \cos\beta_z\right)\left(\frac{\partial z_M}{\partial y_M}\right)\right]. \qquad (2.3\text{-}8b)$$

If the subreflector parameters, x_S and y_S, are considered independent, then

$$\left(\frac{\partial L_p}{\partial x_S}\right) = \left[\left(\cos\alpha_x - \cos\beta_x\right) - \left(\cos\beta_z - \cos\alpha_z\right)\left(\frac{\partial z_S}{\partial x_S}\right)\right]$$

$$+\left(\frac{\partial x_M}{\partial x_S}\right)\left[\cos\beta_x - \left(1 - \cos\beta_z\right)\left(\frac{\partial z_M}{\partial x_M}\right)\right]$$

$$+\left(\frac{\partial x_M}{\partial x_S}\right)\left[\cos\beta_y - \left(1 - \cos\beta_z\right)\left(\frac{\partial x_M}{\partial y_M}\right)\right] \qquad (2.3\text{-}9a)$$

$$\left(\frac{\partial L_p}{\partial y_S}\right) = \left[\left(\cos\alpha_y - \cos\beta_y\right) - \left(\cos\beta_z - \cos\alpha_z\right)\left(\frac{\partial z_S}{\partial y_S}\right)\right]$$

$$+\left(\frac{\partial x_M}{\partial y_S}\right)\left[\cos\beta_x - \left(1 - \cos\beta_z\right)\left(\frac{\partial z_M}{\partial x_M}\right)\right]$$

$$+\left(\frac{\partial y_M}{\partial y_S}\right)\left[\cos\beta_y - \left(1 - \cos\beta_z\right)\left(\frac{\partial z_M}{\partial y_M}\right)\right]. \qquad (2.3\text{-}9b)$$

If the Snell's law requirements, (2.3-5) and (2.3-6), are satisfied and substituted into (2.3-9), then

$$\left(\frac{\partial L_p}{\partial x_S}\right) = 0 \qquad (2.3\text{-}10a)$$

$$\left(\frac{\partial L_p}{\partial y_S}\right) = 0 \qquad (2.3\text{-}10b)$$

so the minimum path length constraint of Fermat's principle is satisfied and the first restriction that Xianzhong considers is proven [3]. Alternately, substituting (2.3-5) and (2.3-6) into (2.3-8) gives

$$\left(\frac{\partial L_p}{\partial x_M}\right) = 0 \qquad (2.3\text{-}11a)$$

$$\left(\frac{\partial L_p}{\partial y_M}\right) = 0. \qquad (2.3\text{-}11b)$$

The other possible combinations of imposed and automatically satisfied restrictions are also considered by Xianzhong and are stated to be correct [3].

This extension of the Levi-Civita theorem makes the analysis or synthesis of the geometry of the canonical Cassegrain reflector antenna system significantly simpler. The Levi-

Civita theorem and the analysis of Section 2.2 or the analysis of Section 2.1 show that Snell's Law is satisfied at the reflector surface for any ray in the focused prime-focus paraboloidal reflector antenna system. Because the main reflector surface in a canonical Cassegrain reflector antenna system is paraboloidal and the hyperboloidal subreflector produces a spherical phase front centered on its first focus when illuminated by a point source at its second focus, the results of the preceding analysis of the prime-focus paraboloidal reflector antenna system can be used to assure the satisfaction of condition (2) of the Xianzhong extension of the Levi-Civita theorem for dual reflector antenna systems.

Condition (1) of this extension can be shown to be satisfied for the hyperboloidal subreflector because the defining characteristic of the hyperbola is that the difference in the distances from any point on the hyperbola to the foci is constant. A distinction is made between the path length of a ray in the prime focus system, $L_{ppf.}$, and the path length of a ray in the Cassegrain system, $L_{pcass.}$, through (2.3-15). For the hyperbola shown in Figure 2.3-1 the defining characteristic can be written as

$$d_{f2} - d_{f1} = \frac{2a}{e} \tag{2.3-12}$$

where

d_{f1}, d_{f2} = the distances from f1 and f2 to a point on the subreflector,

f1, f2 = the focal points of the hyperboloid,

2 a = the distance between the foci of the hyperbola,

e = the eccentricity of the hyperbola.

From (2.2-3)

$$\left|\overline{R}_1\right| + \left|\overline{R}_2\right| = L_{ppf.} \tag{2.3-13}$$

where

$L_{ppf.}$ = the path length of any ray in the prime focus antenna system which is reflected to the feed point.

A hyperboloidal subreflector located in the reflector system with one focus at the focus of the main reflector paraboloid and the other focus at the desired feed point will reduce the length of any ray reflected from the hyperboloidal surface by the distance d_{f1}, the distance between the point on the subreflector and focal point f1, and increase the length of any ray reflected from the hyperboloidal surface by the distance d_{f2}, the distance between the point on the subreflector and focal point f2, as shown in Figure 2.3-1. Therefore, the length of any ray which reflects through the antenna system is

$$\left|\overline{R}_1\right| + \left|\overline{R}_2\right| + d_{f2} - d_{f1} = L_{pcass.} = L_{ppf.} + \frac{2a}{e}. \tag{2.3-14}$$

Since the analysis of Section 2.2 shows that $L_{ppf.}$, the path length of any ray in the prime-focus reflector antenna system, is constant, (2.3-14) shows that $L_{pcass.}$ is constant from the definition of the hyperbola. Thus, condition (1) of the Xianzhong extension of the Levi-Civita theorem is satisfied. Condition (3) is also now known to be satisfied since all of the other conditions have been shown to be satisfied. Avoiding direct application of Snell's law at the subreflector surface through the use of this theorem is advantageous it is more difficult than the calculation of the total path length.

2.4 The Equivalent Paraboloid

The equivalent paraboloid of a dual reflector antenna system is a mathematically constructed prime-focus paraboloidal reflector antenna which produces the same aperture field distribution as the dual reflector antenna system. The equivalent paraboloid has been found to be an accurate predictor of the electromagnetic performance of the modeled dual reflector antenna system but with the advantage of requiring far less computational effort [4]. Rusch et al. [4] developed a general definition of the equivalent paraboloid for offset Cassegrain and Gregorian dual reflector antenna systems with arbitrary aperture shape. The development presented here will concentrate on the case of the canonical Cassegrain reflector antenna system. The notation of Rusch et al. [4] will be used through the end of this chapter to maintain consistency with the referenced article.

Figure 2.4-1 shows the geometry and definition of variables which Rusch et al. [4] use in the derivation of the general equation of the equivalent paraboloid of a Cassegrain reflector system. Rusch et al. [4] use four Cartesian coordinate systems: $\{x_p, y_p, z_p\}$ and $\{x_s, y_s, z_s\}$ which have their origin at the focal point of the main reflector surface and $\{x_f, y_f, z_f\}$ and $\{x_\beta, y_\beta, z_\beta\}$ which have their origin at the second focal point of the subreflector surface. Each coordinate system also has an associated spherical coordinate system. The main reflector surface is paraboloidal and the subreflector surface is hyperboloidal. The main reflector surface is given by

$$\rho_p = \frac{2F}{1 + \cos\theta_p} \qquad (2.4\text{-}1)$$

where

F = the focal length of the paraboloidal main reflector surface.

The subreflector is defined by

$$\rho_f - \rho_s = \frac{2c}{e} \qquad (2.4\text{-}2)$$

where

2c = the interfocal distance of the hyperboloid,

e = the eccentricity of the hyperboloid.

The formulas

$$\rho_f = \frac{c(e^2 - 1)}{e(e\cos\theta_\beta - 1)} \qquad (2.4\text{-}3)$$

$$\tan\frac{\theta_\beta}{2} = \frac{|e - 1|}{e + 1}\left[\tan\frac{\theta_s}{2}\right]^{-1}, \qquad (2.4\text{-}4)$$

derived from (2.4-2), and the identity

$$\tan\frac{\pi - \theta_s}{2} = \left[\tan\frac{\theta_s}{2}\right]^{-1} \qquad (2.4\text{-}5)$$

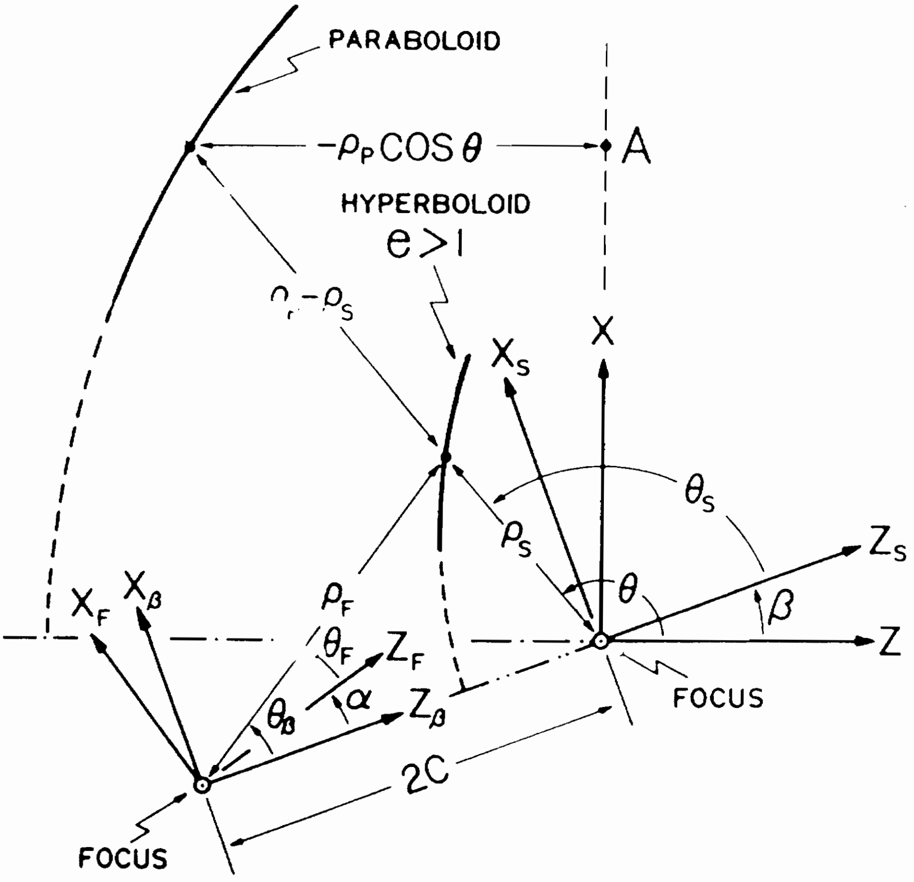

Figure 2.4-1. Geometry definition of the general Cassegrain reflector antenna for the Rusch et al. development of the equivalent paraboloid [4].

are useful in determining the geometrical optics aperture field due to a point source located at the second focus of the hyperboloidal subreflector.

Rusch et al. [4] now find the aperture field at a point A due to a spherical wave emanating from the feed point. The magnitude of this field at a point in the aperture is given by

$$E_A = E(\theta_f, \phi_f)\,\frac{\rho_s}{\rho_f \rho_p} \tag{2.4-6}$$

where

$E(\theta_f, \phi_f) =$ the field pattern of the feed expressed in the spherical feed coordinate system.

Rusch et al. [4] develop the $\frac{\rho_s}{\rho_f \rho_p}$ amplitude term as a function of θ_f and ϕ_f using the formulas

$$\cos\theta_p = \cos\theta_s \cos\beta - \sin\theta_s \cos\phi_s \sin\beta \tag{2.4-7}$$

$$\sin\theta_s = \frac{\rho_f}{\rho_s} \sin\theta_\beta \tag{2.4-8}$$

$$\cos\theta_s = \frac{\rho_f \cos\theta_\beta - 2c}{\rho_s} \tag{2.4-9}$$

and the identities

$$\sin\theta_\beta \cos\phi_\beta = \sin\theta_f \cos\phi_f \cos\alpha + \cos\theta_f \sin\alpha \tag{2.4-10}$$

$$\cos\theta_\beta = -\sin\theta_f \cos\phi_f \sin\alpha + \cos\theta_f \cos\alpha. \tag{2.4-11}$$

After substitution, they show that

$$\frac{\rho_s}{\rho_f \rho_p} = \frac{1}{2F}\left[1 - \frac{2c(1 - e\cos\beta)}{e\rho_f} + \sin\theta_f \cos\phi_f \sin(\alpha + \beta) - \cos\theta_f \cos(\alpha + \beta)\right]. \tag{2.4-12}$$

Since the angle α has not been used yet, it can be chosen arbitrarily. Rusch et al. [4] set α so that the z_f-axis is aligned with the axis of the equivalent paraboloid. This selection causes (2.4-12) to reduce to

$$\frac{\rho_s}{\rho_f \rho_p} = \frac{1 + \cos\theta_f}{2F_{eq}} \tag{2.4-13}$$

where

$$F_{eq} = F\,\frac{|e^2 - 1|}{(e^2 + 1) - 2e\cos\beta}. \tag{2.4-14}$$

So (2.4-6) now has the form

$$E_A = \frac{E(\theta_f, \phi_f)}{\rho_{eq}} \tag{2.4-15}$$

which is the aperture field distribution of a prime-focus paraboloidal reflector antenna system with a focal length of F_{eq}. Finally, (2.4-12) can be solved to determine the required feed tilt angle, α:

$$\sin\alpha = \frac{\left(e^2 - 1\right)\sin\beta}{\left(e^2 + 1\right) - 2e\cos\beta} \tag{2.4-16}$$

$$\cos\alpha = \frac{\left(e^2 + 1\right)\cos\beta - 2e}{\left(e^2 + 1\right) - 2e\cos\beta}. \tag{2.4-17}$$

These equations can be combined to form

$$\tan\alpha = \frac{\left(e^2 - 1\right)\sin\beta}{\left(e^2 + 1\right)\cos\beta - 2e} \tag{2.4-18}$$

or

$$\tan\frac{\alpha}{2} = \frac{e + 1}{e - 1}\tan\frac{\beta}{2}. \tag{2.4-19}$$

Either (2.4-18) or (2.4-19) can be used to find the required feed tilt for an equivalent paraboloid of focal length F_{eq} which will model the Cassegrain reflector antenna system.

Rusch et al. [4] caution that this model is based on geometrical optics principles applied to a focused reflector antenna system. Although defocusing and diffraction effects are ignored, the equivalent paraboloid should provide a reasonably accurate prediction of the near-boresight aperture and radiated fields of the focused dual reflector system it models. In order to minimize these effects, Rusch et al. [4] recommend that the equivalent paraboloid model not be applied to systems which have a subreflector smaller than approximately 10 wavelengths or an edge illumination taper of less than 10 dB on the subreflector.

To demonstrate the accuracy of the equivalent paraboloid as a model of a focused dual reflector system which satisfies the restrictions of (2.4-14) and (2.4-16) through (2.4-19), Rusch et al. [4] considered the system shown in Figure 2.4-2. The far-field electromagnetic

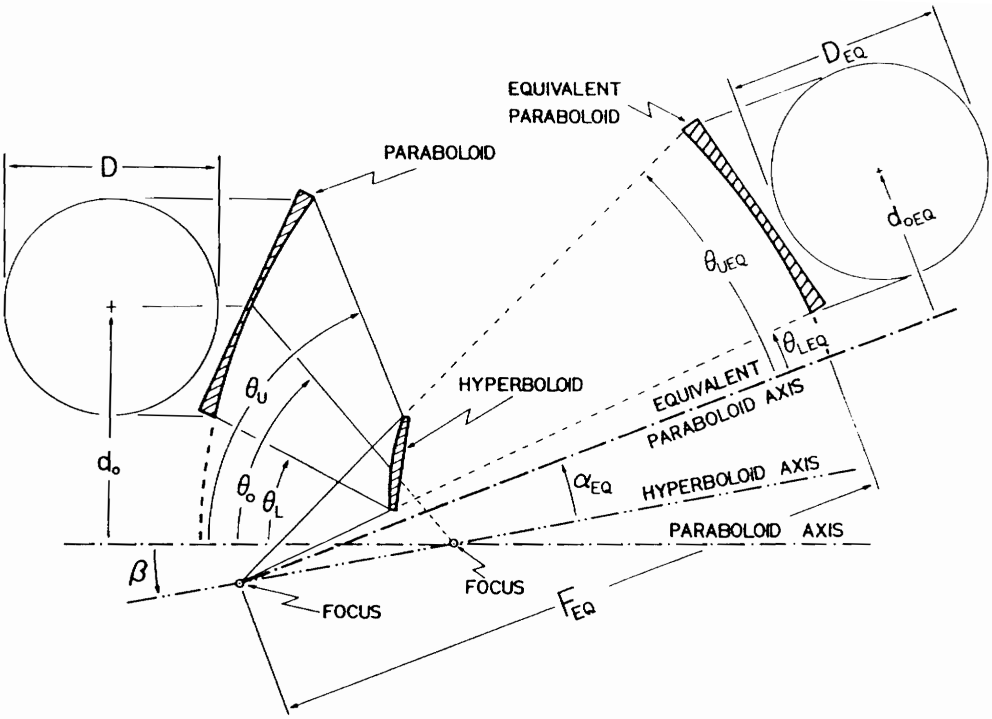

Figure 2.4-2. Geometry definition of a Cassegrain reflector antenna system with a circular aperture as used by Rusch et al. [4].

characteristics of this system and its equivalent paraboloid were calculated using physical optics/surface integration. The characteristics of this system are shown in Table 2.4-1. Figure 2.4-3 [4] shows the principal and 45° plane far-field radiation patterns for the Cassegrain system and its equivalent paraboloid. The equivalent paraboloid has a gain about 0.5 dB greater than the Cassegrain system but otherwise predicts the co-polarized antenna pattern of the Cassegrain system fairly accurately down to as low as 30 dB below the peak. The accuracy of the cross-polarization level prediction by the equivalent paraboloid is not discussed by Rusch et al. [4]. Rusch et al. [4] attribute the differences between the co-polarized patterns of the systems and the cross-polarized component of the Cassegrain system to diffraction effects and spillover at the subreflector surface.

Because the equivalent paraboloid of a dual reflector antenna system is derived under the assumption of a focused system, the equivalent paraboloid is a poor predictor of scan performance. Figure 2.4-4 [4] shows how the accuracy of the performance of the Cassegrain system predicted from the equivalent paraboloid degrades with beam scanning.

2.5 The Minimum Cross-Polarization/Spillover Condition for Offset Dual Reflector Antenna Systems

The second reflector surface in a dual reflector antenna affords the antenna designer additional degrees of freedom in the synthesis of the antenna system. This can be of value during antenna synthesis to improve the performance of the antenna system. For instance, because the main reflector and subreflector can be shaped in a dual reflector system, the designer can develop antenna systems ranging from a spherical main reflector with a phase correcting subreflector for wide-scanning to gain-optimized systems where the subreflector and main reflector are shaped to give a desired aperture distribution. The equivalent paraboloid concept suggests a fundamental configuration selection possibility. If the equivalent paraboloid for a

Table 2.4-1. Reflector geometry used by Rusch et al. [4] to verify the accuracy of the equivalent paraboloid far-field pattern predictions.

Main reflector focal length (F)	$62.5\,\lambda$
Main reflector diameter (D)	$100\,\lambda$
Main reflector offset height (d_o)	$75\,\lambda$
Feed tilt angle (α)	26.64°
Subreflector axis tilt angle (β)	9°
Subreflector eccentricity (e)	1.996
Subreflector interfocal distance (2c)	$20.41\,\lambda$
Equivalent paraboloid focal length (F_{eq})	$179.13\,\lambda$
Feed type	circularly symmetric $\cos^q$ with 10 dB edge illumination

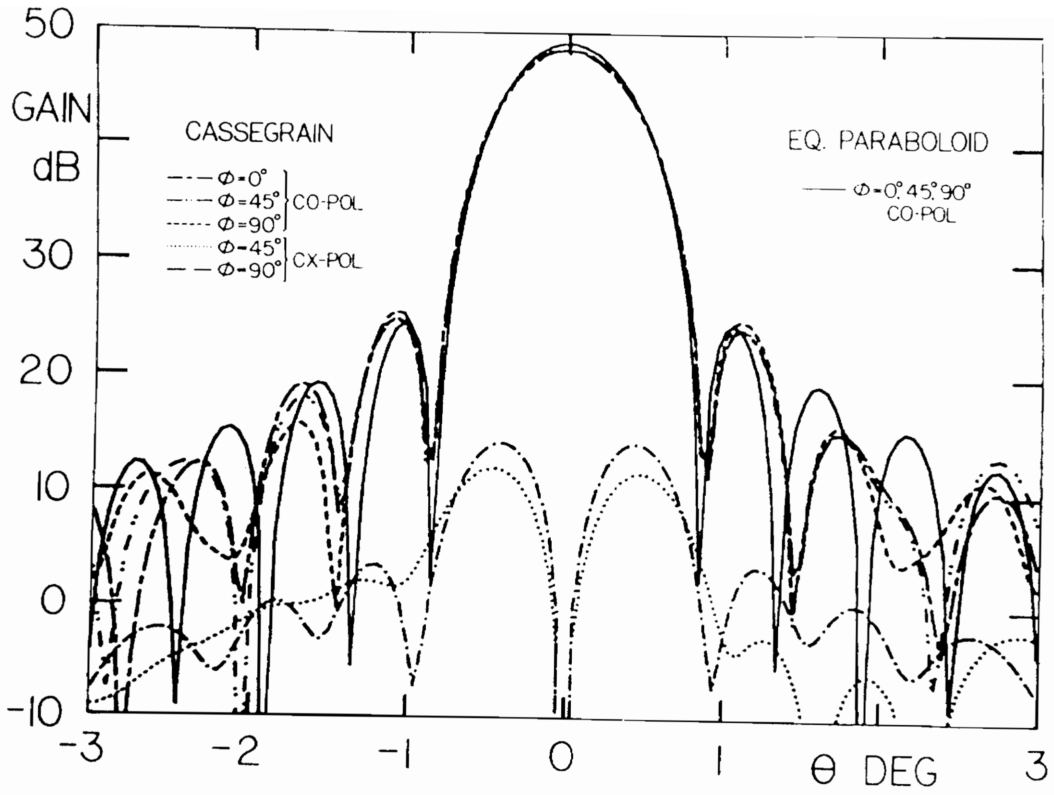

Figure 2.4-3. Equivalent paraboloid physical optics far-field pattern analysis results for the Rusch et al. system of Table 2.4-1. Principal and 45° plane pattern cuts for the Cassegrain reflector antenna system and its equivalent paraboloid [4].

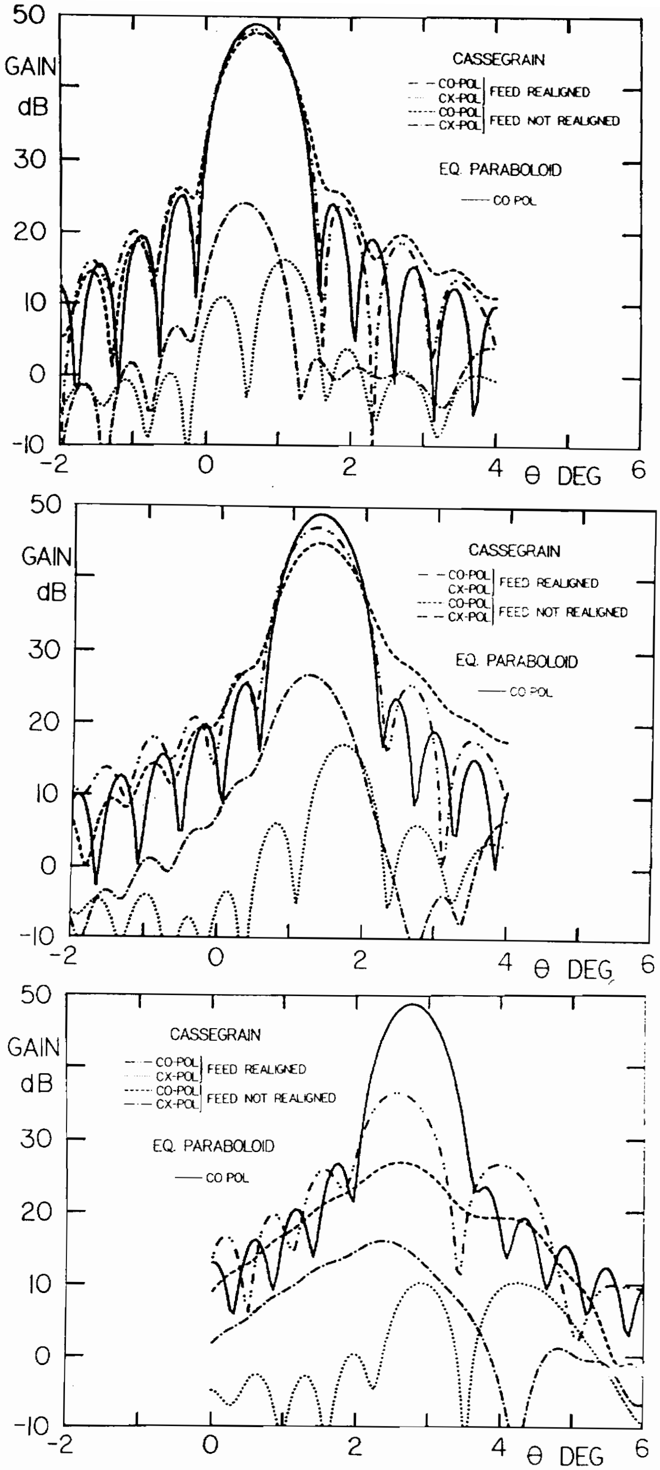

Figure 2.4-4. Equivalent paraboloid physical optics analysis results for the Rusch et al. system of Table 2.4-1. Pattern cuts in the plane of scan for a Cassegrain reflector antenna system and its equivalent paraboloid scanned in the plane of offset [4].

dual reflector antenna system with a circular aperture is axi-symmetric, the cross polarized field component radiated by the antenna due to geometrical offset effects and the antenna efficiency reduction to spillover effects will be simultaneously minimized [4].

Rusch et al. [4] developed a technique based on the equivalent paraboloid concept for simultaneously minimizing feed power spillover and the cross-polarized field component. Figure 2.4-2 [4] shows the geometry used in this development. The most significant change from the geometry used in the development of the equivalent paraboloid is the introduction of D_{eq}, the diameter of the equivalent paraboloid, and $d_{o_{eq}}$, the offset distance of the equivalent paraboloid. Because the development of the equivalent paraboloid, as presented above, is intended to be valid for any ray which reflects from the feed point through the dual reflector system, the equivalent paraboloid is shown to exist but its dimensions are not determined. Specializing this development to dual reflector systems which have circular apertures, allowed Rusch et al. [4] to show that $D = D_{eq}$ and also find $d_{o_{eq}}$, the offset height of the equivalent paraboloid.

Rusch et al. [4] use (2.4-4) , in the y = 0 plane, to write

$$\tan\left(\frac{\theta_f + \alpha}{2}\right) = \frac{|e - 1|}{e + 1}\left[\tan\left(\frac{\theta - \beta}{2}\right)\right]^{-1}. \tag{2.5-1}$$

By expanding the tangent terms and using (2.4-19), they showed that

$$\tan\frac{\theta_f}{2} = \frac{e^2 + 1 - 2e\cos\beta}{|e^2 - 1|}\left(\tan\frac{\theta}{2}\right)^{-1} - \frac{2e}{e^2 - 1}\sin\beta. \tag{2.5-2}$$

Rusch et al. [4] used clockwise angles as negative and use $\theta_{u_{eq}}$ and $\theta_{l_{eq}}$ to represent the angle between the upper and lower equivalent paraboloid edges and the z_f-axis. These conditions lead to:

$$D_{eq} = 2F_{eq}\left(\tan\frac{\theta_{u_{eq}}}{2} - \tan\frac{\theta_{l_{eq}}}{2}\right) \tag{2.5-3}$$

$$d_{o_{eq}} = F_{eq}\left(\tan\frac{\theta_{u_{eq}}}{2} + \tan\frac{\theta_{l_{eq}}}{2}\right). \tag{2.5-4}$$

Substituting (2.4-14) and (2.5-2) into (2.5-3) and (2.5-4) gives

$$D_{eq} = 2F\left(\tan\frac{\theta_l}{2} - \tan\frac{\theta_u}{2}\right) = D \qquad (2.5\text{-}5)$$

and

$$d_{o_{eq}} = \left(d_o - 2F\frac{2e\sin\beta}{e^2 + 1 - 2e\cos\beta}\right) \qquad (2.5\text{-}6)$$

where θ_l and θ_u are the angles between the lower and upper edges of the physical paraboloid of the Cassegrain system and the z-axis as shown in Figure 2.4-2 [4]. Setting $d_{o_{eq}} = 0$ allows the solution of (2.5-6) for the required β for an axi-symmetric equivalent paraboloid:

$$\tan\frac{\theta_c}{2} = \frac{2e\sin\beta}{e^2 + 1 - 2e\cos\beta} \qquad (2.5\text{-}7)$$

where the angle θ_c, as shown in Figure 2.4-2 [4], is the angle between the center of the aperture projected onto the main reflector surface and the -z-axis. In general, radiated cross-polarized fields can be minimized by aligning the feed along the axis of the equivalent paraboloid [4]. The Rusch condition, (2.5-7), forces the axis of the equivalent paraboloid to align with the angular center of the subreflector. This alignment will simultaneously minimize the radiated cross-polarized field component and the spillover [4] and will give the offset Cassegrain reflector antenna system unscanned characteristics similar to those of the axi-symmetric prime-focus paraboloidal reflector antenna system.

References

[1] R. Mittra, F. Hyjazie, and V. Galindo-Israel, "Synthesis of Offset Dual Reflector Antennas Transforming a Given Feed Illumination Pattern into a Specified Aperture Distribution," *IEEE Transactions on Antennas and Propagation*, Vol. AP-30, No. 2, pp. 251-259, March 1982.

[2] Z. Xianzhong, "A Theorem on an Arbitrary Dual Reflector Antenna System," *IEEE AP-S Symposium Digest (Dallas)*, pp. 486-489, May 1990.

[3] W.V.T. Rusch, A. Prata, Jr., Y. Rahmat-Samii, and R.A. Shore, "Derivation and Application of the Equivalent Paraboloid for Classical Offset Cassegrain and Gregorian Antennas," *IEEE Transactions on Antennas and Propagation*, Vol. AP-38, No. 8, pp. 1141-1149, August 1990.

Chapter 3

BEAM SCANNING IN CASSEGRAIN REFLECTOR ANTENNA SYSTEMS

The radiation characteristics of a Cassegrain reflector antenna system are degraded when its main beam is scanned away from the focused boresight direction. The gain of the antenna and the symmetry of the pattern are reduced while the beamwidth and the sidelobe levels are increased. The factors which lead to this degradation must be minimized to achieve good performance during even moderate beam scanning. This chapter identifies the major factors which contribute to the degradation of antenna performance during beam scanning and presents two previous methods of beam scanning for the offset Cassegrain reflector antenna system. This material offers insight into the beam scanning properties of the offset Cassegrain reflector antenna system and facilitates the development of the simplified error functionals in Chapter 5.

3.1 Principles of Beam Scanning

Beam scanning in any antenna system requires a tilted aperture phase surface [1]. This phase taper can be achieved either mechanically by moving the antenna feed system or electrically by imposing a phase taper with an array feed. This work is intended to determine the optimal mechanical motions for beam scanning in an offset Cassegrain reflector antenna system.

To create an asymmetric phase distribution across the aperture of a reflector antenna, the antenna system feed phase center must be moved laterally away from the unscanned feed point. In the offset Cassegrain reflector antenna system this movement can be achieved either by physically moving the feed or by repositioning the subreflector to create a virtual feed movement. While any asymmetric aperture phase taper is sufficient for beam scanning, the formation of a clean scanned beam requires that two sources of beam degradation be minimized; these are discussed in the remainder of this section.

3.1.1 Illumination Error Effects

Aperture illumination amplitude error is a major source of antenna performance degradation during beam scanning. In an offset Cassegrain reflector antenna system, the significant source of illumination amplitude error during beam scanning is misalignment of the illumination pattern with the main reflector caused by the lateral feed translation. A small amount of illumination error is also introduced during beam scanning by edge illumination taper changes resulting from axial feed translation. Illumination misaligment, illustrated in Figure 3.1.1-1, can be significant in subreflector scanned offset Cassegrain reflector antenna systems because the required subreflector tilt repoints the central ray from the feed away from the center of the main reflector.

The effects of the illumination misalignment error can be estimated for an offset Cassegrain reflector antenna system by inducing feed mispointing in the equivalent paraboloid since feed mispointing does not induce defocusing. In order to estimate the effects of illumination misalignment on the far-field pattern on a Cassegrain reflector antenna, uv-plane patterns were generated for its equivalent paraboloid using the TICRA GRASP7 numerical electromagnetics code using physical optics surface integration analysis. As will be discussed in Chapter 4, the equivalent paraboloid of the test case is axi-symmetric and has a diameter, D_{eq}, of 10.63 meters and a focal length, F_{eq}, of 42.48 meters. Viewed from the feed, the equivalent

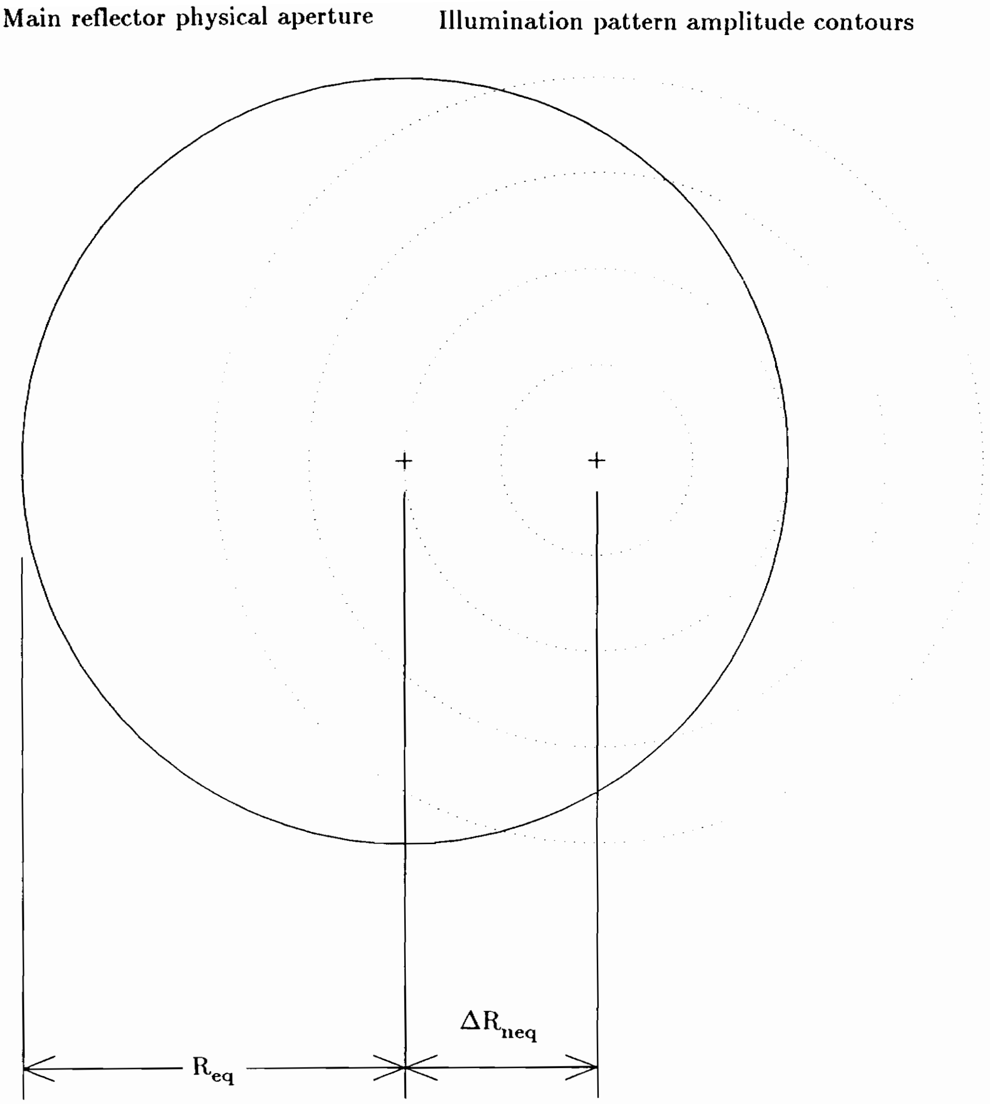

Figure 3.1.1-1. Illumination misalignment in the equivalent paraboloid.

paraboloid subtends a half-angle of 7.159°. For this analysis the reflector was fed by standard Gaussian feed patterns with reflector edge illuminations of -5, -10, -15, -20, and -25 dB. The edge illumination specified for the study of illumination misalignment does not include the spherical spreading loss edge taper, but this effect is less than 0.04 dB. Scan induced illumination misalignment was simulated by pointing the center of the illumination away from the center of the reflector in steps of 0.2 reflector radii, R_{eq}, up to a maximum of $2\,R_{eq}$. The maximum illumination misalignment of $2\,R_{eq}$ was chosen because it causes the feed pattern to just miss the reflector surface.

The actual gain of an aperture antenna, G, is given by

$$G = \frac{4\pi A_e}{\lambda^2} = \varepsilon_{ap}\frac{4\pi A}{\lambda^2} \tag{3.1.1-1}$$

where A is the area of the projection of the main reflector into the aperture plane, and λ is the wavelength of operation. The effective aperture area, $A_e = \varepsilon_{ap} A$, where ε_{ap} is the aperture efficiency of the antenna. Aperture efficiency can be factored as:

$$\varepsilon_{ap} = \varepsilon_{sp}\varepsilon_{ill} = \varepsilon_{sp}\varepsilon_{amp}\varepsilon_{\phi} \tag{3.1.1-2}$$

where ε_{sp} is the spillover efficiency of the reflector antenna system, ε_{ill} is the illumination efficiency of the reflector antenna, ε_{amp} is the illumination amplitude efficiency of the reflector antenna, and ε_{ϕ} is the illumination phase efficiency of the reflector antenna. Spillover efficiency is defined by

$$\varepsilon_{sp} = \frac{\displaystyle\iint_A P_i(r,\theta)\,dA}{P_t} \tag{3.1.1-3}$$

where $P_i(r,\theta)$ is the power density incident on the reflector aperture and P_t is the total power from the reflector feed antenna. Illumination amplitude efficiency is defined by [2]

$$\varepsilon_{amp} = \frac{\left[\displaystyle\iint_A P_i(r,\theta)\,dA\right]^2}{\displaystyle\iint_A [P_i(r,\theta)]^2\,dA}. \tag{3.1.1-4}$$

Illumination phase efficiency, ε_ϕ, is given by

$$\varepsilon_\phi = \frac{\left| \displaystyle\iint_{\text{aperture}} P_i(r,\theta)\, e^{j\Phi}\, dA \right|^2}{\displaystyle\iint_{\text{aperture}} \left| P_i(r,\theta)\, e^{j\Phi} \right|^2 dA} \cdot \frac{1}{\varepsilon_{\text{amp}}} \tag{3.1.1-5}$$

where $P_i(r,\theta)\, e^{j\Phi}$ is the complex power density incident on the reflector aperture and ε_{amp} is the illumination amplitude efficiency found from (3.1.1-4). The illumination amplitude efficiency term is included in illumination phase efficiency to remove the effects of aperture power illumination so that the phase error efficiency is 100% for a focused system.

The far-field radiation patterns of the equivalent paraboloid with illumination misalignment were calculated using GRASP7 physical optics/surface integration at 20 GHz. Figure 3.1.1-2 shows the gain, G, of the equivalent paraboloid as a function of normalized illumination misalignment distance, ΔR_n, for five edge illumination values. The gain loss caused by illumination misalignment can be separated into two loss components corresponding to decreased spillover efficiency and decreased illumination efficiency. As shown by Figure 3.1.1-3, most of the gain loss caused by illumination misalignment consists of spillover loss. Expressed in decibels, the decrease in spillover efficiency relative to the properly aligned case varies from about 13 to 36 dB at an normalized illumination misalignment distance of 2. The remaining gain loss, 3 to 9 dB at an normalized illumination misalignment distance of 2, is comprised of decreased illumination amplitude efficiency as shown in Figure 3.1.1-4. Illumination phase efficiency is 100% for this case since the system is focused. The overall aperture efficiency, ε_{ap}, is shown in Figure 3.1.1-5 as a function of normalized illumination misalignment distance, ΔR_n; this is found from the data in Figure 3.1.1-3 using (3.1.1-1).

Figure 3.1.1-6 shows the sidelobe level, SLL, as a function of normalized illumination misalignment distance, ΔR_n, for the five edge illumination values. Although the plots are not

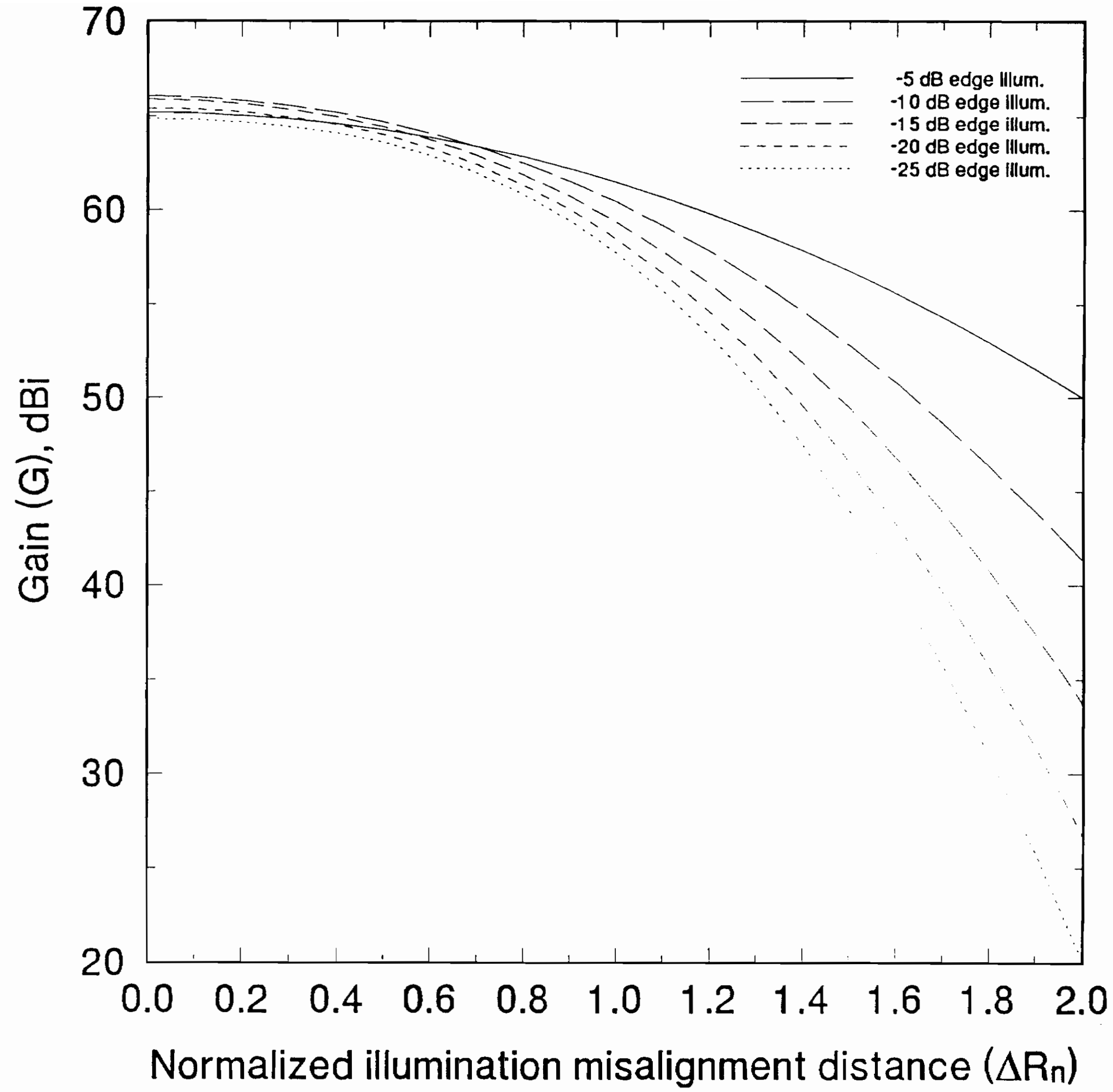

Figure 3.1.1-2. Test case equivalent paraboloid gain (G) as a function of normalized illumination misalignment distance (ΔR_{eqn}).

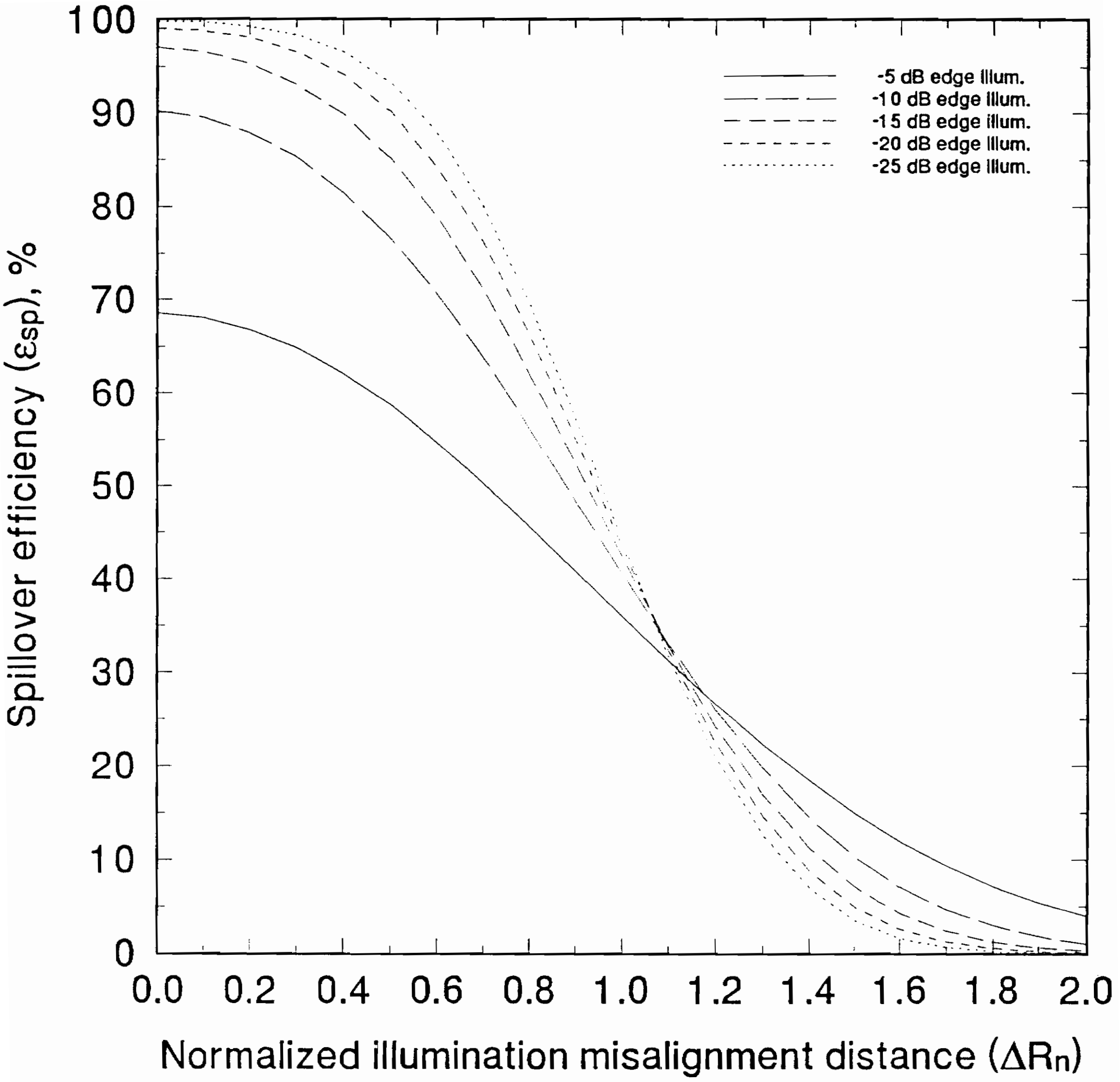

Figure 3.1.1-3. Test case equivalent paraboloid spillover efficiency (ε_{sp}) as a function of normalized illumination misalignment distance (ΔR_{eqn}).

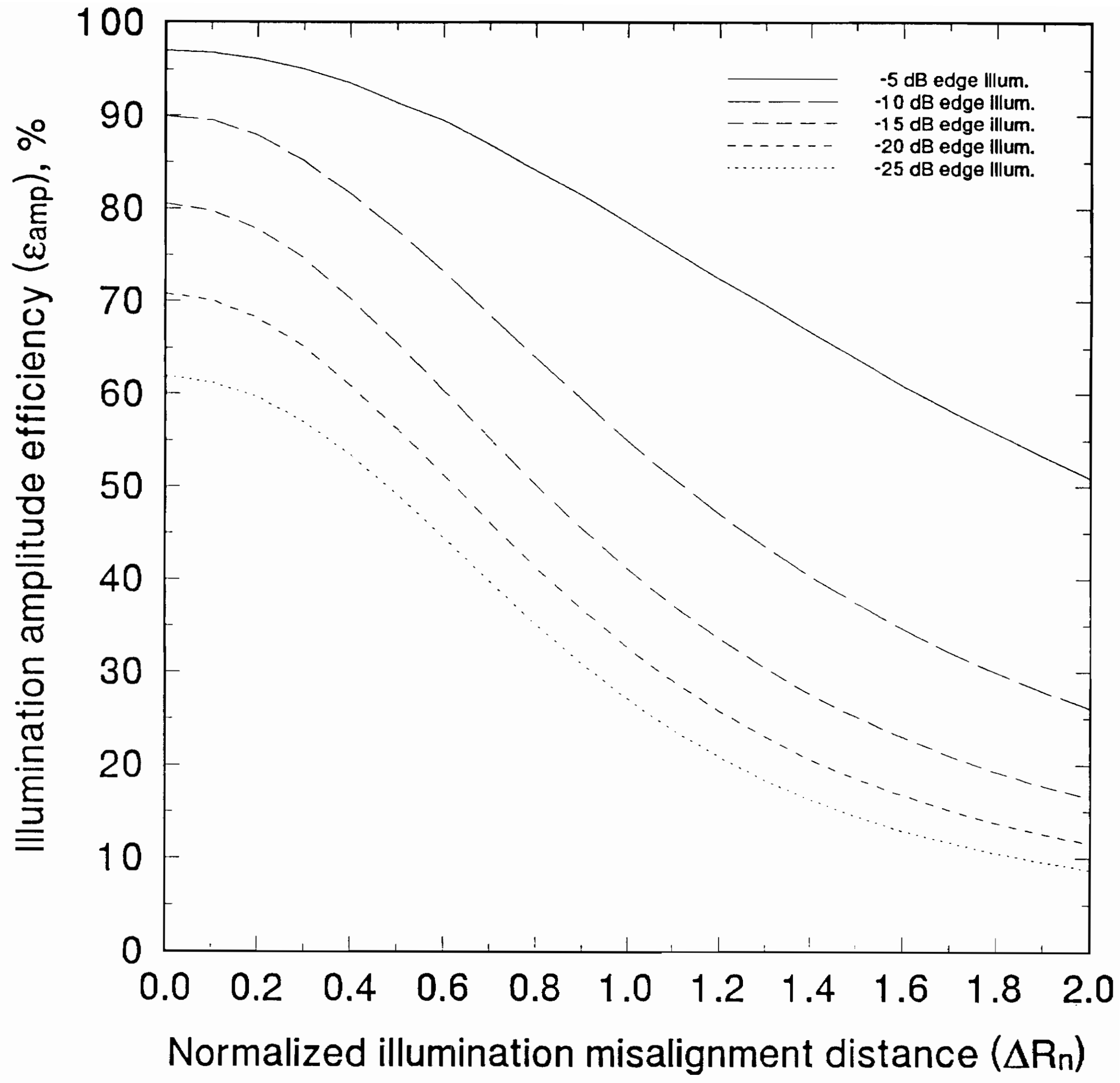

Figure 3.1.1-4. Test case equivalent paraboloid illumination amplitude efficiency ($\varepsilon_{\mathrm{amp}}$) as a function of normalized illumination misalignment distance (ΔR_{eqn}).

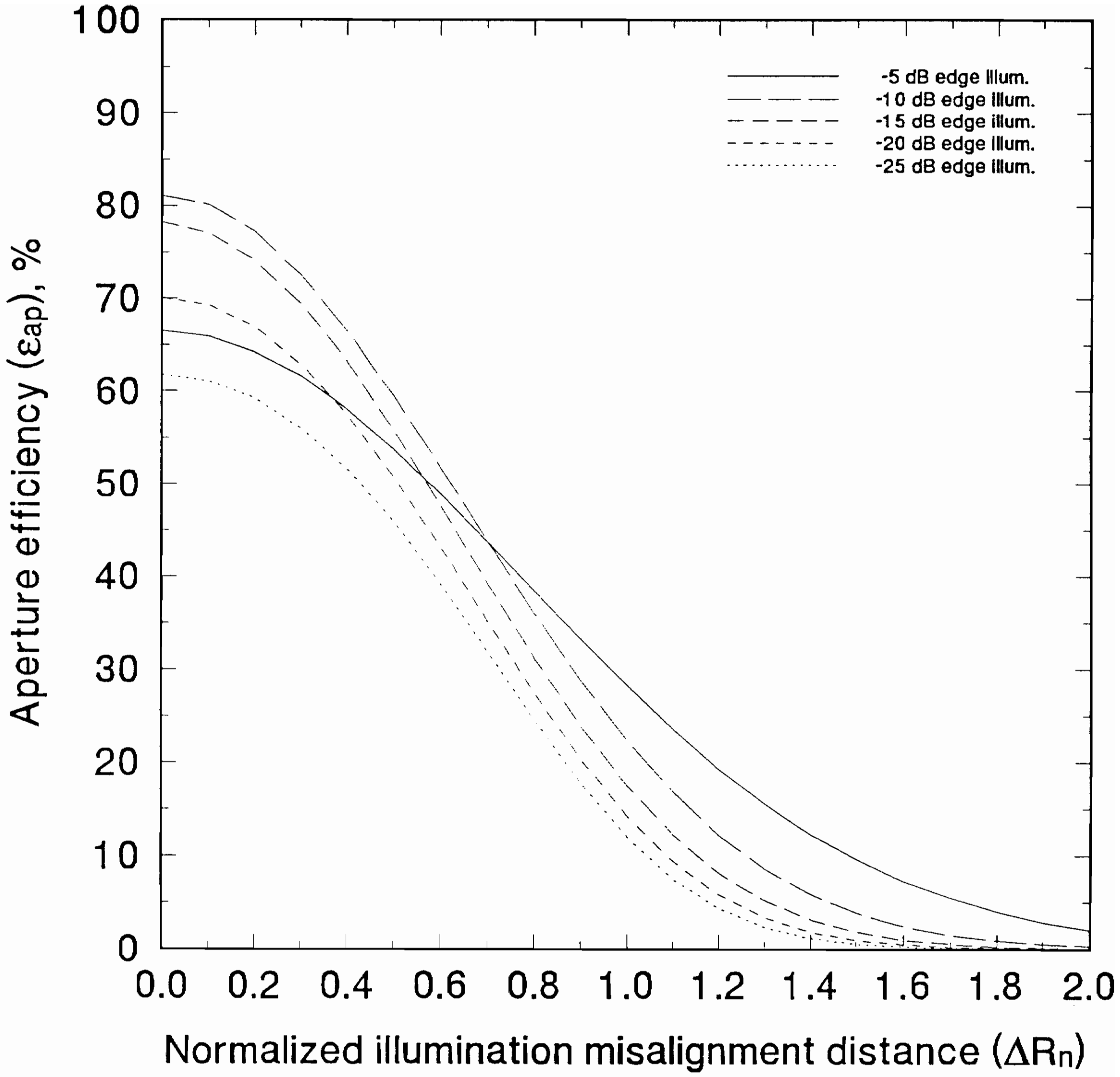

Figure 3.1.1-5. Test case equivalent paraboloid aperture efficiency (ε_{ap}) as a function of normalized illumination misalignment distance (ΔR_{eqn}).

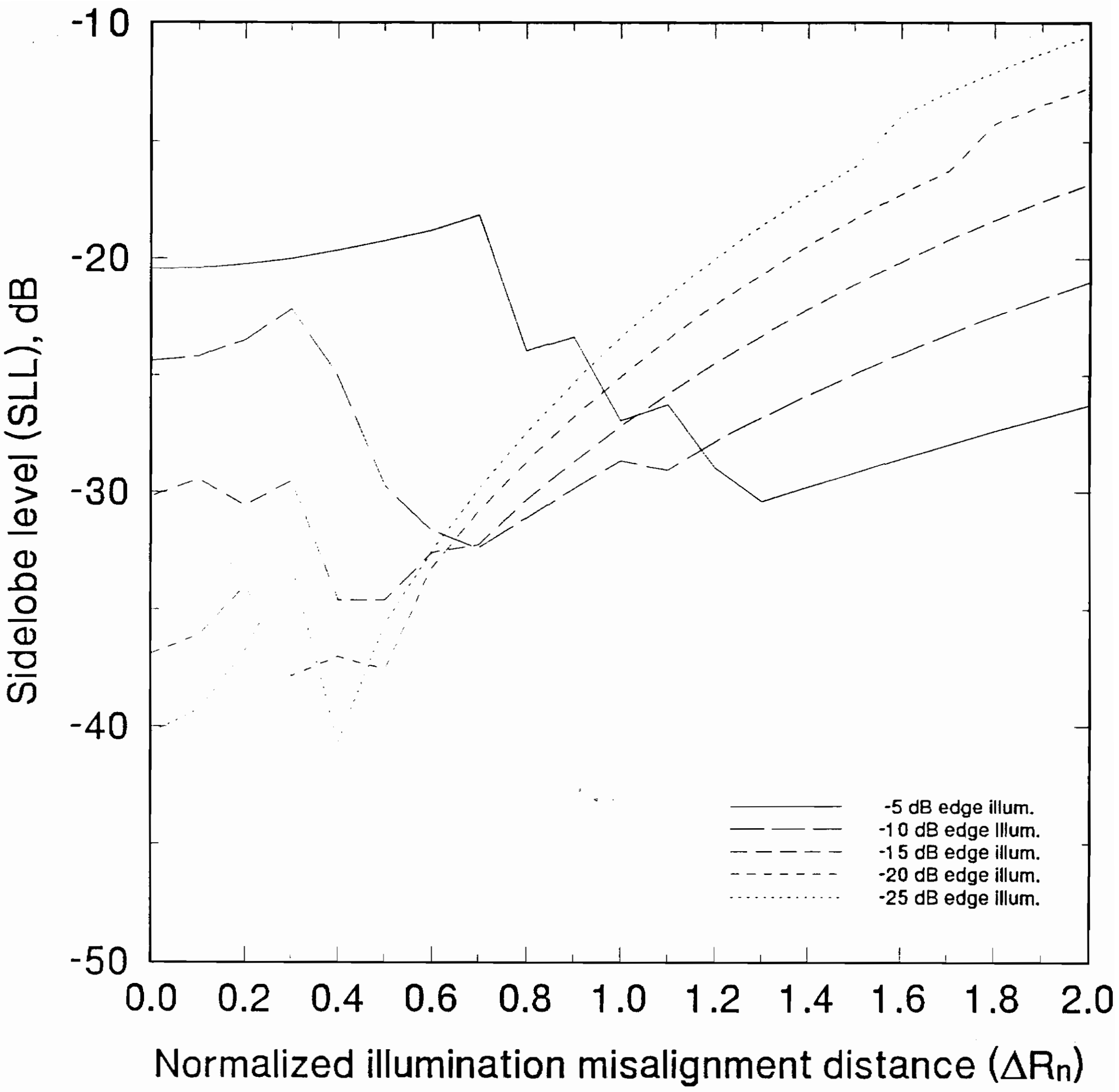

Figure 3.1.1.-6. Test case equivalent paraboloid sidelobe level (SLL) as a function of normalized illumination misalignment distance (ΔR_{eqn}).

smooth, the relative sidelobe level increases monotonically with increasing illumination misalignment. The roughness in the curves is caused by the consecutive blending of the increasing near-in sidelobes with the main lobe. Figure 3.1.1-7 shows the peak cross-polarization level,

$$XPOL = G_{cr}(\theta,\phi)_{max} - G(\theta,\phi)_{max}, \tag{3.1.1-6}$$

as a function of normalized illumination misalignment distance, ΔR_n, for the five edge illumination values. Beam efficiency, defined as

$$BE = \frac{\displaystyle\int_{\theta=0}^{2.5(\theta_{3dB})} \int_{\phi=0}^{2\pi} P(\theta,\phi) \sin\theta \, d\theta \, d\phi}{P_t} \tag{3.1.1-7}$$

where θ_{3dB} is angle from the main beam gain peak to the the half-power point of the pattern, $P(\theta,\phi)$ is the power pattern of the antenna, and P_t is the power transmitted by the feed, is shown in Figure 3.1.1-8 for several edge illumination values. In order to achieve the required 90% beam efficiency, the edge illumination must be lower than -12 dB for a system with no illumination misalignment and still lower if illumination misalignment exists.

3.1.2 Phase Error Effects

The second source of antenna performance degradation during beam scanning is aperture phase error resulting from distortion of the aperture constant phase surface. The effects of aperture phase errors, or aberrations, on antenna performance have been extensively studied by Born and Wolf in connection with optical lens design [3]. Born and Wolf [1] represent aperture phase errors with cylindrical Zernike polynomials of ρ and ϕ to define a constant phase surface above the aperture. For small aberrations, the first five terms of the aberration series are sufficient to describe the constant phase surface [1]. These terms, called the Siedel aberrations, are

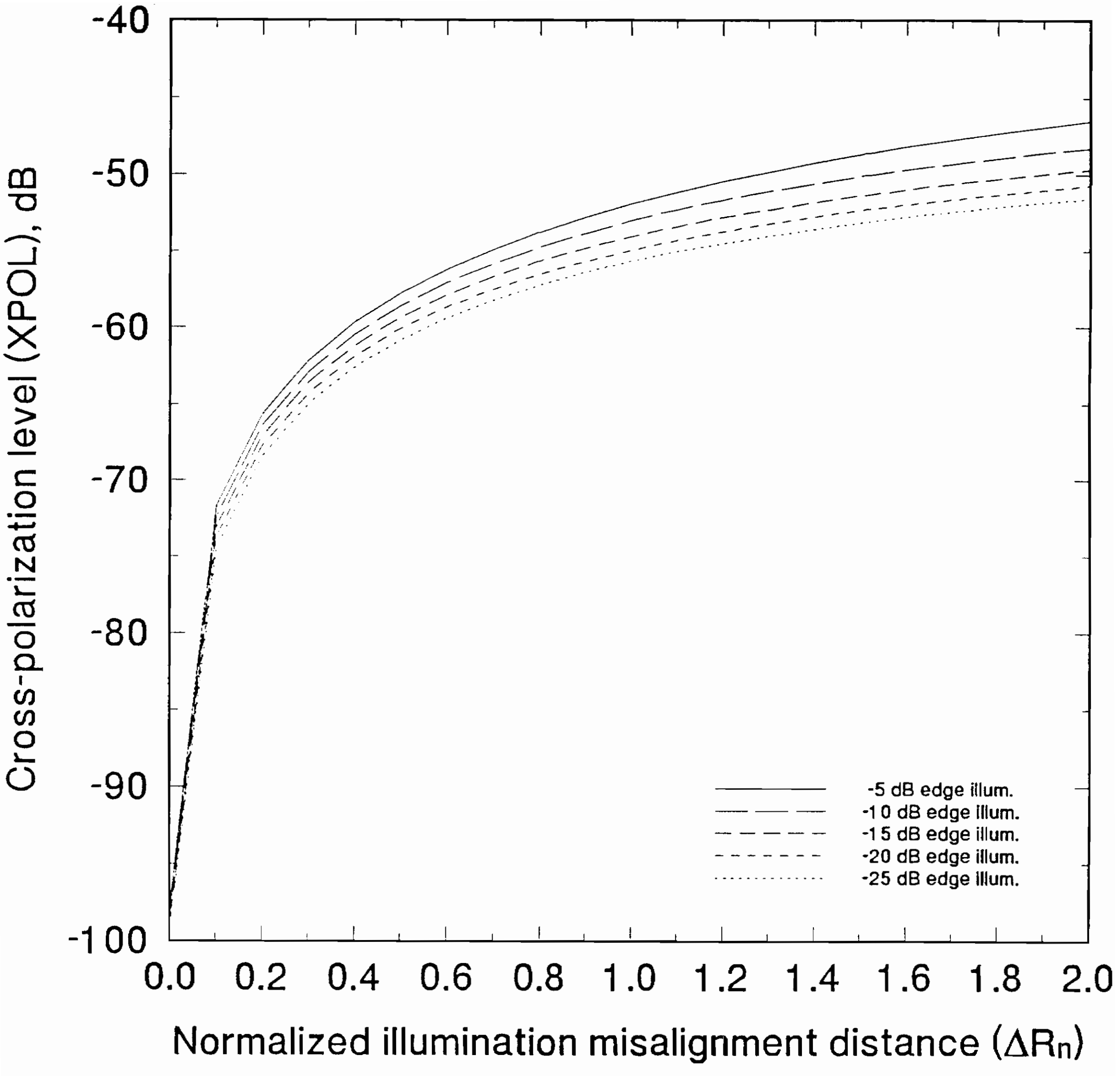

Figure 3.1.1-7. Test case equivalent paraboloid cross-polarization level (XPOL) as a function of normalized illumination misalignment distance (ΔR_{eqn}).

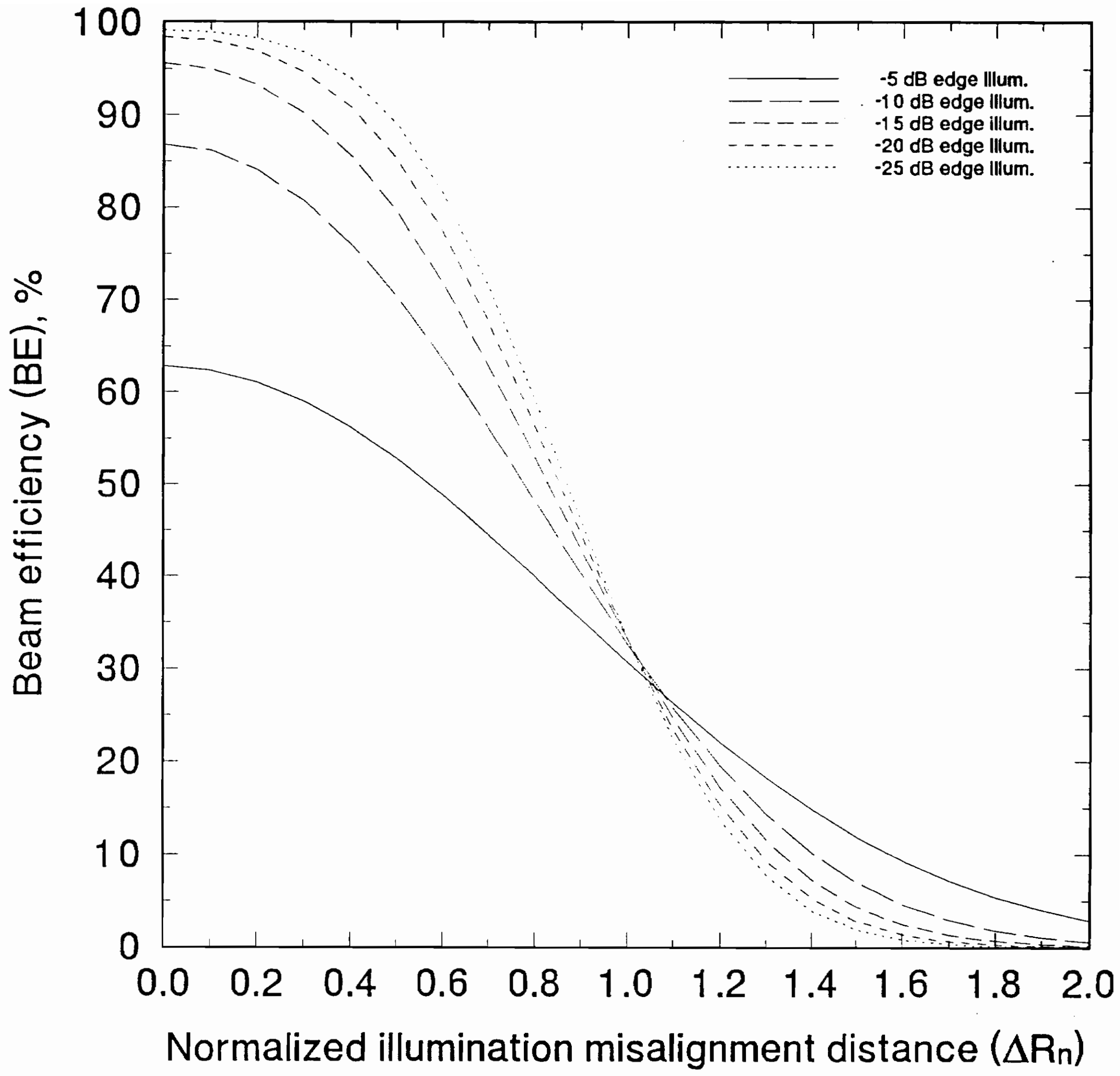

Figure 3.1.1-8. Test case equivalent paraboloid beam efficiency (BE) as a function of normalized illumination misalignment distance (ΔR_{eqn}).

$$\Delta L(\rho,\phi) = \alpha\rho\cos\phi + \beta\rho^2 + \gamma\rho^2\cos 2\phi + \delta\rho^3\cos\phi + \varepsilon\rho^4 \tag{3.1.2-1}$$

and are known, respectively, as distortion, curvature of field, astigmatism, coma, and spherical aberration [1]. The constant aperture phase surface produced by each these aberration terms is shown in Figure 3.1.2-1 [1]. The effects of these aberrations on antenna patterns are usually obtained by the simplification of the Zernike polynomial to a one-dimensional polynomial by setting ϕ equal to either 0 or $\frac{\pi}{2}$ [1]. With this simplification, the Siedel aberration series becomes

$$\Delta L(\rho) = \alpha\rho + (\beta + \gamma)\rho^2 + \delta\rho^3 + \varepsilon\rho^4 \tag{3.1.2-2}$$

in the $\phi = 0$ plane.

The linear phase error term, $\alpha\rho$, does not degrade the antenna pattern but rather steers the beam away from the unscanned boresight direction [1]. The amount of beam scanning caused by this aberration is

$$\theta_o = \sin^{-1}\left(\frac{\alpha\lambda}{D_M\pi}\right) \tag{3.1.2-3}$$

where D_M is the diameter of the antenna aperture and λ is the wavelength at the frequency of operation [1]. This is the desired constant aperture phase surface which should be attained during beam scanning while minimizing the other aberration terms and illumination errors. A secondary pattern effect which is associated with this aberration term is a small change in the size of the projected aperture. For a symmetric aperture which is perpendicular to the unscanned beam, this change is a reduction of the projected aperture diameter which is proportional to $\cos\theta_o$.

The quadratic phase error term, $(\beta + \gamma)\rho^2$, has no beam scanning effect since it represents a symmetric aperture phase taper. This aberration will, however, lead to an increase in the overall sidelobe level and pattern null-filling [1]. The exact effects of quadratic phase error can be determined by an analysis presented by Silver [4]. This analysis gives the far-field

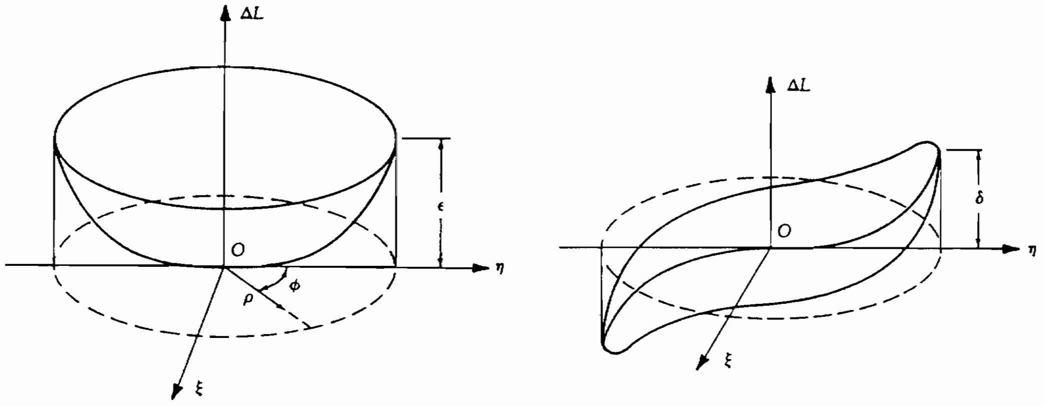

Spherical: $\Delta L = \varepsilon\rho^4$

Coma: $\Delta L = \delta\rho^3\cos\phi$

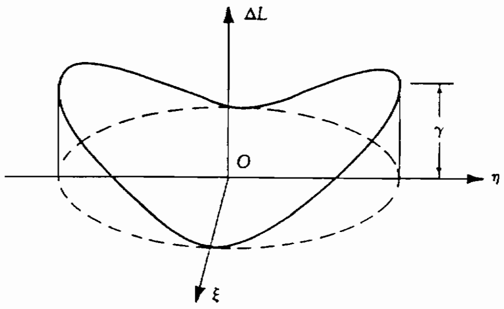

Astigmatism: $\Delta L = \gamma\rho^2\cos 2\phi$

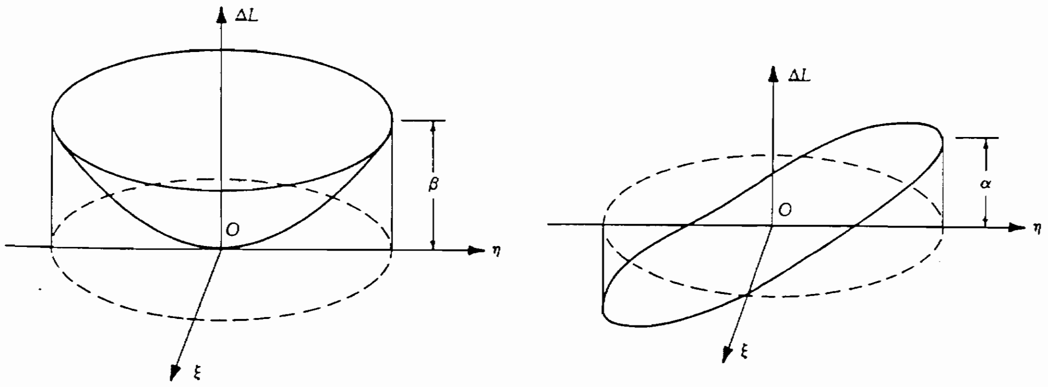

Curvature of field: $\Delta L = \beta\rho^2$

Distortion: $\Delta L = \alpha\rho\cos\phi$

Figure 3.1.2-1. The constant phase surfaces of the Siedel aberration terms [1].

radiation pattern of the aperture from

$$g(u) = \frac{a}{2} \int_{-1}^{1} f(\rho)\, e^{j[u\rho - \beta\rho^2]}\, d\rho \tag{3.1.2-4}$$

where $u = \left(\frac{\pi D_M}{\lambda}\right) \sin\theta$ and $f(\rho)$ is assumed to be an even function which represents the amplitude distribution across the aperture [1]. For small quadratic phase aberrations, the far-field power pattern is

$$P(u) \simeq \frac{D_M^{\,2}}{4} \left\{ g_o^{\,2}(u) + \beta^2 \left[g_o''(u) \right]^2 \right\} \tag{3.1.2-5}$$

where $g_o(u)$ is the far-field radiation pattern with no aberration and $g_o''(u)$ is the second derivative of the aberration free far-field radiation pattern [1]. The effects of the quadratic phase error term on the pattern of an aperture with a uniform amplitude are shown in Figure 3.1.2-2 for $\beta = 0$, $\frac{\pi}{4}$, and $\frac{\pi}{2}$ [1]. As β increases, the pattern continues to deteriorate with the main lobe eventually bifurcating but symmetry is maintained about the $\theta = 0$ axis [1].

The cubic phase error term, $\delta\rho^3$, introduces additional beam scanning since it represents an asymmetric aperture phase taper and also raises the peak sidelobe level [1]. Using Silver's method to find the effects of the cubic phase error term on the far-field power pattern results in

$$P(u) \simeq \frac{D_M^{\,2}}{4} \left\{ g_o(u) + \delta\, g_o'''(u) \right\}^2 \tag{3.1.2-6}$$

where $g_o(u)$ is the far-field radiation pattern with no aberration and $g_o'''(u)$ is the third derivative of the aberration free far-field radiation pattern [1]. The effects of the cubic phase error term on the pattern of an aperture with a uniform amplitude are shown in Figure 3.1.2-3 for $\gamma = 0$, $\frac{\pi}{4}$, and $\frac{\pi}{2}$ [1]. The cubic phase error term causes the main beam of the aperture to be steered farther away from the unscanned boresight direction, $\theta = 0$, as γ increases. Also, the sidelobes increase on the side of the main beam away from $\theta = 0$ while the sidelobes on the side of the main beam toward $\theta = 0$ decrease.

Like the quadratic phase error term, the quartic phase error term, $\varepsilon\rho^4$, has no beam

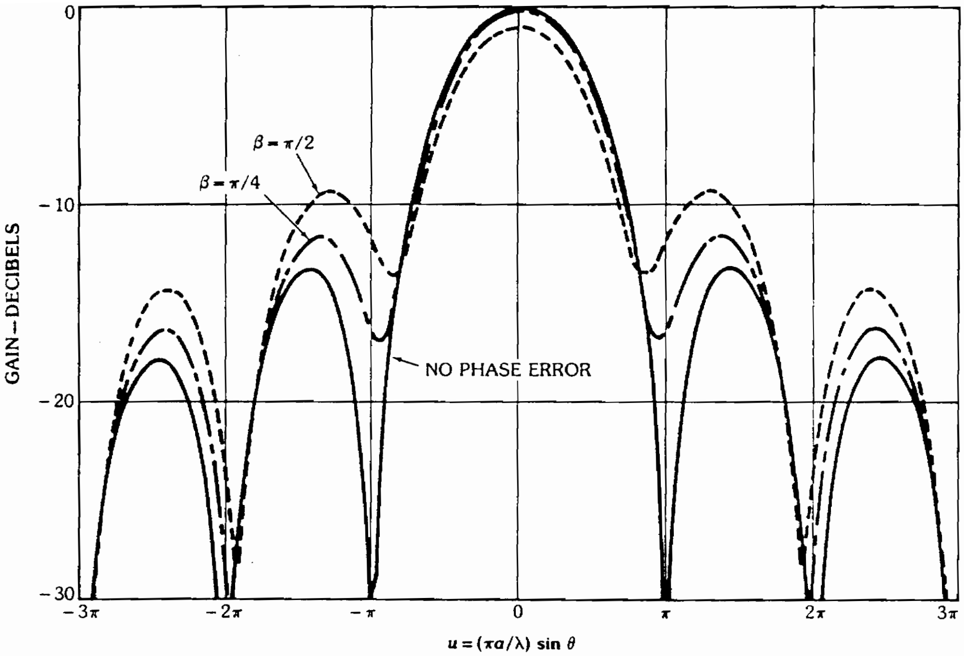

Figure 3.1.2-2. Effects of quadratic phase error on an antenna pattern [1].

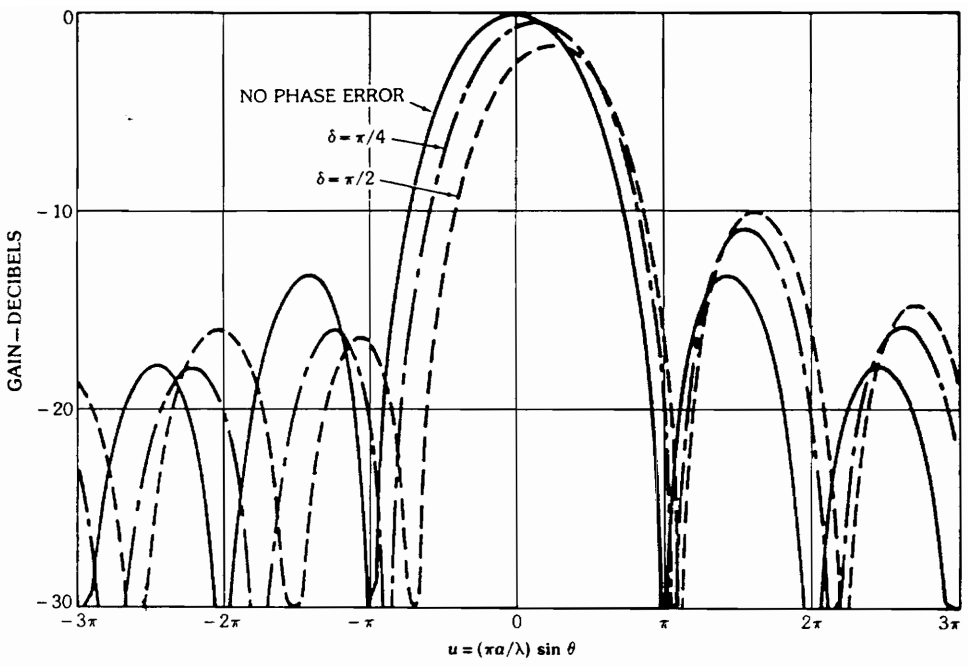

Figure 3.1.2-3. Effects of cubic phase error on an antenna pattern [1].

scanning effect since it represents a symmetric aperture phase taper. Also, like the quadratic phase error term, the quartic aberration will increase the overall sidelobe level and fill in the pattern nulls although the pattern degrades less than for a quadratic phase error of the same peak value [1]. Using Silver's analysis, as for the quadratic and cubic phase error terms, the far-field power pattern of the quartic phase error term is

$$P(u) \simeq \frac{D_M{}^2}{4}\left\{g_o{}^2(u) + \varepsilon^2\left[g_o{}^{(4)}(u)\right]^2\right\} \qquad (3.1.2\text{-}7)$$

where $g_o(u)$ is the far-field radiation pattern with no aberration and $g_o{}^{(4)}(u)$ is the fourth derivative of the aberration free far-field radiation pattern [1]. The effects of the quartic phase error term on the pattern of an aperture with a uniform amplitude are shown in Figure 3.1.2-4 for $\varepsilon = 0, \frac{\pi}{4}$, and $\frac{\pi}{2}$ [1]. As expected from the similarities between (3.1.2-7) and (3.1.2-5), Figure 3.1.2-4 is much the same as Figure 3.1.2-2 except with a smaller pattern degradation for a given peak aberration [1].

The boresight gain loss for quadratic, cubic, and quartic phase errors is shown in Figure 3.1.2-5 [1]. With the exception of the cubic phase error, the effect of an aberration with a given peak phase error decreases with increasing order. The effect of cubic phase error is greater because the beam peak is scanned away from boresight by the resulting asymmetric phase distribution. This relationship between aberration order and pattern degradation for a given peak phase error can be explained by noting that for a given peak phase error, the total error decreases with increasing aberration order as shown in Figure 3.1.2-6. In addition to gain loss, as shown for each of the non-linear phase error terms, aberrations of quadratic or higher order also cause an increase in peak sidelobe level and can cause the filling of pattern nulls [1]. Of the Siedel aberrations, cubic phase errors exhibit the greatest pattern degradation for a given peak phase error [1].

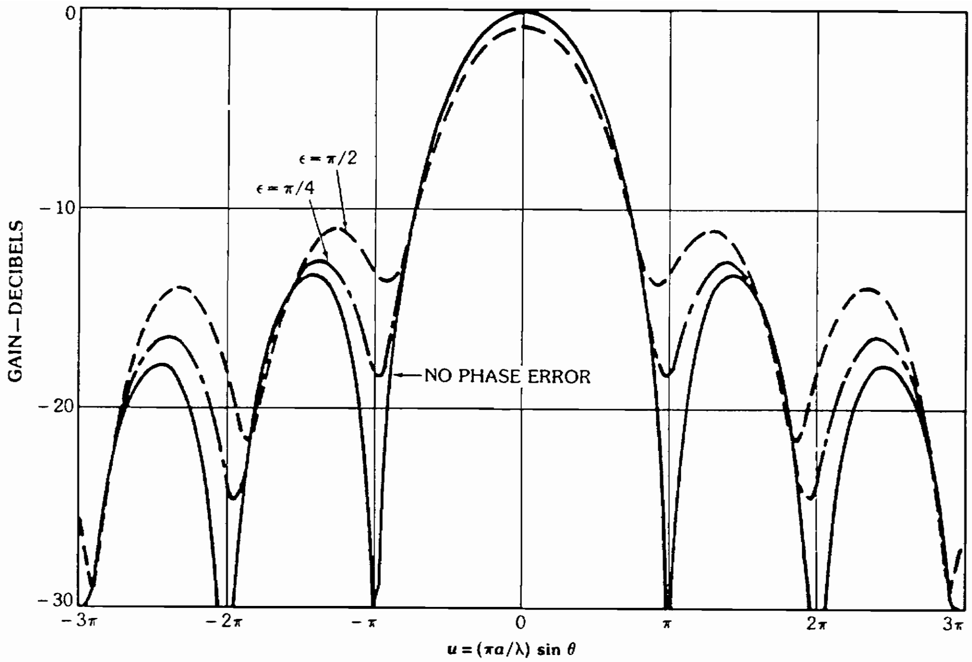

Figure 3.1.2-4. Effects of quartic phase error on an antenna pattern [1].

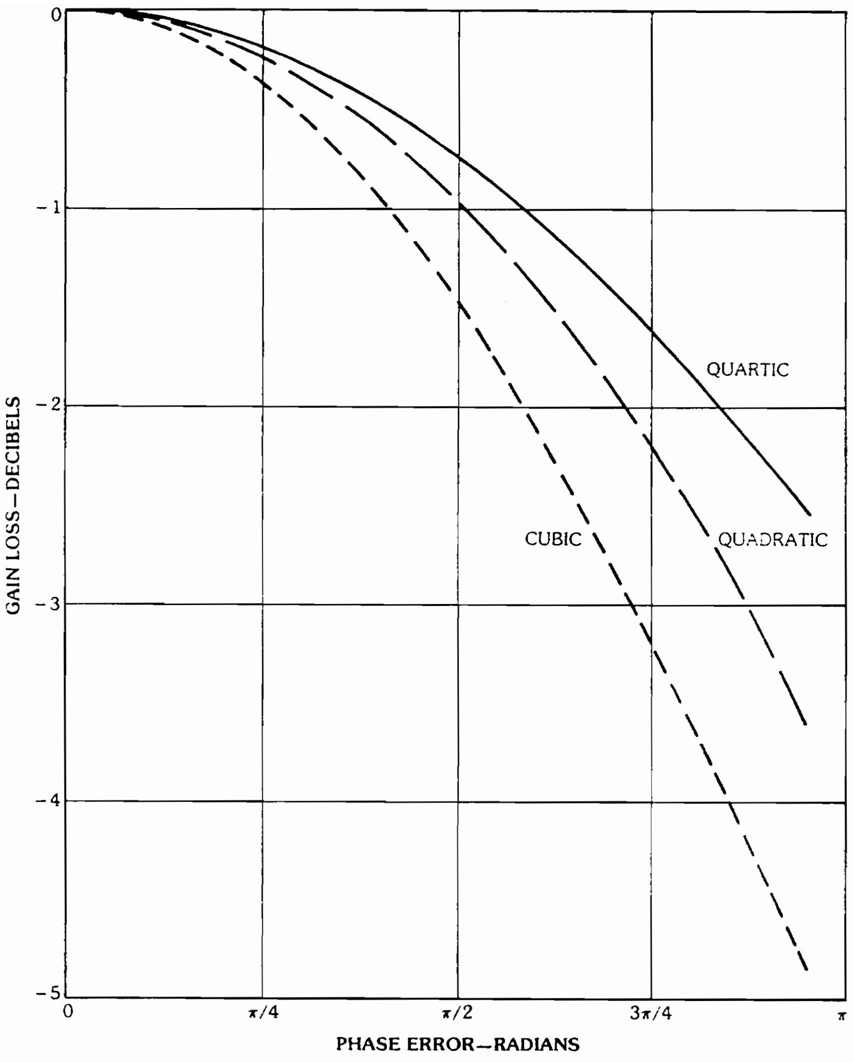

Figure 3.1.2-5. Boresight antenna gain loss for the Siedel aberration terms [1].

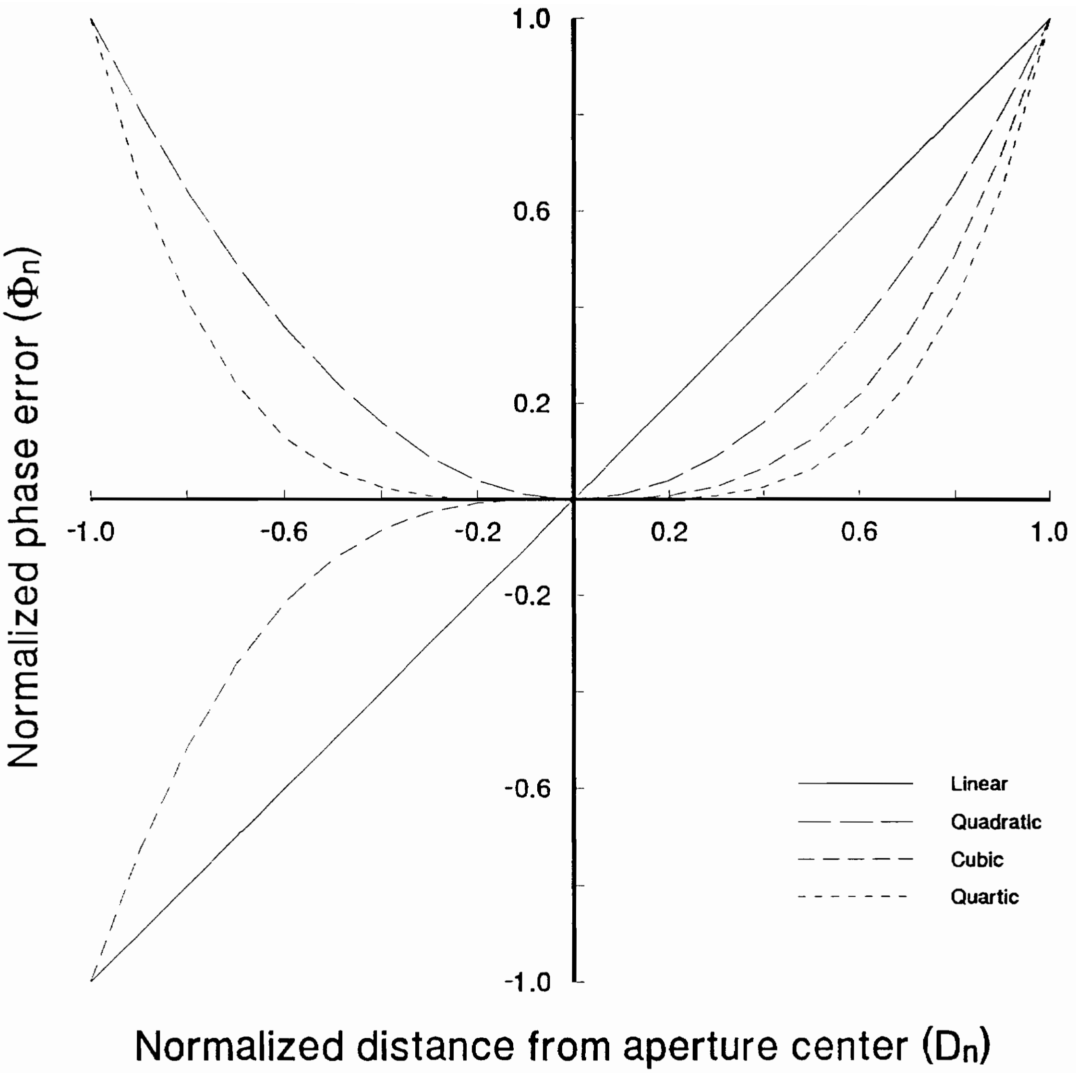

Figure 3.1.2-6. Phase error as a function of distance from aperture center for a one dimensional aperture.

3.2 Beam Scanning Effects of Equivalent Paraboloid Offset

As discussed in Sections 2.4, a Cassegrain reflector system can be represented with reasonable accuracy by an equivalent paraboloid, which may or may not be offset, for offset Cassegrain systems. Because this equivalence is developed using geometrical optics it is only valid for focused systems. For a scanning offset Cassegrain reflector antenna system this means that unscanned performance, especially cross-polarization level, can be improved by using the Rusch condition discussed in Section 2.5. The additional concern for scanning offset Cassegrain reflector antenna systems is that scan performance might be degraded by the use of a reflector system geometry which has an axi-symmetric equivalent paraboloid.

Parameters of offset Cassegrain reflector antenna systems with three equivalent paraboloid offsets are summarized in Table 3.2-1. These systems were studied to determine the effect of equivalent paraboloid offset on the scanning characteristics of offset Cassegrain reflector antennas. The three systems were synthesized using the main reflector of the test case which will be discussed in Chapter 4. The feed point was allowed to vary to create systems with either an axi-symmetric equivalent paraboloid or an equivalent paraboloid which was just fully offset above or below the axis of symmetry. The scanning performance of these systems was determined by using GRASP7 analysis with geometrical optics/geometrical theory of diffraction at the subreflector and physical optics/surface integration at the main reflector. The geometries of these three systems with their equivalent paraboloids are shown in Figure 3.2-1.

3.2.1 Feed Motion Scanning

The study of the effect of equivalent paraboloid offset on offset Cassegrain reflector antenna scanning characteristics was first performed using feed motion to scan the systems. During this trial, the feed of each system was translated in three dimensions to achieve the

Table 3.2.-1. Characteristics of three offset Cassegrain reflector antenna system using the same main reflector but with three different equivalent paraboloids.

Main reflector diameter (D_M)	10.63 meters
Main reflector offset height (H_o)	7.795 meters
Main reflector focal length (F_M)	13.5 meters
Subreflector interfocal distance (2c)	6.9 meters
Subreflector eccentricity (e)	1.919
Equivalent paraboloid focal length (F_{eq})	42.5 meters
Equivalent paraboloid offset height (H_{oeq})	0 and ± 5 meters
Feed point (x_f, y_f, z_f)	near (-0.442, 0.0, 6.614)
Feed pattern	-15 dB subreflector edge illumination Gaussian pattern
Frequency of analysis	20 GHz

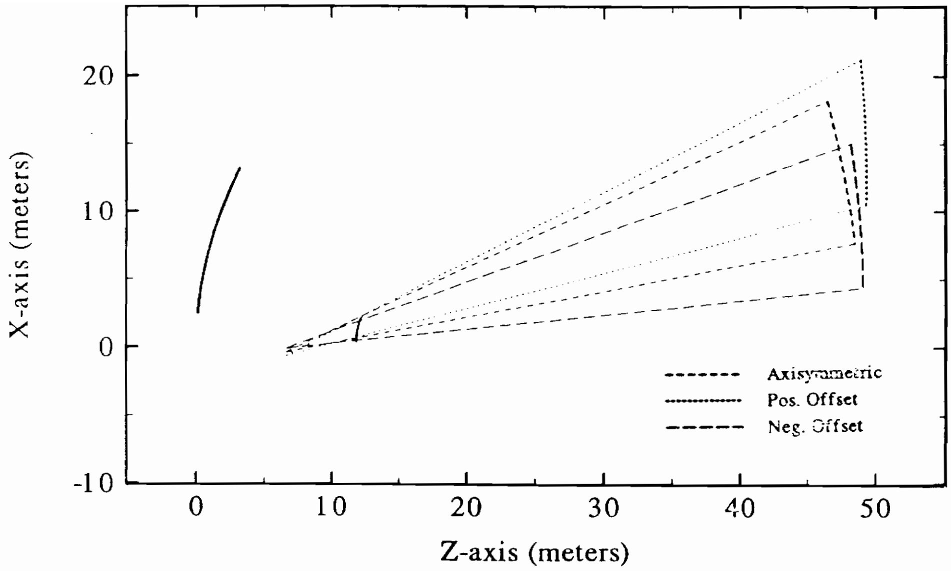

Figure 3.2-1. Offset Cassegrain reflector systems and their equivalent paraboloids.

lowest possible aperture phase error as defined by the transmit mode raytracing error functional which will be described in Section 5.2. The transmit mode raytracing error functional was used to position the feed to allow the same error functional to be used for both feed and subreflector motion scanning. The systems were fed by a feed pattern which produced a -15 dB edge illumination for the analysis. The feed pattern was held fixed at the optimal unscanned pointing for each system to simplify the synthesis and analysis.

The gain, G, of the three systems is shown in Figure 3.2.1-1. As for the unscanned case, the gain of a scanned offset Cassegrain reflector antenna is essentially unchanged by equivalent paraboloid offset. Spillover efficiency, $\varepsilon_{\mathrm{sp}}$, shown in Figure 3.2.1-2, is also relatively unchanged by equivalent paraboloid offset. The sidelobe level of the three systems could not be calculated because phase errors caused null filling at relatively low scan angles. The only significant effect of equivalent paraboloid offset on the scan performance of offset Cassegrain reflector antenna systems is in cross-polarization level. The cross-polarization levels, XPOL, of the three systems are shown in Figure 3.2.1-3. The system with the axi-symmetric equivalent paraboloid both reaches the lowest cross-polarization level and generally performs the best although the systems with offset equivalent paraboloids each exhibit a lower cross-polarized component over a small portion of the scan region. This effect is caused by the change in illumination due to the required scanning motion.

3.2.2 Subreflector Motion Scanning

The study of the effect of equivalent paraboloid offset distance on the scanning characteristics of offset Cassegrain reflector antennas was also performed using subreflector translation and rotation to scan the three systems of Table 3.2-1. The subreflector position was determined to minimize the aperture phase error as defined by the transmit mode raytracing error functional which will be discussed in Section 5.2 as in the feed motion scanning study.

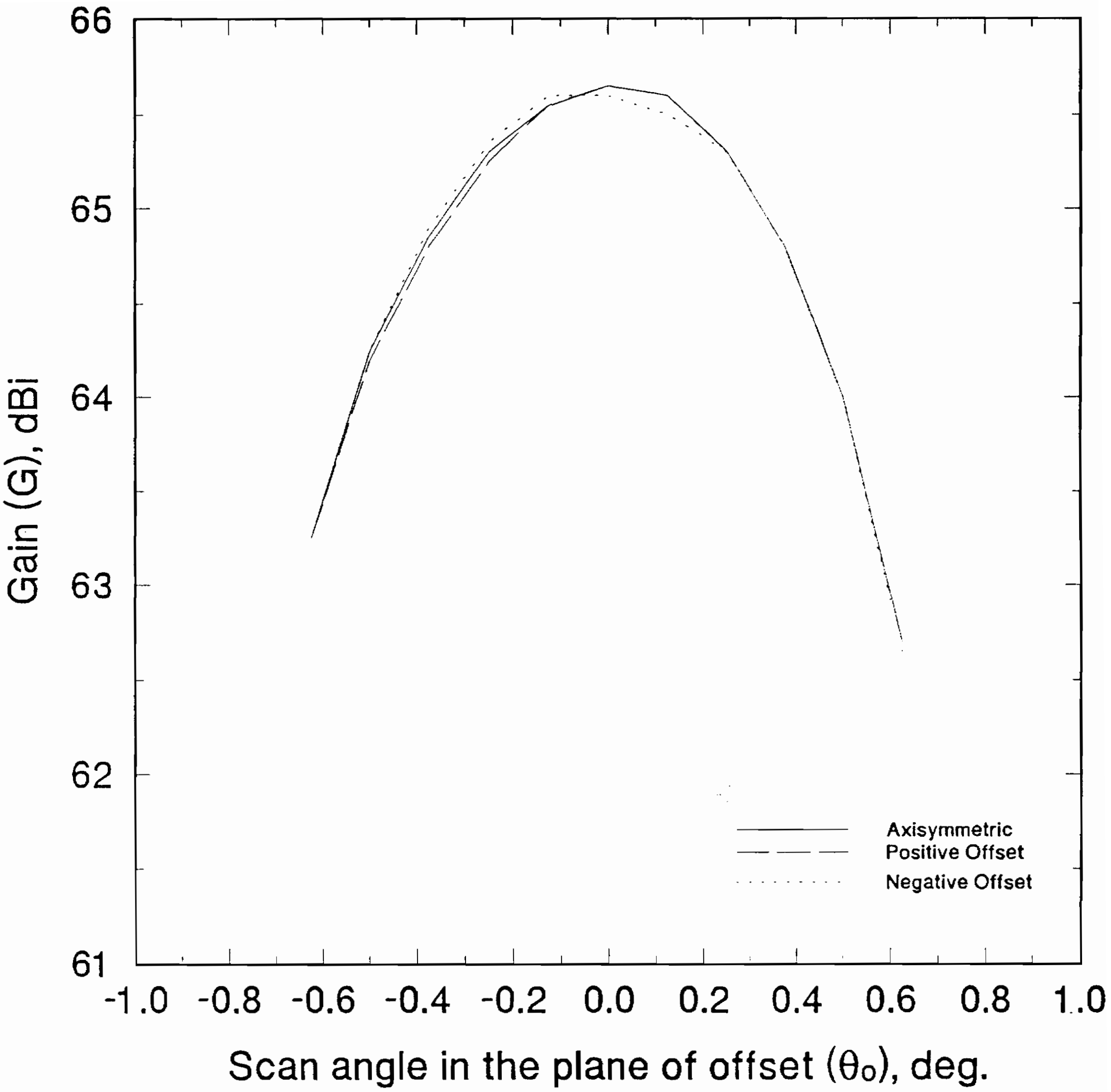

Figure 3.2.1-1. Feed scanned antenna gain (G) as a function of scan angle in the plane of offset (θ_0) for three offset Cassegrain systems with three different equivalent paraboloids.

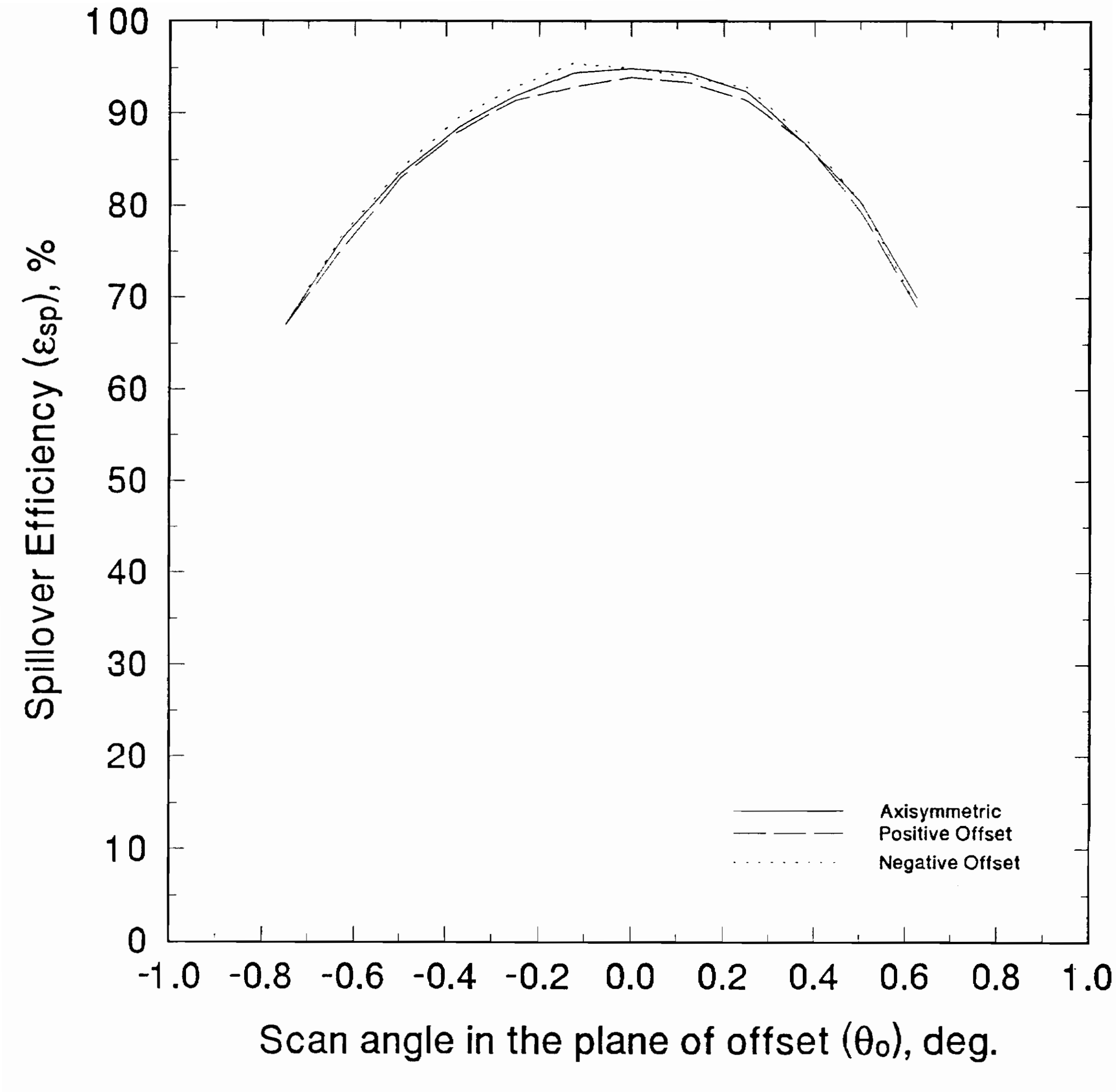

Figure 3.2.1-2. Feed scanned spillover efficiency (ε_{sp}) as a function of scan angle in the plane of offset (θ_o) for three offset Cassegrain systems with three different equivalent paraboloids.

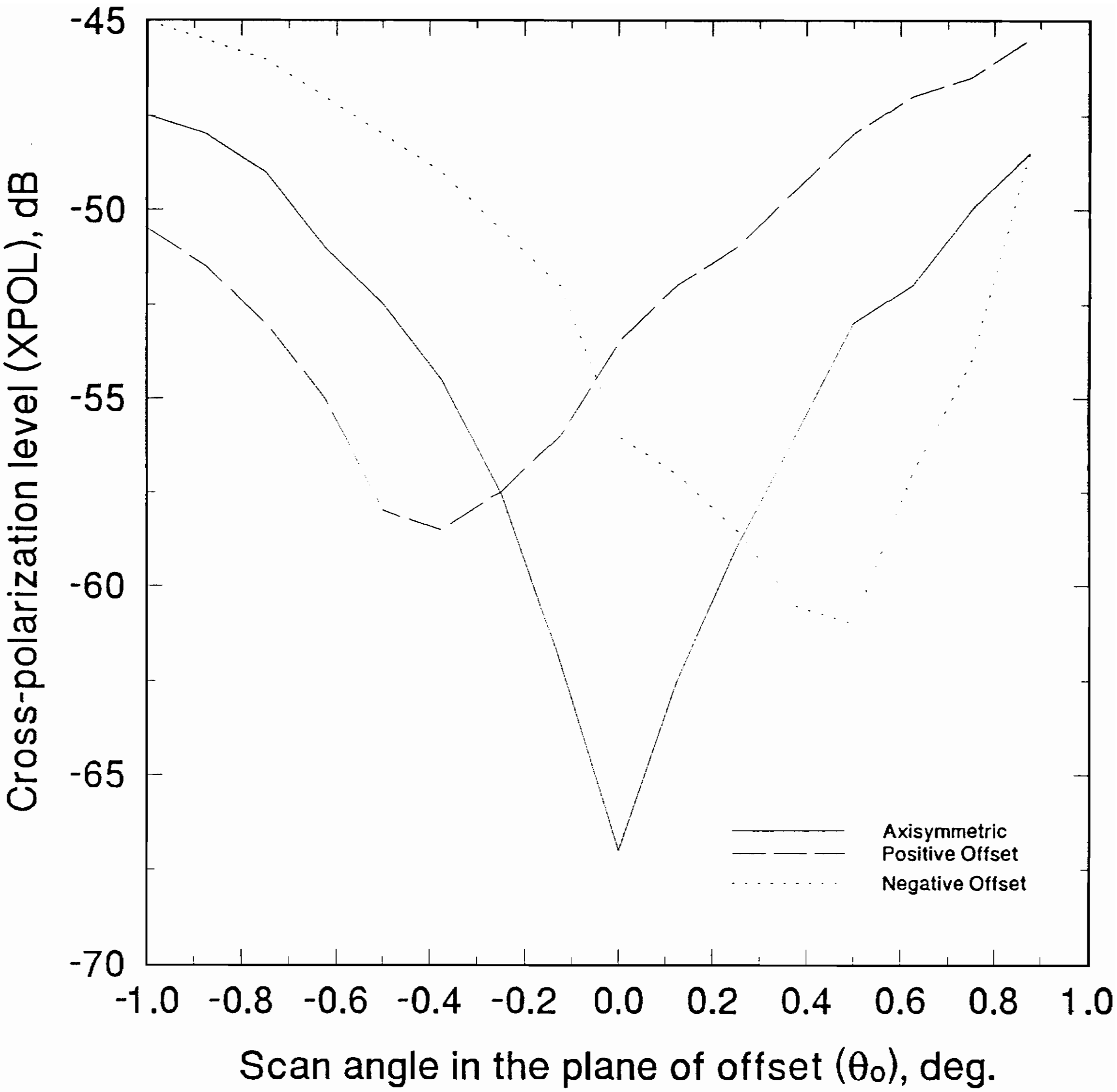

Figure 3.2.1-3. Feed scanned cross-polarization level (XPOL) as a function of scan angle in the plane of offset (θ_o) for three offset Cassegrain systems with three different equivalent paraboloids.

Also, the feed illumination was again geometrically defined to produce a -15 dB edge illumination and was fixed to the optimum unscanned feed pattern pointing.

Figure 3.2.2-1 shows the gain, G, of the three systems as a function of scan angle in the plane of offset, θ_o. Again, the gain variation caused by equivalent paraboloid offset is small although the difference in scanned gain is greater than for the feed scanned case. The spillover efficiency, ε_{sp}, of the three systems is shown in Figure 3.2.2-2 and, like gain, is relatively insensitive to equivalent paraboloid offset. Sidelobe level, SLL, could be found for the subreflector scanned case and is also nearly unaffected by equivalent paraboloid offset as shown in Figure 3.2.2-3. As for the feed scanned case, cross-polarization level, XPOL, is the only pattern characteristic which was found to be strongly affected by equivalent paraboloid offset. Figure 3.2.2-4 shows that the cross-polarized component is minimized in the system with an axi-symmetric equivalent paraboloid but can be lower in certain regions of the scan range for either system which has an offset equivalent paraboloid.

3.3 Beam Scanning the Offset Cassegrain Antenna by Feed Displacement

The conventional method of mechanical beam scanning with the offset Cassegrain reflector antenna system is lateral feed displacement [5]. Lateral feed displacement is in common use to form multiple spot beams using a single prime focus paraboloidal reflector antenna for satellite-to-ground applications [6-8]. Increasing geostationary satellite antenna performance requirements prompted INTELSAT to commission a study by Krichevsky and DiFonzo at COMSAT of beam scanning offset Cassegrain reflector antennas by optimal feed displacement [9]. This study developed a method to determine the optimal feed location for any desired main beam direction. Krichevsky and DiFonzo give results for beam scanning in the same offset Cassegrain reflector antenna system using lateral feed displacement so that the

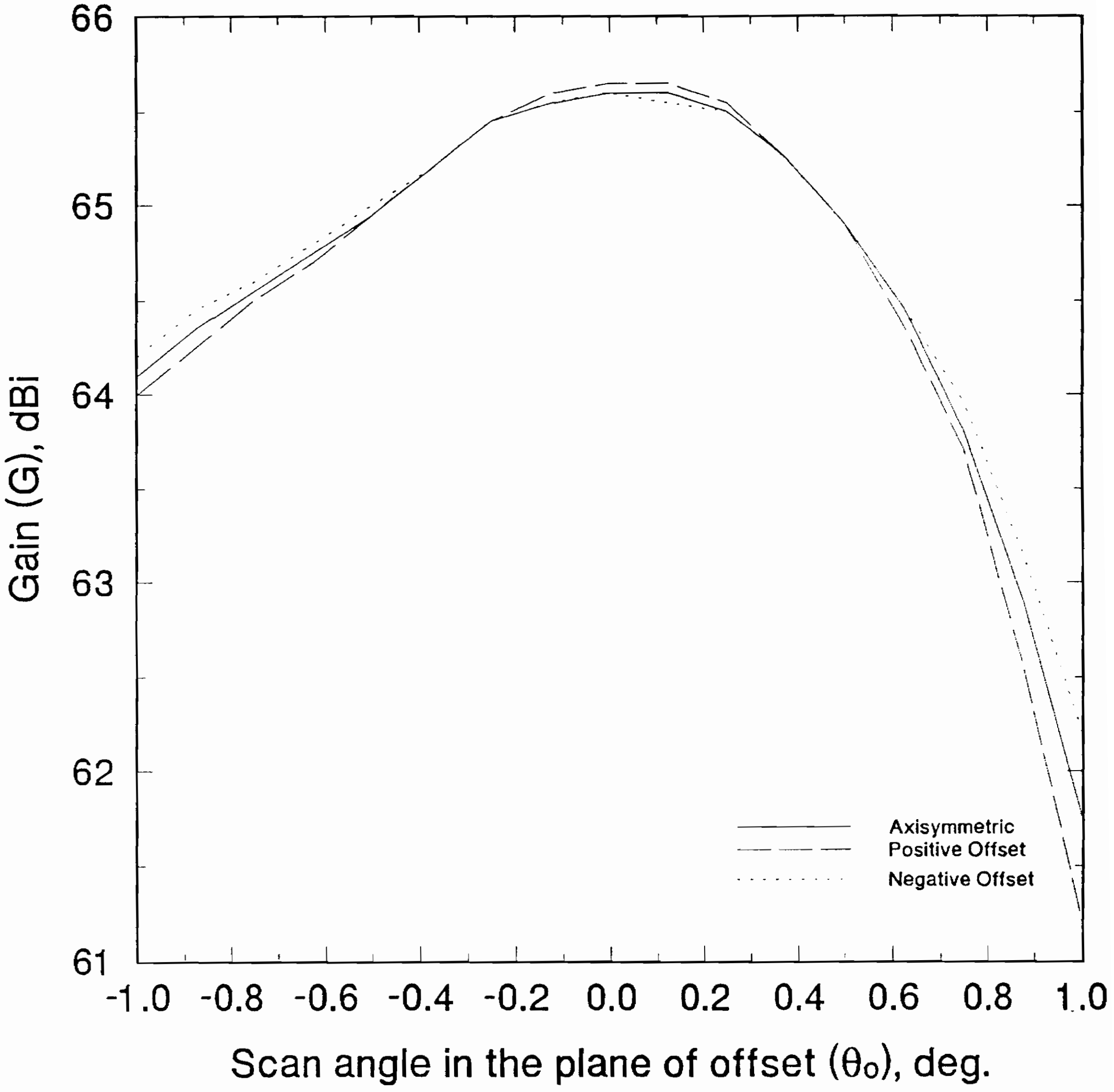

Figure 3.2.2-1. Subreflector scanned antenna gain (G) as a function of scan angle in the plane of offset (θ_o) for three offset Cassegrain systems with three different equivalent paraboloids.

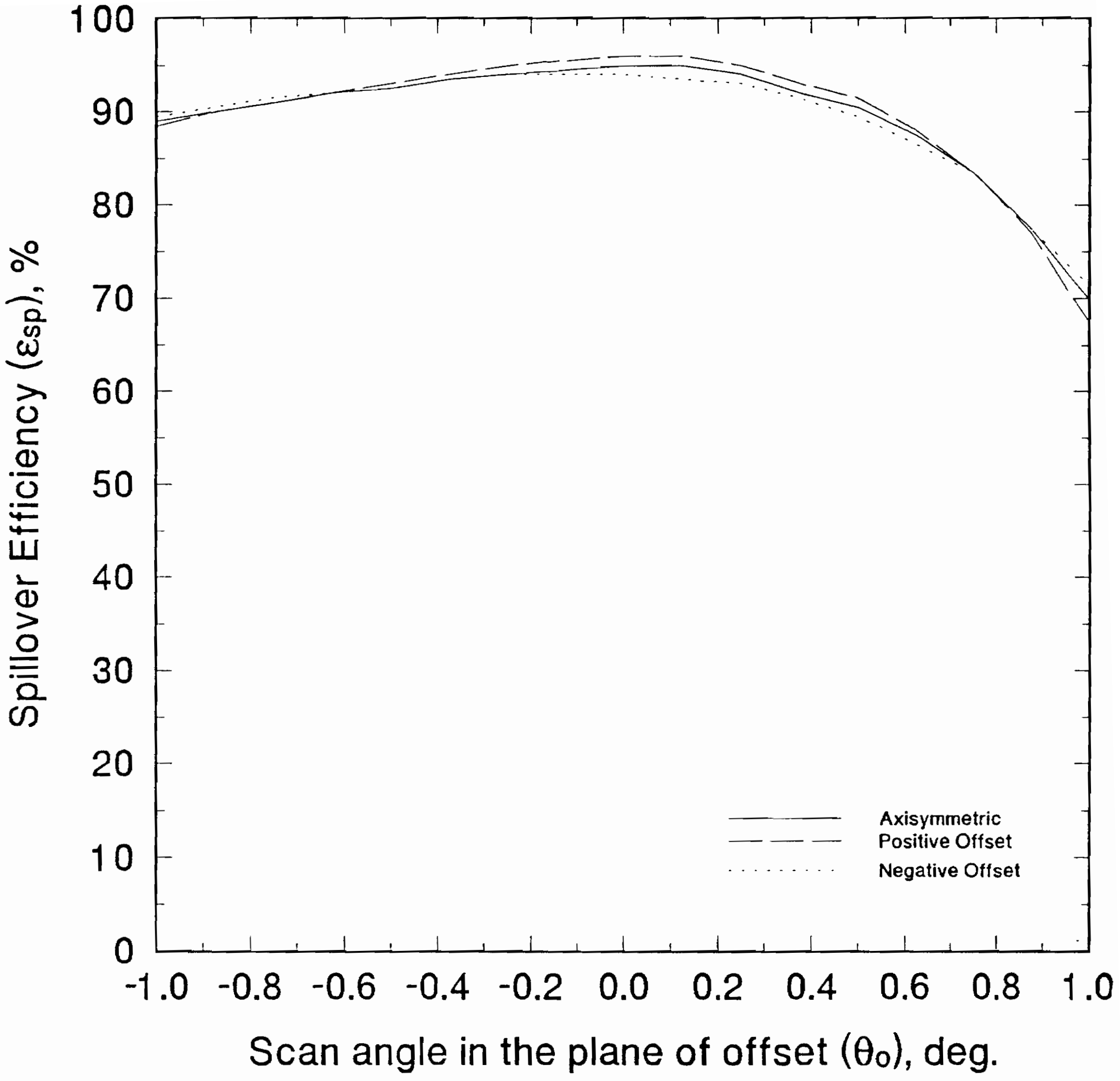

Figure 3.2.2-2. Subreflector scanned spillover efficiency (ε_{sp}) as a function of scan angle in the plane of offset (θ_o) for three offset Cassegrain systems with three different equivalent paraboloids.

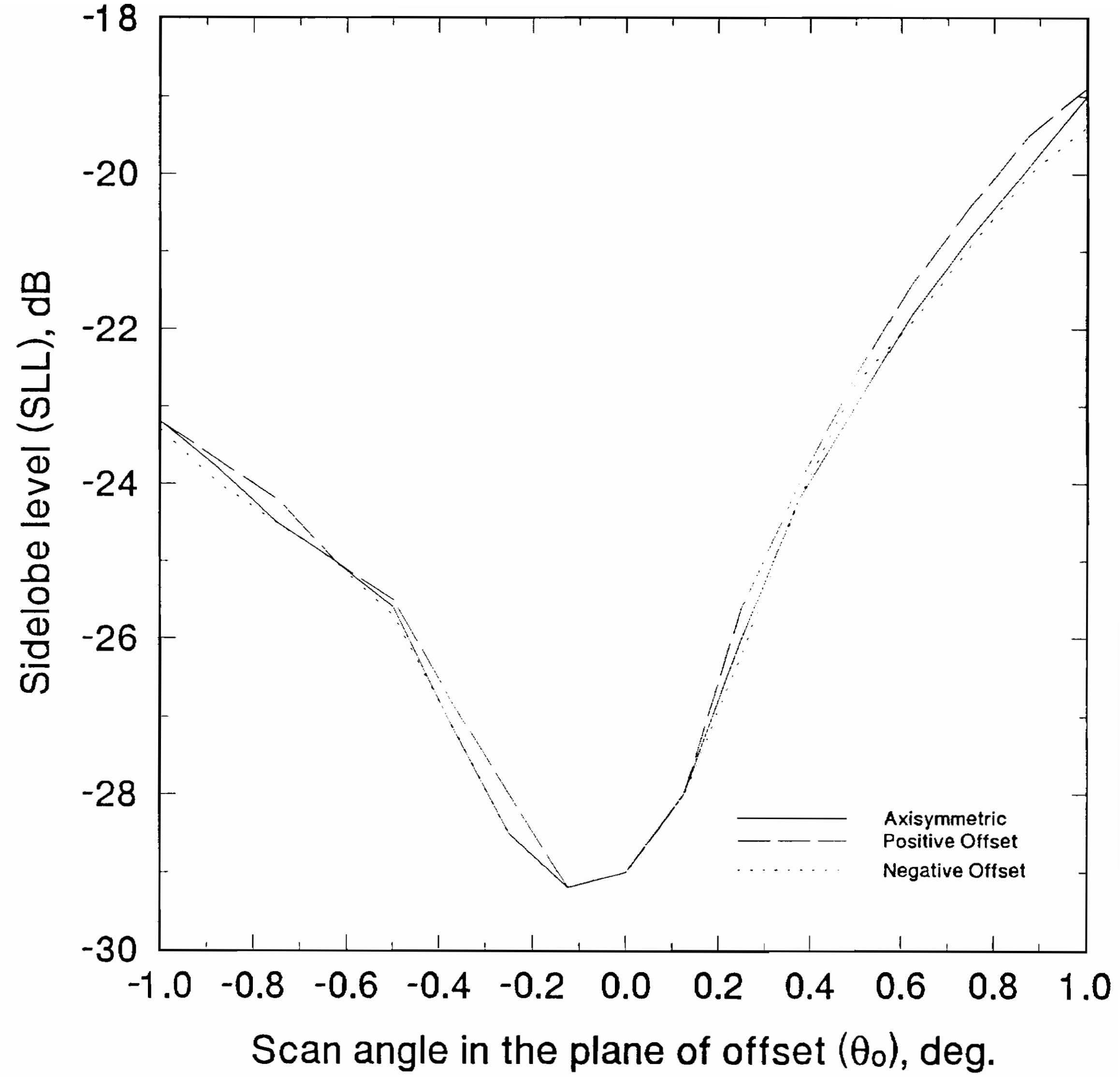

Figure 3.2.2-3. Subreflector scanned sidelobe level (SLL) as a function of scan angle in the plane of offset (θ_o) for three offset Cassegrain systems with three different equivalent paraboloids.

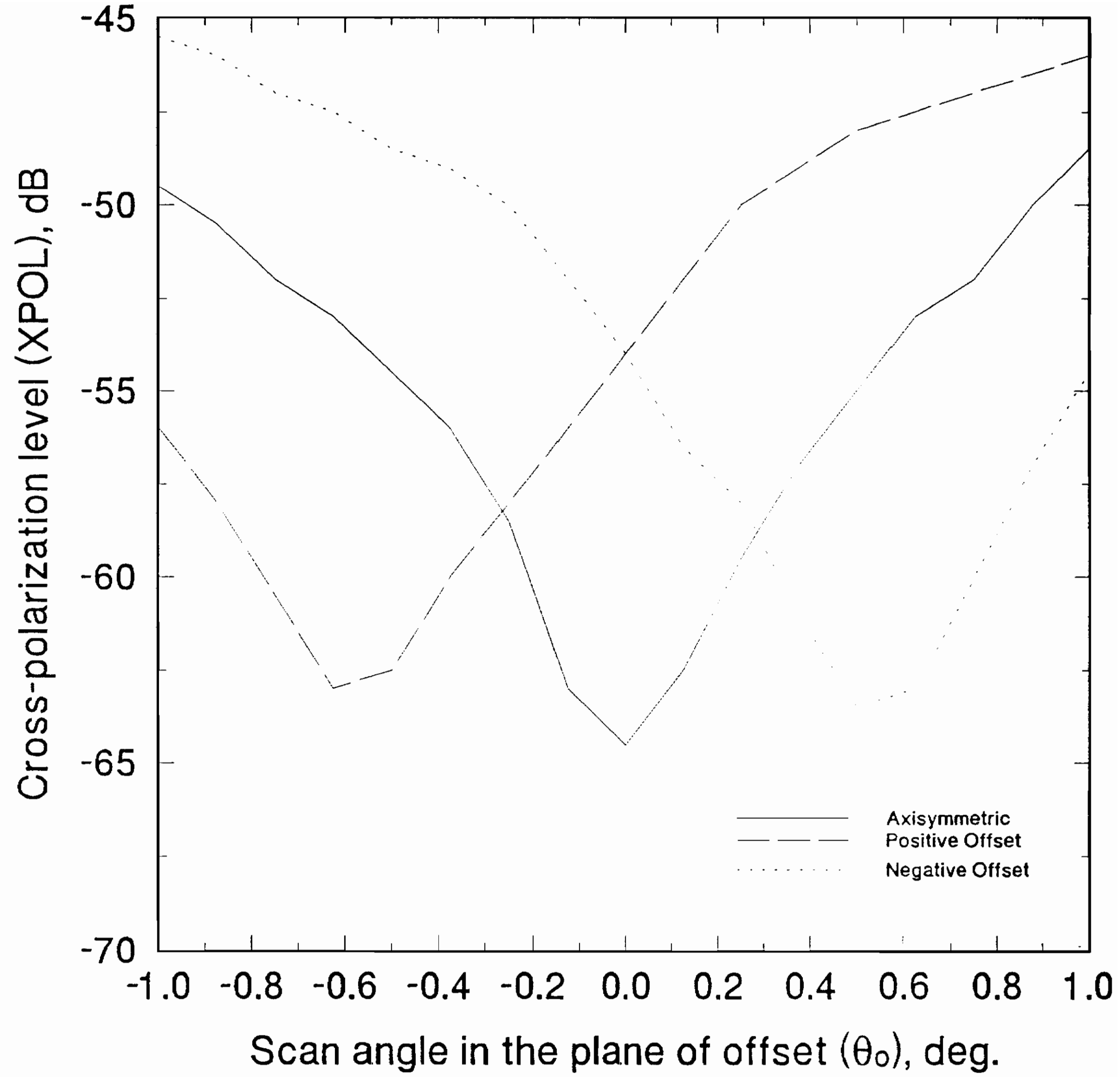

Figure 3.2.2-4. Subreflector scanned cross-polarization level (XPOL) as a function of scan angle in the plane of offset (θ_0) for three offset Cassegrain systems with three different equivalent paraboloids.

increased performance of their optimum feed position scanning method can be shown [5].

The Krichevsky and DiFonzo study of optimal beam scanning used the reflector system geometry shown in Figure 3.3-1 [5]. This system consists of a paraboloidal main reflector with a focal point at F_1, a hyperboloidal subreflector with focal points at F_1 and F_2, and a point source feed located at F_2 when the system is unscanned [5]. The coordinate system is constructed such that F_2 lies at the origin and the unscanned aperture plane is perpendicular to the z-axis [5]. The subreflector rim is defined by the intersection of a cone with its vertex at F_2 and the hyperboloidal surface on which the subreflector lies [5]. The angle between the axis of the cone which defines the subreflector edge and the +z-axis is θ_1 and the half-angle of the cone is θ_2 [5]. Main reflector size is determined by the area illuminated by the ray bundles which are reflected from the subreflector for all beam directions after the optimal feed positions are found [5]. This method of sizing the main reflector is much less stringent because it assures that no spillover will occur at the main reflector. Krichevsky and DiFonzo defined the plane of lateral feed displacement as the plane which contains F_2 and is perpendicular to the axis of the cone which defines the subreflector edge [5].

Krichevsky and DiFonzo determined the optimum feed position for a given beam direction by finding the intersection of the locus of feed positions which produce the desired beam direction with the locus of feed positions which yield the minimum aperture phase error [5]. For simplicity, in the analysis presented here, that of Krichevsky and DiFonzo [5], the antenna system is assumed to be cylindrical and only rays which lie in the xy-plane are considered. The complete derivation of the optimum feed position is available in Krichevsky [9].

The locus of feed positions which produce the desired beam direction is found by tracing rays transmitted from a point source feed at $Q(0, y_0, z_0)$ as shown in Figure 3.3-1 [5]. The total optical path length of a ray which satisfies the conditions imposed by geometrical optics at the

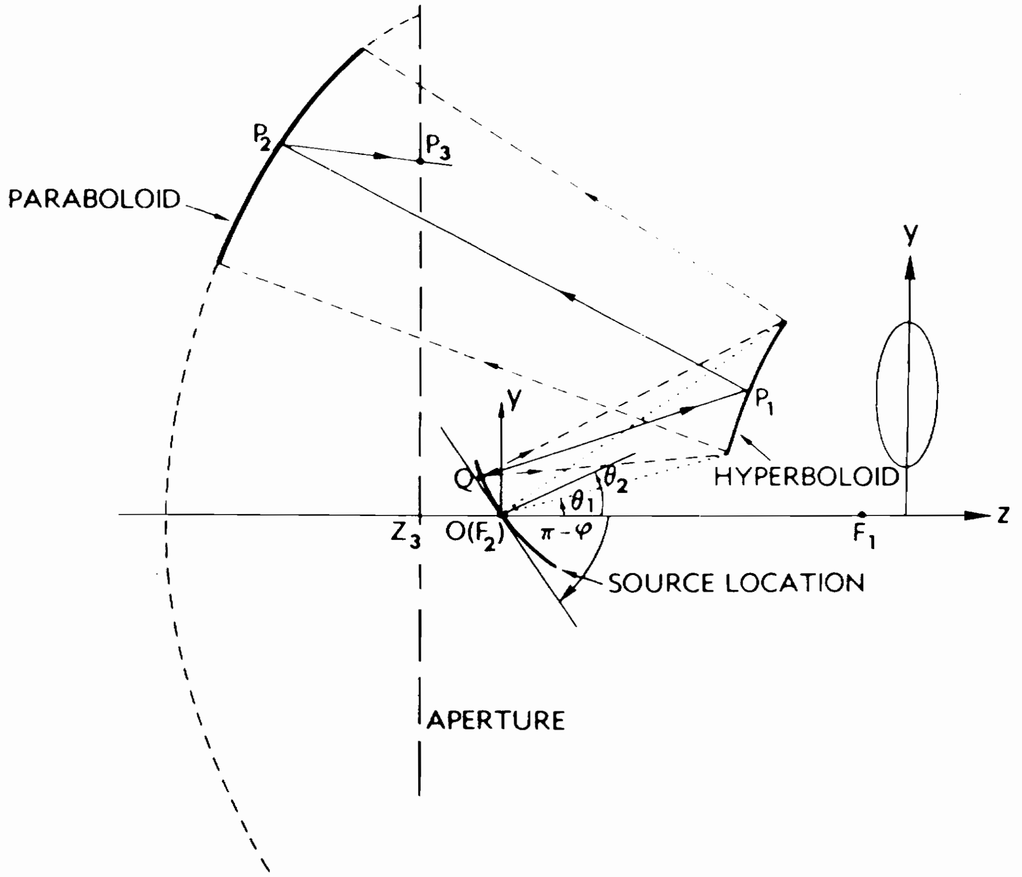

Figure 3.3-1. Antenna system geometry for the Optimum Feed Position Scanning of Krichevsky and DiFonzo [5].

main and subreflectors and strikes the subreflector at $P_1(0, y_1, z_1)$, the main reflector at $P_2(0, y_2, z_2)$, and the aperture plane at $P_3(0, y_3, z_3)$ is given by

$$L = \sum_{i=1}^{3} L_i \tag{3.3-1}$$

where

$$L_i = \sqrt{(y_i - y_{i-1})^2 + (z_i - z_{i-1})^2} \tag{3.3.2}$$

for i = 1, 2, or 3 [5]. The total optical path lengths and points of intersection with the aperture plane of the upper and lower rays in the system are given by L_u and L_l and (y_u, z_u) and (y_l, z_l) as shown in Figure 3.3-2 [5]. From these parameters, the beam direction can be approximated by

$$\alpha \approx \frac{L_u - L_l}{y_u - y_l} \tag{3.3-3}$$

for small scan angles and feed displacements [5].

Krichevsky and DiFonzo next present the series expansions of the total optical path length and transmitted ray/aperture plane intersection:

$$L = L^{(0)} \sum_{m=0}^{v} \sum_{k=0}^{m} c_{m,k}\, y_0^{\,k}\, z_0^{\,m-k} \tag{3.3-4}$$

and

$$y = y^{(0)} \sum_{m=0}^{v} \sum_{k=0}^{m} T_{m,k}\, y_0^{\,k}\, z_0^{\,m-k} \tag{3.3-5}$$

where $L^{(0)}$ and $y^{(0)}$ are equal to L and y when the point source feed is at the unscanned feed point F_2 [5]. The value of v in the series expansions is the order of the desired approximation:

a) first order approximation: $\frac{R}{F_H} \ll 1$

b) second order approximation: $\left(\frac{R}{F_H}\right)^2 \ll 1$

where R is the displacement of the point source feed from the unscanned feed point F_2 and F_H is half the interfocal length of the parent hyperboloid of the subreflector [5]. By substituting (3.3-4) and (3.3-5) into (3.3-3), Krichevsky and DiFonzo find the series expansion for the locus of feed positions which produce a constant beam direction:

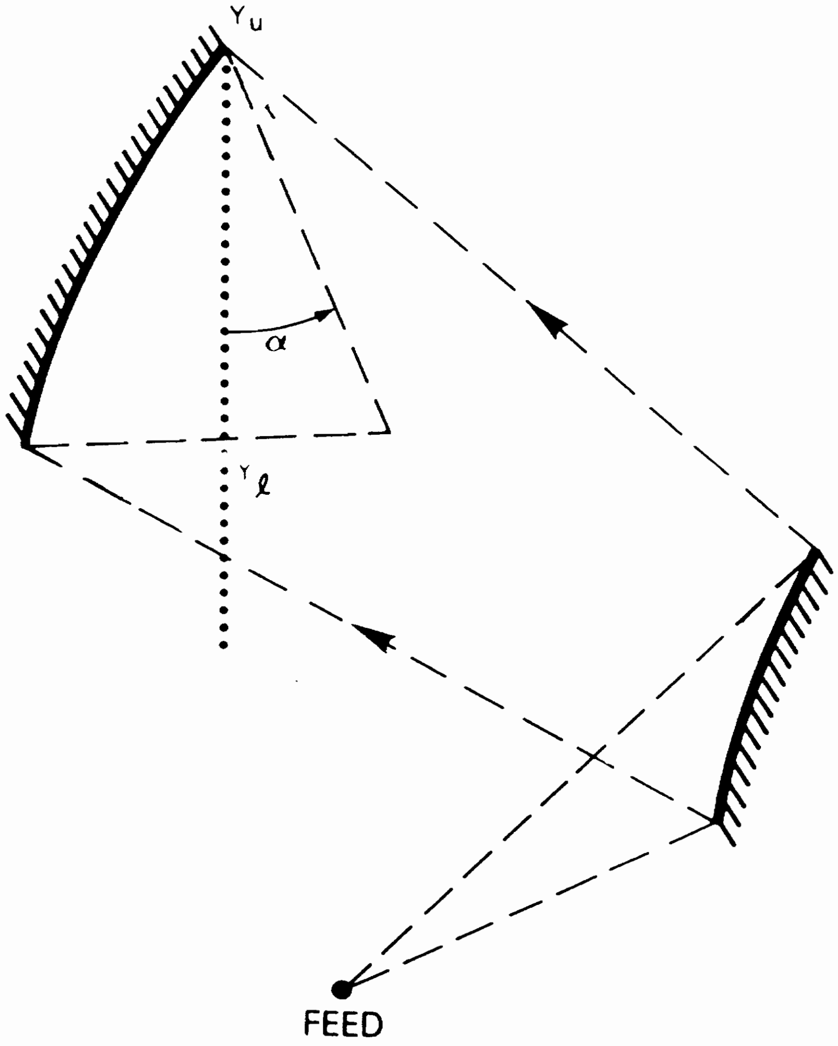

Figure 3.3-2. Krichevsky and DiFonzo [5] definition of beam scan angle.

$$\alpha = \sum_{m=0}^{v} \sum_{k=0}^{m} A_{m,k}\, y_0^{\,k}\, z_0^{\,m-k} \qquad (3.3\text{-}6)$$

where $A_{m,k}$ is a series of coefficients which are defined in terms of the geometrical parameters of the offset Cassegrain reflector antenna system [5]. The coefficients, $A_{m,k}$, and their derivation are presented in Krichevsky and DiFonzo [5] and Krichevsky [9]. The constant beam direction feed locus can be found from (3.3-6) by solving for y_0 in terms of z_0, α, and the coefficients, $A_{m,k}$.

Figure 3.3-3 shows several constant beam direction feed position loci for the offset Cassegrain reflector antenna system summarized by Table 3.3-1 [5]. The first-order, linear approximation to (3.3-6) for each constant beam direction feed locus is shown in Figure 3.3-3 by a dashed line which is labeled with the angular beam displacement caused [5]. The second-order approximation to (3.3-6) is shown by a solid line which crosses the corresponding first-order approximation [5]. Figure 3.3-4 shows the beam pointing error as a function of the beam direction predicted by the constant beam direction loci shown in Figure 3.3-3 [5]. The beam directions used to determine the accuracy of the constant beam direction feed loci were calculated using a computer based pattern analysis code [5]. The second-order approximation is, as expected, more accurate with a maximum beam pointing direction error of less than 0.05° compared to a maximum error of about 1.1° for the first-order approximation [5].

Krichevsky and DiFonzo [5] calculated the optimum feed position locus by dividing the subreflector and tracing n rays from the unscanned feed point to the subreflector with the same angular separation between the rays. This, in effect, divides the antenna for which the optimum feed position locus is being determined into n-1 small antennas [5]. The substitutions,

$$\theta_{2,n} = \frac{\theta_2}{n} \qquad (3.3\text{-}7)$$

and

$$\theta_{1,m,n} = \frac{\theta_2}{n}(2m - 1) + \theta_1 - \theta_2, \qquad (3.3\text{-}8)$$

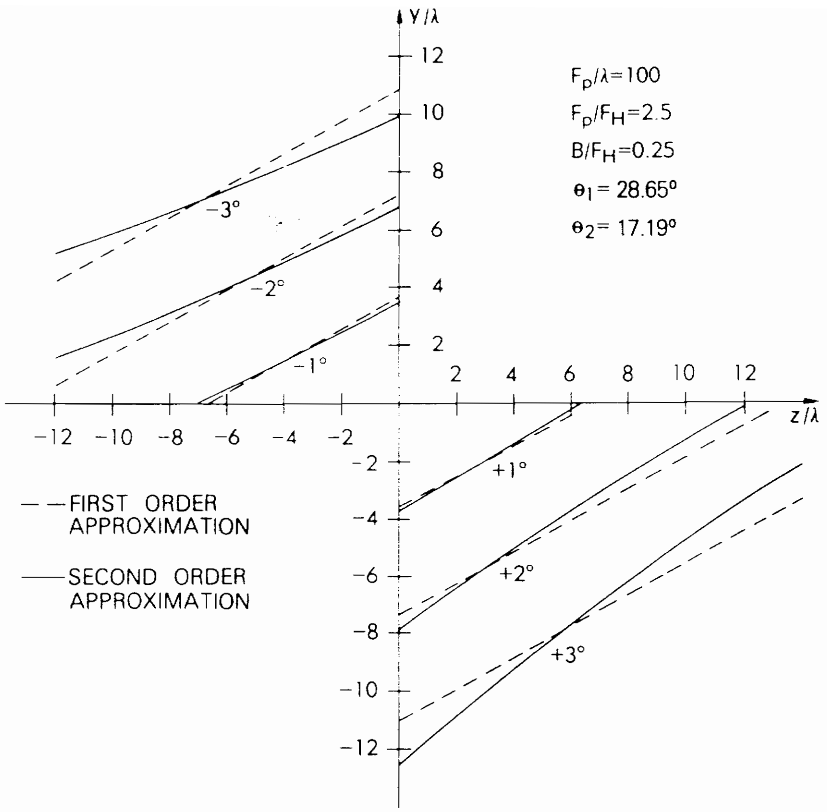

Figure 3.3-3. First and second order approximations to the Constant Beam Direction Locus of Krichevsky and DiFonzo [5] for the system of Table 3.3-1.

Table 3.3-1. Characteristics of the Krichevsky and DiFonzo [5] offset Cassegrain reflector antenna system used for Optimum Feed Position Scanning.

Main reflector focal length (F_1)	100λ
Subreflector focal length (F_2)	40λ
Subreflector interfocal distance (2c)	20λ
Feed angle subtended by subreflector	34.38°

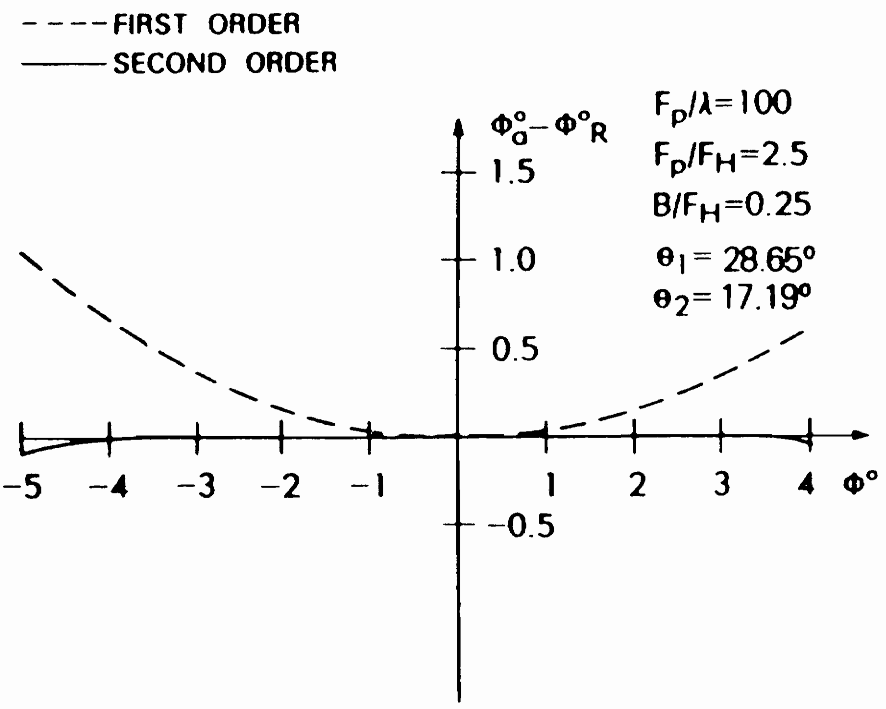

Figure 3.3-4. Beam pointing error given by physical optics analysis for the Constant Beam Direction locus of the system of Table 3.3-1 [5].

where m is the ray number from 1 to n, allow the use of the constant beam direction solution method to find the beam direction for each of the subdivisions [5]. The difference between the scan beam directions of the subdivisions can be minimized by using the constraint

$$G(y_0, z_0) = \lim_{n\to\infty} \left\{ \frac{1}{n} \sum_{m=1}^{n} (\alpha_{m,n} - \alpha)^2 \right\} \tag{3.3-9}$$

where α is the overall beam direction since the beam direction for each of the subdivisions is $\alpha_{m,n}$ [5]. Since the solution must also lie on one of the constant beam direction loci, the complete error function is

$$I(y_0, z_0, \mu) = G(y_0, z_0) + \mu[y_0 - f_v(z_0, \alpha, A_{m,k})] \tag{3.3-10}$$

where μ is a Lagrangian multiplier [5]. After trigonometric and algebraic simplification of (3.3-9), Krichevsky and DiFonzo found the following closed form solution for the optimum feed position:

$$\sum_{m=1}^{v} \sum_{k=0}^{m} I_{m,k}\, Y_0^{\,k}\, Z_0^{\,m-k} = 0 \tag{3.3-11}$$

where $I_{m,k}$ is a series of coefficients which are defined in terms of the geometrical parameters of the offset Cassegrain reflector antenna system [5]. The coefficients, $I_{m,k}$, and their derivation are presented in Krichevsky and DiFonzo [5] and Krichevsky [9]. As for the constant beam direction feed loci, v corresponds to the order of the desired approximation: either 1 for a first-order, linear approximation or 2 for a second-order approximation [5].

The locus of optimum feed positions and the second-order approximation to the constant beam direction loci for the system of Table 3.3-1 are shown in Figure 3.3-5 [5]. The dotted line in Figure 3.3-5 represents the possible feed positions for lateral feed displacement while the dashed and solid lines represent the first- and second-order approximations to the optimum feed position locus [5]. The optimum feed position for each beam direction can be found at the intersection of the second-order approximation of the appropriate constant beam direction loci and the second-order approximation of the optimum feed position locus [5]. The

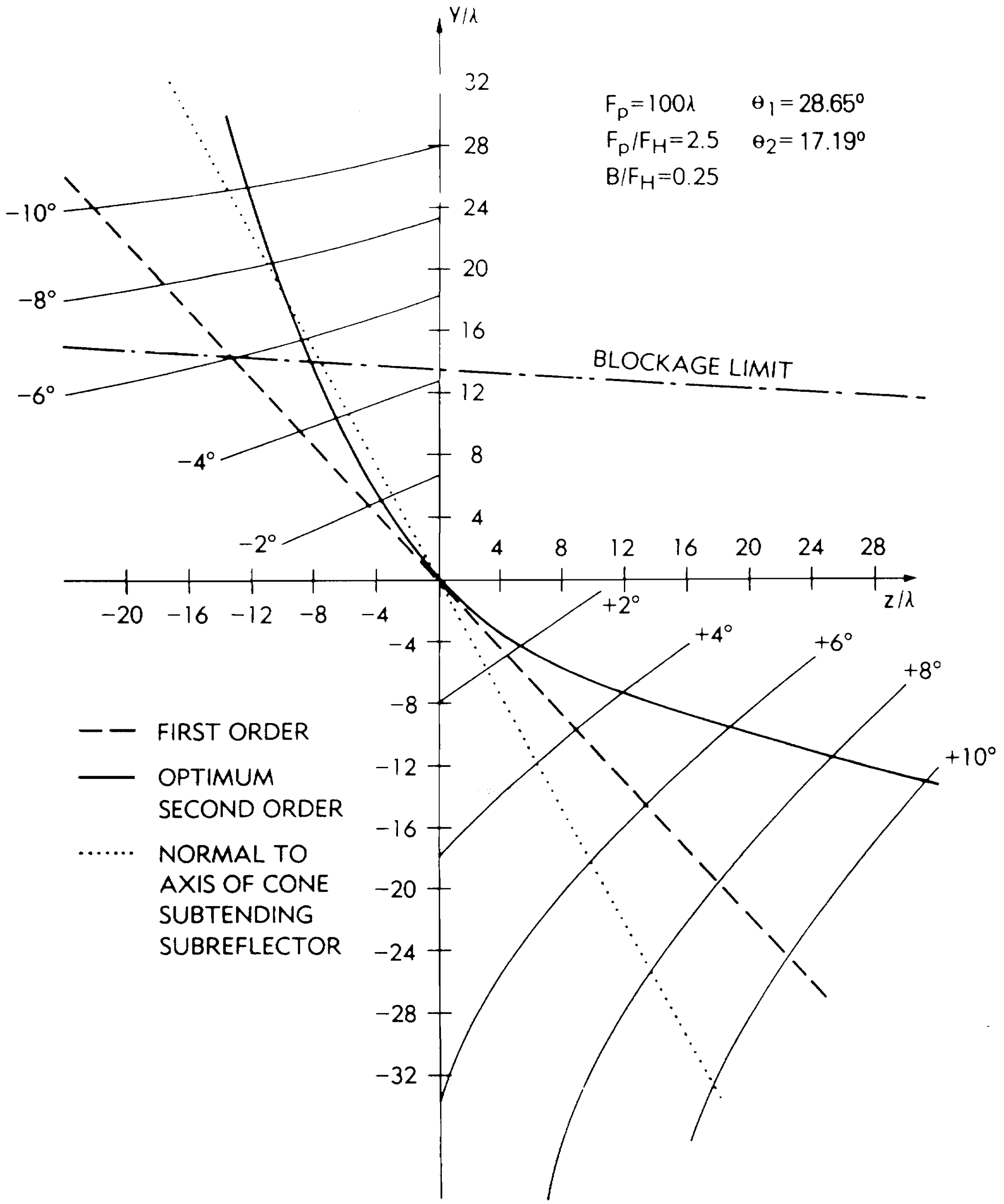

Figure 3.3-5. Optimum Feed Position loci and Constant Beam Direction loci of Krichevsky and DiFonzo [5] for the system of Table 3.3-1.

required motion for optimum feed positioning beam scanning requires both a lateral and a longitudinal feed displacement.

Krichevsky and DiFonzo [5] used physical optics to find the far-field patterns of the optimum feed position movement scanned system of Table 3.3-1. The reflector system was analyzed for a Potter horn feed with a radius of 2.3λ at the optimum feed position for each beam direction [5]. The feed was repointed at each optimum feed position to align the axis of the feed with the angular center of the subreflector to minimize spillover [5]. Also, as mentioned above, the main reflector surface size was determined by allowing no spillover at the main reflector [5]. Figure 3.3-6 shows several scanned beams for the offset Cassegrain reflector antenna system with the feed for each beam located at the optimum feed position [5]. Figure 3.3-7 shows several scanned beams from the offset Cassegrain reflector antenna system fed by a 3.1λ Potter horn which was displaced laterally [5]. In both cases, the pattern of the offset Cassegrain reflector antenna system tends to deteriorate less rapidly during downward beam scanning, but the optimum feed position scanned system shows less overall pattern deterioration. Note that the aperture is partly blocked by the subreflector for beams which are scanned more than about 5.8° below the unscanned boresight [5].

3.4 Beam Scanning the Offset Cassegrain Reflector Antenna by Subreflector Tilt - The Foldes Type 6 System

A reflector antenna system was proposed by Peter Foldes for use in the NASA Mission to Planet Earth radiometer design. This system, referred to as the Type 6 system, is summarized by Figure 3.4-1 and Table 3.4-1. The Type 6 system was designed to scan by subreflector tilt. For simplicity, the scanned systems were synthesized by tilting the subreflector to an angle and then finding the resulting beam scan from the physical optics analysis result. This also assured that the performance of the Type 6 system was maximized. Unfortunately,

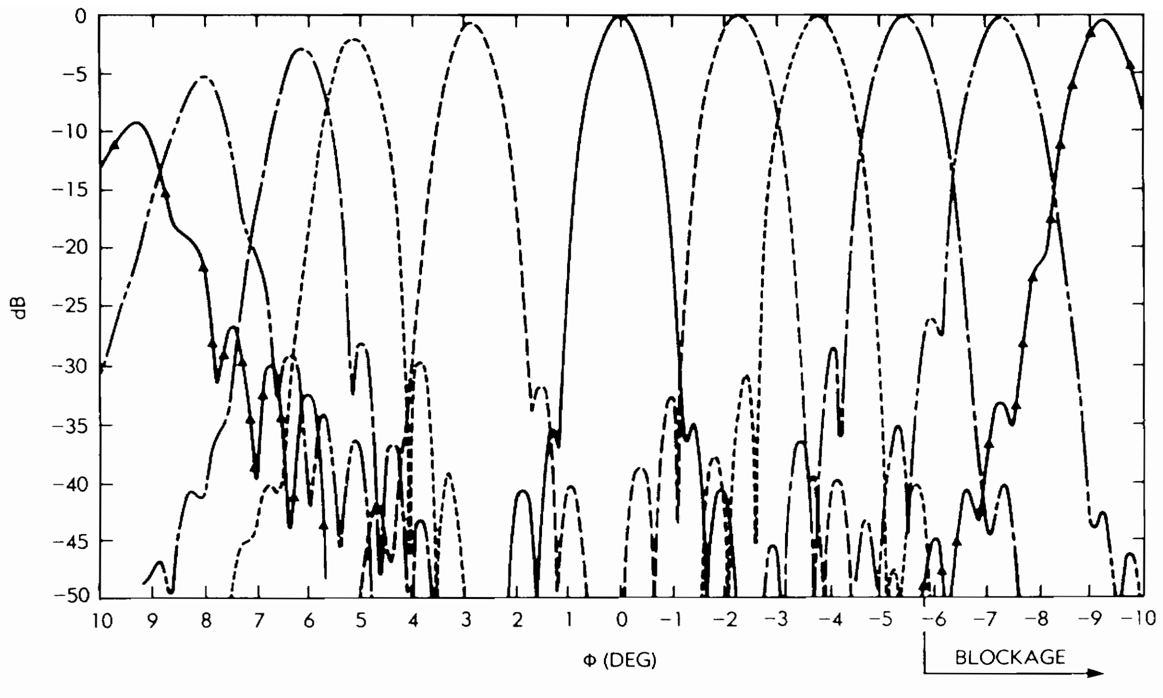

Figure 3.3-6. Scanned beams of the system of Table 3.3-1 produced by the second order Optimum Feed Position scanning of Krichevsky and DiFonzo [5].

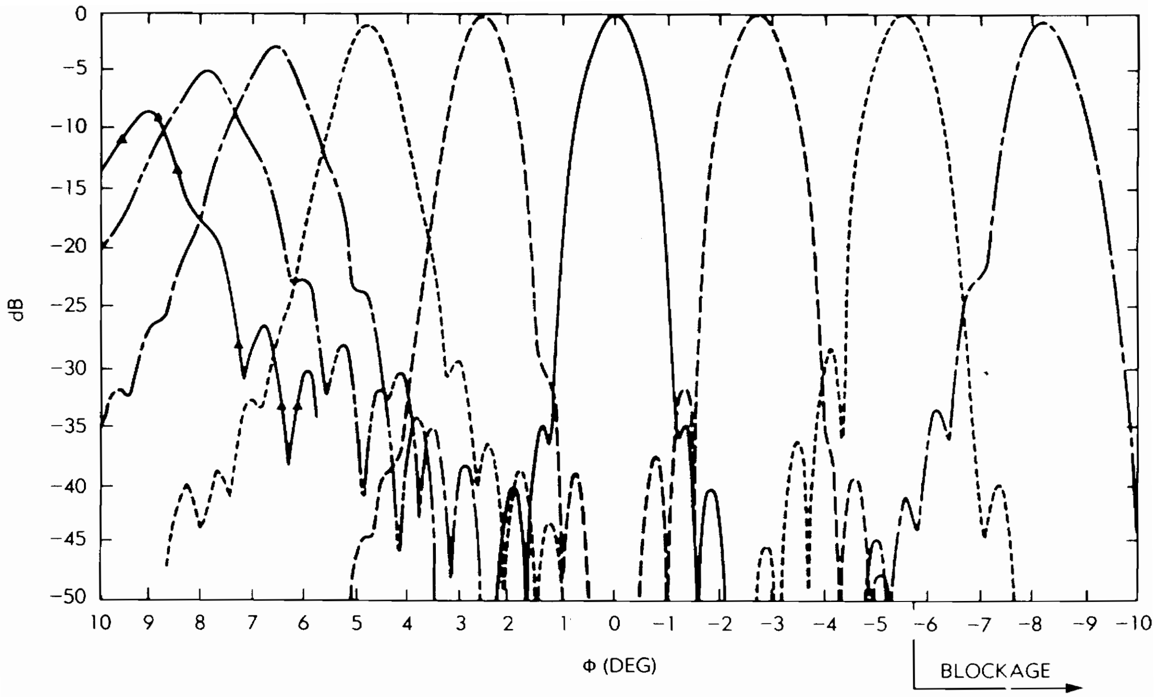

Figure 3.3-7. Scanned beams of the system of Table 3.3-1 produced by lateral feed displacement scanning [5].

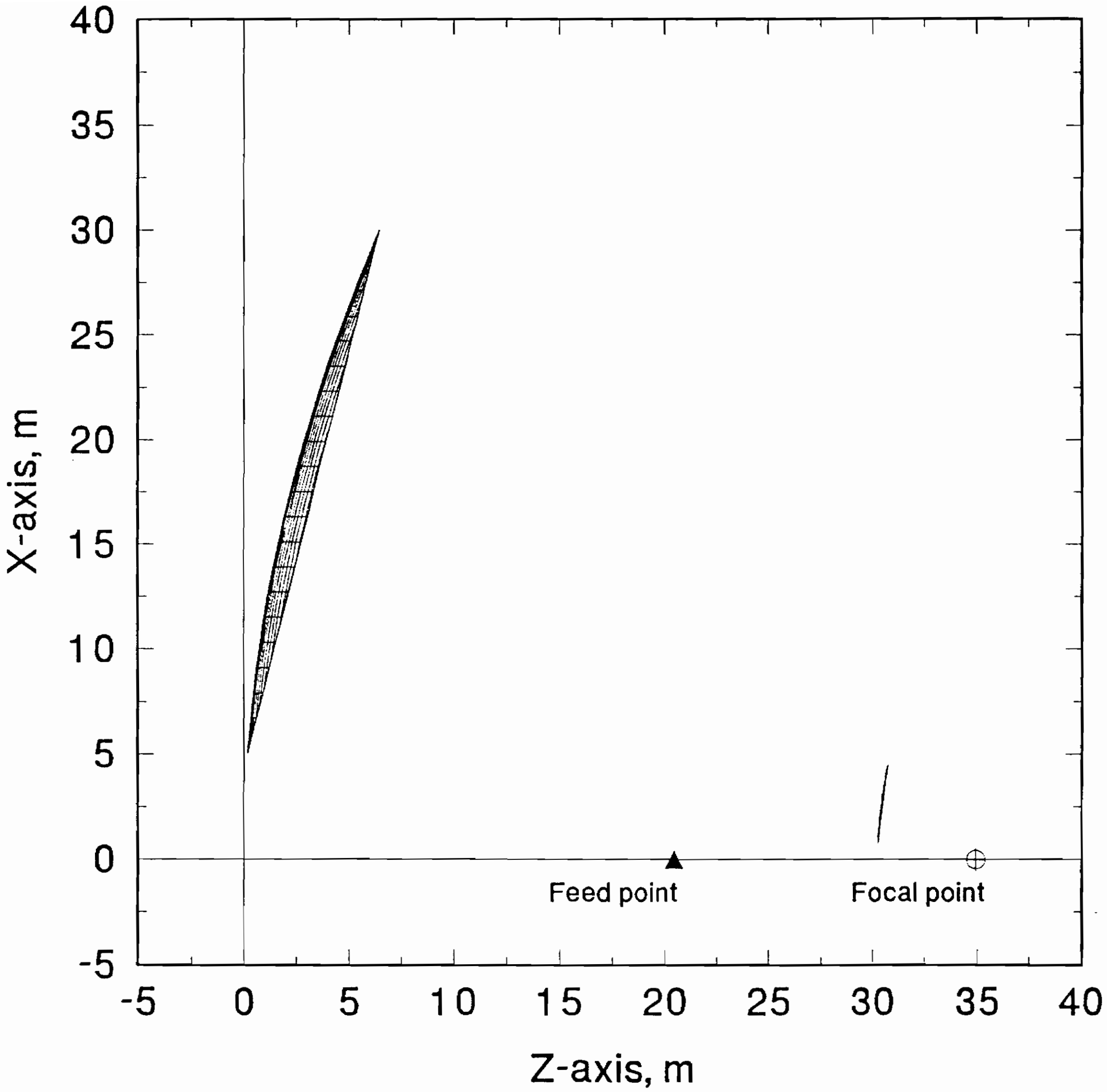

Figure 3.4-1. Plane of offset view of the Type 6 reflector antenna system geometry of Foldes [10].

Table 3.4-1. Characteristics of the Type 6 reflector antenna system of Foldes [10].

Main reflector focal length (F_M)	35 meters
Main reflector diameter (D_M)	25 meters
Main reflector offset height (H_o)	17.5 meters
Subreflector eccentricity (e)	2.81
Subreflector interfocal distance (2c)	14.5 meters
Subreflector axis tilt angle (β)	0°
Subreflector diameter (D_S)	3.56 meters
Areal efficiency, $\left(\frac{{D_M}^2}{{D_M}^2 + {D_S}^2}\right)$	98%
Feed tilt angle (α)	17°
Intended scan range	± 0.5°
Frequency of analysis	10, 20, and 40 GHz
Feed pattern used for analysis	-15 dB Gaussian edge taper

this method for determining beam scanning parameters is not applicable to more sophisticated system because the multiple degrees of freedom would require excessive time to analyze as briefly discussed in Chapter 5.

The feed pattern was not specified by Peter Foldes and so was chosen to produce a -15 dB edge taper based on the beam efficiency results shown in Section 3.1. The scan performance results shown here were calculated using the TICRA GRASP7 reflector antenna code. The system was analyzed using geometrical optics/geometrical theory of diffraction at the subreflector and physical optics surface integration at the main reflector. For purposes of later comparison, the Foldes Type 6 system was analyzed at 10, 20, and 40 GHz.

Figure 3.4-2 shows the gain, G, of the Foldes Type 6 reflector antenna system as a function of frequency and scan angle in the plane of offset, θ_o. The system displays the expected 6 dB increase in gain for each octave increase in operating frequency. The significant increase in scan induced gain loss with increasing frequency indicates that the main source of error in the Foldes Type 6 reflector antenna system is aperture phase error. This conclusion is supported by the relative flatness of the curves for spillover efficiency, ε_{sp}, shown in Figure 3.4-3. As expected the spillover efficiency is essentially frequency independent with the slight variation being due to the increase electrical size of the system causing less diffraction effects. The illumination amplitude efficiency, ε_{amp}, shown in Figure 3.4-4 as a function of scan angle in the plane of offset, θ_o, was estimated for the Foldes Type 6 system by using the results presented in Section 3.1.1 because the presence of both amplitude and phase taper in the aperture field of a scanned reflector antenna prevent determining the amplitude efficiency factor independently. The illumination amplitude efficiency is essentially frequency independent and its small range supports the conclusion that the main source of scan loss in the Type 6 system is phase error. The illumination phase efficiency, ε_{ϕ}, of the Foldes Type 6 reflector antenna system is shown in

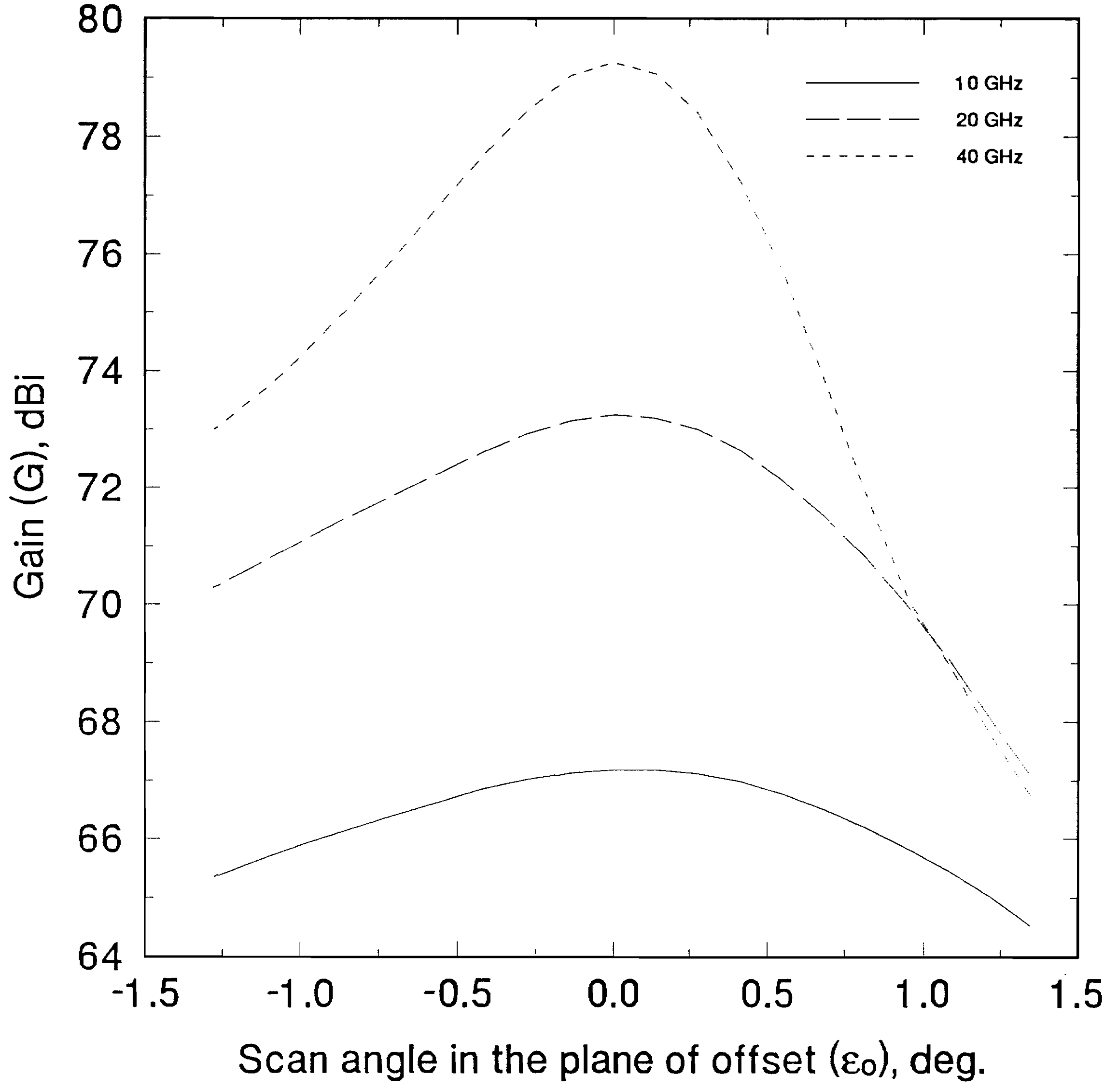

Figure 3.4-2. Gain (G) as a function of scan angle in the plane of offset (θ_o) for the Type 6 reflector antenna system of Foldes.

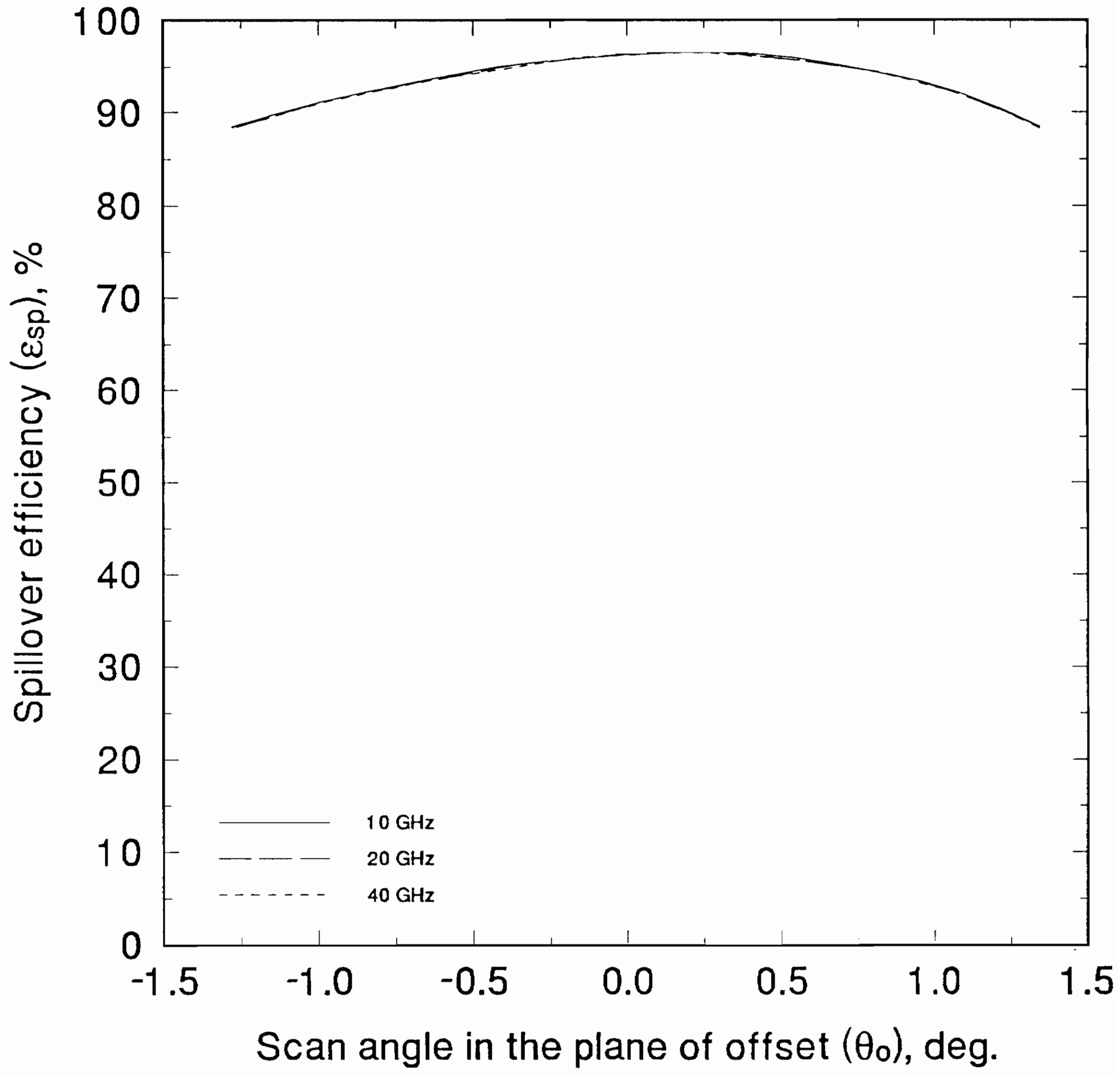

Figure 3.4-3. Spillover efficiency (ε_{sp}) as a function of scan angle in the plane of offset (θ_o) for the Type 6 reflector antenna system of Foldes.

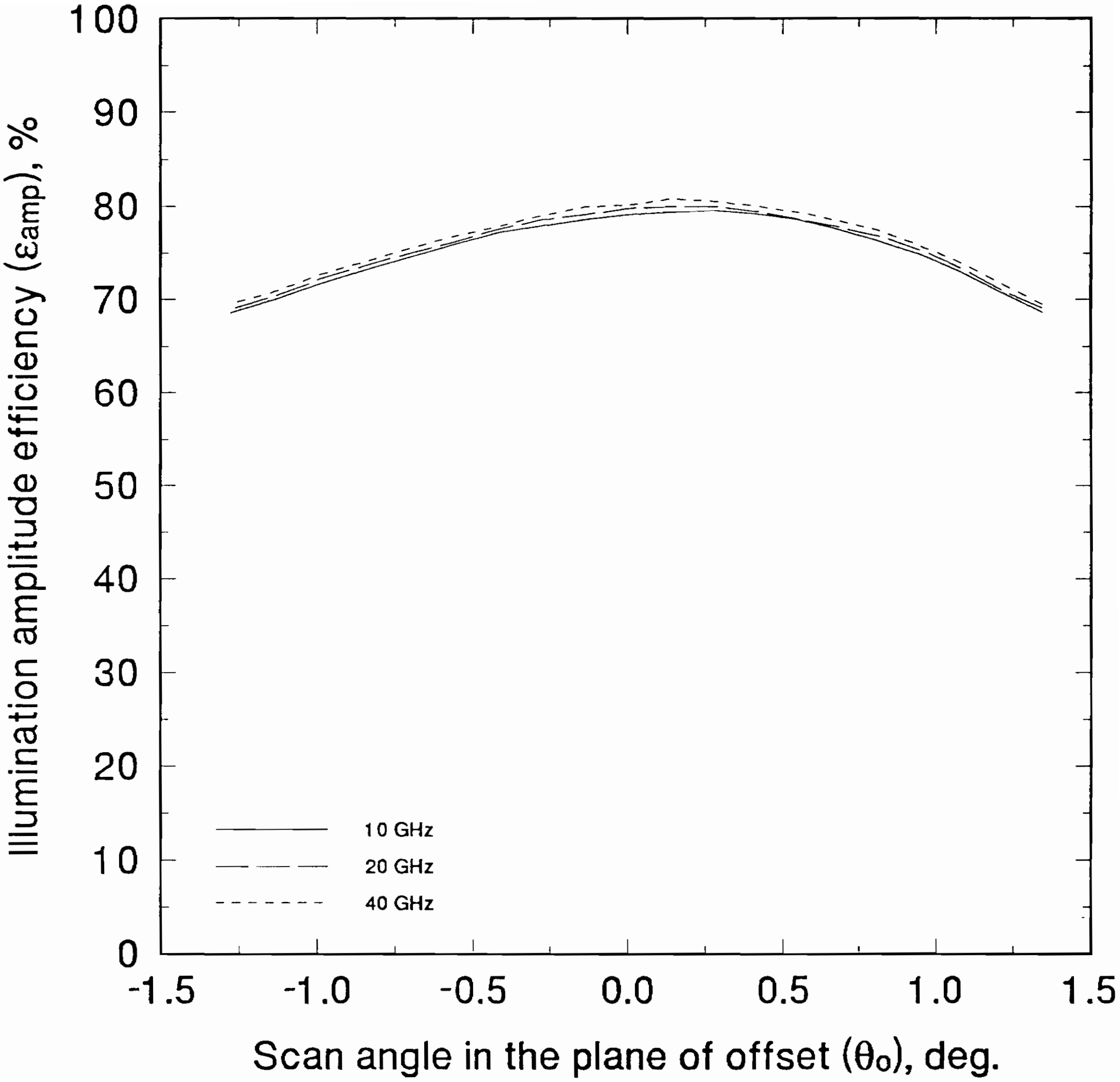

Figure 3.4-4. Illumination amplitude efficiency ($\varepsilon_{\mathrm{amp}}$) as a function of scan angle in the plane of offset (θ_{o}) for the Type 6 reflector antenna system of Foldes.

Figure 3.4-5 as a function of frequency and scan angle in the plane of offset, θ_o. Although the illumination phase efficiency of the Type 6 system is fairly high at 10 GHz, at 20 and 40 GHz phase errors are clearly the dominant scan loss mechanism. Like the illumination amplitude efficiency, the illumination phase efficiency should be considered a diagnostic tool rather than an exact measurement because the illumination amplitude efficiency estimate was used in the calculation of the illumination phase efficiency. The overall aperture efficiency, ε_{ap}, of the Type 6 system is shown in Figure 3.4-6.

Figure 3.4-7 shows the sidelobe level, SLL, for the Foldes Type 6 reflector antenna system as a function of frequency and scan angle in the plane of offset, θ_o. The sidelobe level should increase monotonically but blending of the increasing sidelobes with the main lobe and null filling cause the observed roughness in the curve. Figure 3.4-8 shows the cross-polarization level, XPOL, for the Type 6 system. The generally low cross-polarization level is caused by the long effective focal length, 101.5 meters, of the system. The offset of the equivalent paraboloid can be observed in the monotonic decrease in relative cross-polarization level with increasing negative beam scan. The beam efficiency, BE, of the Foldes Type 6 reflector antenna system is shown in Figure 3.4-9. As with the illumination phase efficiency, the beam efficiency is a strong function of frequency. Since the limit of the scan range is 90% beam efficiency, the scan range of the Type 6 system is about 1.5° at 10 GHz, 0.8° at 20 GHz, and 0.6° at 40 GHz.

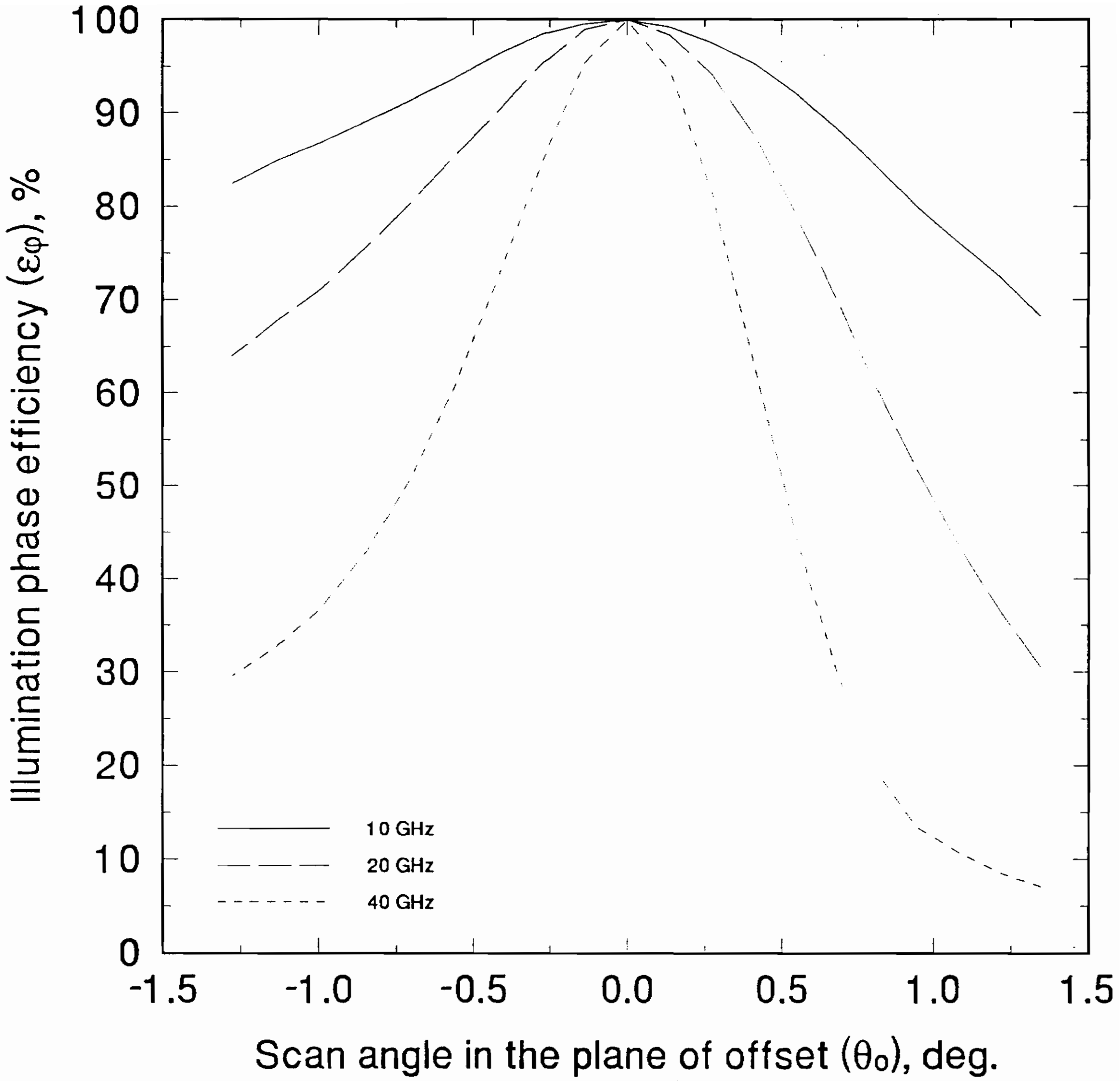

Figure 3.4-5. Illumination phase efficiency (ε_{ϕ}) as a function of scan angle in the plane of offset (θ_o) for the Type 6 reflector antenna system of Foldes.

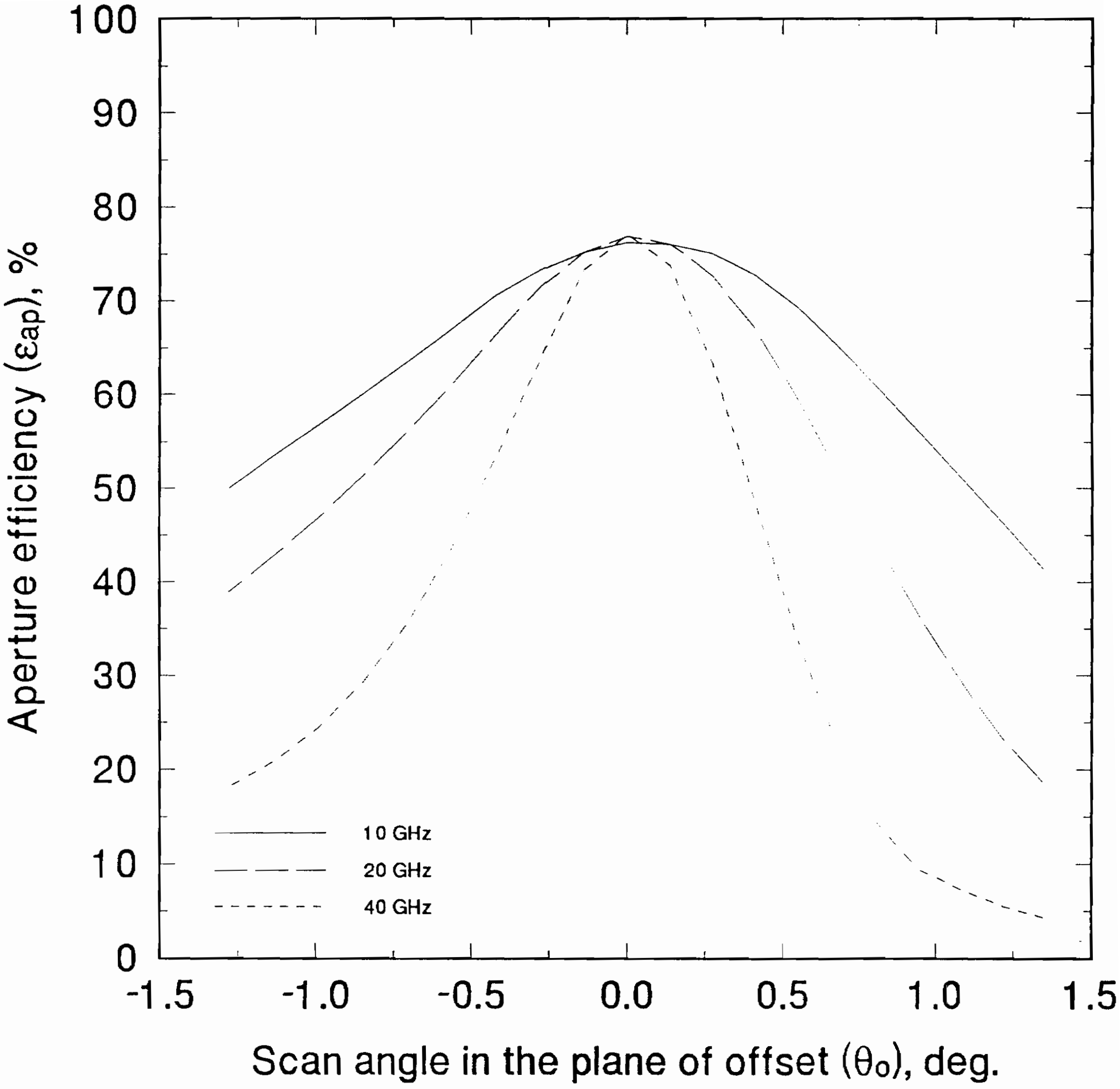

Figure 3.4-6. Aperture efficiency ($\varepsilon_{\mathrm{ap}}$) as a function of scan angle in the plane of offset (θ_{o}) for the Type 6 reflector antenna system of Foldes.

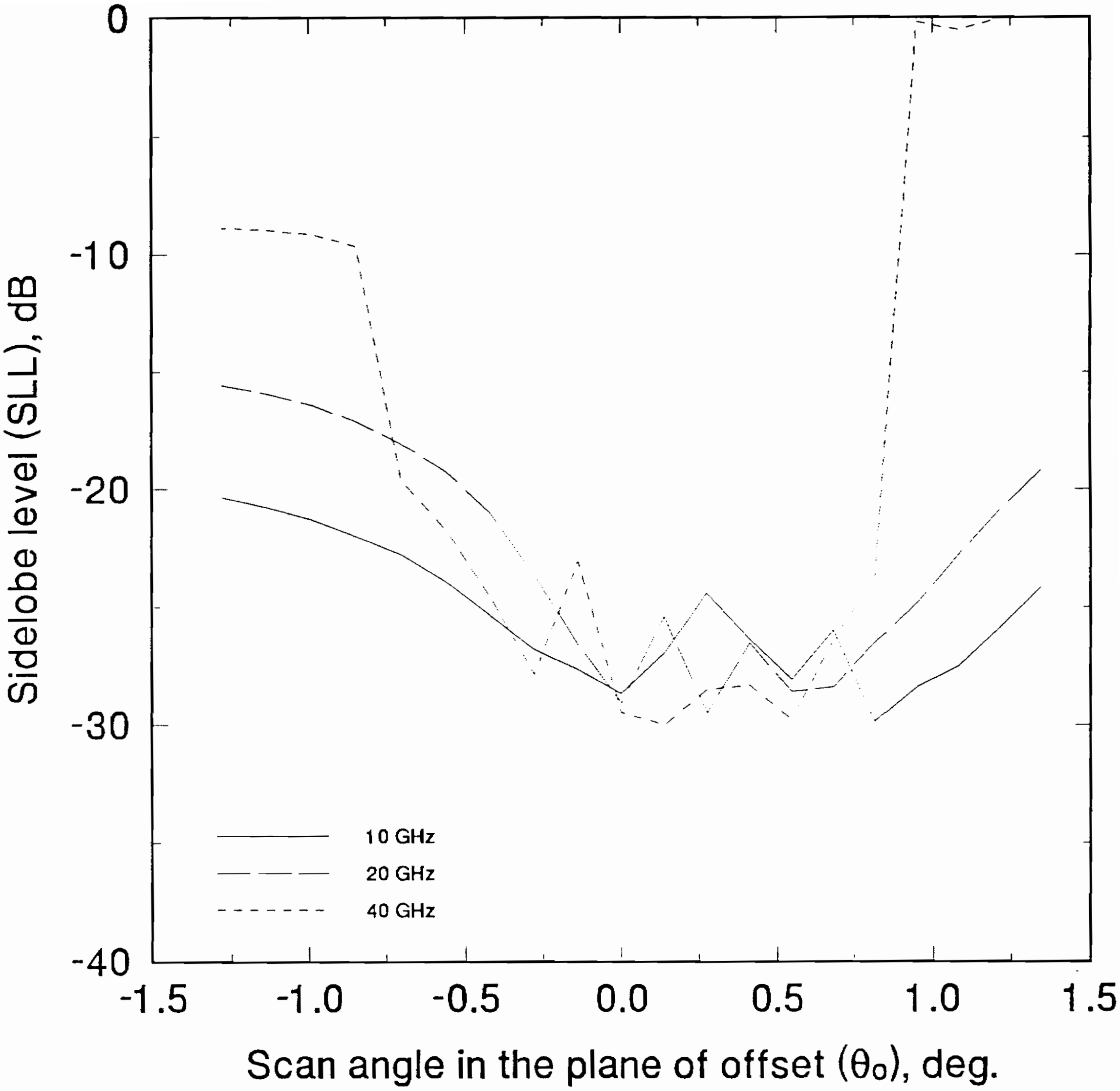

Figure 3.4-7. Sidelobe level (SLL) as a function of scan angle in the plane of offset (θ_o) for the Type 6 reflector antenna system of Foldes.

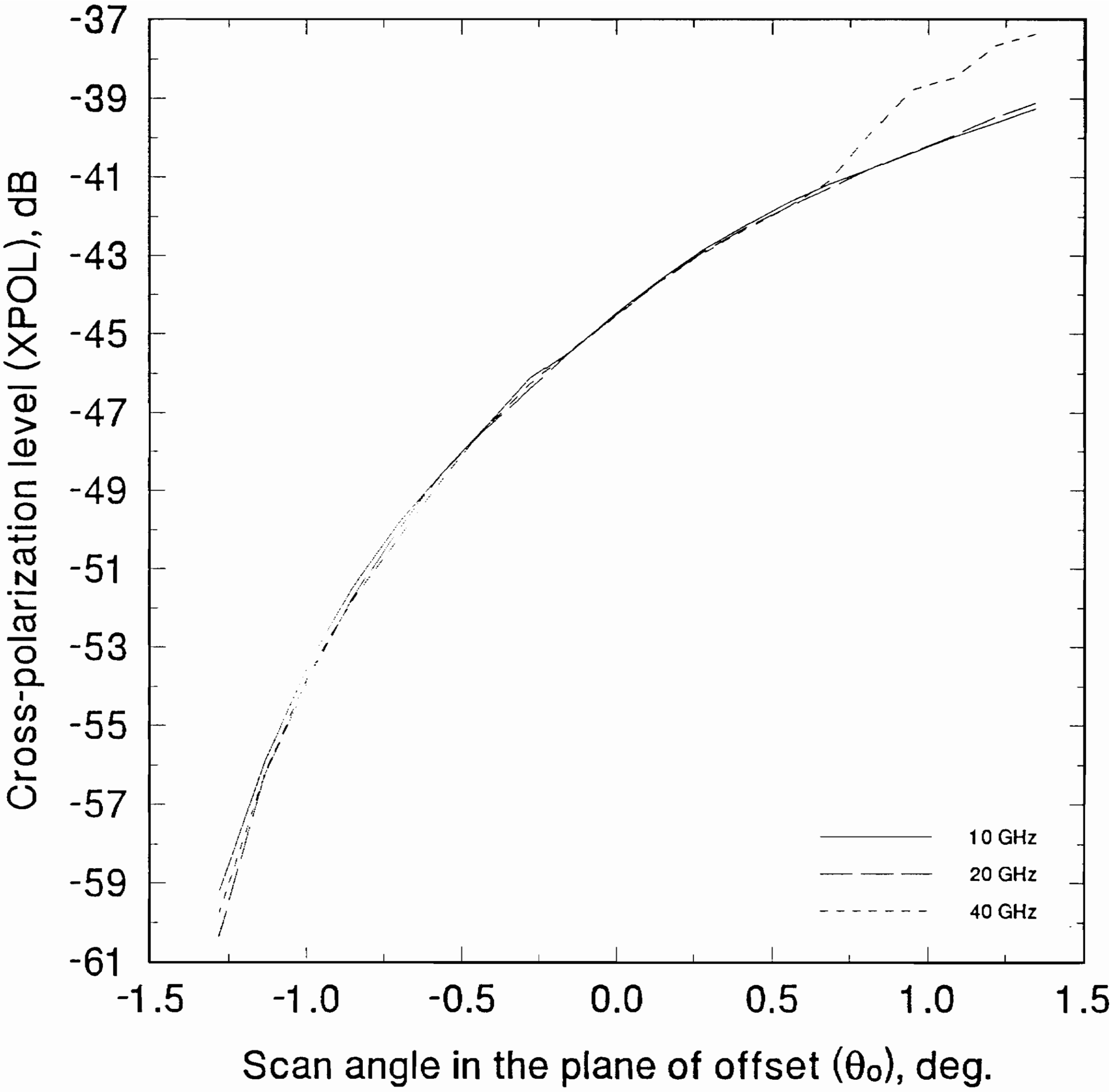

Figure 3.4-8. Cross-polarization level (XPOL) as a function of scan angle in the plane of offset (θ_o) for the Type 6 reflector antenna system of Foldes.

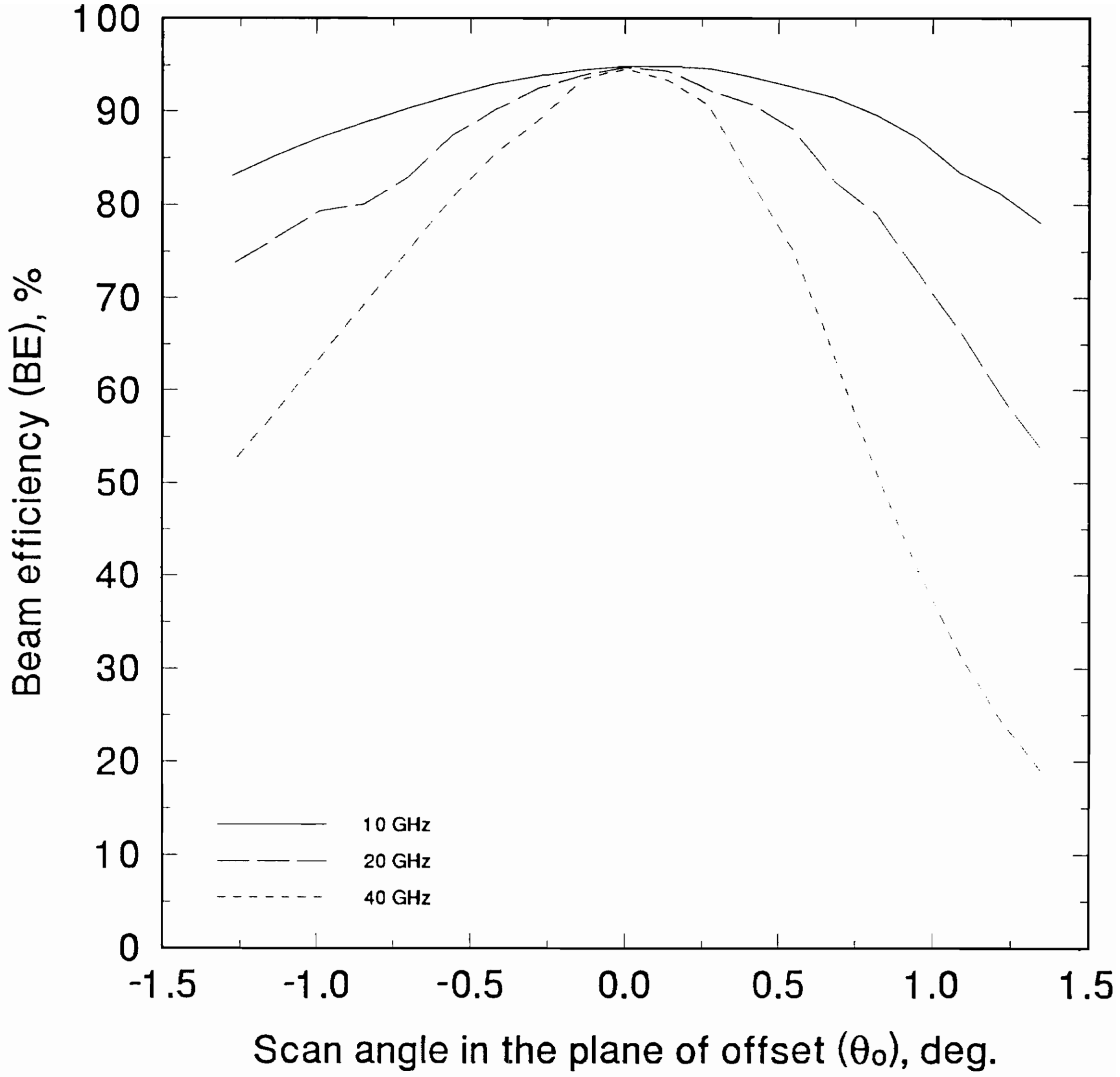

Figure 3.4-9. Beam efficiency (BE) as function of scan angle in the plane of offset (θ_0) for the Type 6 reflector antenna system of Foldes.

References

[1] J.J. Lee, "Lens Antennas," *Antenna Handbook*, Chap. 16, pp. 16-12-16-19, Y.T. Lo and S.W. Lee, editors, Van Nostrand Reinhold Co., New York, New York, 1988.

[2] W.L. Stutzman and G.A. Thiele, *Antenna Theory and Design*, John Wiley & Sons, Inc., New York, New York, 1981.

[3] M. Born and E. Wolf, *Principles of Optics*, 3rd edition, pp. 211-218 and 468-484, Pergamon Press, New York, New York, 1965.

[4] S. Silver, editor, *Microwave Antenna Theory and Design*, Sect. 6.7, McGraw-Hill Book Co., New York, New York, 1949.

[5] V. Krichevsky and D.F. Difonzo, "Optimum feed locus for beam scanning in the symmetry plane of offset Cassegrain antennas: Two dimensional case," *Comsat Technical Review*, Vol. 11, No. 1, pp. 131-157, Spring 1981.

[6] R.W. Kreutel et al., "Antenna Technology for Frequency Reuse Satellite Communications," *Proceedings of the IEEE*, Vol. 65, No. 3, pp. 370-378, March 1977.

[7] F. Taormina et al., "INTELSAT IV-A Communications Antenna - Frequency Reuse through Spatial Isolation," ICC '76 *Conference Digest*, Vol. 1, pp. 4-10-4-14.

[8] G.H. Schennum and H.T. Ward, "INTELSAT V Spacecraft Antenna Subsystem," ICC '80 *Conference Digest*, Vol. 2, pp. 25.1.1-25.2.6.

[9] V. Krichevsky, *Optimum Beam Scanning in Offset Single and Dual Reflector Antennas*, Vol. 1, COMSAT Laboratories, April 1983.

[10] W.L. Stutzman et al., Semiannual Status Report for "Feasibility Study of a Synthesis Procedure for Array Feeds to Improve Radiation Performance of Large Distorted Reflector Antennas," February 1992.

Chapter 4

TEST CASE GEOMETRY SELECTION

The selection of a test case geometry for this study is motivated by the antenna performance characteristics required by the Mission to Planet Earth. A NASA microwaves radiometric earth observation science steering panel met twice in 1990 to determine the mission parameters which would allow the project to make a significant contribution to the knowledge of climatic and meteorological phenomena [1]. The requirements recommended by the panel are summarized in Table 1.2-1. The frequency and beamwidth restrictions require an aperture efficiency of 70% since a Virginia Tech study of the issues presented by large space antenna structures found that an antenna of up to 25 meters diameter can be launched by a single Shuttle Transportation System (STS) mission [1, 2].

As mentioned in Chapter 1, the necessity of sharing a geostationary platform with other experiments requires that the antenna be capable of beam scanning by sub-optics motion to avoid disturbing other experiments. The aperture efficiency required by the desired beamwidth and frequency of operation effectively eliminates conventional spherical reflector antenna systems from consideration despite their degradation-free scan performance. The Cassegrain reflector antenna was selected since it is the simplest and most compact reflector configuration that allows beam scanning by subreflector motion. The high beam efficiency requirement indicates that an offset antenna configuration would be desirable to eliminate aperture blockage by the subreflector/feed assembly.

The test case main reflector has a diameter of $D_M = 10.63$ meters, a focal length of $F_M = 13.5$ meters, and an offset distance of $H_o = 7.795$ meters. These dimensions were chosen to allow possible verification of the synthesis procedure using a NASA Langley Antenna and Microwave Research Branch test article [3]. The configuration and dimensions of the test article are shown in Figure 4-1. This test article is a 42.52% scale model of the proposed 25 meter radiometric earth observation reflector antenna.

Since the results given in Section 3.2 show that the scan characteristics of Cassegrain reflector antenna systems are insensitive to equivalent paraboloid offset, the test case geometry was chosen to have an axi-symmetric equivalent paraboloid. This geometry selection should minimize the overall cross-polarization experienced by the system across the scan range. The Rusch condition for this system can be found using (2.5-7) with a center angle, θ_c, of 32.207°:

$$\tan\frac{32.207}{2} = \frac{2\,e\,\sin\beta}{e^2 + 1 - 2\,e\,\cos\beta}. \tag{4-1}$$

The eccentricity of the subreflector hyperboloid was chosen to be 1.919 to approximate the relative subreflector size of the 25 meter diameter Foldes Type 6 reflector antenna system which was originally proposed. This results in a subreflector diameter of about 1.4 meters for the test case. The subreflector area used in the synthesis and the GRASP7 physical optics analysis is the illuminated portion of the parent hyperboloid during unscanned conditions as determined by geometrical optics raytracing.

The tilt angle, β, of the line between the hyperboloid foci can now be found to be $\beta = 3.676°$ from (2.6-1). The interfocal length of the hyperboloid was chosen to be 6.900 meters to place the feed point near the the subreflector/feed boom. These selections lead to a feed point located at $\{0.442,\ 0.000,\ 6.614\}$ meters. The feed tilt angle, α, which will align the feed boresight with the angular center of the subreflector and the axis of the equivalent paraboloid can now be found using (2.4-19):

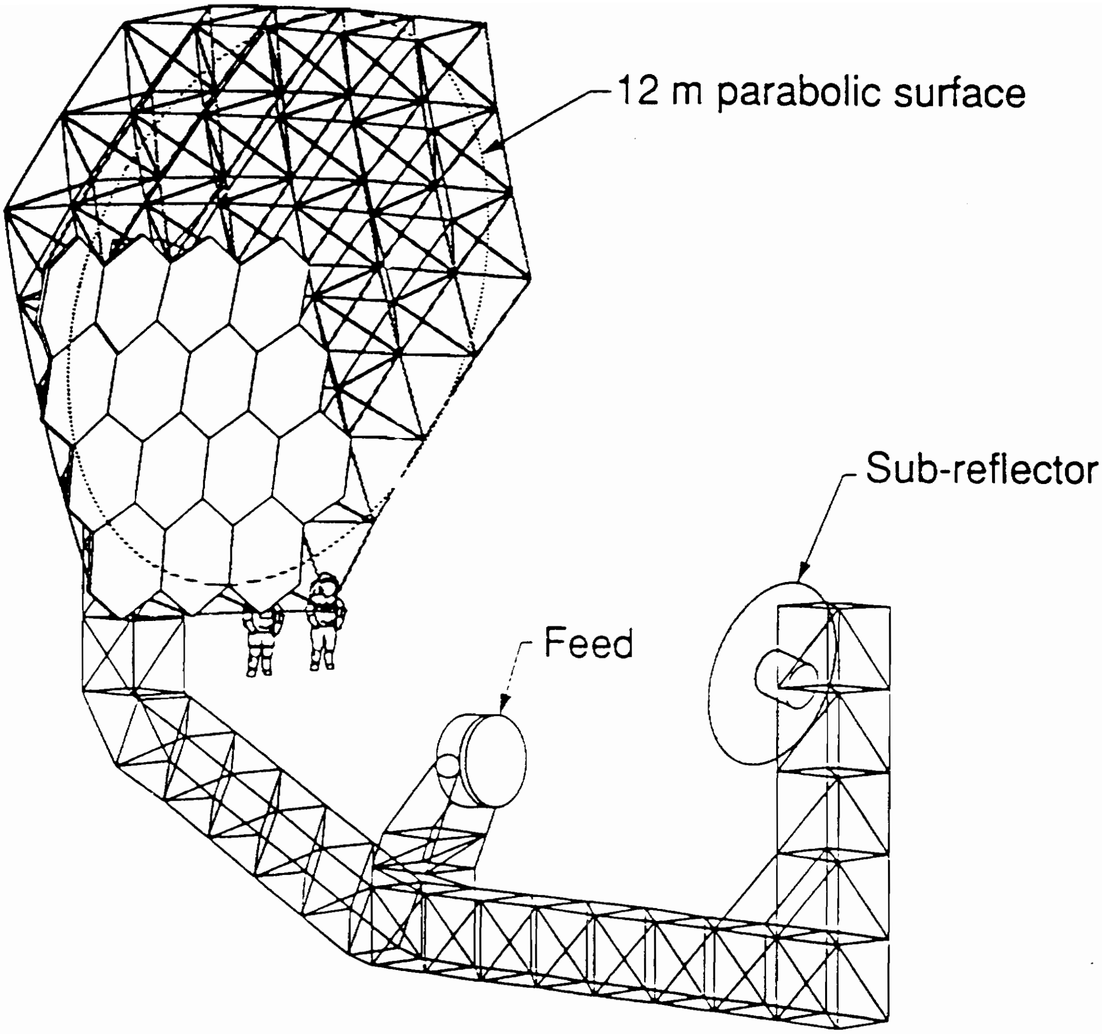

Figure 4-1. NASA Langley AMRB test article configuration and dimensions [3].

$$\tan\frac{\alpha}{2} = \frac{e+1}{e-1}\tan\left(\frac{\beta}{2}\right). \tag{4-2}$$

Solving (4-2) with these selections of e and β gives $\alpha = 11.640^\circ$. The test case is fed with an x-polarized feed. The feed pattern is defined independent of frequency to produce a 15 dB edge taper on the subreflector. This edge taper was chosen based on the beam efficiency results of Section 2.1.1. The geometry of the test case is given by Figure 4-2 and Table 4-1.

The unscanned far-field pattern of the test case was evaluated using the TICRA GRASP7 reflector analysis code. The evaluation was performed by geometrical theory of diffraction analysis at the subreflector and physical optics/surface integration at the main reflector. The gain pattern, G(u,v), of the unscanned test case system is shown in Figure 4.3 over a rectangular uv-grid of $\pm 0.57^\circ$. The cross-polarization pattern, XPOL(u,v), of the unscanned test case system is shown in Figure 4.4. The far-field pattern characteristics of the unscanned test case are summarized in Table 4.2.

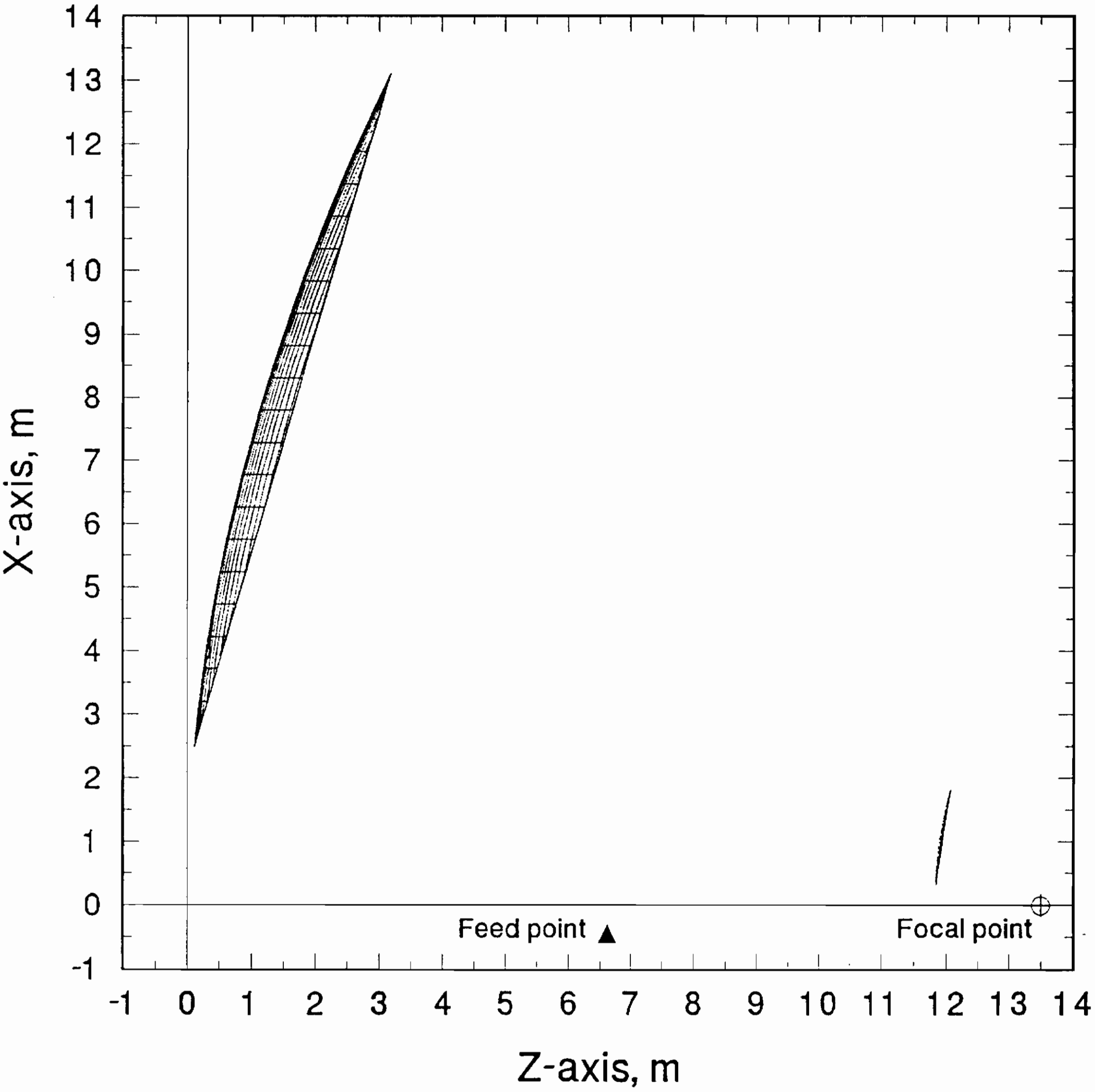

Figure 4-2. Plane of offset view of the final test case configuration.

Table 4-1. Characteristics of the final test case geometry.

Main reflector diameter (D_M)	10.63 meters
Main reflector focal length (F_M)	13.5 meters
Main reflector offset height (H_o)	7.795 meters
Subreflector axis tilt angle (β)	3.676°
Subreflector eccentricity (e)	1.919
Subreflector interfocal length (2c)	6.9 meters
Subreflector diameter (D_S)	1.4 meters
Areal efficiency $\left(\frac{D_M^2}{D_M^2 + D_S^2}\right)$	98.3%
Subreflector scanning motions	x, y, and z translations α and β rotations
Feed point (f)	{-0.442, 0.000, 6.614} meters from the main reflector vertex
Feed tilt angle (α)	11.64°
Feed pattern	Gaussian pattern with 15 dB edge taper at 7.157°
Frequency of operation	20, 40, and 80 GHz

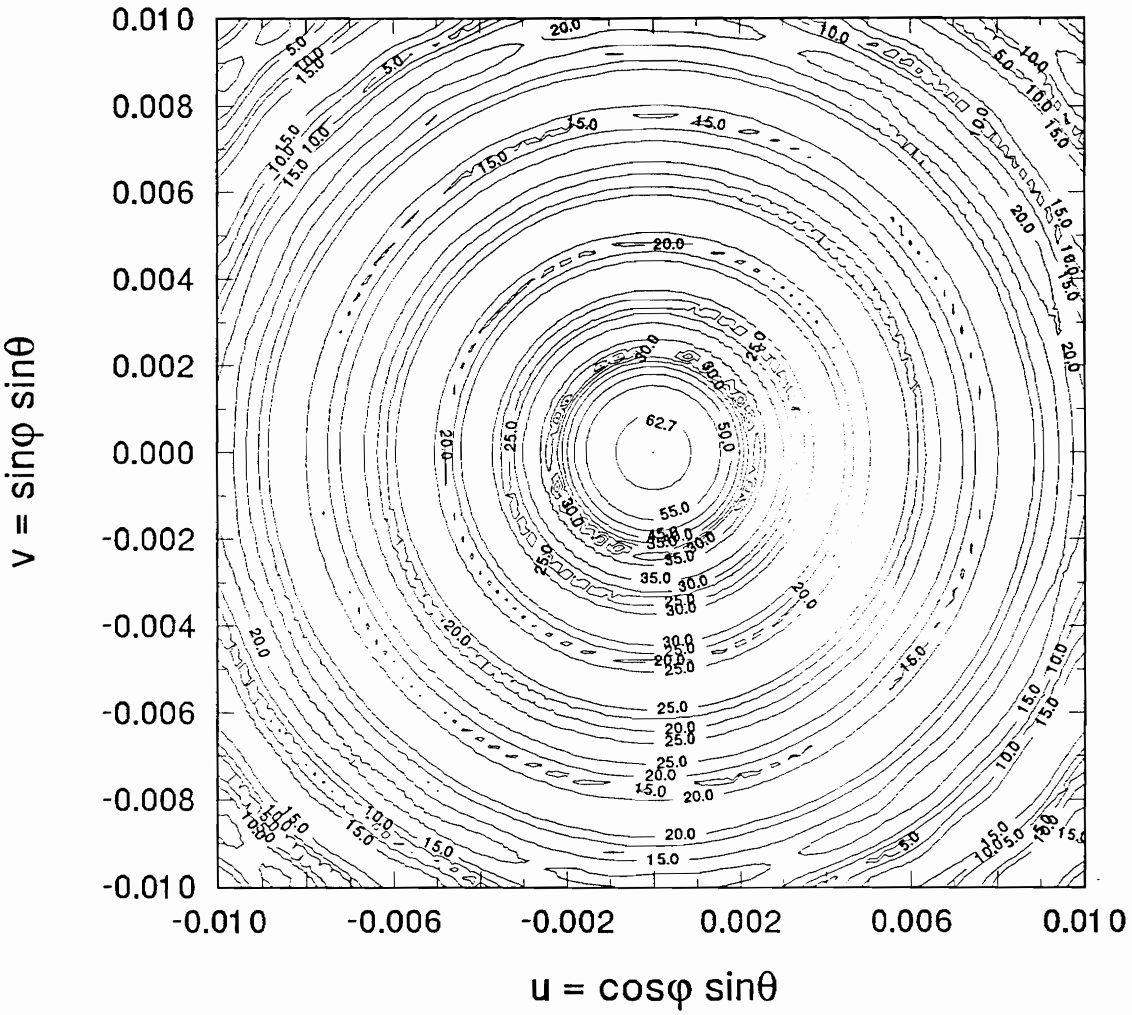

Figure 4-3. Gain pattern $\left(G(u,v)\right)$ of the unscanned test case system at 20 GHz.

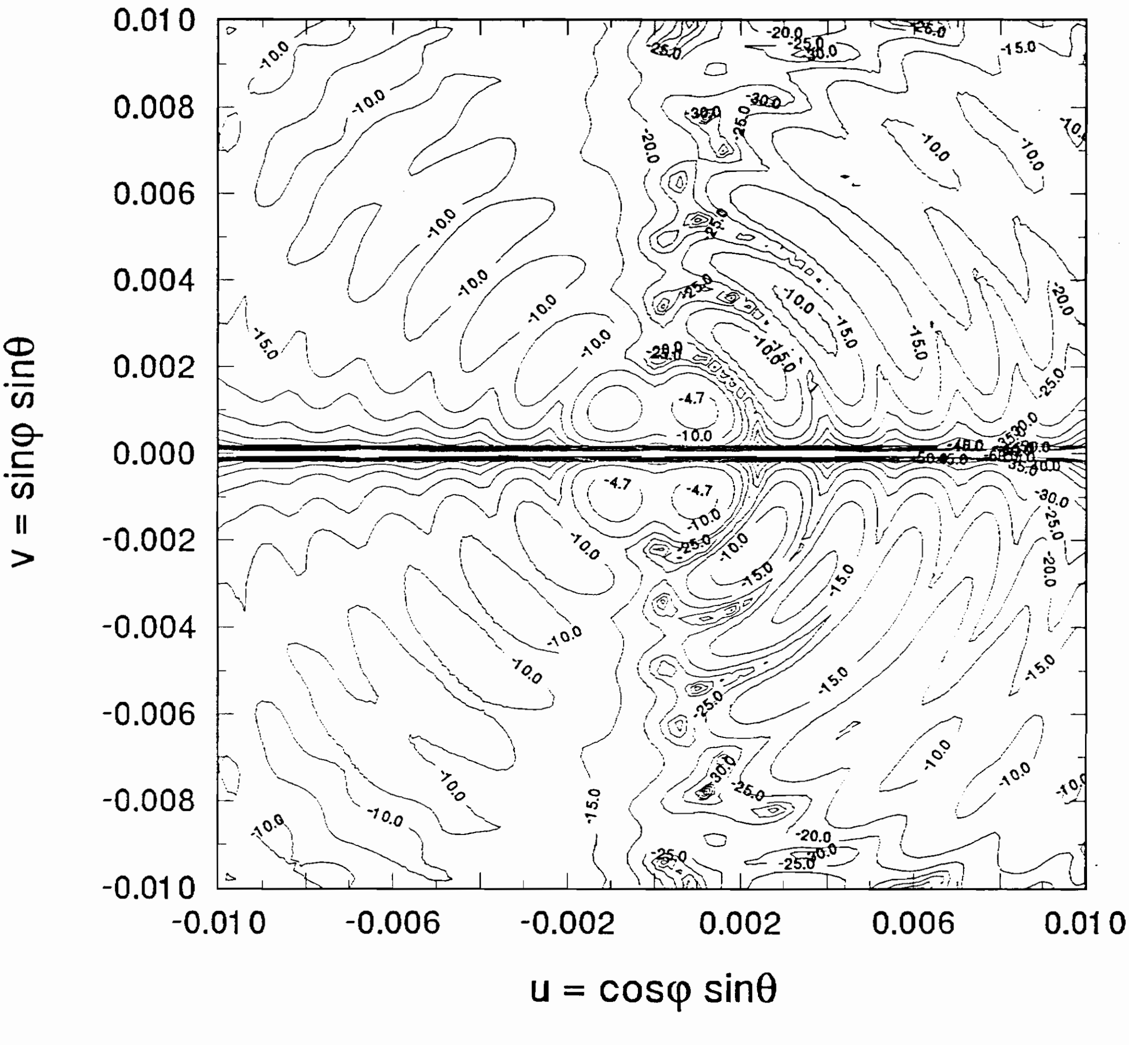

Figure 4-4. Cross-polarization pattern (XPOL(u,v)) of the unscanned test case system at 20 GHz.

Table 4-2. Far-field pattern characteristics of the unscanned test case system.

Far-field pattern characteristic	Frequency, GHz			Units
	20	40	80	
Gain, G	65.67	71.72	77.78	dBi
Sidelobe level, SLL	-29.00	-29.32	-29.45	dB
Cross-polarization level, XPOL	-67.33	-73.40	-74.70	dB
Beam efficiency, BE	93.28	93.44	93.63	%
Aperture efficiency, $\varepsilon_{\mathrm{ap}}$	74.44	74.95	75.63	%
Spillover effiency, $\varepsilon_{\mathrm{sp}}$	94.74	94.85	94.98	%
Illumination amplitude effiency, $\varepsilon_{\mathrm{amp}}$	78.57	79.02	79.63	%
Half-power beamwidth, HPBW	0.092	0.046	0.023	°

References

[1] W. L. Stutzman and G. S. Brown, "The Science Benefits of and the Antenna Requirements for Microwave Remote Sensing From Geostationary Orbit," NASA Contractor Report 4408, October 1991.

[2] C.A. Rogers and W. L. Stutzman, "Large Deployable Antenna Program, Phase 1: Technology Assesment and Mission Architecture," NASA Contractor Report 4410, October 1991.

[3] Unpublished NASA Langley Research Center Antenna and Microwave Research Branch Memorandum

Chapter 5

SIMPLIFIED ERROR FUNCTIONALS FOR GEOMETRICAL OPTICS SYNTHESIS

As discussed previously, the test case developed in Chapter 4 beam scans by subreflector motion. While the primary goal of this effort is the maximization of beam efficiency during beam scanning, analysis of the pattern of the antenna to determine beam efficiency is impractical for use as an error functional in determining the optimal position of the subreflector during beam scanning. The physical optics analysis required to determine the far-field pattern of a Cassegrain reflector antenna system of this size requires approximately 6 minutes using a 50 MHz 80486 computer. An error functional of this complexity would result in an optimization which would require over one month of computer time for a single scan direction. It is highly desirable then to create a simple, computationally efficient estimate of the antenna's performance.

The desire that the error functional be easy to evaluate requires that the error functional be defined as a geometrical optics process with a minimal number of mathematical operations. Two error functionals, the correcting subreflector surface fitting error functional and the transmit mode raytracing error functional, were investigated. Both of these error functionals involve a minimum of mathematical evaluation; each requires only a single summation and is tolerant of a much coarser analysis grid than is physical optics analysis. Each error functional was tested by using it to determine the optimum subreflector position for several scanned beam directions. Each case was then analyzed using the geometrical theory of diffraction at the subreflector and physical optics/surface integration at the main reflector using the TICRA GRASP7 reflector antenna analysis package.

5.1 The Correcting Subreflector Surface Fitting Error Functional

The correcting subreflector surface fitting error functional determines the optimum position for the unscanned subreflector by fitting the repositioned unscanned subreflector to a correcting subreflector for the desired scan direction. Because the optimization is based on fitting the available subreflector to a fully illuminated correcting subreflector, this error functional should be expected to emphasize the minimization of illumination amplitude errors at the expense of illumination phase errors. A simpler version of this error functional was proposed by Kitsuregawa [1] for beam scanning by subreflector motion in reflector antenna systems where the main reflector and feed cannot be moved. The fitting error used by Kitsuregawa is given by

$$\epsilon_k = \sum_{i=1}^{N} [(S'_i - S_i)\cdot\hat{n}_{Si}]^2, \qquad (5.1\text{-}1)$$

where S'_i is the i th point on the repositioned unscanned subreflector, S_i is the i th point on the correcting subreflector for the desired direction of scan, and $\hat{n}_{Si}$ is the unit normal of the correcting subreflector at the i th point [1]. While Kitsuregawa [1] uses this error functional in a system of least squares equations, it can also be used as an error estimate for optimization.

5.1.1 Analytic Development of the Correcting Subreflector

The test case reflector antenna system discussed in Chapter 4 is described by grids of points which define the parent surface of the main and subreflectors. These grids are found by using geometrical optics raytracing in the test case geometry. As discussed in Section 2.3, Snell's law is satisfied at the main reflector and the total path length of the rays from the aperture plane through the system to the feed point is held constant to find the subreflector points. This procedure, developed by Werntz [2], is also used in the correcting subreflector surface fitting error function to find the phase error correcting subreflector for the scanned system.

Figure 5.1.1-1 shows the geometry used to determine the subreflector points. The rays used to define the system form a 25 × 25 grid in the aperture plane which circumscribes the projected aperture of the antenna system. A ray incident on the main reflector from the aperture plane has a unit vector

$$\hat{r}_1 = \left\{-\sin\theta_o \cos\phi_o\, \hat{x},\ -\sin\theta_o \sin\phi_o\, \hat{y},\ \cos\theta_o\, \hat{z}\right\}, \tag{5.1.1-1}$$

where θ_o is the scan angle from the z-axis and ϕ_o is the scan angle from the x-axis toward the y-axis as shown in Figure 5.1.1-2.

The length of a ray from the aperture plane to the main reflector is

$$\left|R_1\right| = \cos\theta_o \left(z_A + \tan(-\theta_o)\cos\phi_o x_M + \tan(-\theta_o)\sin\phi_o y_M + z_M\right), \tag{5.1.1-2}$$

where z_A is the z-coordinate of the intersection of the aperture plane and the z-axis and $\left\{x_M, y_M, z_M\right\}$ is a point on the main reflector.

The unit vector of a ray reflected from the main reflector is found by satisfying Snell's law at the main reflector. This gives

$$\hat{r}_2 = \hat{r}_1 - 2(\hat{r}_1 \cdot \hat{n}_M)\hat{n}_M, \tag{5.1.1-3}$$

where $\hat{n}$ is the unit normal at the main reflector point given by (2.1-11)

$$\hat{n}_M = \left(\sqrt{x_M{}^2 + y_M{}^2 + 4F^2}\right)^{-1} \left\{-x_M\hat{x},\ -y_M\hat{y},\ 2F\hat{x}\right\}, \tag{5.1.1-4}$$

where F is the focal length of the main reflector paraboloid. Five intermediate results are next calculated to simplify the equations for the subreflector point. These are

$$I_1 = \frac{\hat{r}_{1x} - 2(\hat{r}_1 \cdot \hat{n}_M)\hat{n}_{Mx}}{\hat{r}_{1z} - 2(\hat{r}_1 \cdot \hat{n}_M)\hat{n}_{Mz}}, \tag{5.1.1-5}$$

$$I_2 = \hat{r}_{1y} - 2(\hat{r}_1 \cdot \hat{n}_M)\hat{n}_{My}, \tag{5.1.1-6}$$

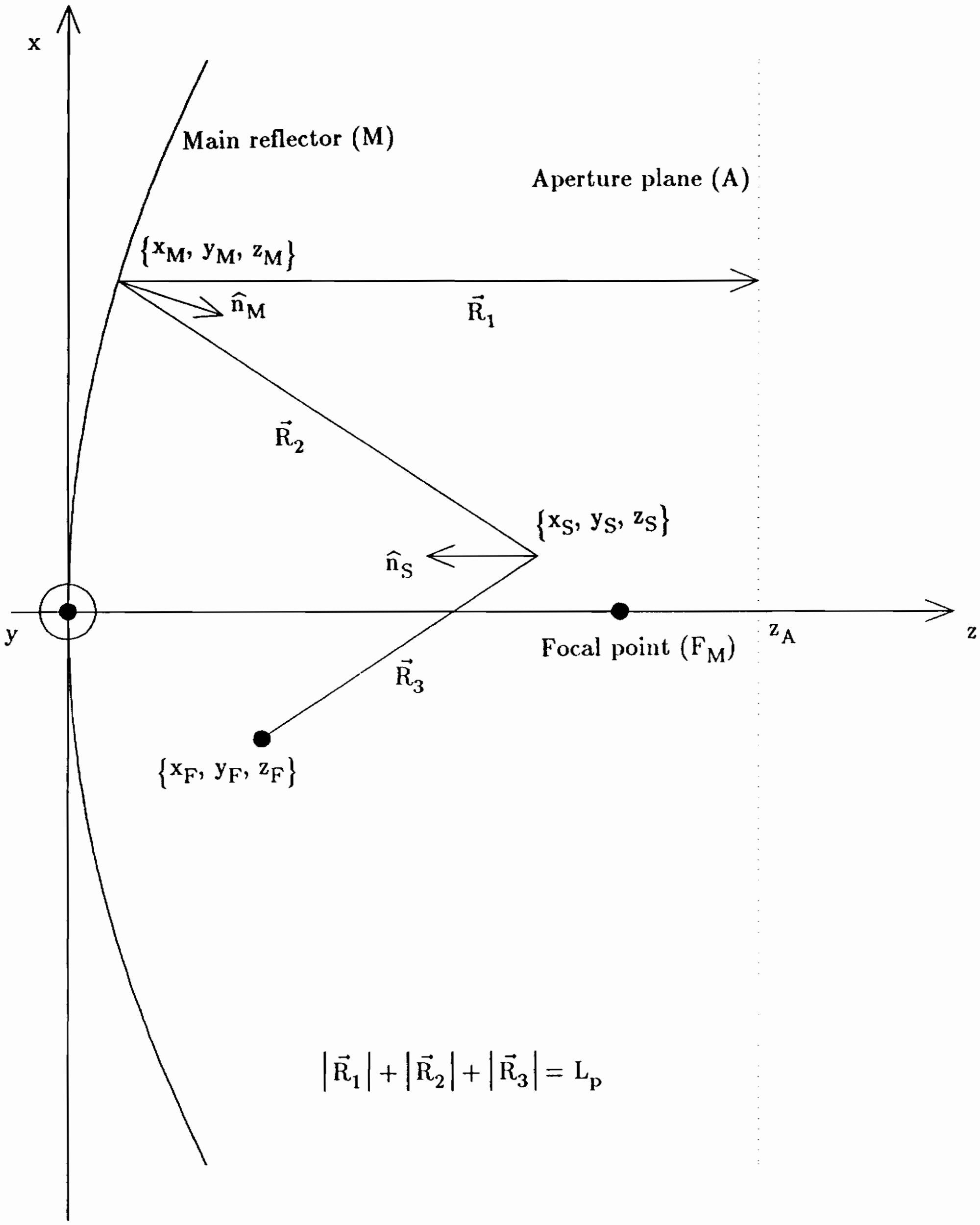

Figure 5.1.1-1. Correcting subreflector synthesis geometry.

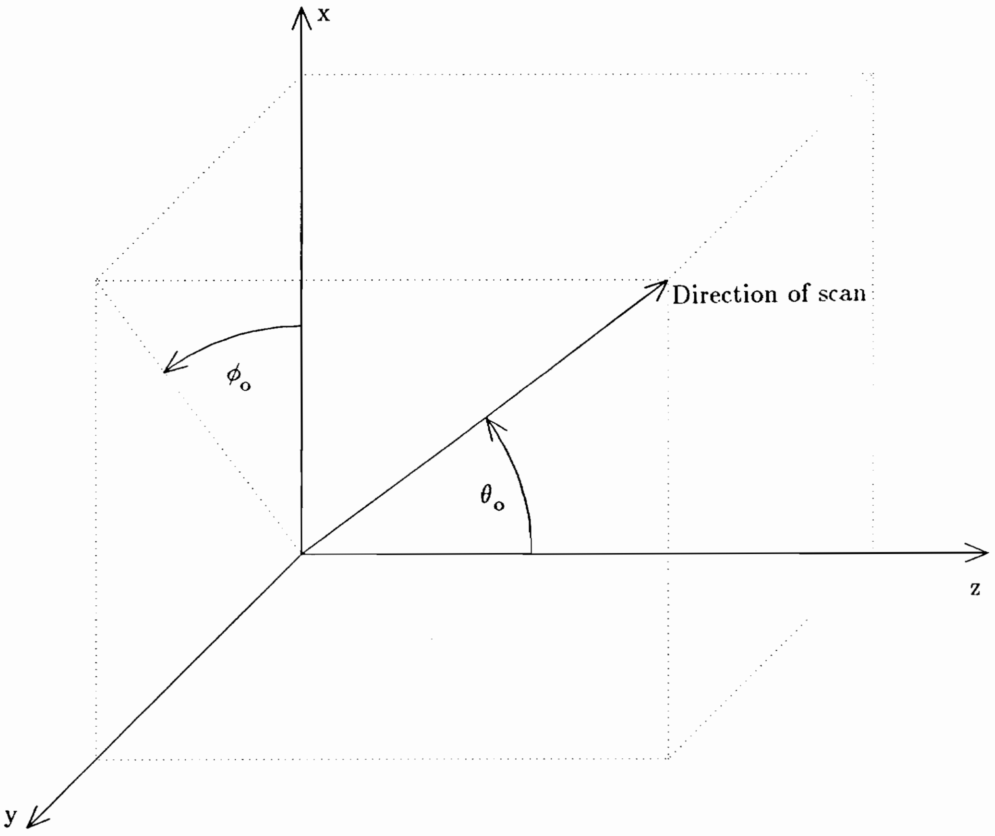

Figure 5.1.1-2. Definition of scan angles.

$$I_3 = I_2\sqrt{\frac{1+I_1^2}{1-I_2^2}}, \tag{5.1.1-7}$$

$$I_4 = L_p - |R_1|, \text{ and} \tag{5.1.1-8}$$

$$I_5 = 2\left[I_4\sqrt{1+I_1^2+I_3^2} + I_1(x_M - x_f) + I_3(y_M - y_f)\right]$$

where L_p is the desired path length through the system and $\{x_f, y_f, z_f\}$ is the feed point. The subreflector point, $\{x_S, y_S, z_S\}$, can now be found by

$$z_S = \frac{I_4^2 + I_5 z_M - (x_f - x_M)^2 - (y_f - y_M)^2 + z_M^2 - z_f^2}{I_5 + 2z_M - 2z_f}, \tag{5.1.1-9a}$$

$$x_S = I_1(z_S - z_M) + x_M, \tag{5.1.1-9b}$$

$$y_S = I_3(z_S - z_M) + y_M. \tag{5.1.1-9c}$$

The length of the ray from the subreflector point to the feed point is

$$|R_3| = \sqrt{(x_S - x_f)^2 + (y_S - y_f)^2 + (z_S - z_f)^2} \tag{5.1.1-10}$$

so the unit vector of the ray from the subreflector point to the feed point is

$$\hat{r}_3 = \left\{ \frac{x_f - x_S}{|R_3|}\hat{x}, \frac{y_f - y_S}{|R_3|}\hat{y}, \frac{z_f - z_S}{|R_3|}\hat{z} \right\}. \tag{5.1.1-11}$$

The subreflector unit normal can now be found by taking the difference between $\hat{r}_2$ and $\hat{r}_3$. This results in

$$\hat{n}_s = \frac{(\hat{r}_{3x} - \hat{r}_{2x})\hat{x} + (\hat{r}_{3y} - \hat{r}_{2y})\hat{y} + (\hat{r}_{3z} - \hat{r}_{2z})\hat{z}}{\sqrt{(\hat{r}_{3x} - \hat{r}_{2x})^2 + (\hat{r}_{3y} - \hat{r}_{2y})^2 + (\hat{r}_{3z} - \hat{r}_{2z})^2}}. \tag{5.1.1-12}$$

The set of subreflector points and normals generated by this procedure is either saved to a data file in the case of test case synthesis or used in the error functional as the correcting subreflector during optimization.

5.1.2 Correcting Subreflector Surface Fitting Optimization Implementation - CSSFT1

The correcting subreflector surface fitting error functional is a slight extension of the error functional of Kitsuregawa [1] given by (5.1-1). For the optimization, the error function is expanded to a double summation over the grid of points of the subreflector but is otherwise unchanged. This results in

$$\epsilon_{cs} = \sum_{i=1}^{M} \sum_{j=1}^{N} \left[\left(S'_{i,j} - S_{i,j} \right) \cdot \hat{n}_{Si,j} \right]^2, \tag{5.1.2-1}$$

where $S'_{i,j}$ is the i,j $\underline{th}$ point on the repositioned test case subreflector, $S_{i,j}$ is the i,j $\underline{th}$ point on the correcting subreflector found using the method on Section 5.1.1, and $\hat{n}_{Si,j}$ is the normal of the correcting subreflector. This error functional is then used to estimate the pattern error caused by the current position of the test case subreflector. To achieve this, the error functional is used in the two-stage optimization process which has the function blocks shown in Figure 5.1.2-1. The FORTRAN source code which implements this process is listed in Appendix 1.

The inner loop is a five-dimensional Powell's method optimization [3] which positions the test case subreflector to best fit the correcting subreflector. The test case subreflector can be translated in the x-, y-, and z-directions and rotated about its center grid point in α- and β-tilts as shown in Figure 5.1.2-2. The position of a translated and rotated test case subreflector point is given by

$$x_{S'} = x_t + x_{\bar{S}r} + \cos\alpha_r (x_{\bar{S}} - x_{\bar{S}r}) + \sin\alpha_r \sin\beta_r (y_{\bar{S}} - y_{\bar{S}r}) + \sin\alpha_r \cos\beta_r (z_{\bar{S}} - z_{\bar{S}r}), \tag{5.1.2-2a}$$

$$y_{S'} = y_t + y_{\bar{S}r} + \cos\beta_r (y_{\bar{S}} - y_{\bar{S}r}) - \sin\beta_r (z_{\bar{S}} - z_{\bar{S}r}), \text{ and} \tag{5.1.2-2b}$$

$$z_{S'} = z_t + z_{\bar{S}r} + \sin\alpha_r (x_{\bar{S}} - x_{\bar{S}r}) + \cos\alpha_r \sin\beta_r (y_{\bar{S}} - y_{\bar{S}r}) + \cos\alpha_r \cos\beta_r (z_{\bar{S}} - z_{\bar{S}r}) \tag{5.1.2-2c}$$

where $\{ x_{S'}, y_{S'}, z_{S'} \}$ is the repositioned test case subreflector point, $\{ x_{\bar{S}}, y_{\bar{S}}, z_{\bar{S}} \}$ is the test case subreflector point, $\{ x_{\bar{S}r}, y_{\bar{S}r}, z_{\bar{S}r} \}$ is the point about which the rotations occur, and $\{ x_t, y_t, z_t \}$ is the vector of translations. The outer optimization loop is a Golden Section optimization process [4] which varies the path length through the antenna system to allow the calculation of a family of correcting subreflectors. This step is necessary because the curvature of the correcting subreflector is greater for higher total path lengths.

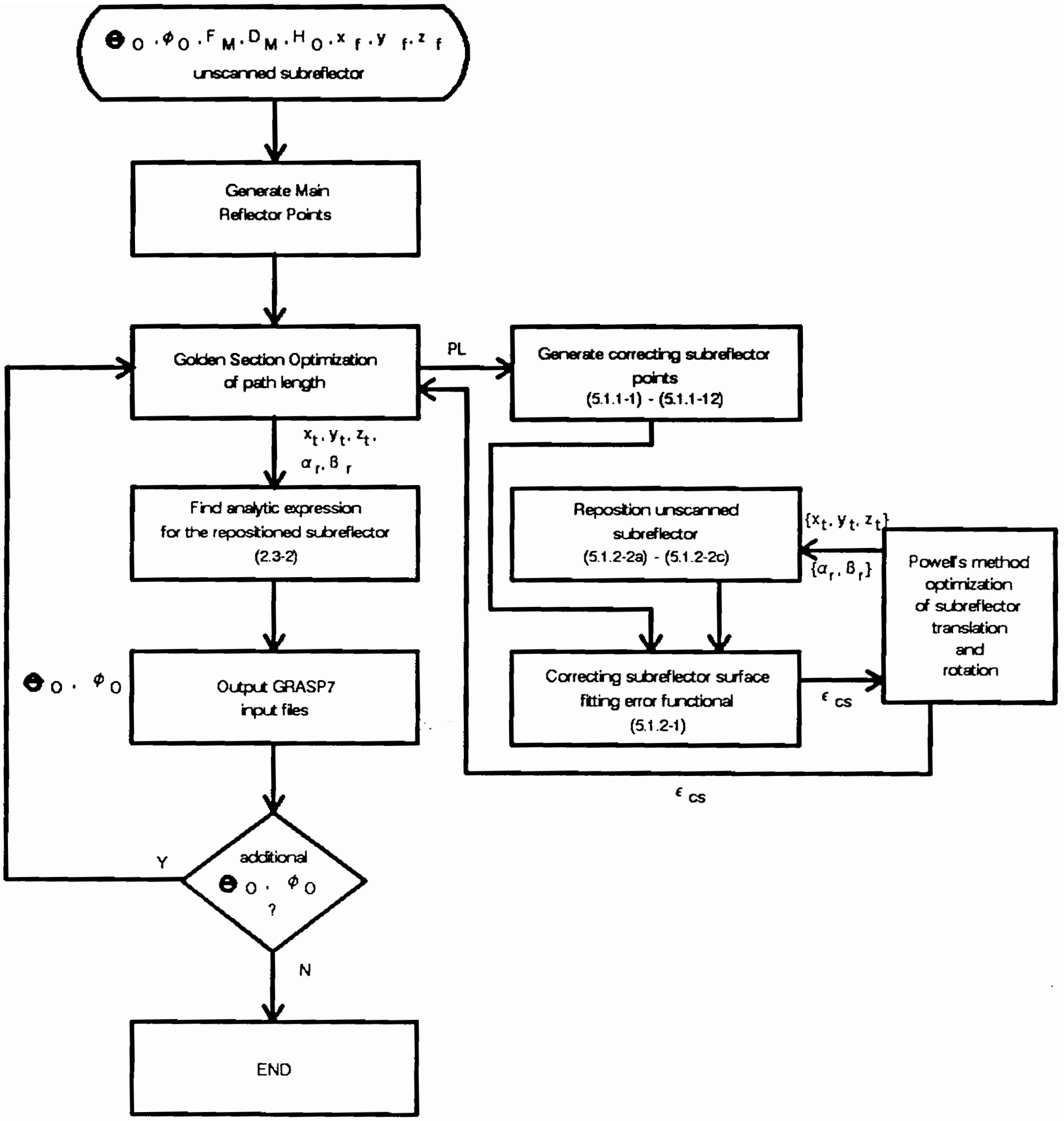

Figure 5.1.2-1. Correcting subreflector surface fitting error functional optimization algorithm structure.

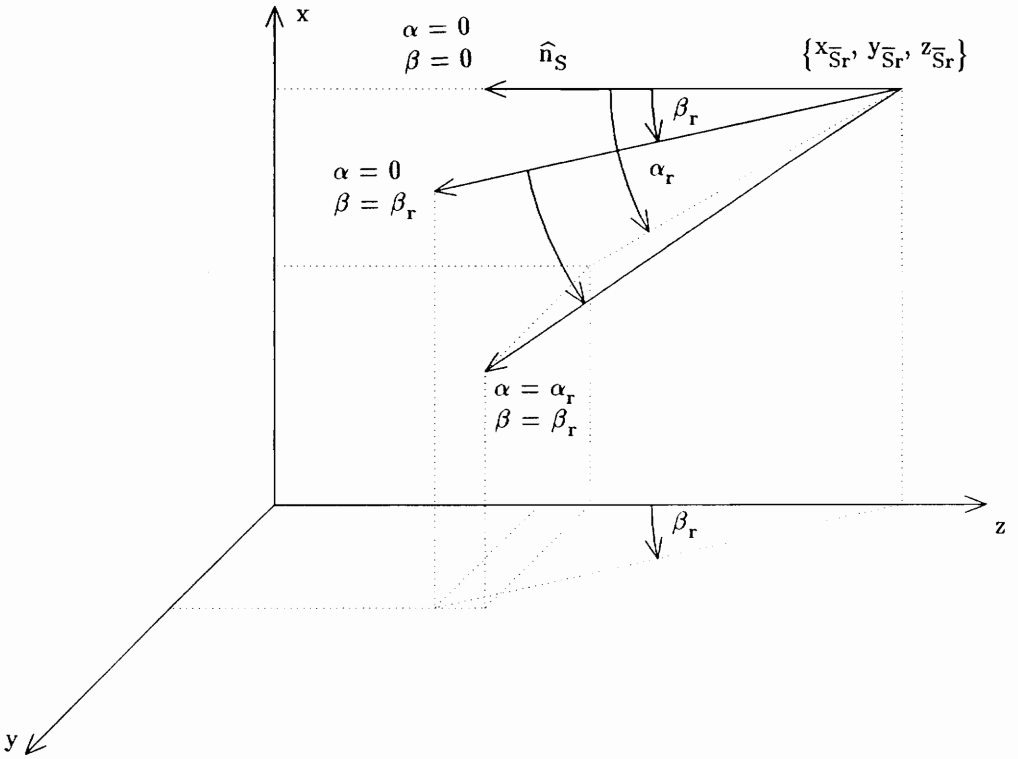

Figure 5.1.2-2. Definition of subreflector tilt angles.

5.1.3 Predicted Subreflector Motions

The optimum subreflector positions were determined using the correcting subreflector surface fitting error functional for three scan paths: a scan from θ_o = -1.0° to θ_o = 1.0° for ϕ_o = 0°, a scan from ϕ_o = 0° to ϕ_o = 180° for θ_o = 0.5°, and a scan from ϕ_o = 0° to ϕ_o = 180° for θ_o = 1.0°. These scan paths represent 39 individual scan directions with a average computational time of nearly 45 minutes per direction or a total time of just over 29 hours. An earlier version of the optimization which used five linear optimization routines instead of the Powell's method inner optimization loop was noted to be substantially slower.

The constant ϕ scan path from θ_o = -1.0° to θ_o = 1.0° was approximated by 21 discrete scan directions at 0.1° intervals. The subreflector motion for this scan path consists of only x- and z-translations and α-rotation since the main beam is being scanned in the plane of offset. The x-, y-, and z-translations required for this scan path are shown in Figure 5.1.3-1 as a function of scan angle in the plane of offset. The maximum translation for this scan path is about 0.25 meter at either limit of scan. The α- and β-rotations required for this scan path are shown in Figure 5.1.3-2 as a function of scan angle in the plane of offset. The maximum rotation required for this scan path is less than 1°.

The constant θ scan paths at θ_o = 0.5° and θ_o = 1.0° were each approximated by 11 discrete scan directions from ϕ_o = 0° to ϕ_o = 180° at 18° intervals. The x-, y-, and z-translations required for these scan paths are shown in Figure 5.1.3-3. The required total translations for these scan paths are nearly constant at approximately 0.11 meter for θ_o = 0.5° and 0.25 meter for θ_o = 1.0°. The α- and β-rotations required for these scan paths are shown in Figure 5.1.3-4. As for the case of scanning in the plane of offset, the maximum required rotation is slightly less than 1°.

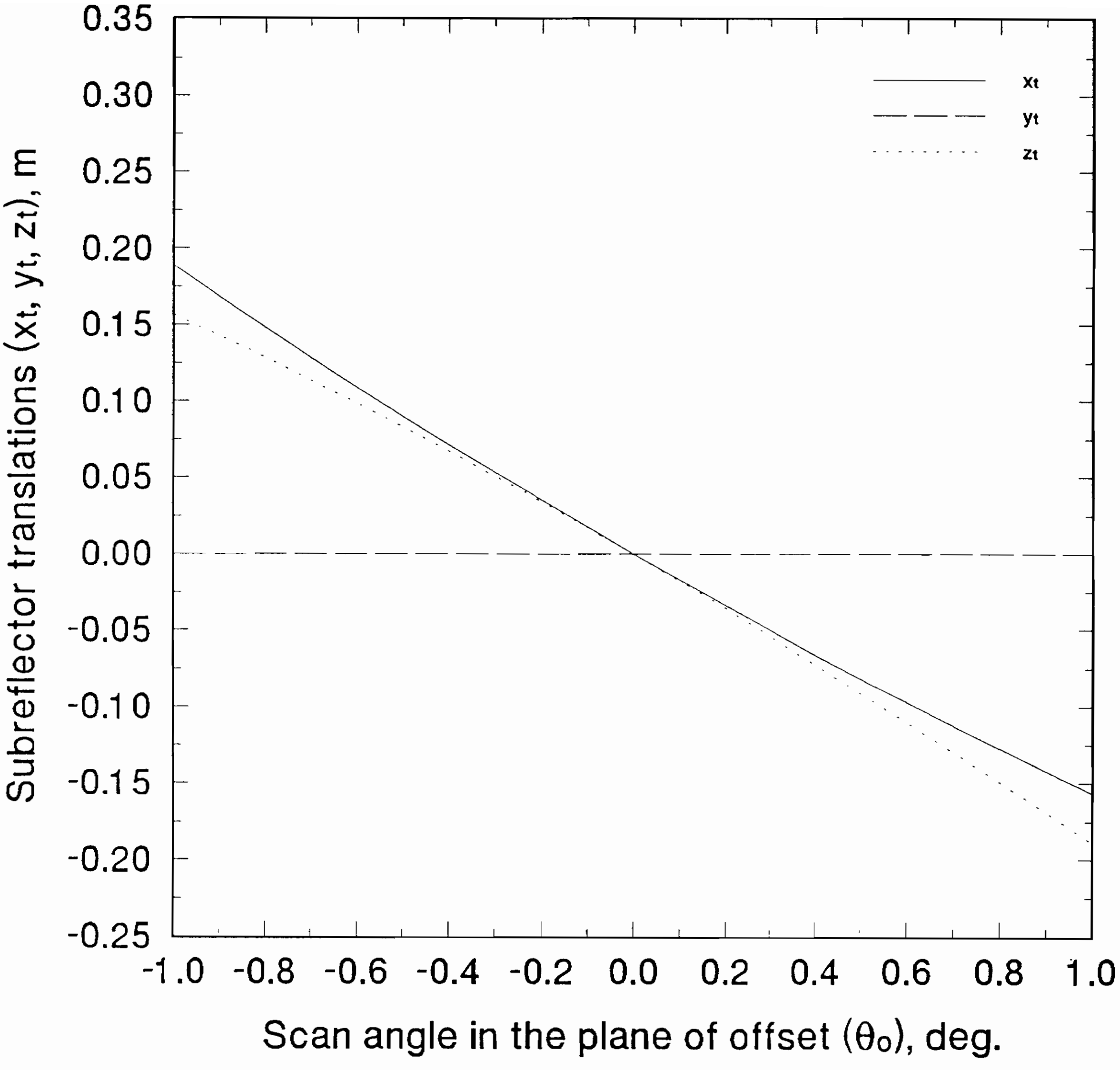

Figure 5.1.3-1. Optimum subreflector x-, y-, and z-translations (x_t, y_t, z_t) for the test case system as determined using the correcting subreflector error functional as a function of scan angle in the plane of offset (θ_o).

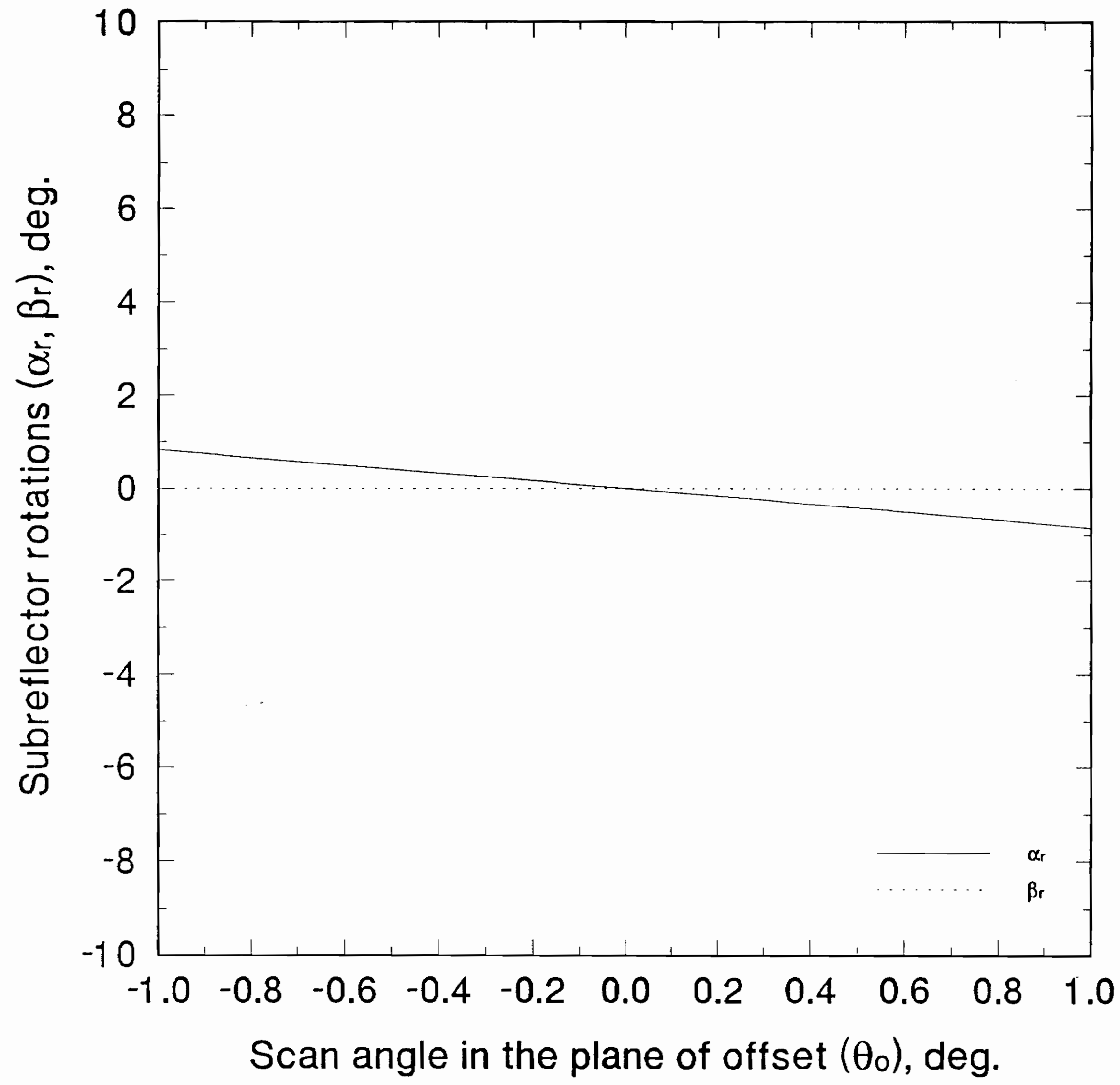

Figure 5.1.3-2. Optimum subreflector α- and β-rotations (α_r, β_r) for the test case system as determined using the correcting subreflector error functional as a function of scan angle in the plane of offset (θ_o).

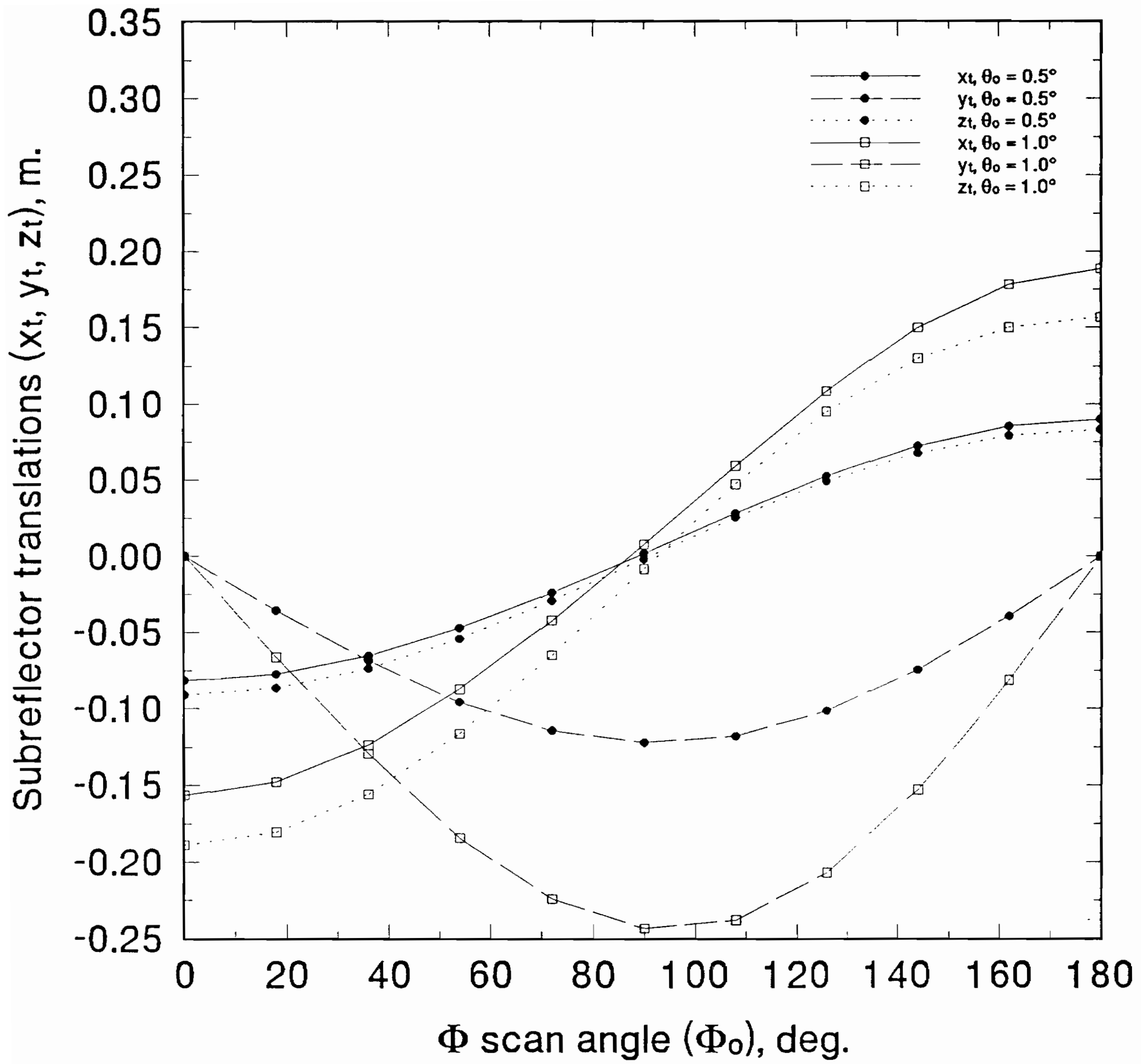

Figure 5.1.3-3. Optimum subreflector x-, y-, and z-translations (x_t, y_t, z_t) for the test case system as determined using the correcting subreflector error functional as a function of ϕ scan angle (ϕ_o) for $\theta_o = 0.5°$ and $\theta_o = 1.0°$.

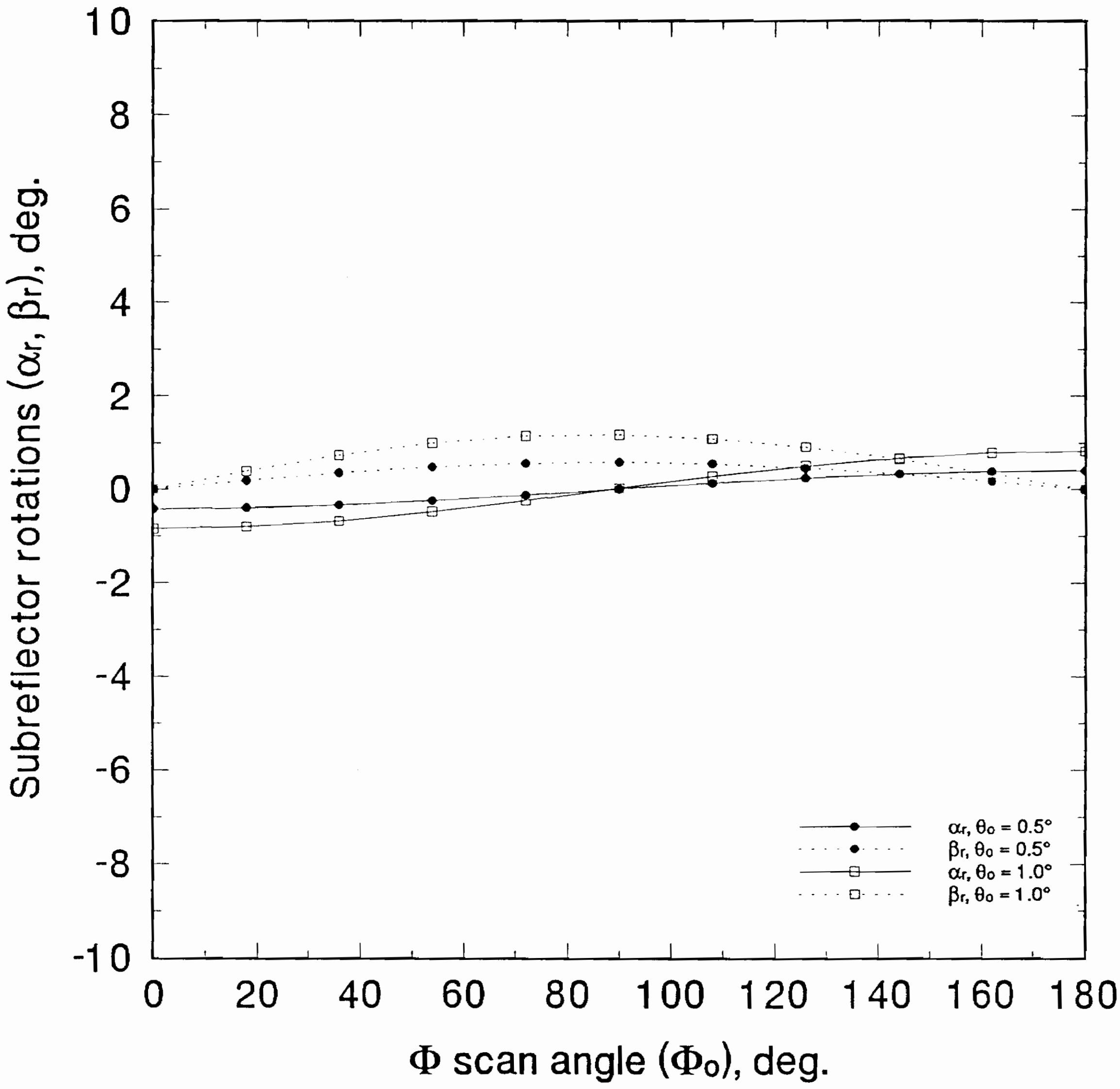

Figure 5.1.3-4. Optimum subreflector α- and β-rotations (α_r, β_r) for the test case system as determined using the correcting subreflector error functional as a function of ϕ scan angle (ϕ_o) for $\theta_o = 0.5°$ and $\theta_o = 1.0°$.

5.1.4 Computational Results using TICRA GRASP7 Physical Optics Analysis

The performance of the correcting subreflector surface fitting error functional was evaluated by performing physical optics analysis to find the far-field radiation pattern characteristics of the scanned test case geometries at 20, 40, and 80 GHz. These frequencies were chosen to allow comparison with the results for the Foldes Type 6 reflector antenna system discussed in Section 3.4. Also, the two octave frequency range assists in the determination of the reasons for pattern degradation during beam scanning.

The selection of geometrical theory of diffraction analysis at the subreflector and physical optics/surface integration analysis at the main reflector was mandated by the excessive time required for physical optics/physical optics analysis. At 20 GHz a dual physical optics analysis requires approximately 2 hours to complete on a 50 MHz 80486 computer. Furthermore, the time required for a PO/PO analysis increases roughly as the cube of the frequency. A further reduction in computing time was realized by limiting the output far-field pattern to an area on the uv-plane which contained a constant number of sidelobes with respect to frequency. This reduction in the output pattern area allowed the number of integration points in the main reflector surface integration to remain constant rather than quadrupling with each octave increase in frequency.

Figure 5.1.4-1 shows the gain, G, of the test case reflector antenna system as a function of scan angle in the plane of offset, θ_o. As expected, the unscanned gain increases 6 dB for each octave increase in frequency indicating no loss of efficiency with increasing frequency. However, the scan loss varies greatly with frequency indicating phase error across the aperture. The sidelobe level, SLL, of the test case is shown in Figure 5.1.4-2 as a function of scan angle in the plane of offset, θ_o. The sudden changes in sidelobe level at the higher frequencies are caused by sidelobes blending with the main lobe and indicate that significant phase errors are occurring.

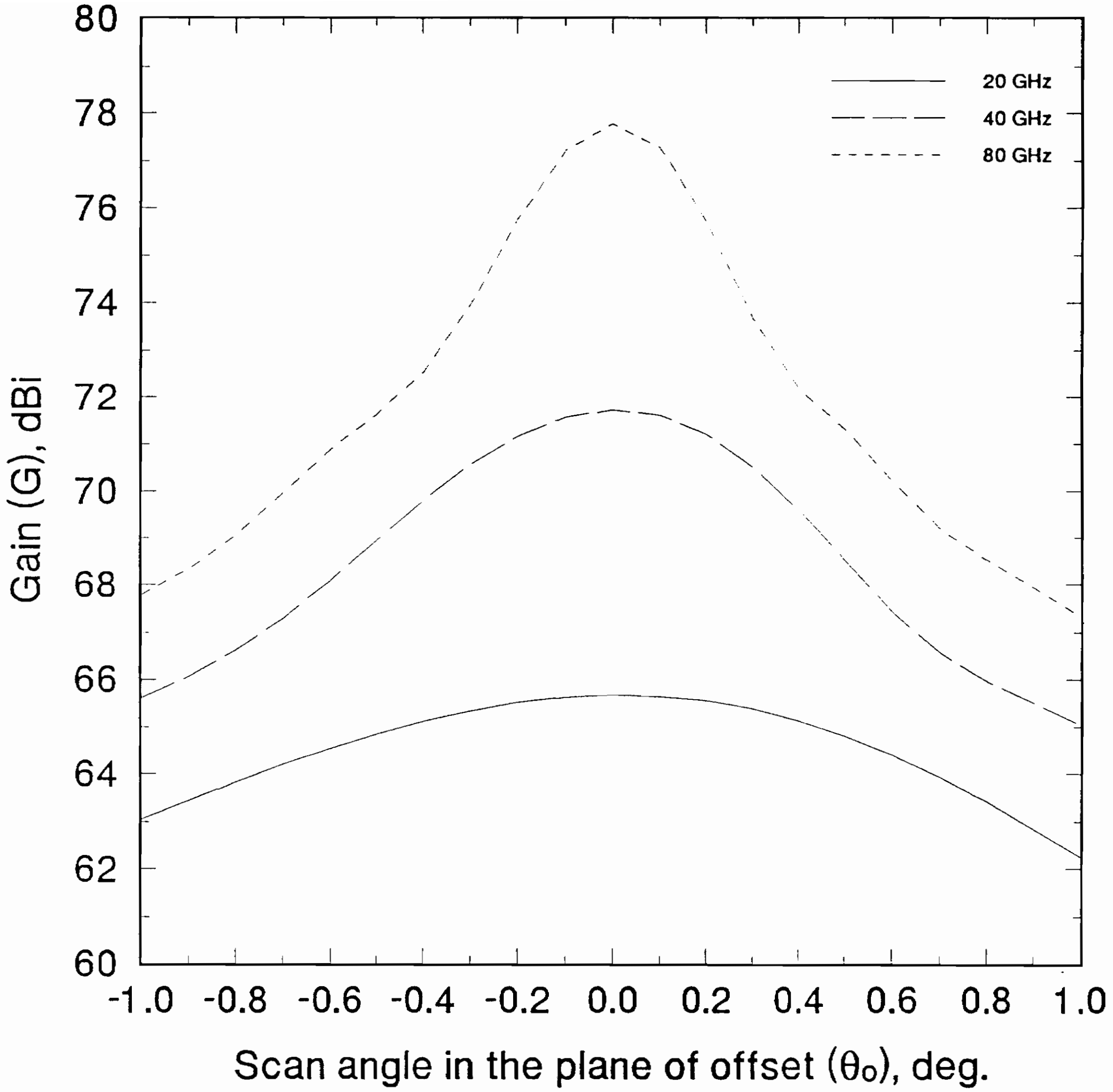

Figure 5.1.4-1. Gain (G) of the test case system as a function of scan angle in the plane of offset (θ_o) for optimized scanning using the correcting subreflector surface fitting error functional.

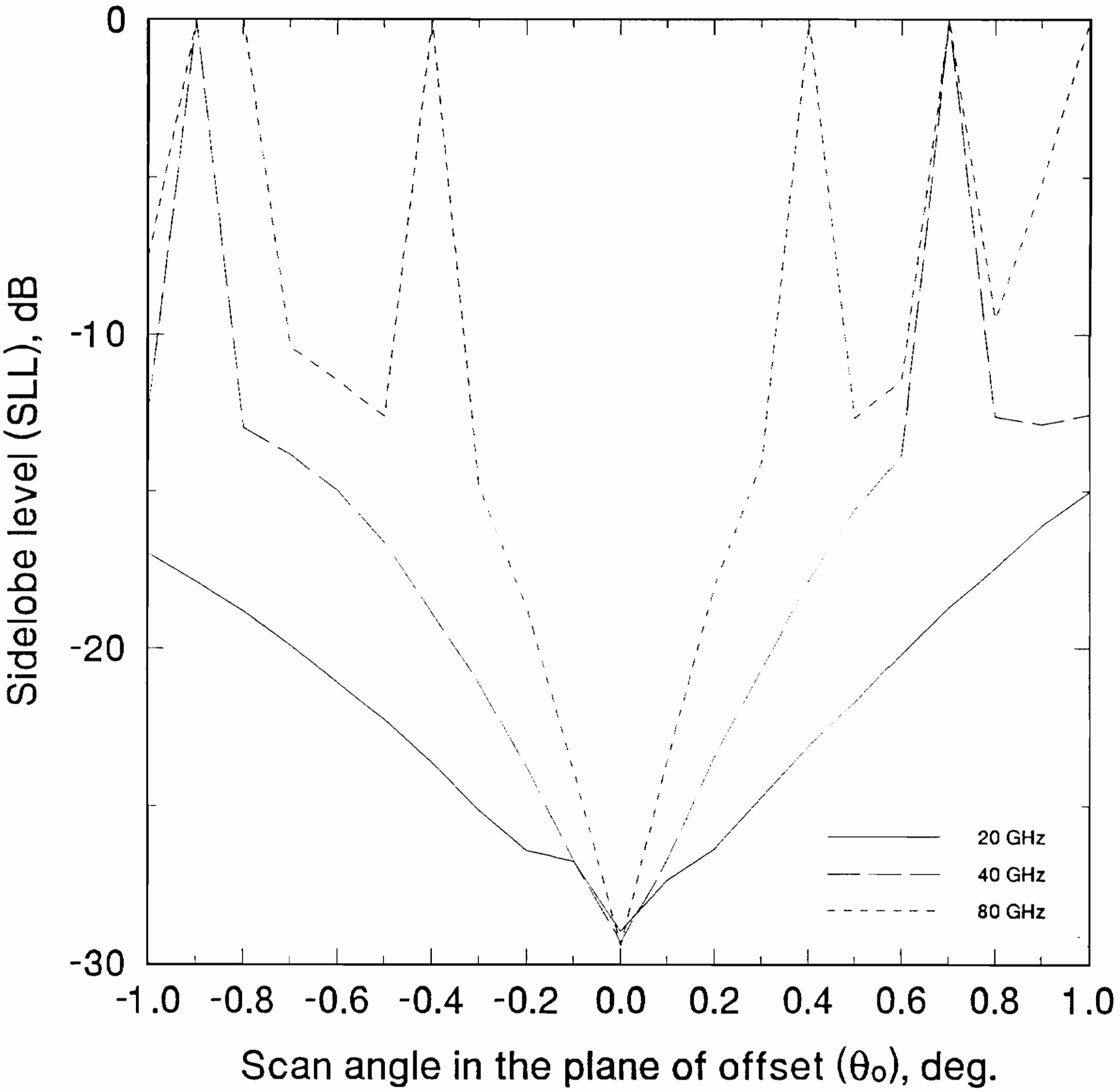

Figure 5.1.4-2. Sidelobe level (SLL) of the test case system as a function of scan angle in the plane of offset (θ_o) for optimized scanning using the correcting subreflector surface fitting error functional.

The cross-polarization level, XPOL, of the test case, shown in Figure 5.1.4-3, is below -50 dB at all three frequencies. The beam efficiency, BE, of the test case is shown in Figure 5.1.4-4. Since the 90% beam efficiency point is taken to be the limit of scan, the test case has a scan range of 0.86° at 20 GHz, 0.42° at 40 GHz, and 0.22° at 80 GHz.

The aperture efficiency, ε_{ap}, of the test case system is shown in Figure 5.1.4-5. Figure 5.1.4-6 shows the spillover efficiency, ε_{sp}, of the scanned test case system. The feed mispointing results of Section 3.1.1 were used with the aperture efficiency and spillover efficiencies to approximate the illumination amplitude and phase efficiencies, ε_{amp} and ε_{ϕ}, of the test case system. These results, shown in Figure 5.1.4-7 and 5.1.4-8, suggest that most of the scan induced pattern degradation is caused almost exclusively by phase error as expected.

Figures 5.1.4-9 through 5.1.4-16 summarize the analysis results for the constant θ scan paths. In general, these results show that the worst pattern degradation occurs for scan in the $\phi_o = 90°$ region.

5.2 The Transmit Mode Raytracing Error Functional

The transmit mode raytracing error functional determines the optimum position for the subreflector by minimizing the cross-product of the rays exiting the system with a unit vector in the desired scanned beam direction. This is equivalent to minimizing the variation in the path lengths of the rays transmitted through the system using the repositioned subreflector [5]. The transmit mode raytracing error functional is defined

$$\epsilon_{tm} = \sum_{i=1}^{M} \sum_{j=1}^{N} \left| \hat{r}_{1i,j} \times \hat{r}_D \right|^2 \tag{5.2-1}$$

where $\hat{r}_{1i,j}$ is the unit vector of the i,j th ray in the system and $\hat{r}_D$ is a unit vector in the desired scanned main beam direction. Unlike the correcting subreflector surface fitting error functional

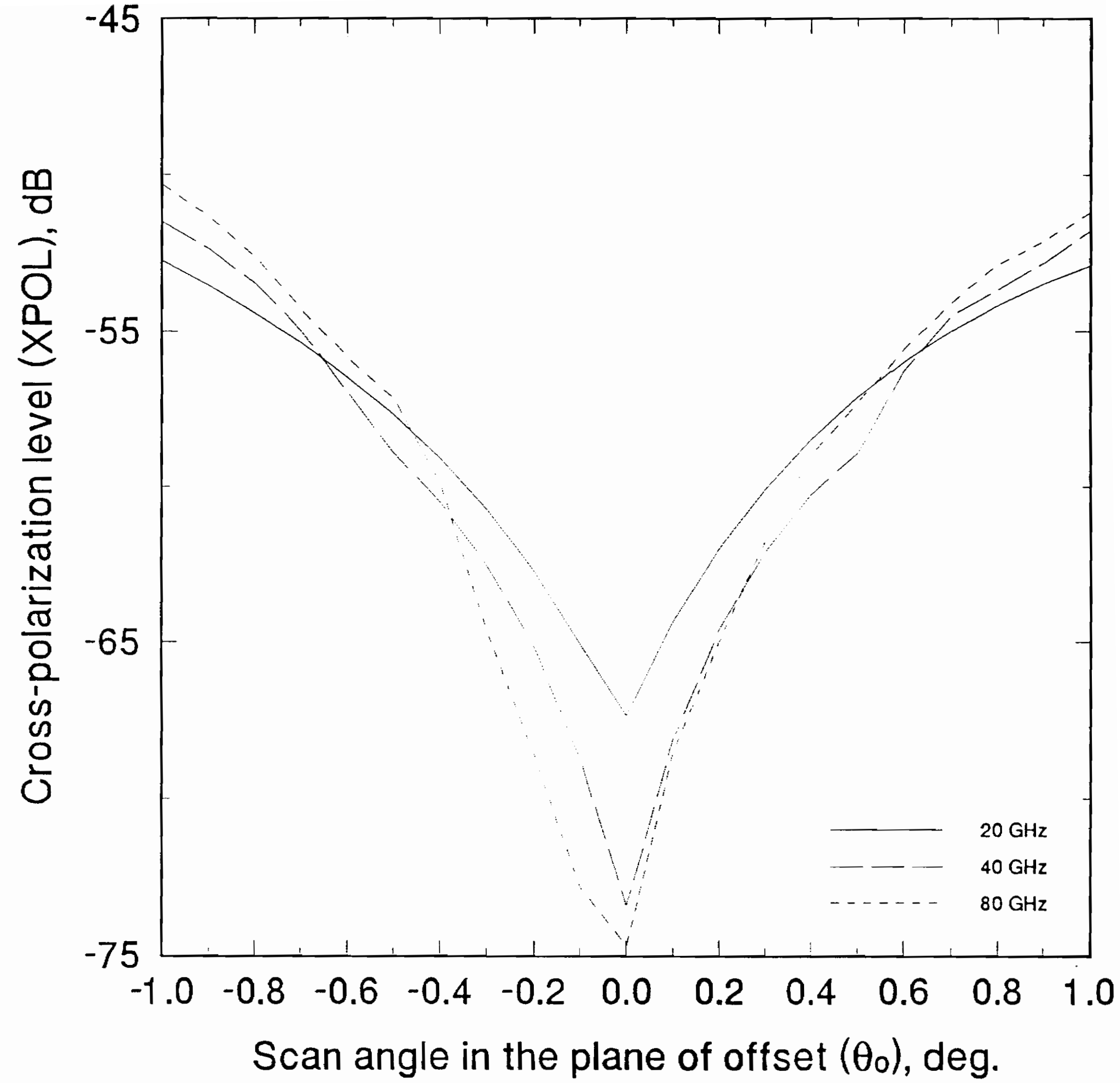

Figure 5.1.4-3. Cross-polarization level (XPOL) of the test case system as a function of scan angle in the plane of offset (θ_0) for optimized scanning using the correcting subreflector surface fitting error functional.

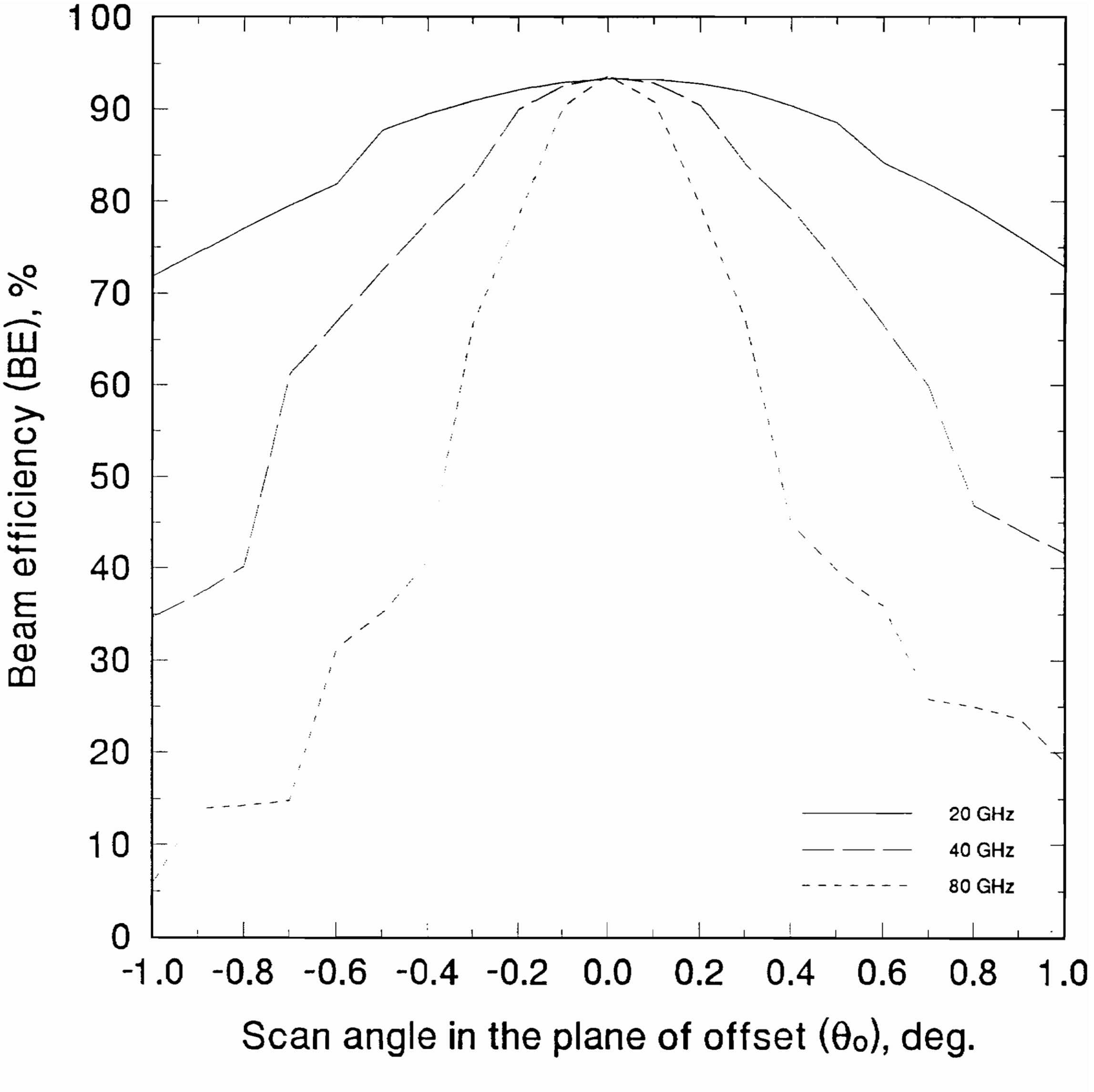

Figure 5.1.4-4. Beam efficiency (BE) of the test case system as a function of scan angle in the plane of offset (θ_o) for optimized scanning using the correcting subreflector surface fitting error functional.

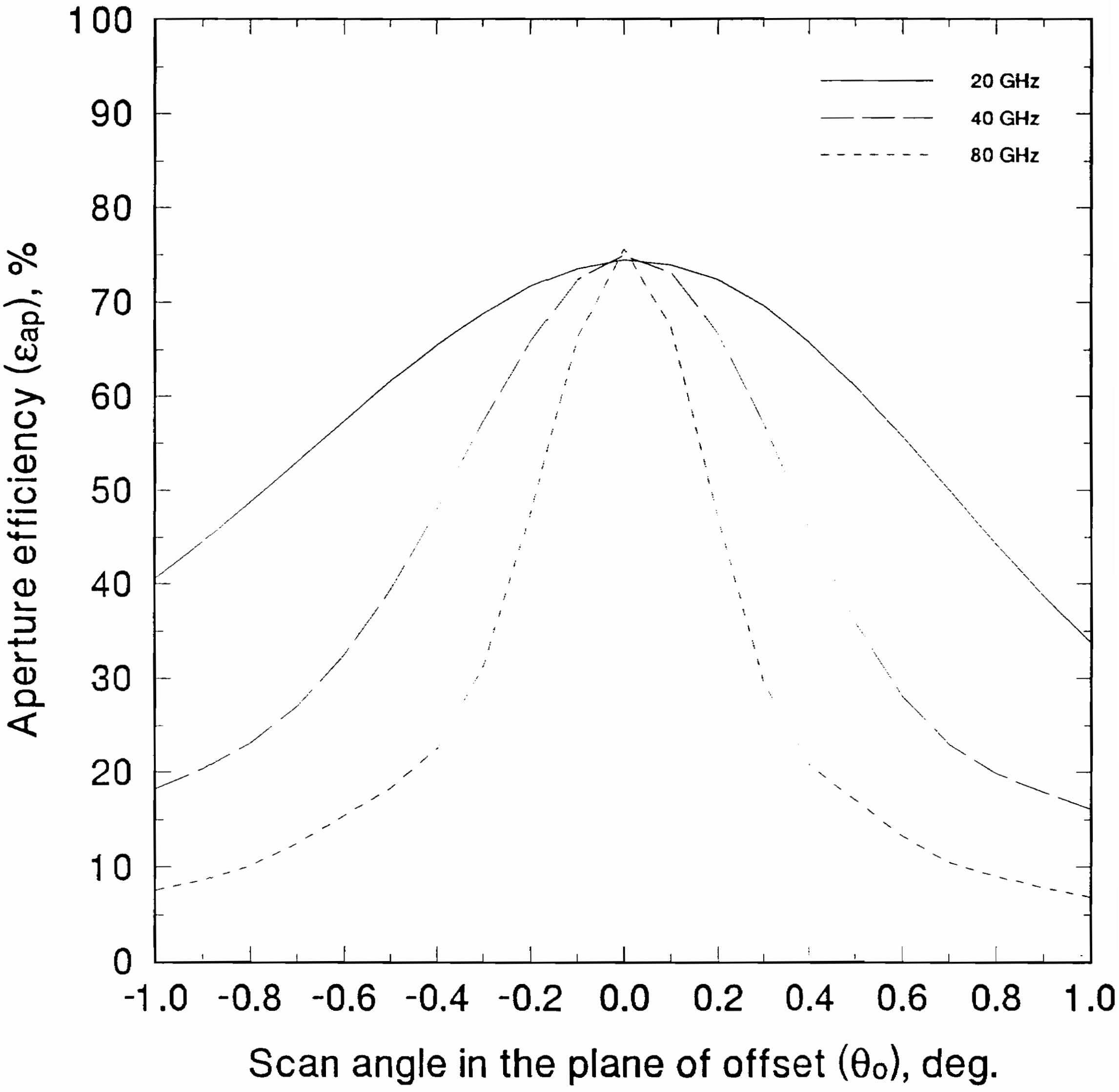

Figure 5.1.4-5. Aperture efficiency (ε_{ap}) of the test case system as a function of scan angle in the plane of offset (θ_o) for optimized scanning using the correcting subreflector surface fitting error functional.

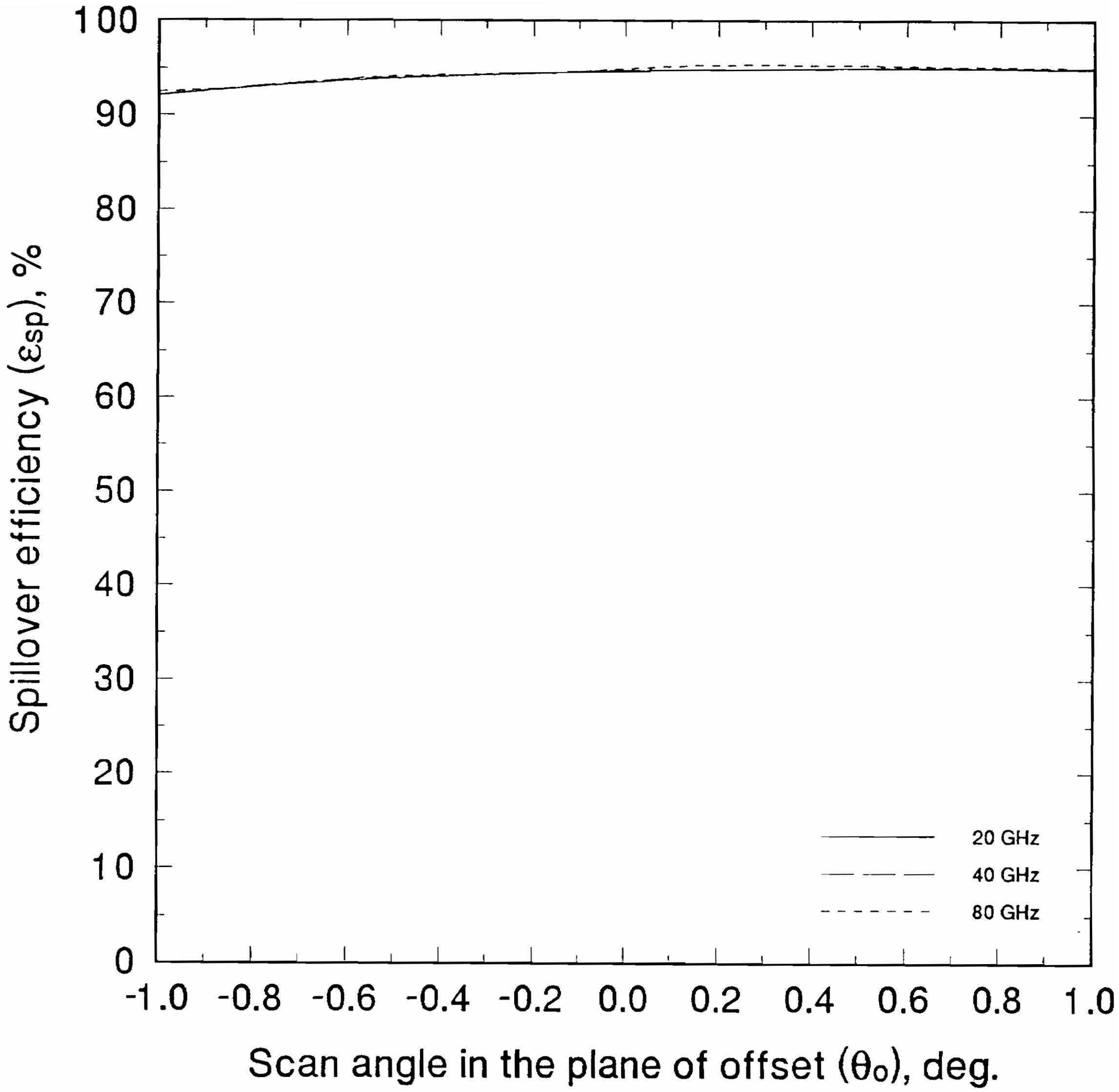

Figure 5.1.4-6. Spillover efficiency (ε_{sp}) of the test case system as a function of scan angle in the plane of offset (θ_o) for optimized scanning using the correcting subreflector surface fitting error functional.

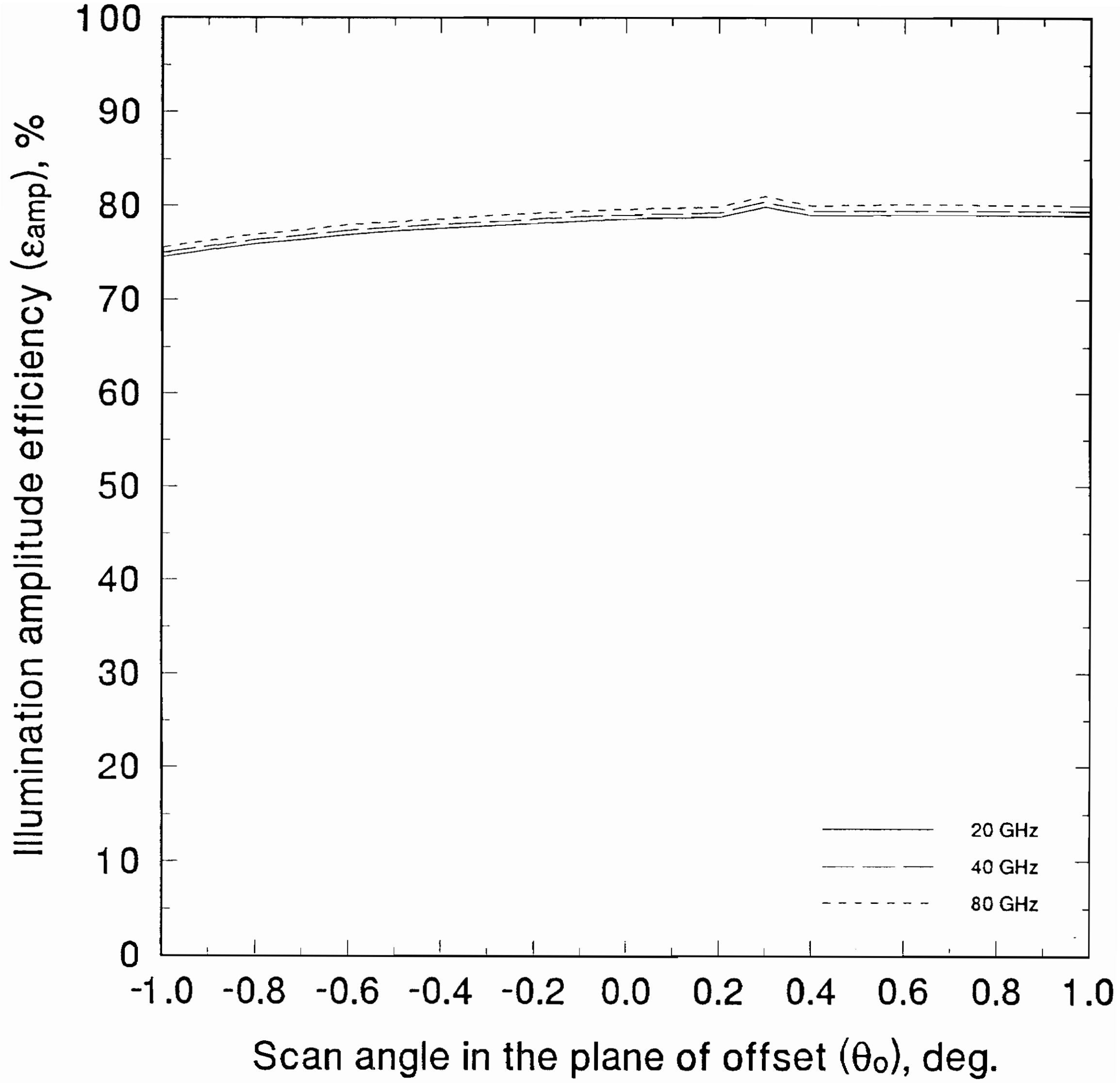

Figure 5.1.4-7. Illumination amplitude efficiency ($\varepsilon_{\mathrm{amp}}$) of the test case system as a function of scan angle in the plane of offset (θ_o) for optimized scanning using the correcting subreflector surface fitting error functional.

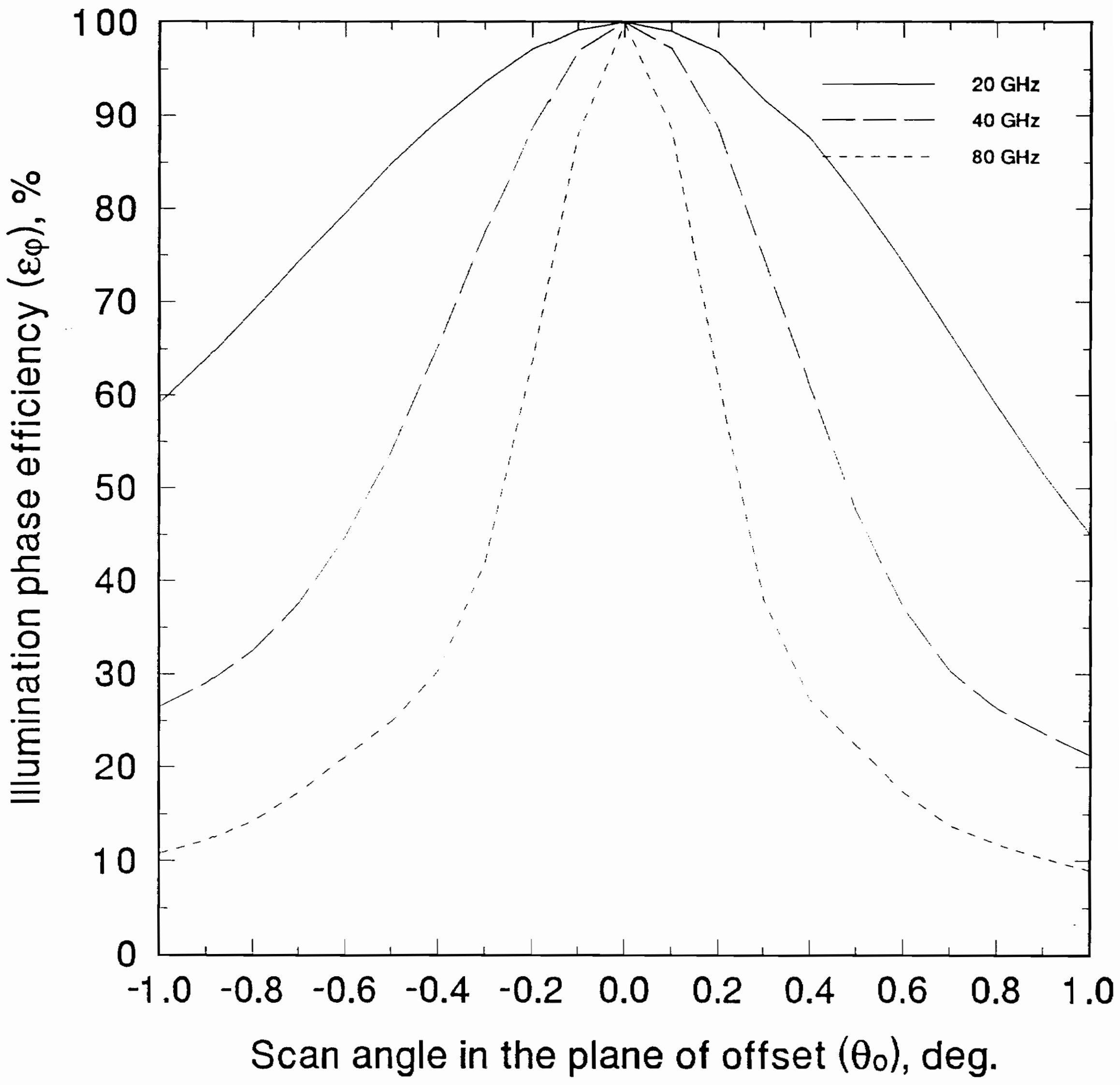

Figure 5.1.4-8. Illumination phase efficiency (ε_{ϕ}) of the test case system as a function of scan angle in the plane of offset (θ_o) for optimized scanning using the correcting subreflector surface fitting error functional.

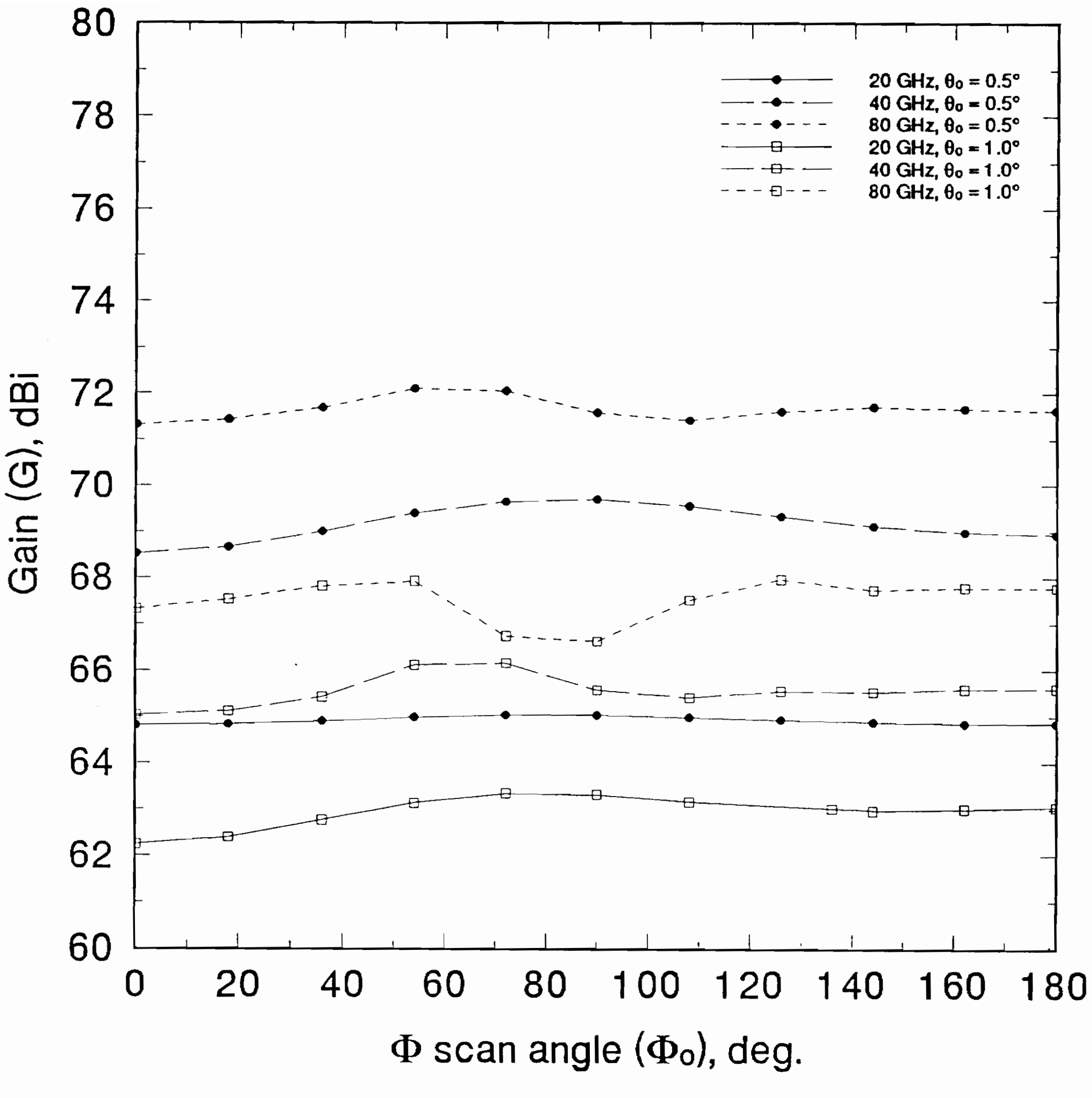

Figure 5.1.4-9. Gain (G) of the test case system as a function of ϕ scan angle (ϕ_o) for $\theta_o = 0.5°$ and $\theta_o = 1.0°$ for optimized scanning using the correcting subreflector surface fitting error functional.

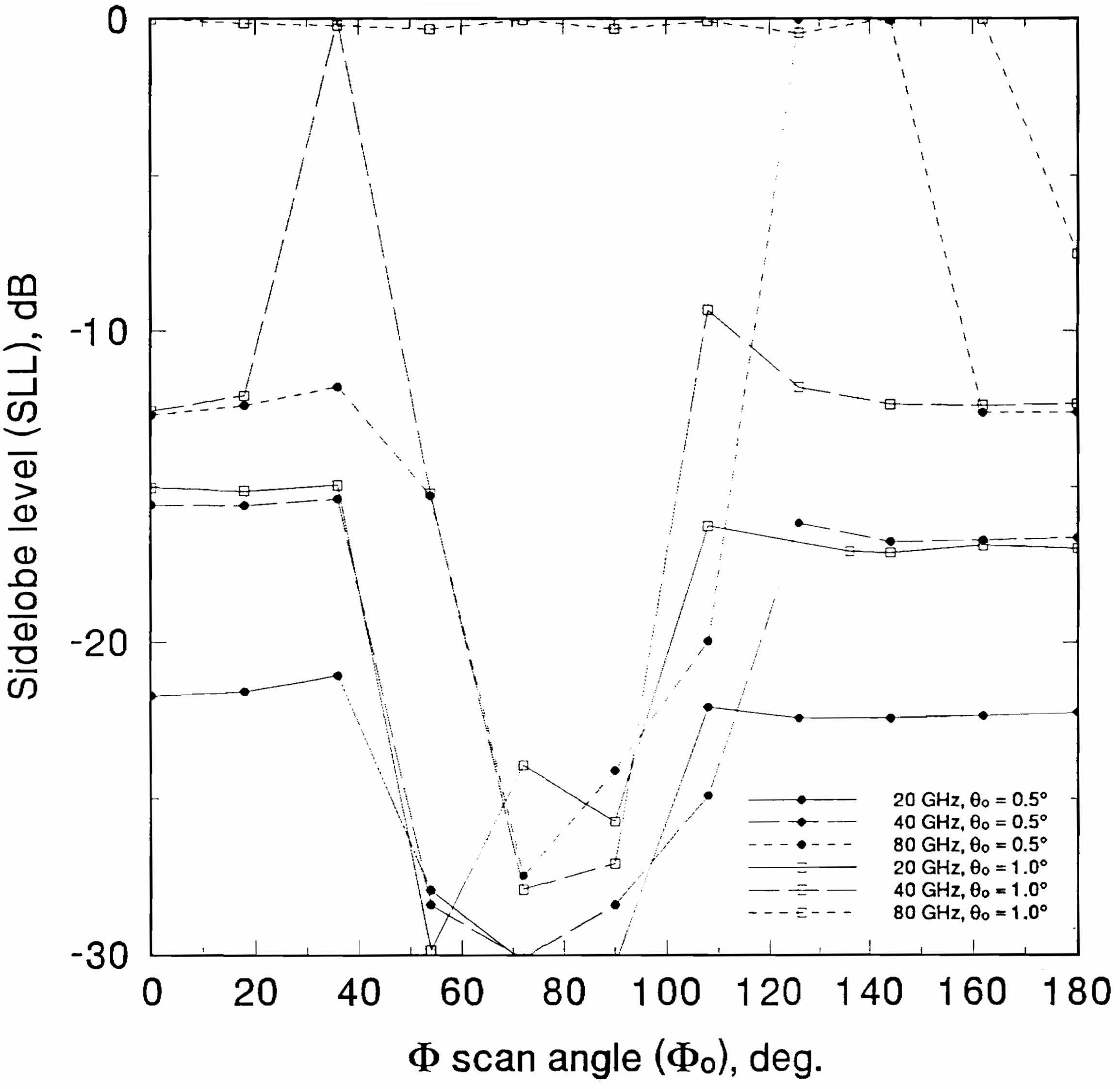

Figure 5.1.4-10. Sidelobe level (SLL) of the test case system as a function of ϕ scan angle (ϕ_o) for $\theta_o = 0.5°$ and $\theta_o = 1.0°$ for optimized scanning using the correcting subreflector surface fitting error functional.

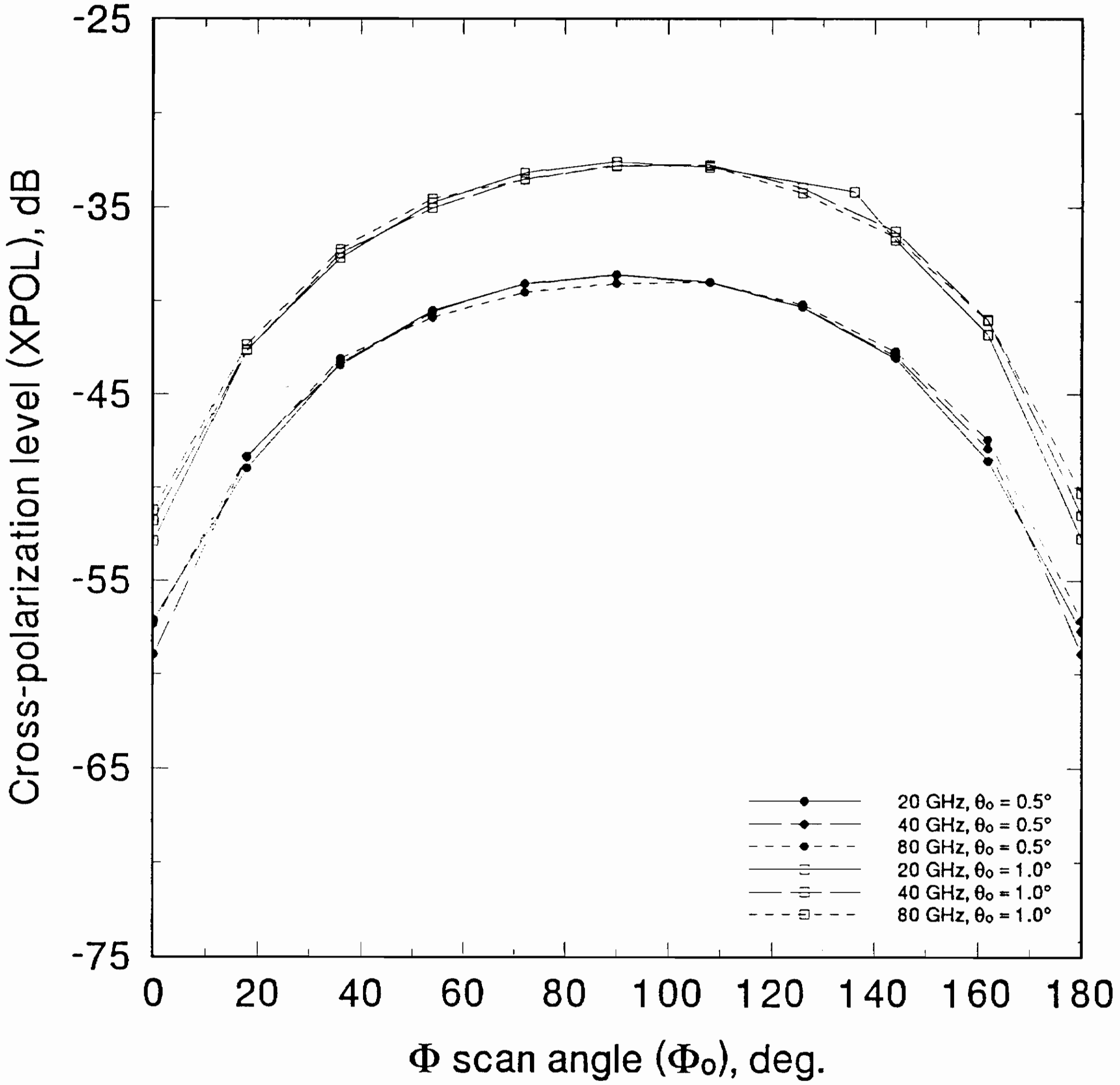

Figure 5.1.4-11. Cross-polarization level (XPOL) of the test case system as a function of ϕ scan angle (ϕ_o) for $\theta_o = 0.5°$ and $\theta_o = 1.0°$ for optimized scanning using the correcting subreflector surface fitting error functional.

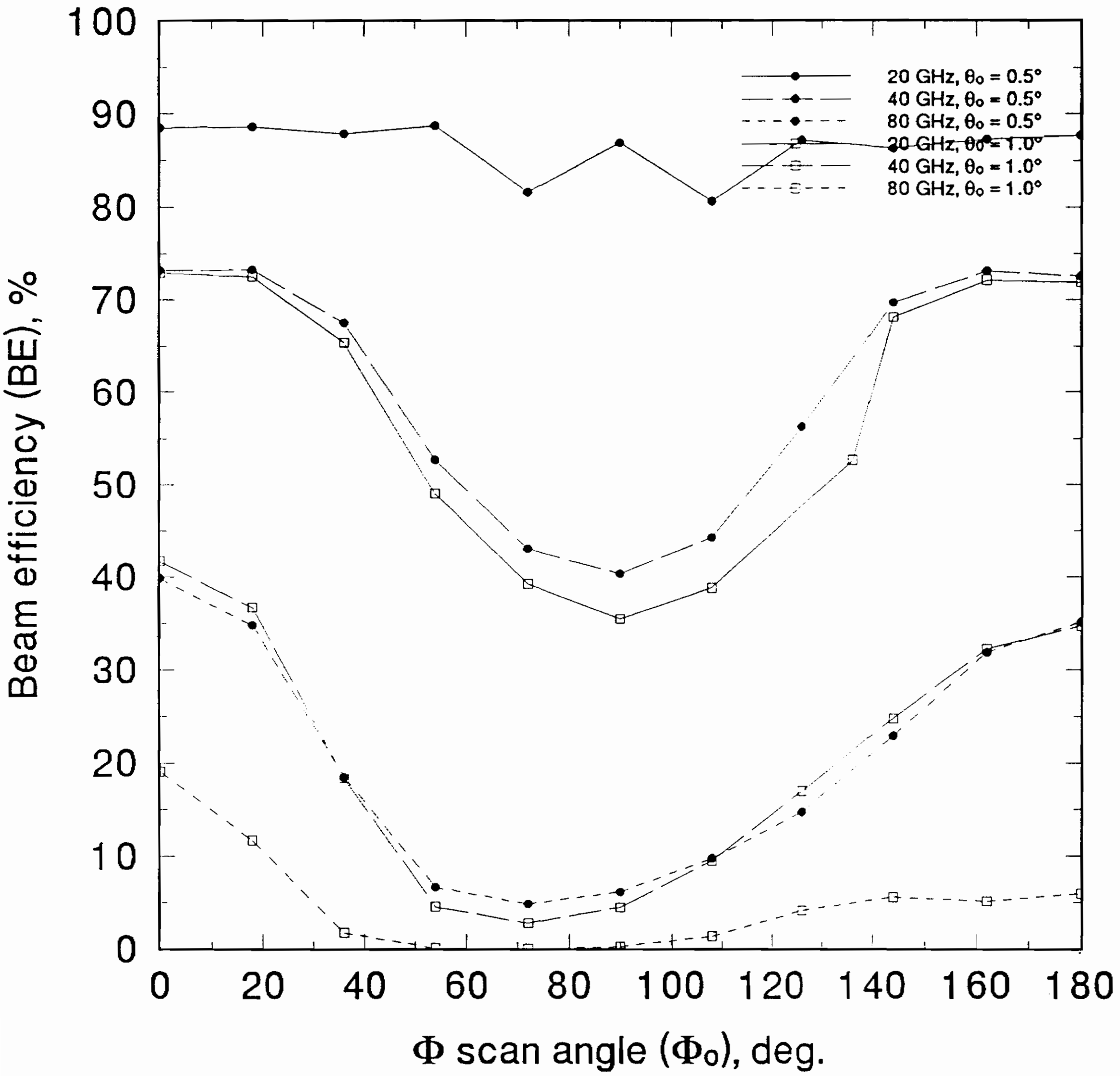

Figure 5.1.4-12. Beam efficiency (BE) of the test case system as a function of ϕ scan angle (ϕ_o) for $\theta_o = 0.5°$ and $\theta_o = 1.0°$ for optimized scanning using the correcting subreflector surface fitting error functional.

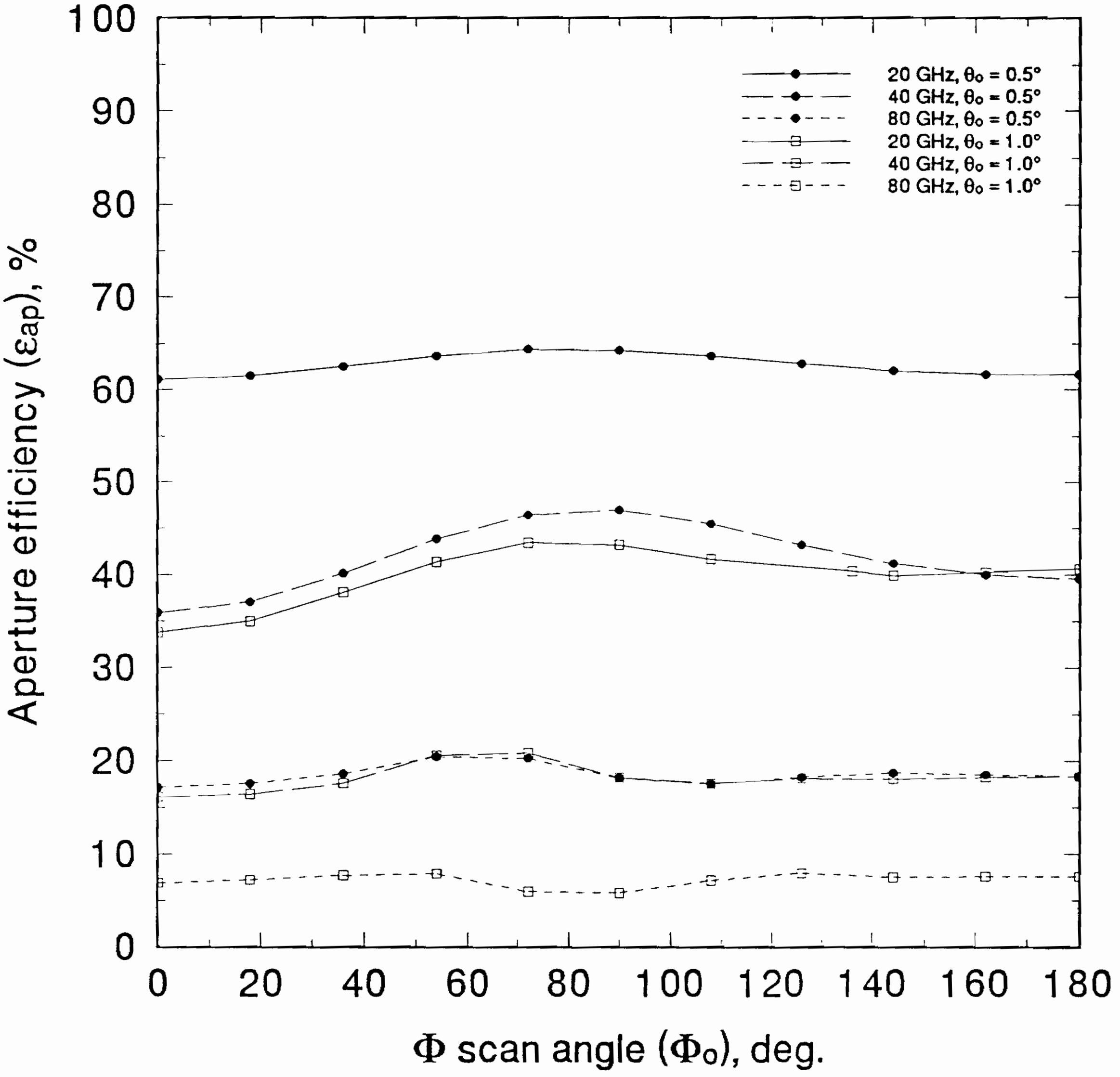

Figure 5.1.4-13. Aperture efficiency (ε_{ap}) of the test case system as a function of ϕ scan angle (ϕ_o) for $\theta_o = 0.5°$ and $\theta_o = 1.0°$ for optimized scanning using the correcting subreflector surface fitting error functional.

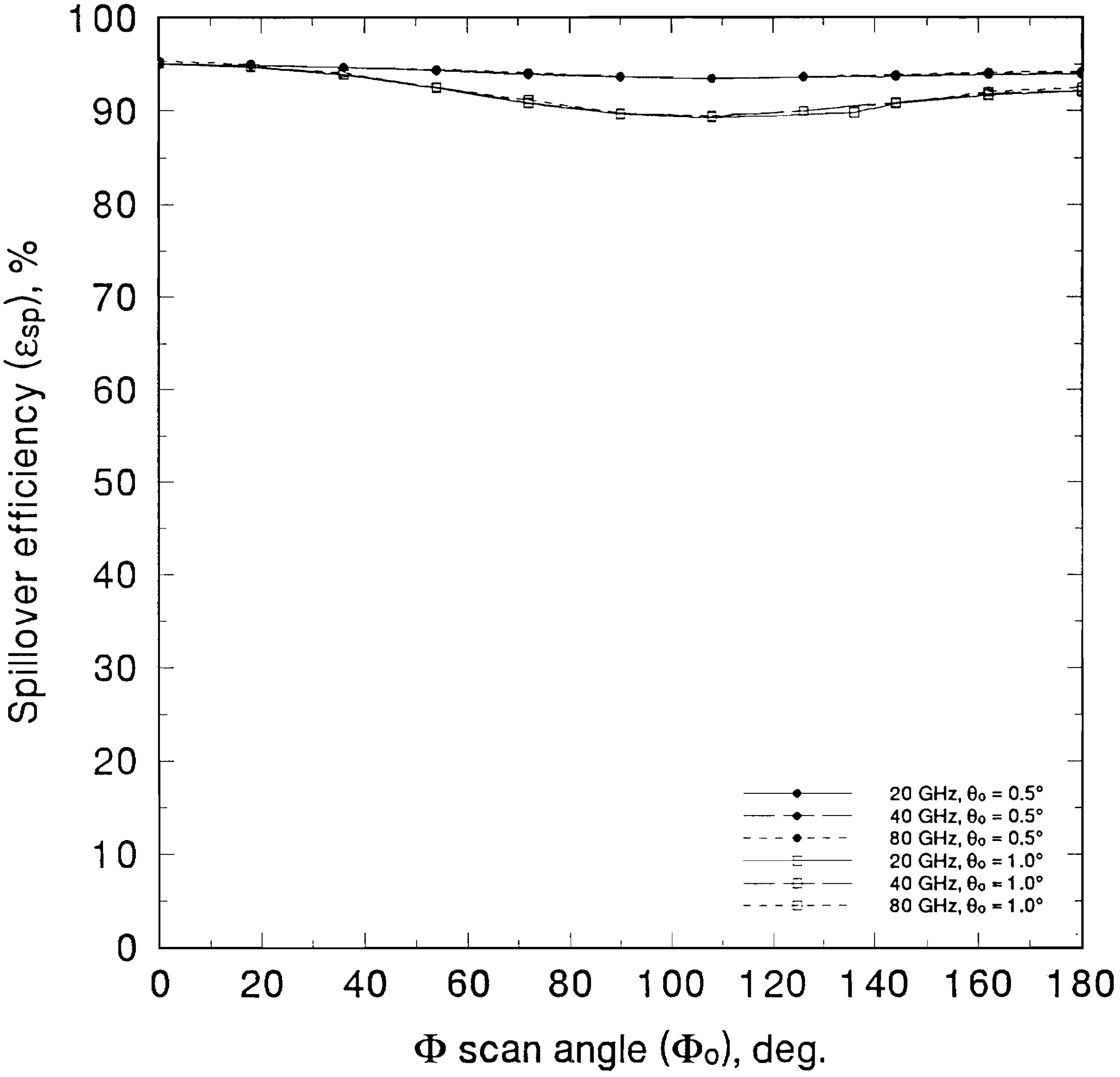

Figure 5.1.4-14. Spillover efficiency (ε_{sp}) of the test case system as a function of ϕ scan angle (ϕ_o) for $\theta_o = 0.5°$ and $\theta_o = 1.0°$ for optimized scanning using the correcting subreflector surface fitting error functional.

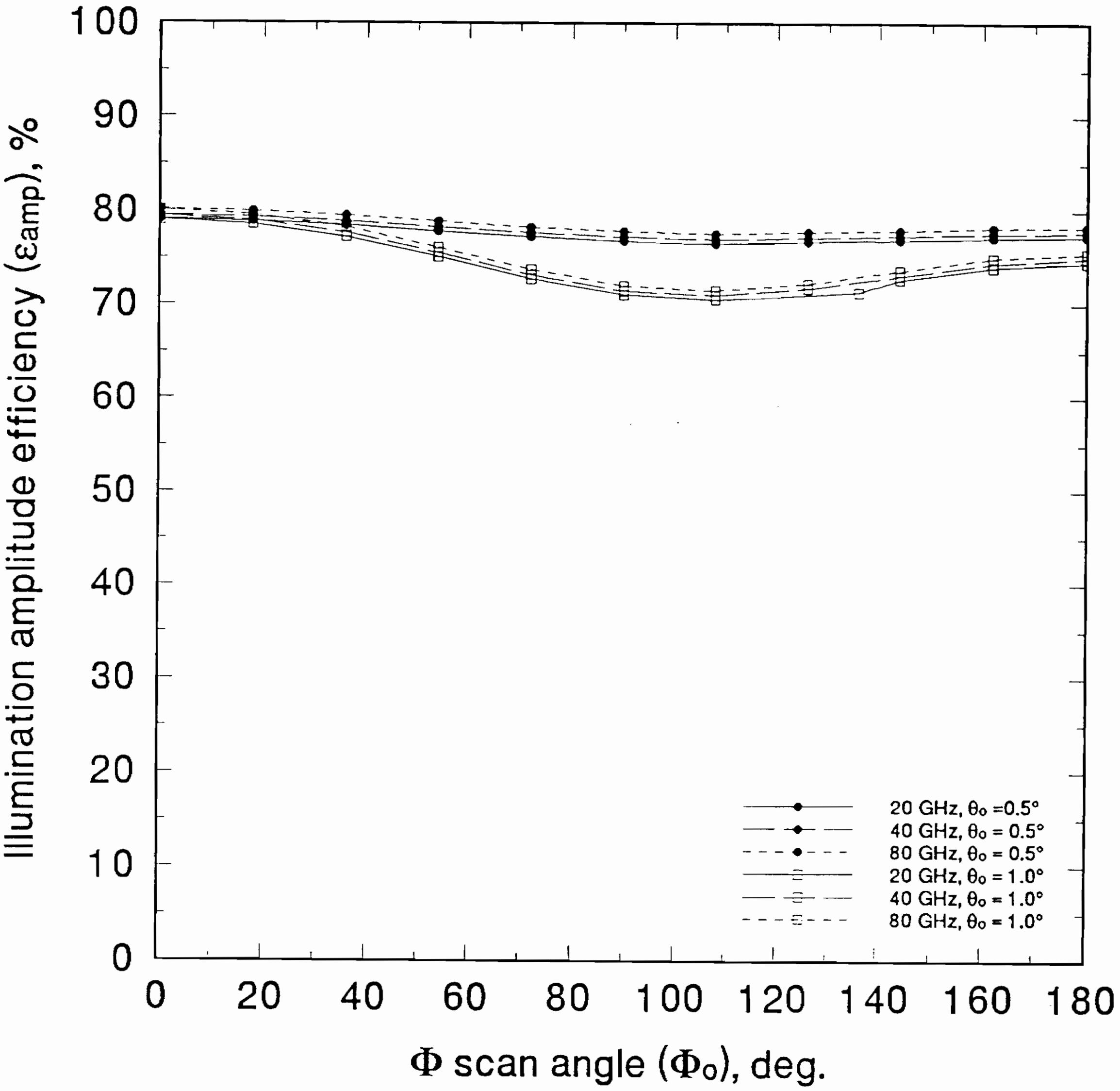

Figure 5.1.4-15. Illumination amplitude efficiency ($\varepsilon_{\mathrm{amp}}$) of the test case system as a function of ϕ scan angle (ϕ_{o}) for $\theta_{\mathrm{o}} = 0.5^{\circ}$ and $\theta_{\mathrm{o}} = 1.0^{\circ}$ for optimized scanning using the correcting subreflector surface fitting error functional.

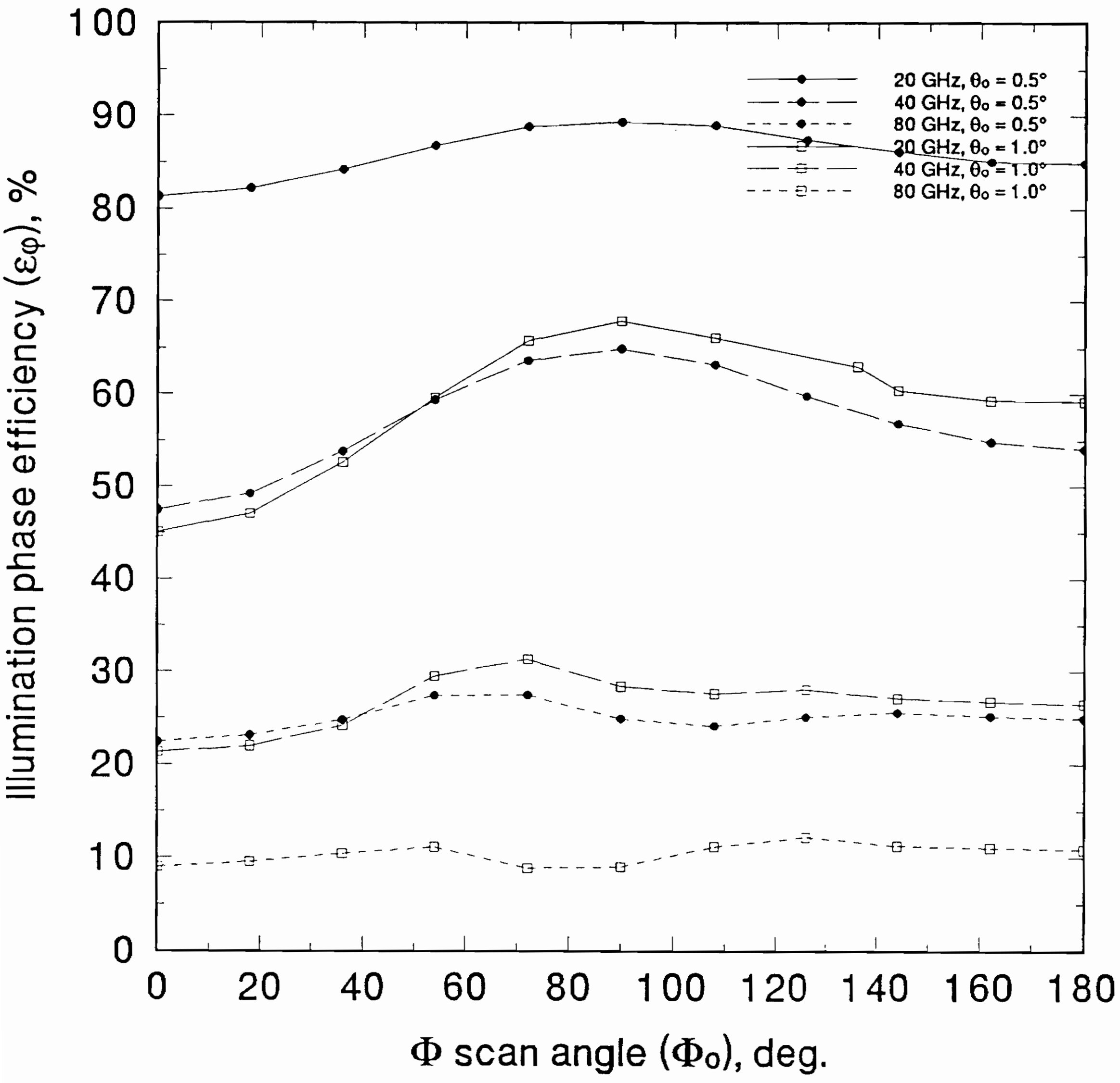

Figure 5.1.4-16. Illumination phase efficiency (ε_ϕ) of the test case system as a function of ϕ scan angle (ϕ_o) for $\theta_o = 0.5°$ and $\theta_o = 1.0°$ for optimized scanning using the correcting subreflector surface fitting error functional.

which emphasizes illumination amplitude error, this error functional evaluates only illumination phase error to provide an estimate of scanned pattern degradation.

5.2.1 Transmit Mode Raytracing Optimization Implementation - TMRT1

Optimization of the subreflector motions for scanned beams is much the same for the transmit mode raytracing error functional as for the correcting subreflector surface fitting error functional. The single major difference between the optimization procedures is the elimination of the outer path length optimization loop required by the correcting subreflector surface fitting error functional. The general scheme for optimization using the transmit mode raytracing error functional is shown in Figure 5.2.1-1. First, the subreflector is positioned using (5.1.2-2a) through (5.1.2-2c) and a geometrical optics ray is traced through the system from the feed to the main reflector. Next, a ray is traced from the feed point to each of the grid points on the repositioned subreflector. The unit vector of this ray is

$$\hat{r}_3 = \left\{ \frac{x_f - x_{S'}}{|R_3|}\hat{x},\ \frac{y_f - y_{S'}}{|R_3|}\hat{y},\ \frac{z_f - z_{S'}}{|R_3|}\hat{z} \right\}. \tag{5.2.1-1}$$

where

$$|R_3| = \sqrt{(x_{S'} - x_f)^2 + (y_{S'} - y_f)^2 + (z_{S'} - z_f)^2}. \tag{5.2.1-2}$$

Snell's law is then used with this unit vector and the unit normal of the subreflector to find the unit vector of the ray from the subreflector to the main reflector, $\hat{r}_2$.

Unlike in the optimization using the Correction Subreflector Surface Fitting error functional, the main reflector is analytically defined for the transmit mode raytracing error functional. This allows an exact solution for the intersection of the ray from the subreflector with the parent paraboloid of the main reflector. The length of the ray from the subreflector to the main reflector, $|R_2|$, can be found by using the quadratic formula

$$|R_2| = \frac{\sqrt{b^2 - 4ac} - b}{2a} \tag{5.2.1-3}$$

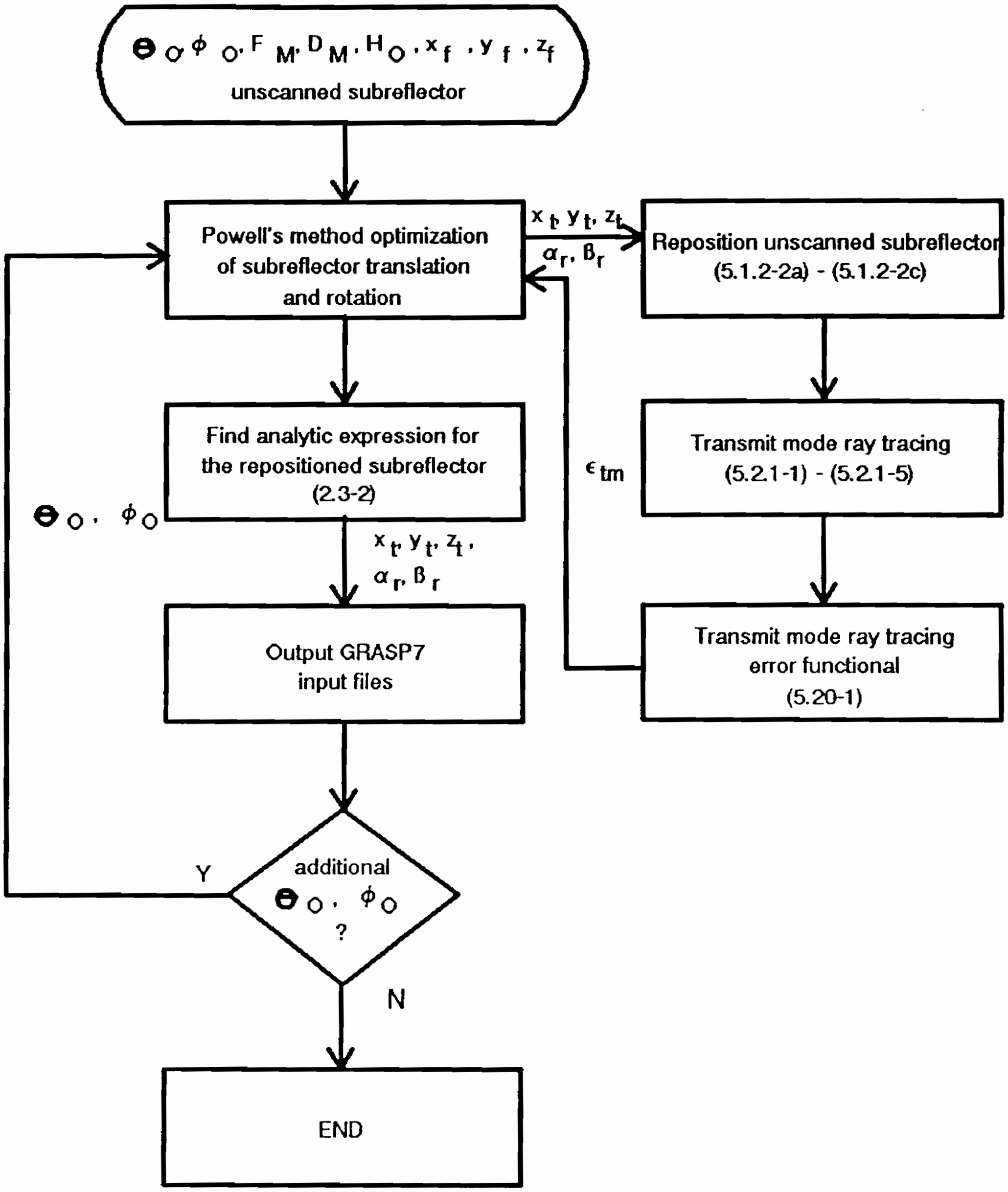

Figure 5.2.1-1. Transmit mode raytracing error functional optimization algorithm structure.

with

$$a = \hat{r}_{2x}^{\,2} + \hat{r}_{2y}^{\,2} \tag{5.2.1-4a}$$

$$b = 2\hat{r}_{2x}x_{S'} + 2\hat{r}_{2y}y_{S'} - 4\hat{r}_{2z}F \tag{5.2.1-4b}$$

$$c = x_{S'}^{\,2} + y_{S'}^{\,2} - 4z_{S'}F. \tag{5.2.1-4c}$$

The intersection of the ray and the parent paraboloid of the main reflector is then

$$M = \left\{ x_{S'} + \hat{r}_{2x}|R_2|,\ y_{S'} + \hat{r}_{2y}|R_2|,\ z_{S'} + \hat{r}_{2z}|R_2| \right\}. \tag{5.2.1-5}$$

The unit normal of the parent paraboloid of the main reflector, $\hat{n}_M$ can now be found from (2.1-11). Using this unit normal with the unit vector $\hat{r}_2$ in Snell's law gives the unit vector of the ray which is reflected from the main reflector, $\hat{r}_1$. This unit vector is calculated for each ray which is traced through the system.

The other necessary component of the transmit mode raytracing error functional is the unit vector of a ray exiting the system in the desired scan direction, $\hat{r}_D$. This unit vector is given by the negative of (5.1.1-1), the unit vector of a ray entering the system from the desired scan direction. After $\hat{r}_1$ is found for each of the rays in the system, the error is found from (5.2-1). This error is used in the Powell's method optimization which repositions the subreflector.

5.2.2 Predicted Subreflector Motions

The optimum subreflector positions were determined for the test case with the transmit mode raytracing error functional as with the correcting subreflector surface fitting error functional for three scan paths: a scan from $\theta_o = -1.0°$ to $\theta_o = 1.0°$ for $\phi_o = 0°$, a scan from $\phi_o = 0°$ to $\phi_o = 180°$ for $\theta_o = 0.5°$, and a scan from $\phi_o = 0°$ to $\phi_o = 180°$ for $\theta_o = 1.0°$. A significant decrease in the computational effort required was noted with a time of slightly less than 7 minutes per scan direction and a total time of 4 hours 29 minutes for all 39 scan directions. This is over a six-fold reduction in the optimization time required.

The required x-, y-, and z-translations for the scan path in the plane of offset are shown in Figure 5.2.2-1 as a function of scan angle in the plane of offset. The α- and β-rotations required for the scan path are shown in Figure 5.2.2-2 as a function of scan angle in the plane of offset. The scan motions produced by the transmit mode raytracing error functional are larger because the subreflector is not constrained to be located along the central ray reflected from the main reflector as in the correcting subreflector surface fitting optimization. The x-, y-, and z-translations and α- and β-rotations required for the constant θ scan paths at $\theta_o = 0.5^\circ$ and $\theta_o = 1.0^\circ$ are shown in Figures 5.2.2-3 and 5.2.2-4.

5.2.3 Computational Results using TICRA GRASP7 Physical Optics Analysis

The scanned test case systems created using the transmit mode raytracing error functional were analyzed as discussed in Section 5.1.4. Figure 5.2.3-1 shows the gain, G, of the scanned test case system as a function of scan angle in the plane of offset, θ_o. The gain increases approximately 6 dB for each octave frequency increase as with the correcting subreflector surface fitting error functional, but, the loss during scan at each frequency is essentially independent of frequency for the transmit mode raytracing error functional. This difference indicates that the scan loss is probably not being caused by illumination phase error. The low overall sidelobe levels, SLL, shown in Figure 5.2.3-2 confirm this indication. Figure 5.2.3-3 shows the cross-polarization level, XPOL, as a function of scan angle in the plane of offset, θ_o. Figure 5.2.3-4 shows the beam efficiency, BE, of the test case system when optimized for beam scanning using the transmit mode raytracing error functional. The beam efficiency produced with this optimization approach is comparable with that using the correcting subreflector surface fitting error functional of Section 5.1 at 20 GHz and much higher at the higher frequencies across the scan path. The scan range as defined by a minimum beam efficiency of 90% is 0.72° at 20 GHz, 0.82° at 40 GHz, and 0.80° at 80 GHz. This is a scan range of 35 half-power beamwidths at 80

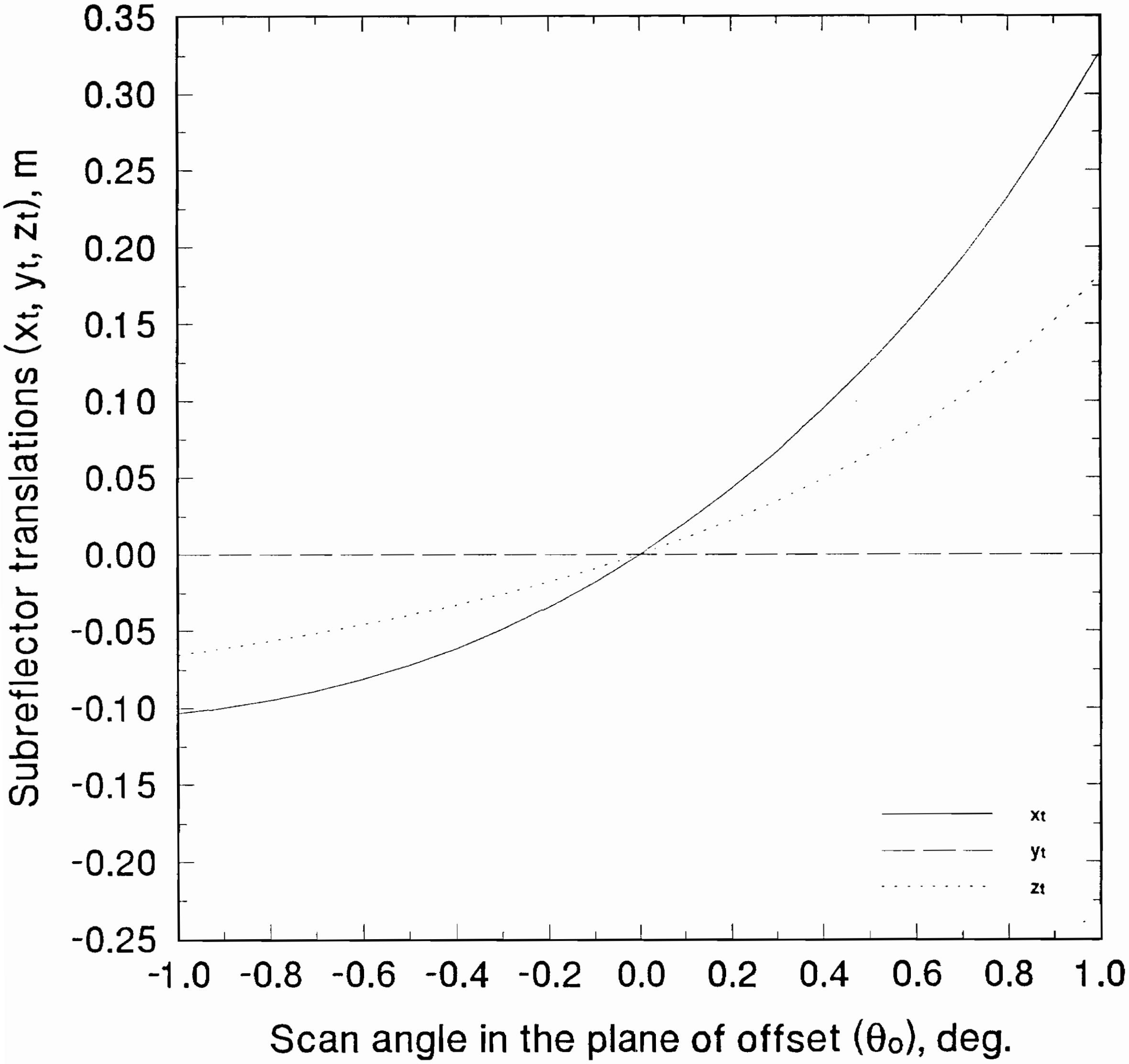

Figure 5.2.2-1. Optimum subreflector x-, y-, and z-translations (x_t, y_t, z_t) for the test case system as determined using the transmit mode raytracing error functional as a function of scan angle in the plane of offset (θ_o).

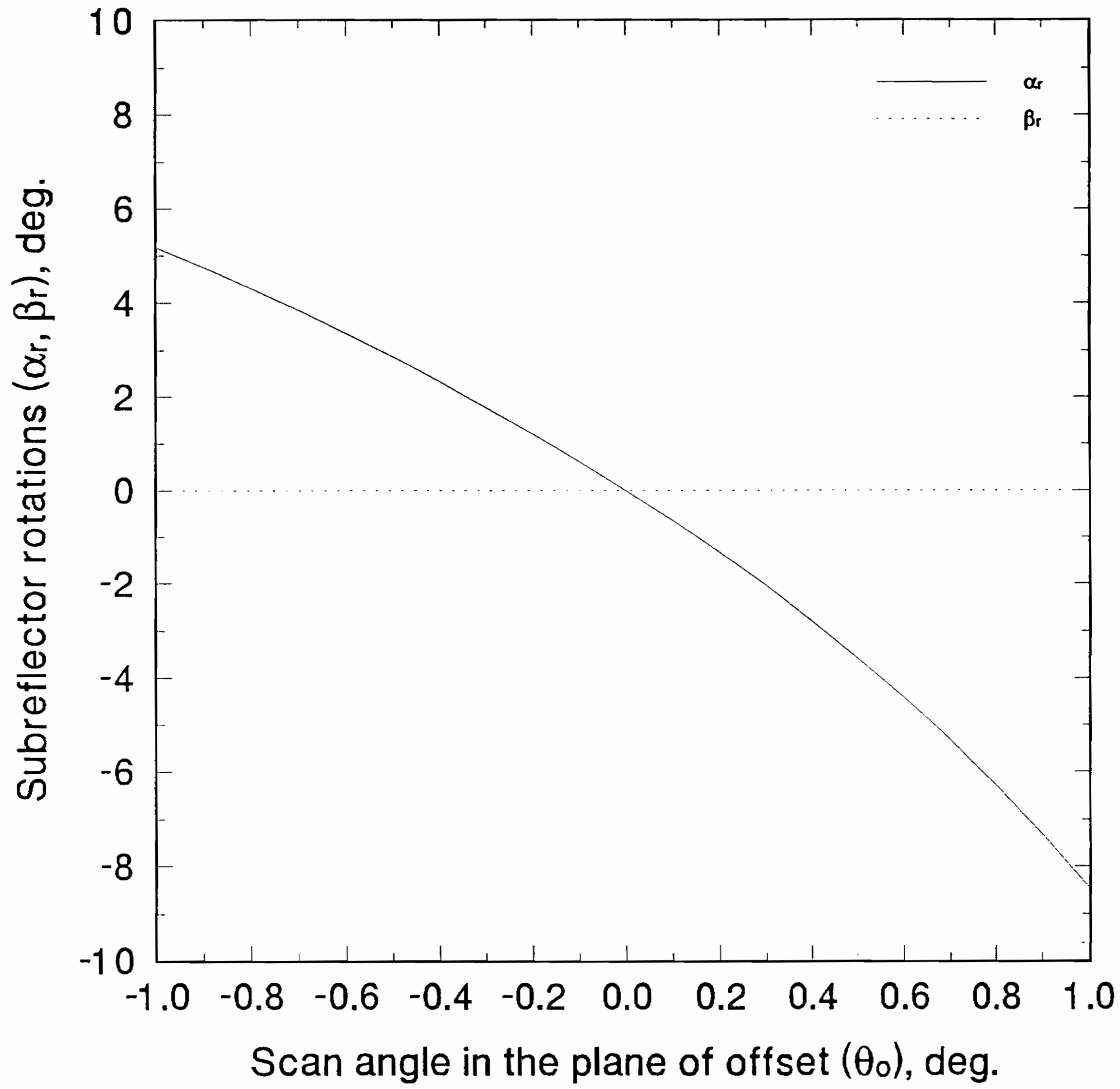

Figure 5.2.2-2. Optimum subreflector α- and β-rotations (α_r, β_r) for the test case system as determined using the transmit mode raytracing error functional as a function of scan angle in the plane of offset (θ_o).

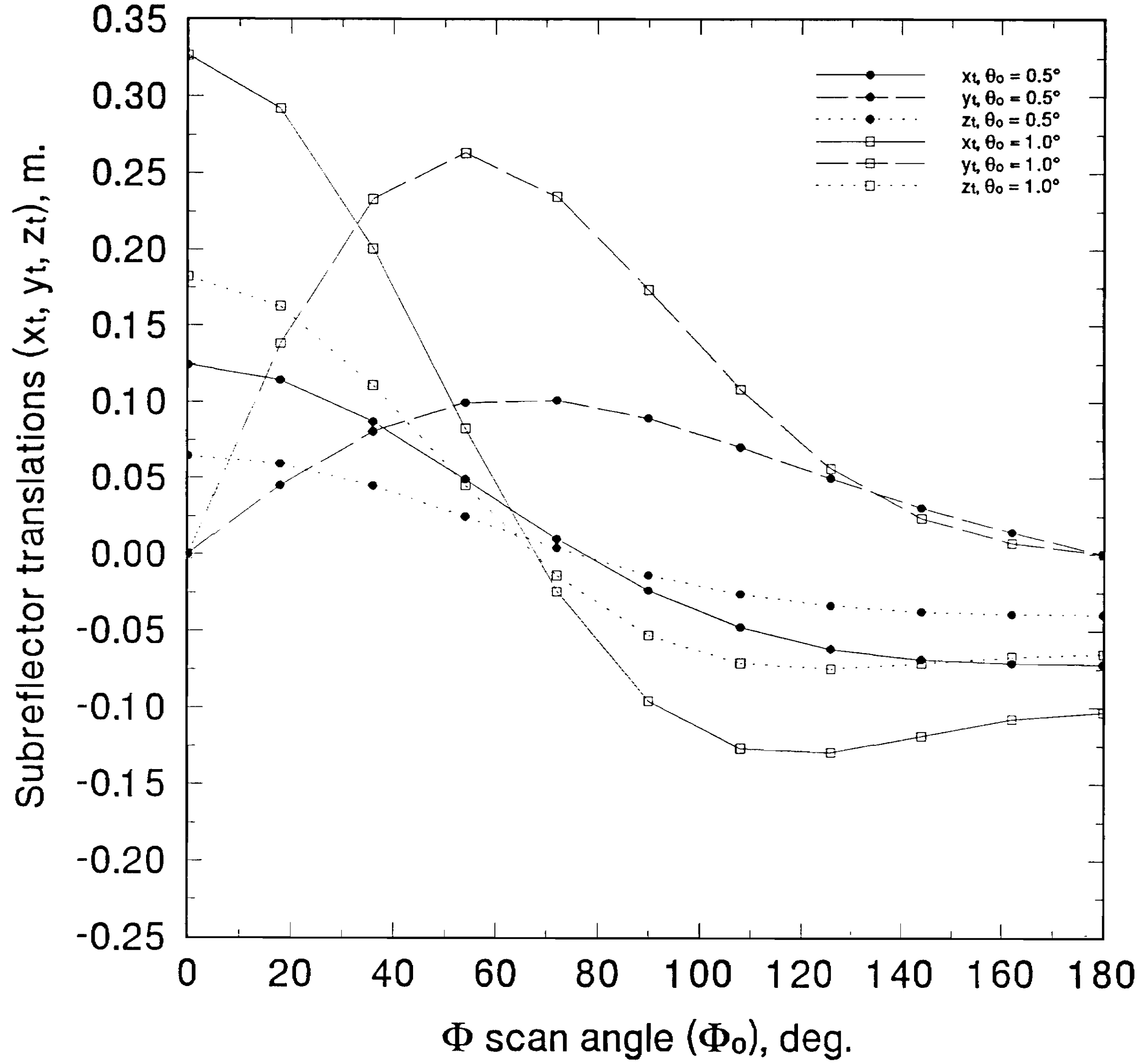

Figure 5.2.2-3. Optimum subreflector x-, y-, and z-translations (x_t, y_t, z_t) for the test case system as determined using the transmit mode raytracing error functional as a function of ϕ scan angle (ϕ_o) for $\theta_o = 0.5°$ and $\theta_o = 1.0°$.

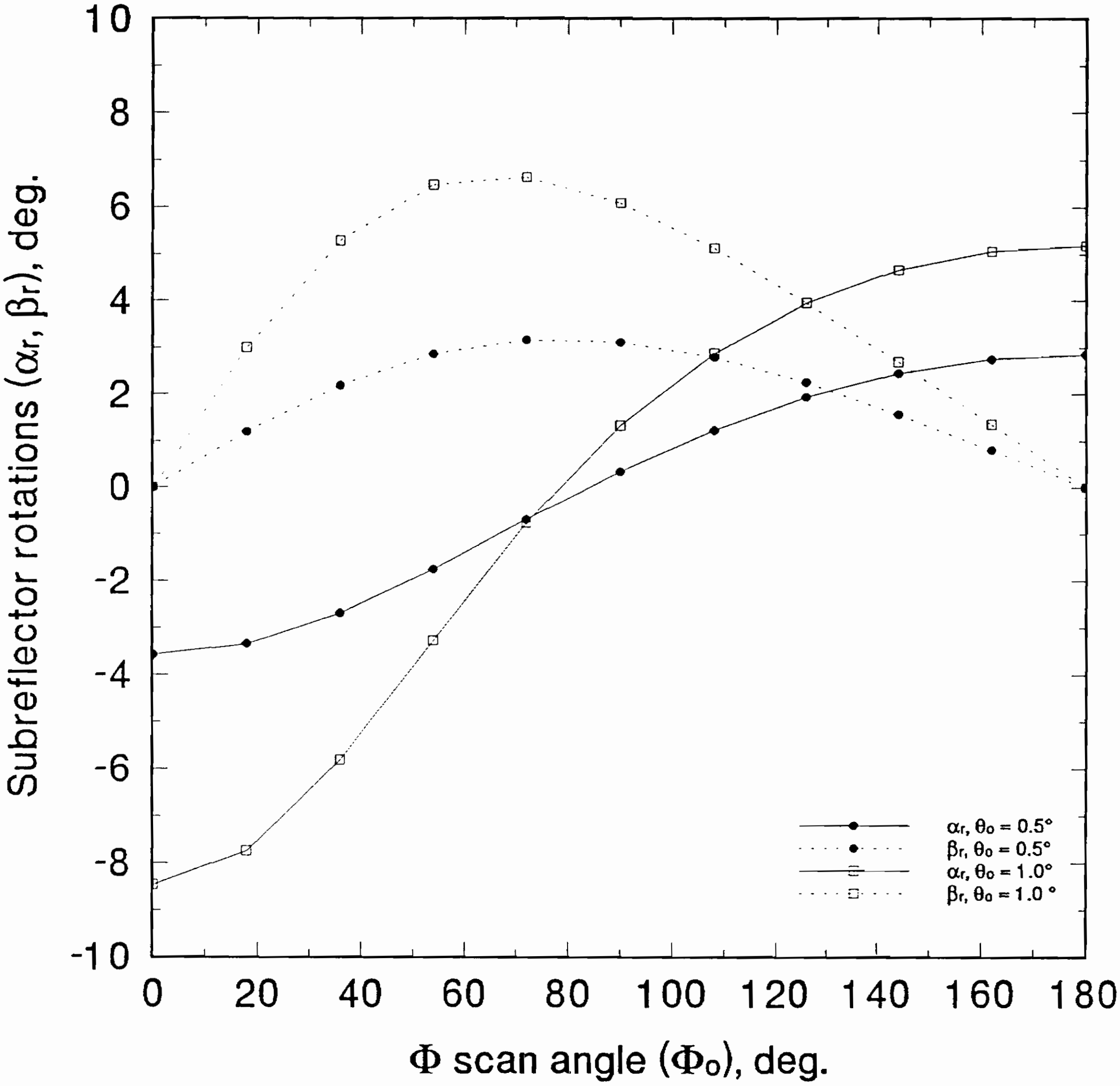

Figure 5.2.2-4. Optimum subreflector α- and β-rotations (α_r, β_r) for the test case system as determined using the transmit mode raytracing error functional as a function of ϕ scan angle (ϕ_o) for $\theta_o = 0.5°$ and $\theta_o = 1.0°$.

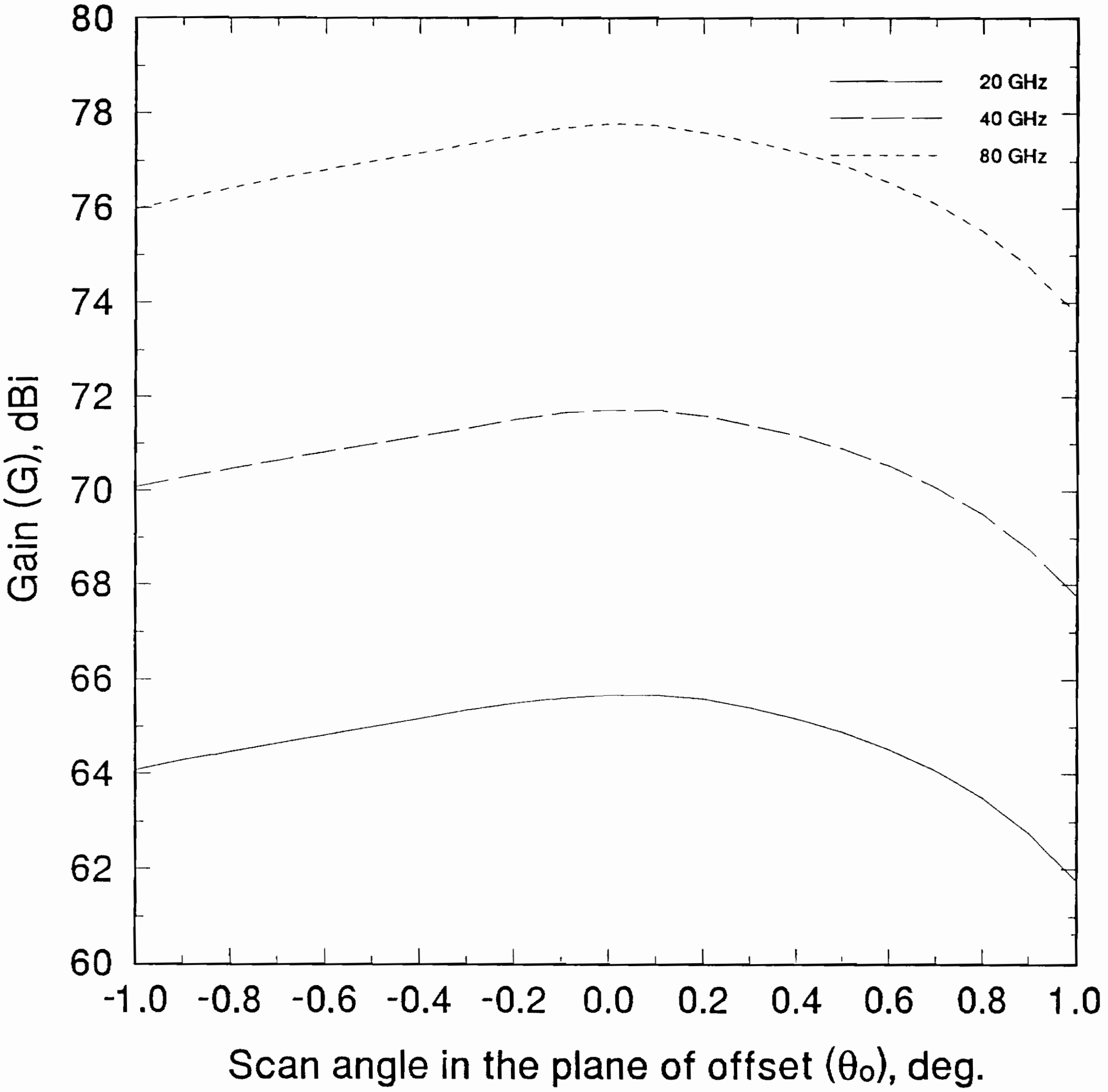

Figure 5.2.3-1. Gain (G) of the test case system as a function of scan angle in the plane of offset (θ_o) for optimized scanning using the transmit mode raytracing error functional.

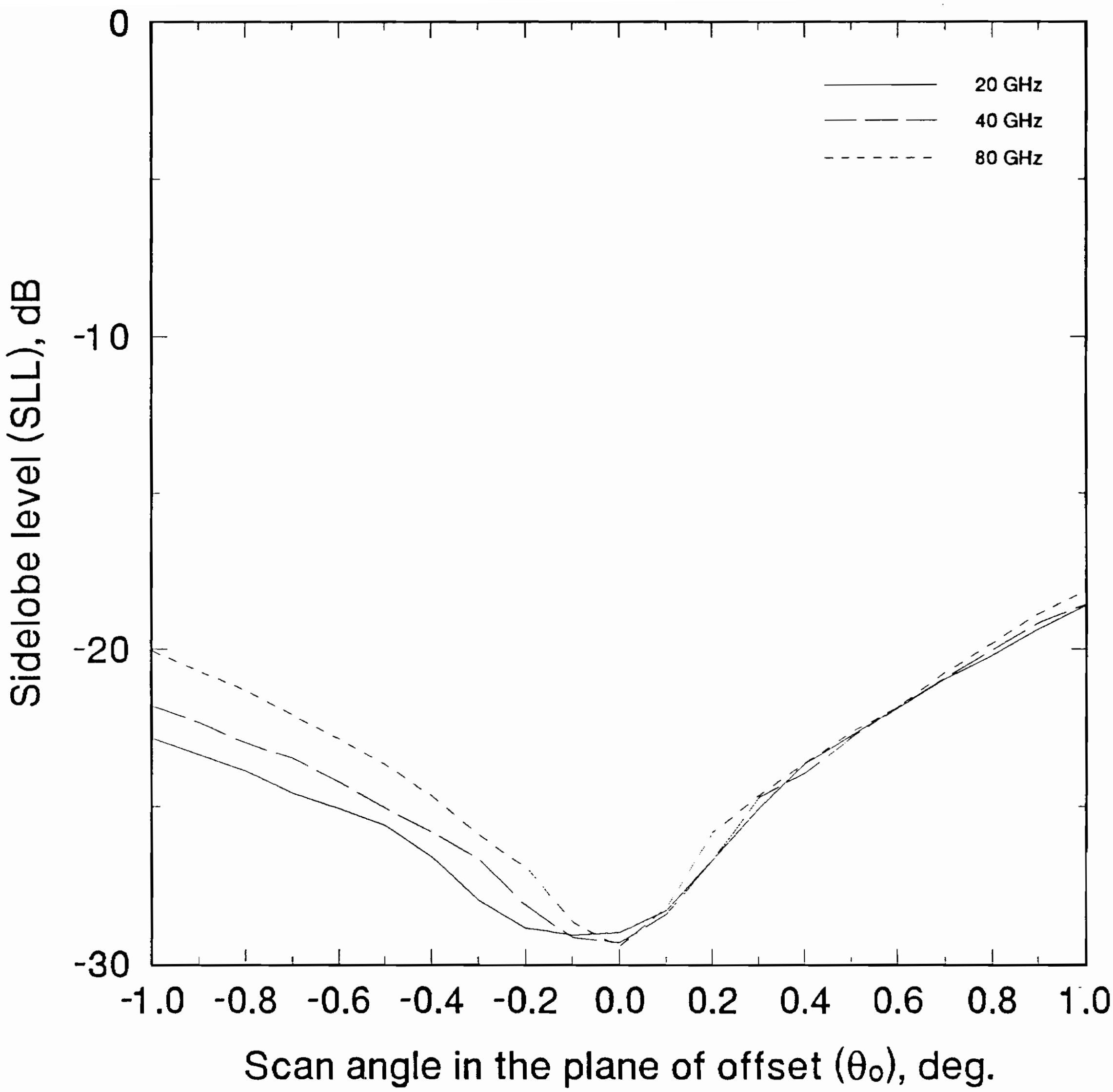

Figure 5.2.3-2. Sidelobe level (SLL) of the test case system as a function of scan angle in the plane of offset (θ_0) for optimized scanning using the transmit mode raytracing error functional.

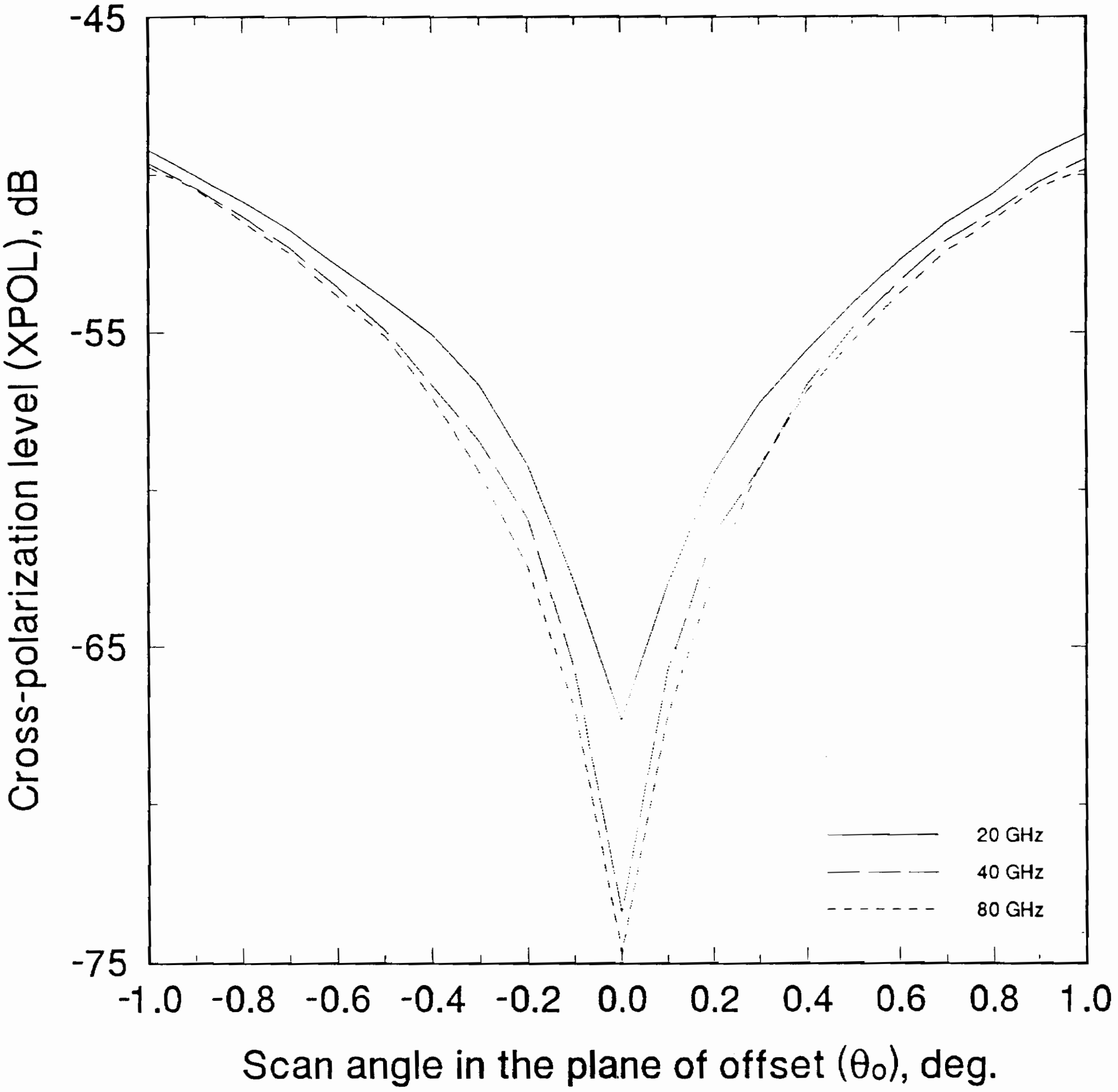

Figure 5.2.3-3. Cross-polarization level (XPOL) of the test case system as a function of scan angle in the plane of offset (θ_0) for optimized scanning using the transmit mode raytracing error functional.

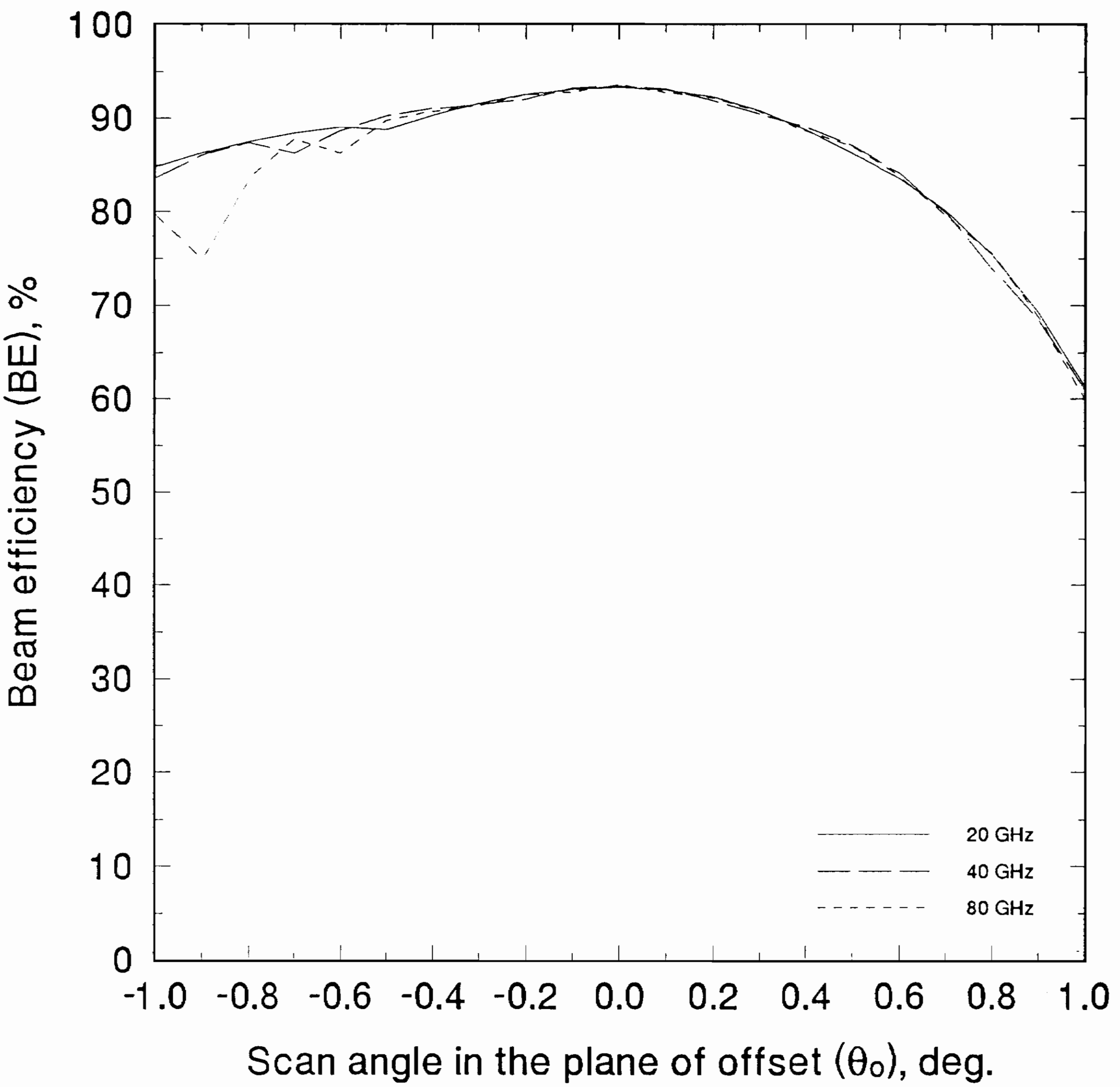

Figure 5.2.3-4. Beam efficiency (BE) of the test case system as a function of scan angle in the plane of offset (θ_o) for optimized scanning using the transmit mode raytracing error functional.

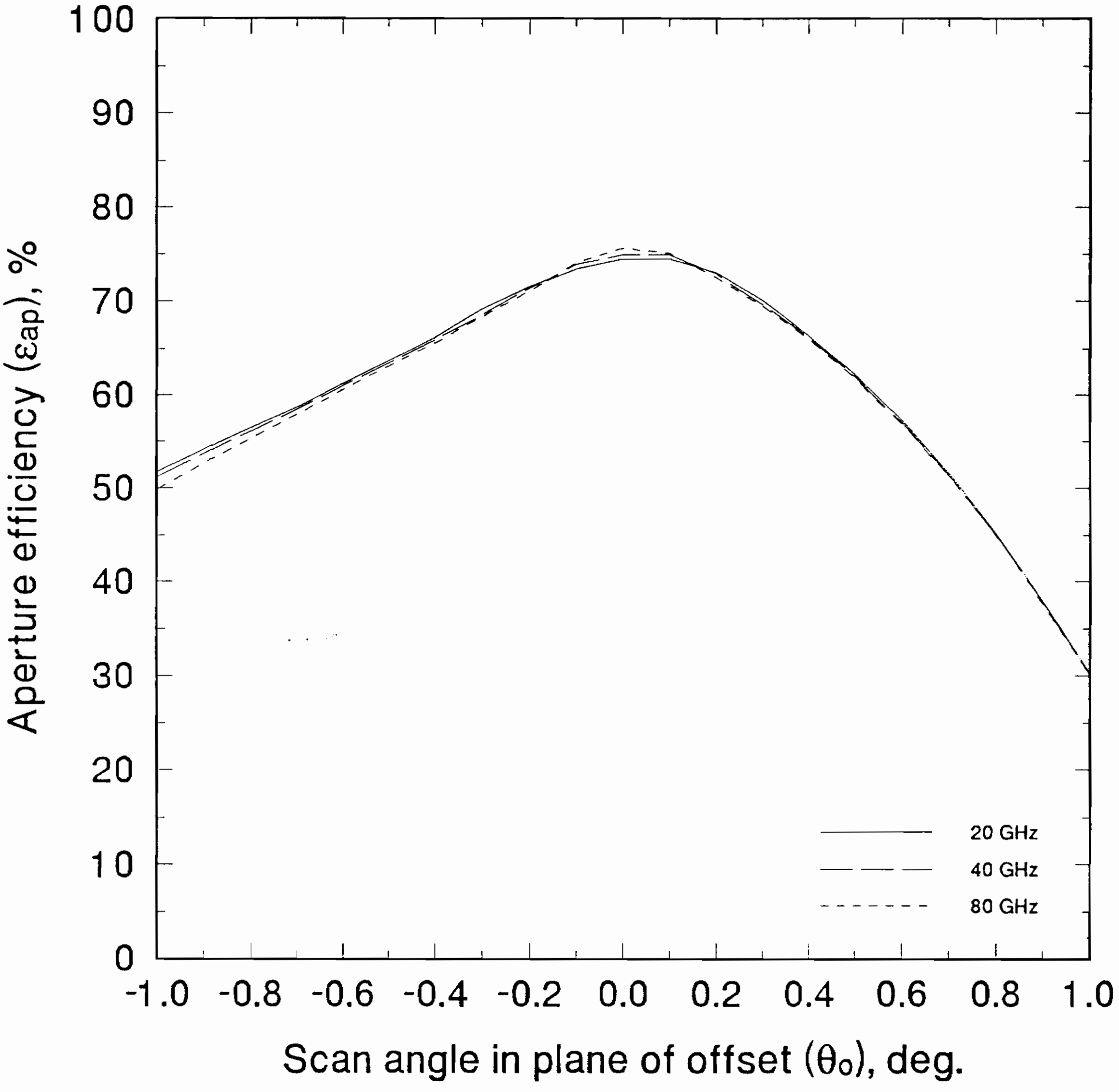

Figure 5.2.3-5. Aperture efficiency ($\varepsilon_{\mathrm{ap}}$) of the test case system as a function of scan angle in the plane of offset (θ_{o}) for optimized scanning using the transmit mode raytracing error functional.

GHz.

The aperture efficiency, ε_{ap}, of the scanned test case system is shown in Figure 5.2.3-5 as a function of scan angle in the plane of offset, θ_{o}. The spillover effiency, ε_{ap}, given by GRASP7, is shown in Figure 5.2.3-6. As before, the results of Section 3.1.1 were used to generate approximate illumination amplitude and phase efficiencies, ε_{amp} and ε_{ϕ}, for the system. These efficiencies are shown in Figures 5.2.3-7 and 5.2.3-8. As expected, the scan loss in the test case systems synthesized using the transmit mode raytracing error functional is dominated by spillover and illumination amplitude losses.

Figures 5.2.3-9 through 5.2.3-16 summarize the analysis results for the constant θ scan paths. These results show that the worst pattern degradation occurs for scan to positive θ_{o} angles in the $\phi_{\text{o}} = 0^\circ$ region for the transmit mode raytracing error functional. This behavior is caused by the extreme motions selected by the error functional in this region as shown in Figures 5.2.2-1 through 5.2.2-3.

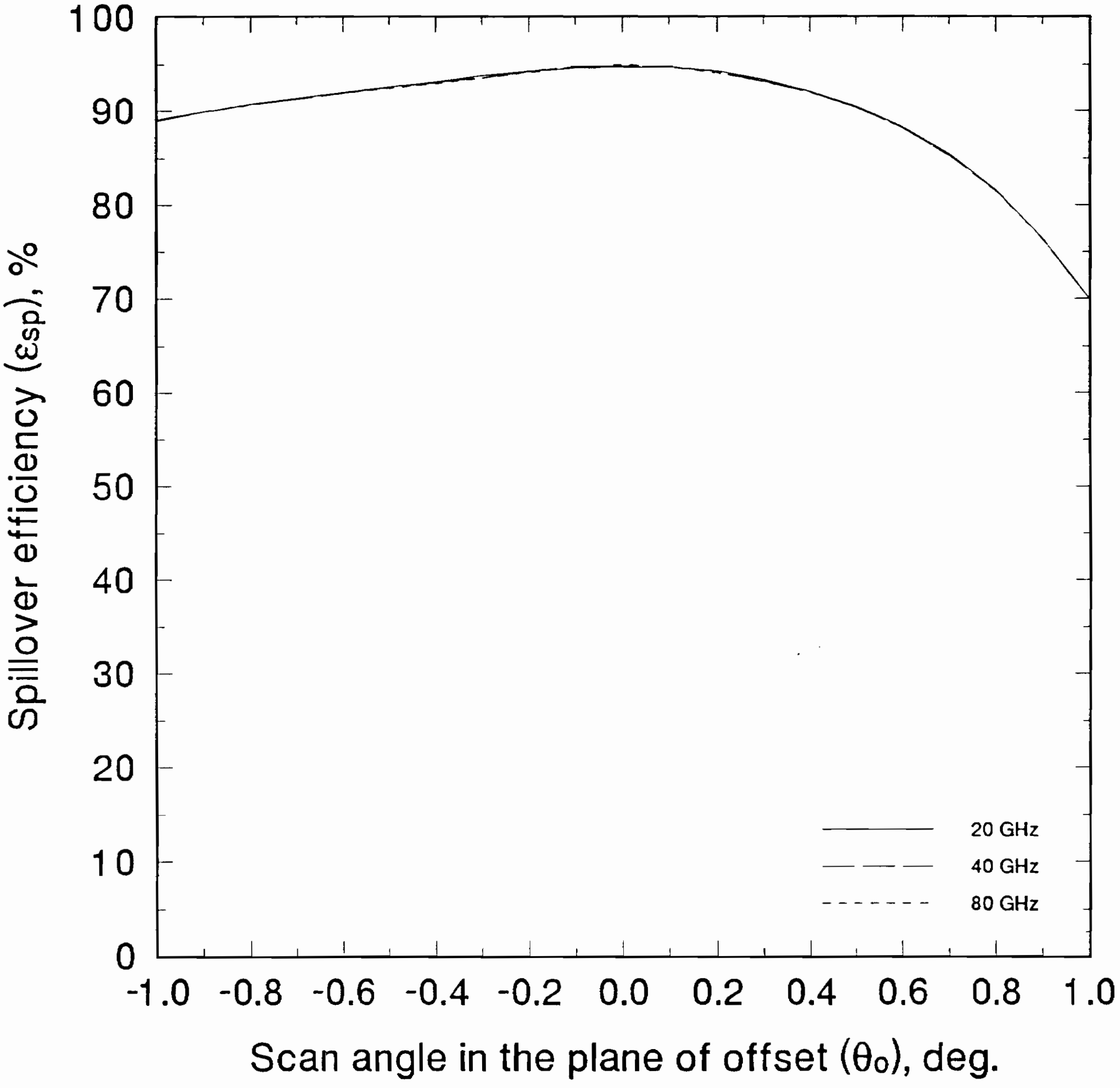

Figure 5.2.3-6. Spillover efficiency (ε_{sp}) of the test case system as a function of scan angle in the plane of offset (θ_o) for optimized scanning using the transmit mode raytracing error functional.

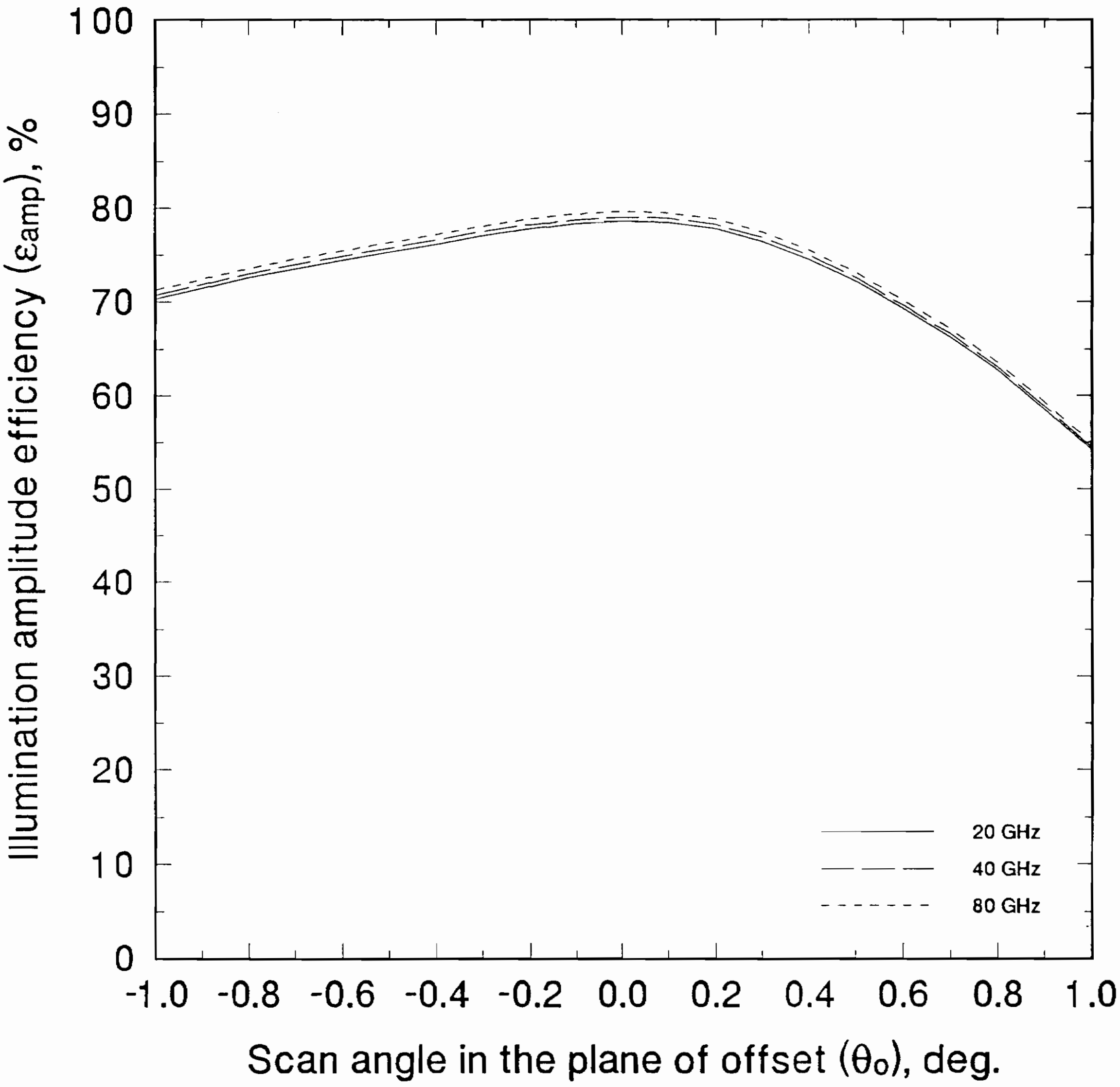

Figure 5.2.3-7. Illumination amplitude efficiency ($\varepsilon_{\mathrm{amp}}$) of the test case system as a function of scan angle in the plane of offset (θ_{o}) for optimized scanning using the transmit mode raytracing error functional.

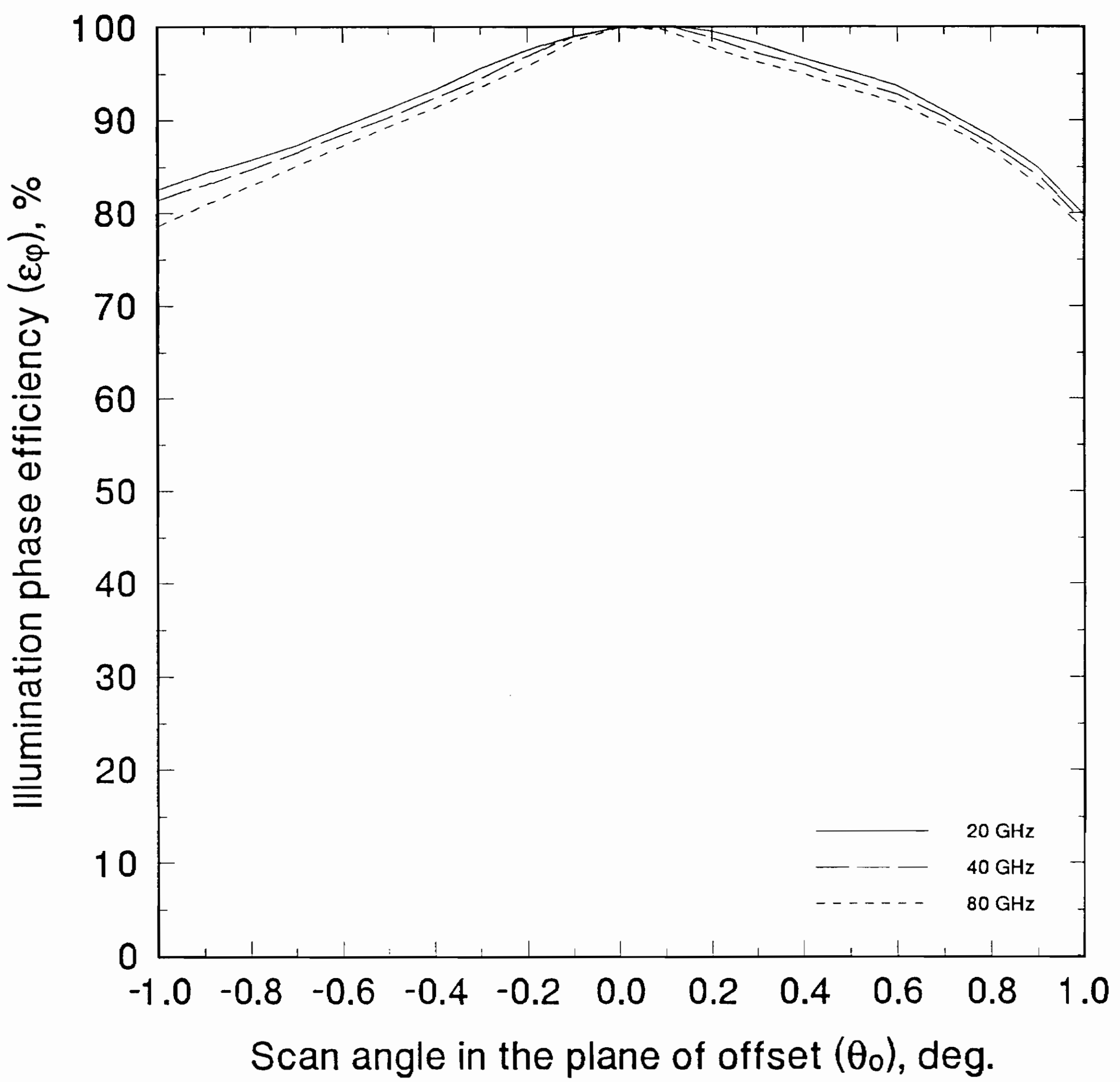

Figure 5.2.3-8. Illumination phase efficiency (ε_ϕ) of the test case system as a function of scan angle in the plane of offset (θ_o) for optimized scanning using the transmit mode raytracing error functional.

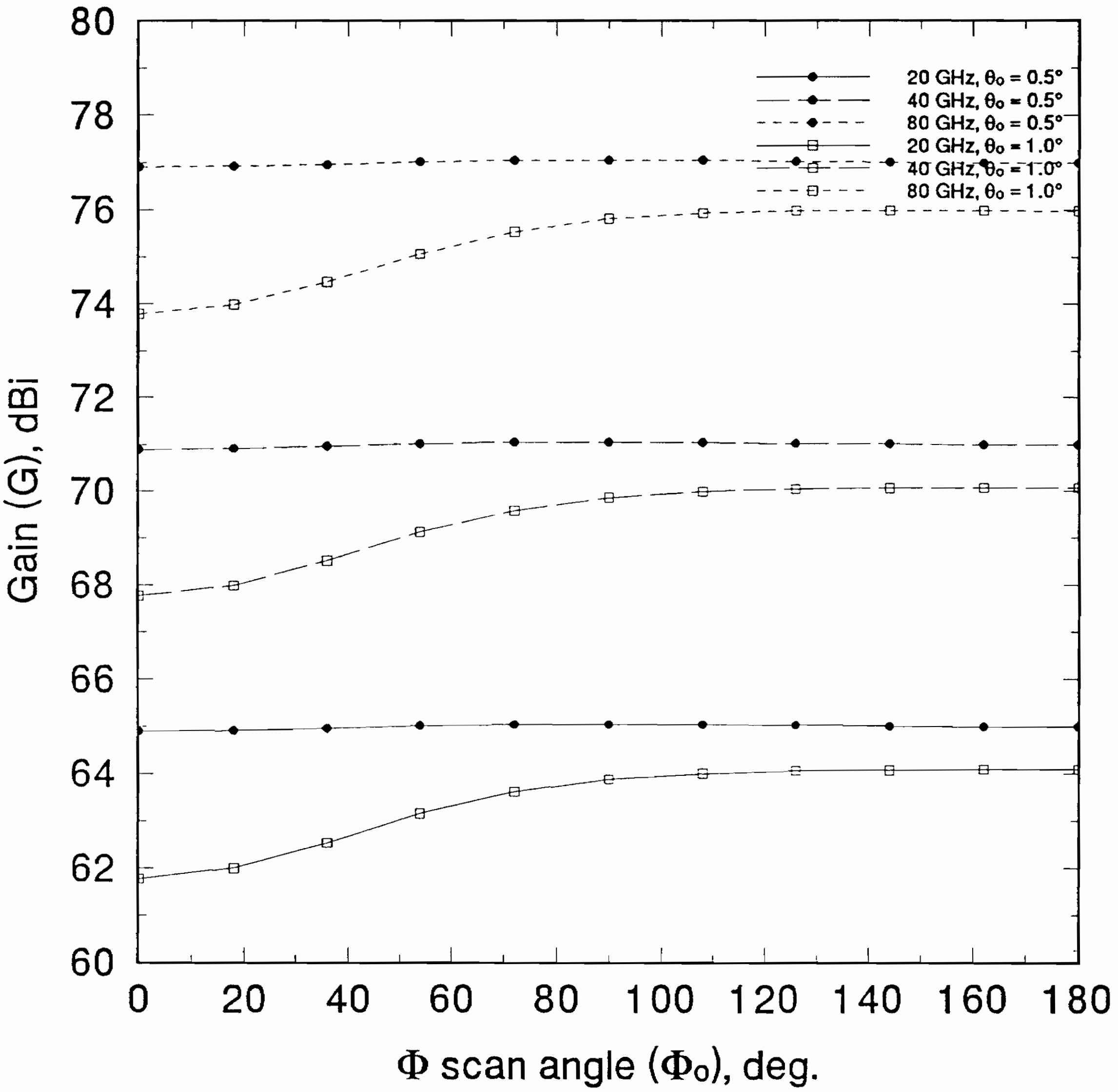

Figure 5.2.3-9. Gain (G) of the test case system as a function of ϕ scan angle (ϕ_o) for $\theta_o = 0.5°$ and $\theta_o = 1.0°$ for optimized scanning using the transmit mode raytracing error functional.

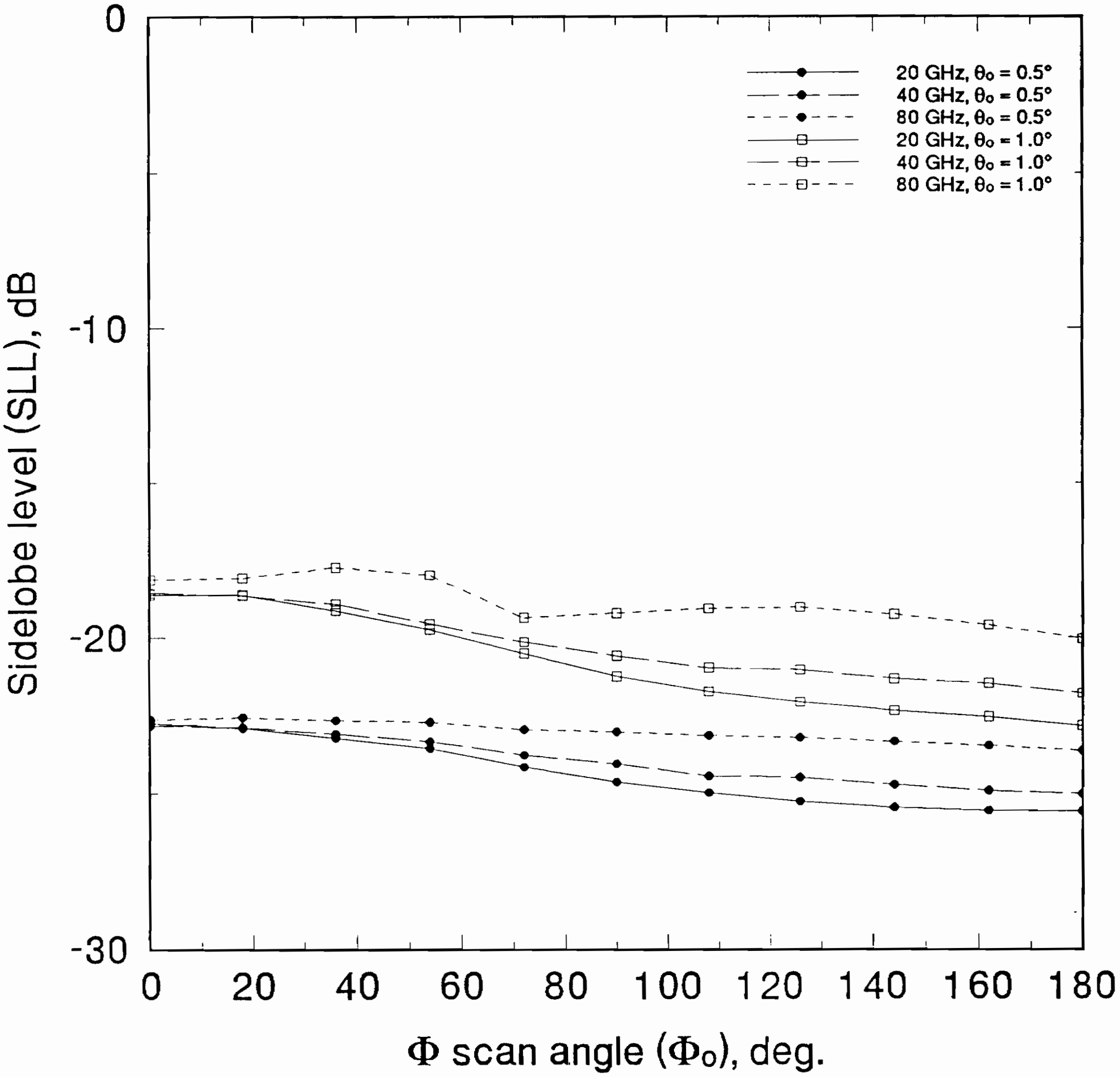

Figure 5.2.3-10. Sidelobe level (SLL) of the test case system as a function of ϕ scan angle (ϕ_o) for $\theta_o = 0.5°$ and $\theta_o = 1.0°$ for optimized scanning using the transmit mode raytracing error functional.

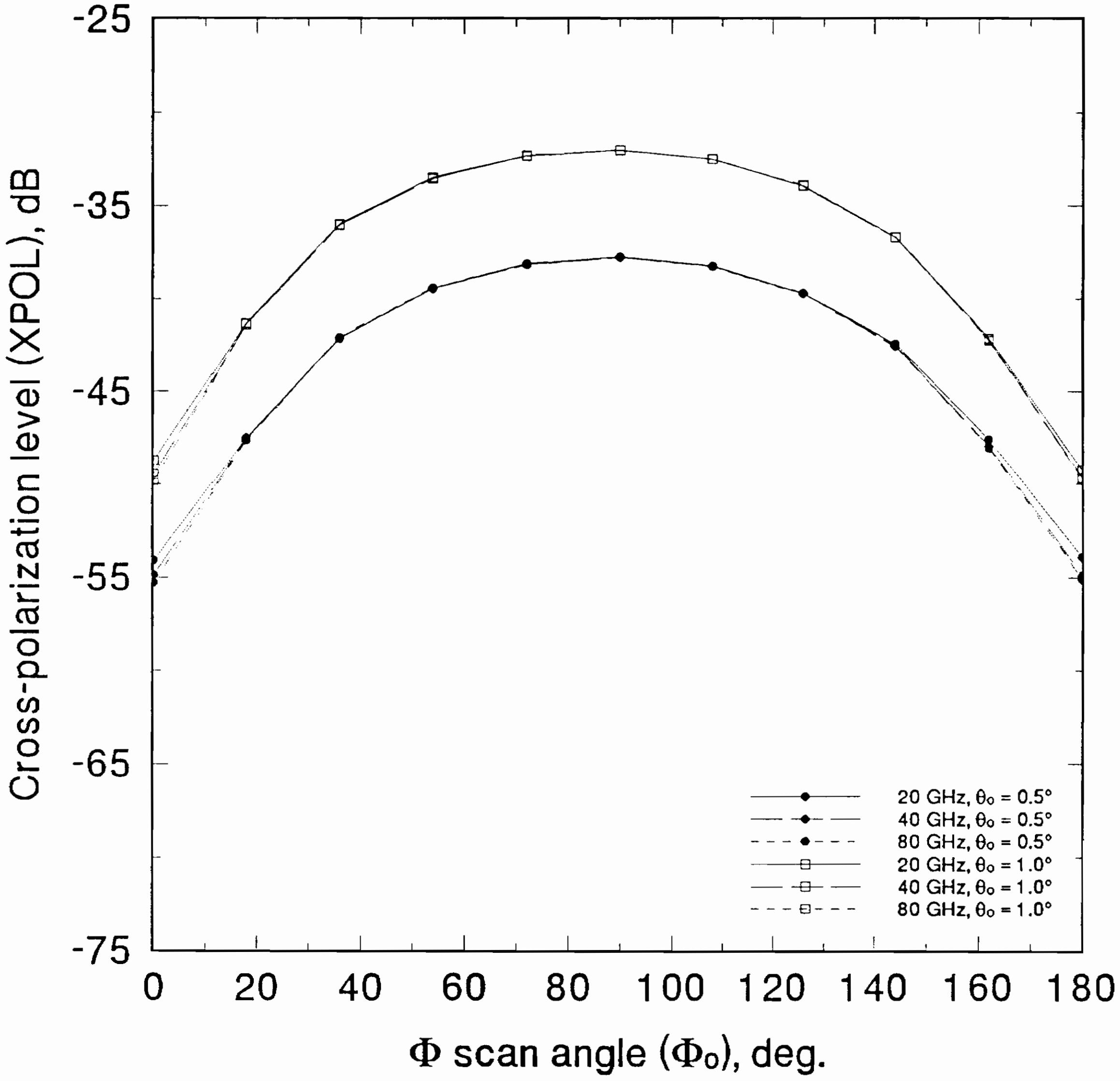

Figure 5.2.3-11. Cross-polarization level (XPOL) of the test case system as a function of ϕ scan angle (ϕ_o) for $\theta_o = 0.5°$ and $\theta_o = 1.0°$ for optimized scanning using the transmit mode raytracing error functional.

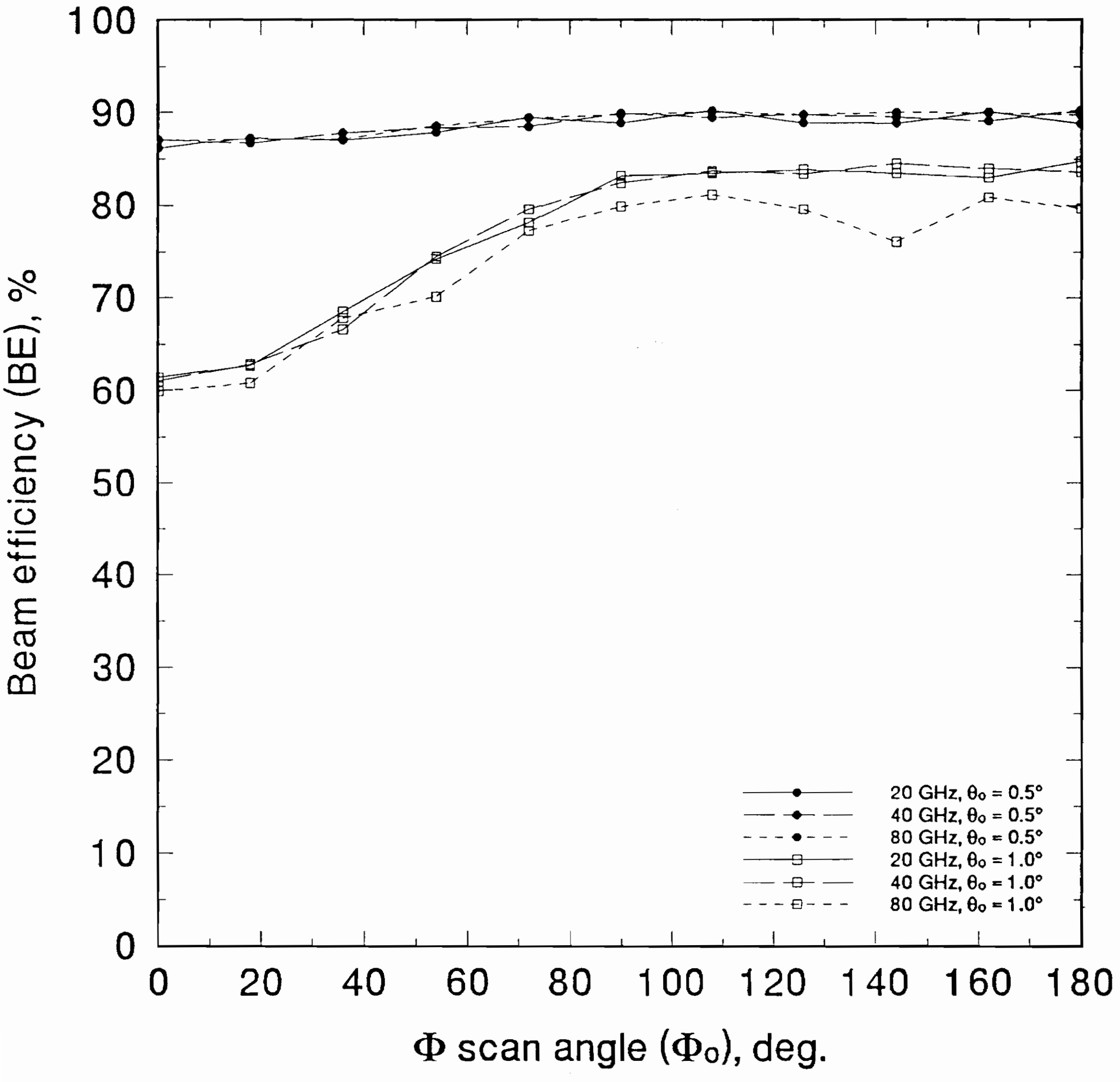

Figure 5.2.3-12. Beam efficiency (BE) of the test case system as a function of ϕ scan angle (ϕ_o) for θ_o = 0.5° and θ_o = 1.0° for optimized scanning using the transmit mode raytracing error functional.

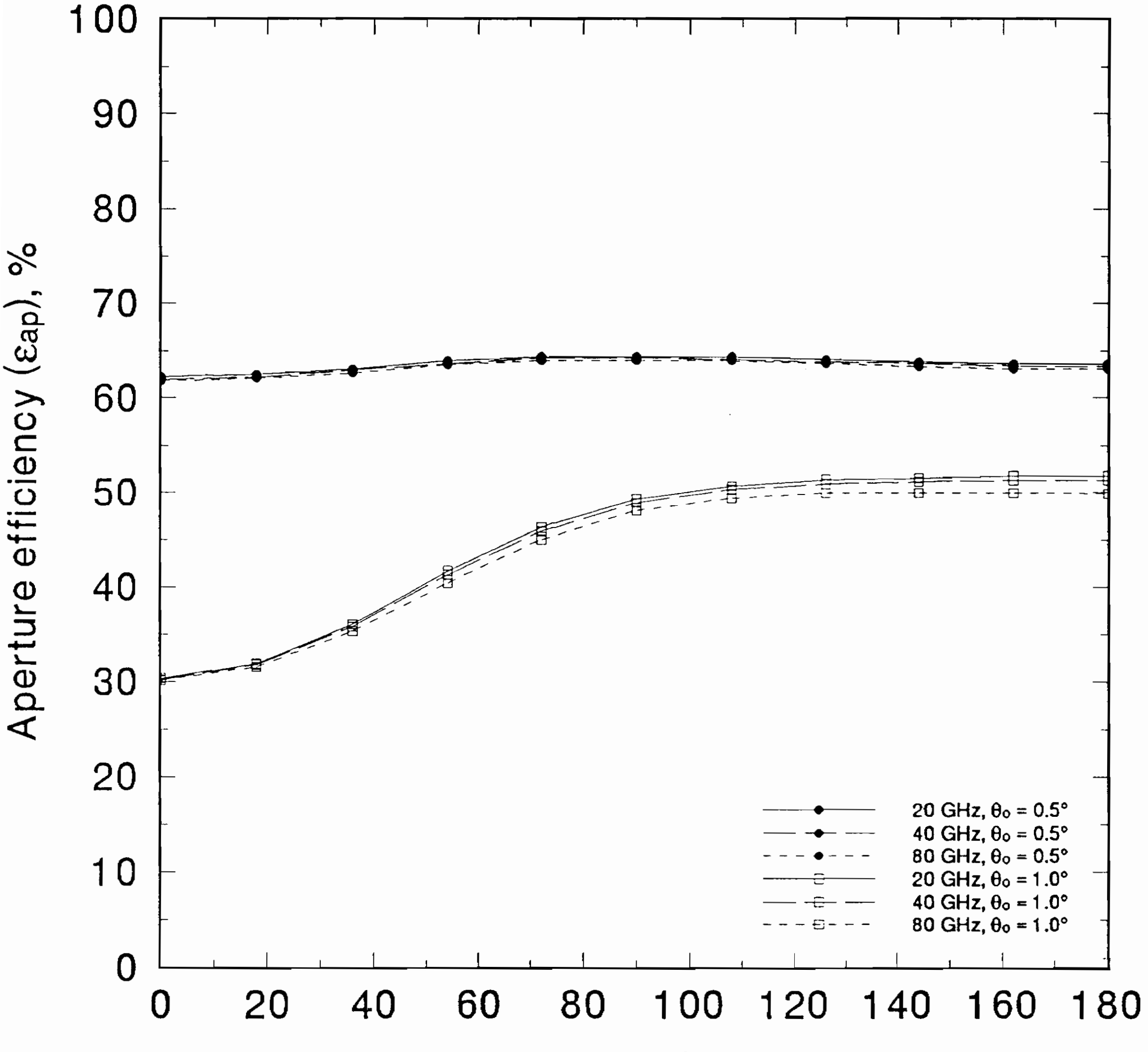

Figure 5.2.3-13. Aperture efficiency (ε_{ap}) of the test case system as a function of ϕ scan angle (ϕ_o) for $\theta_o = 0.5°$ and $\theta_o = 1.0°$ for optimized scanning using the transmit mode raytracing error functional.

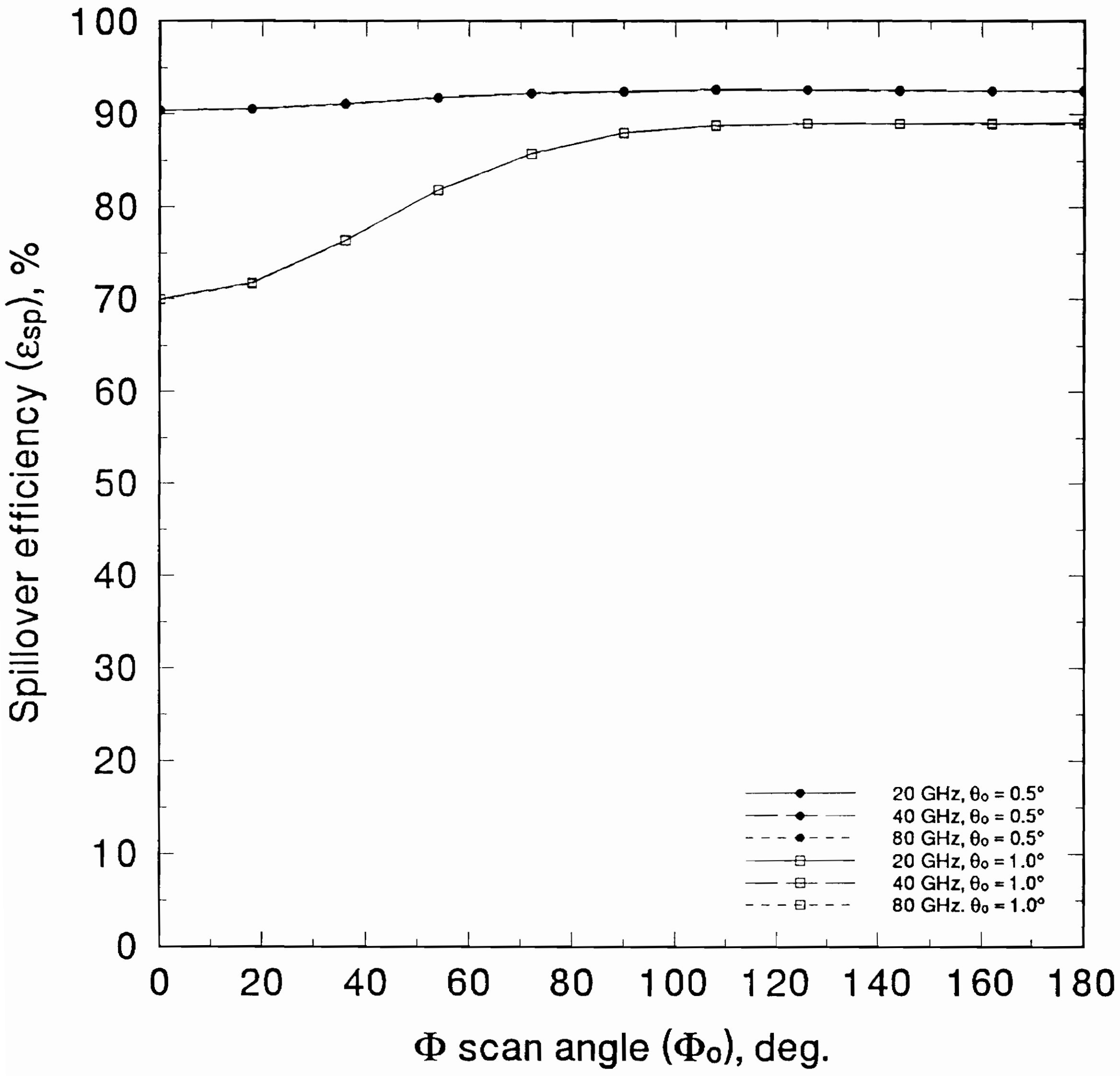

Figure 5.2.3-14. Spillover efficiency (ε_{sp}) of the test case system as a function of ϕ scan angle (ϕ_o) for $\theta_o = 0.5°$ and $\theta_o = 1.0°$ for optimized scanning using the transmit mode raytracing error functional.

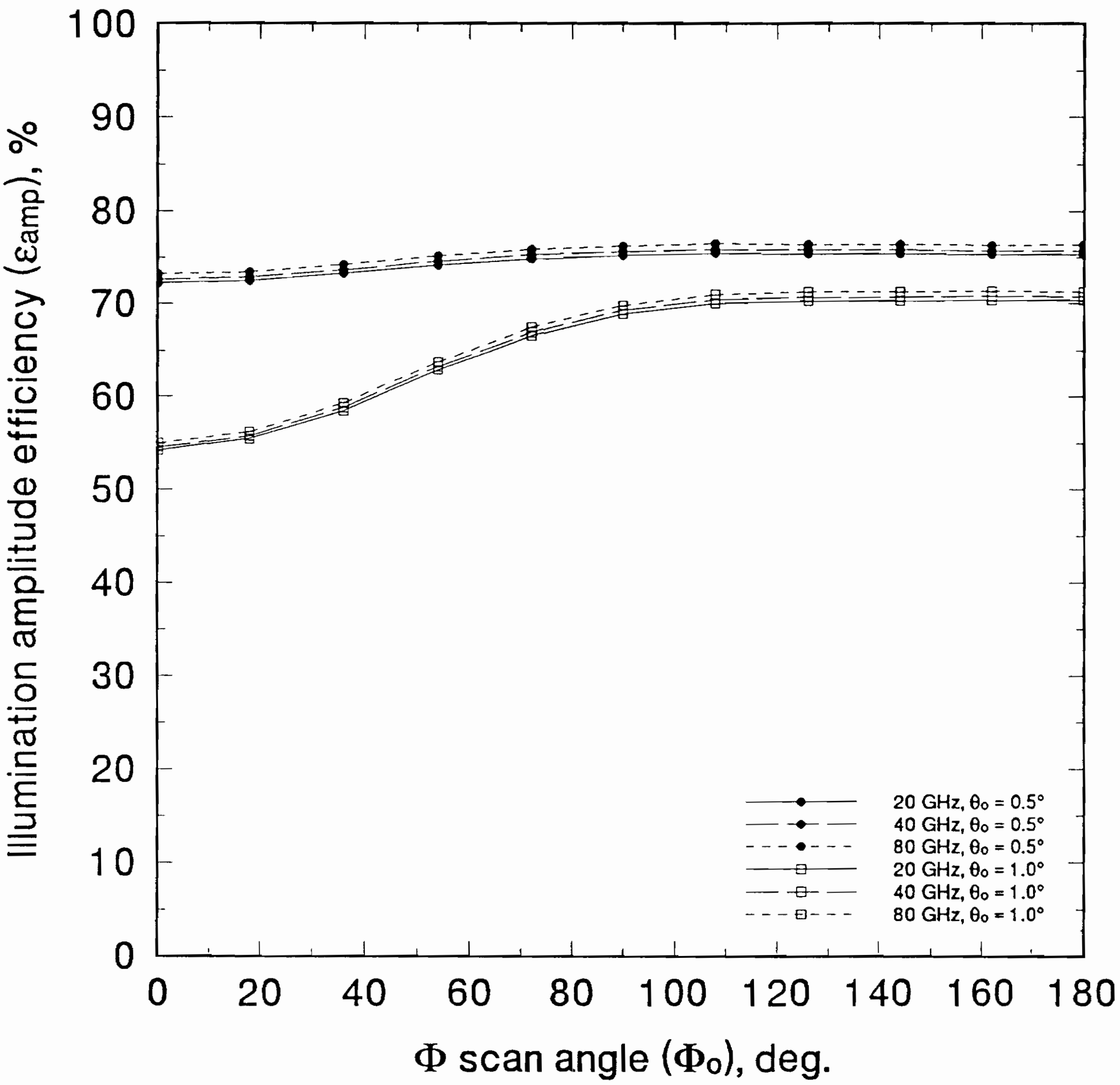

Figure 5.2.3-15. Illumination amplitude efficiency ($\varepsilon_{\mathrm{amp}}$) of the test case system as a function of ϕ scan angle (ϕ_o) for $\theta_o = 0.5°$ and $\theta_o = 1.0°$ for optimized scanning using the transmit mode raytracing error functional.

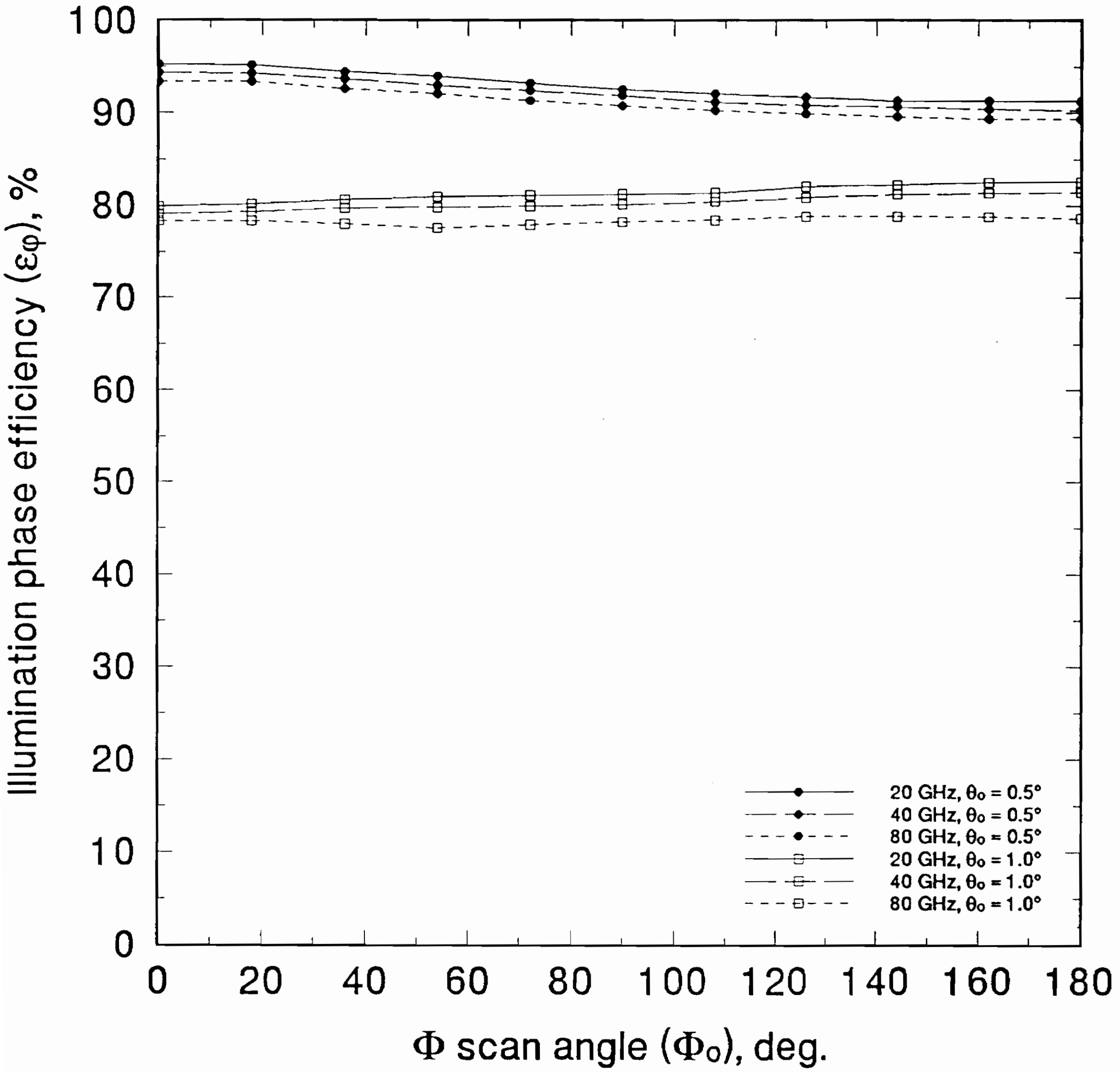

Figure 5.2.3-16. Illumination phase efficiency (ε_ϕ) of the test case system as a function of ϕ scan angle (ϕ_o) for $\theta_o = 0.5°$ and $\theta_o = 1.0°$ for optimized scanning using the transmit mode raytracing error functional.

References

[1] T. Kitsuregawa, "Section 2.6 Steerable Beam Antennas," *Advanced Technology in Satellite Communications Antennas*, pp. 177-178, Artech House, Boston, MA, 1990.

[2] Personal conversation with Paul Werntz.

[3] W.H. Press, et al., "10.5 Direction Set (Powell's) Methods in Multidimensions," *Numerical Recipes*, pp. 294-301, Cambridge University Press, New York, NY, 1990.

[4] W.H. Press, et al., "10.1 Golden Section Search in One Dimension," *Numerical Recipes*, pp. 277-282, Cambridge University Press, New York, NY, 1990.

[5] B. Shen, "2.3. Applications of Fermat's Principle," *Multiple Reflector Scanning Antennas*, Ph.D. Dissertation, pp. 13-17, Virginia Polytechnic Institute and State University, 1993.

Chapter 6

SUMMARY

6.1 Conclusions

The goal of this work was to develop a high gain, wide scanning reflector antenna system for use in a geostationary, microwave radiometric system for the Mission to Planet Earth. The design constraints imposed by the radiometric requirements of this mission are summarized in Table 1.1. Beam efficiency, given by (3.1.1-7), is the far-field pattern characteristic that is of greatest concern during beam scanning. The beam efficiency must be as high as possible for this mission because radiometry measures thermal noise. This means that the ratio of desirable noise, the scene which is being observed, to undesirable noise, the rest of the universe, must be as large as possible. Also, beam efficiency should be constant with frequency because the radiometric measurements must be performed on several frequency bands simultaneously.

The canonical offset Cassegrain reflector antenna configuration was chosen to complement the more complex structures being designed by Werntz [1] with the tri-reflector configurations, by Shen [2] using the spherical main reflector configurations, and by Takamizawa [3] using shaped-reflector configurations. The test case, summarized by Figure 4.2 and Table 4.1, was chosen to fit a 42.52% scale test article developed at NASA Langley Research Center to allow possible experimental verification of the resulting beam scanning system. This is the simplest system which is capable of scanning by subreflector motion only and has an areal efficiency of greater than 98%. The test case achieves an unscanned aperture effiency of nearly 75% using a single feed rather than an array feed system for simplicity.

Two geometrical optics based error functionals were used to generate the optimum scanning motions of the subreflector. The first of these, the transmit mode raytracing error functional of Section 5.2, minimizes the far-field pattern degradation by minimizing the mispointing between the rays exiting the system and a ray in the desired scan direction. The test case system has a 90% beam efficiency scan range of 8 HPBW for $D_M = 709\lambda$, 18 HPBW for $D_M = 1417\lambda$, and 35 HPBW for $D_M = 2835\lambda$ when optimized using this error functional. Optimization of the test case system with the transmit mode raytracing error functional for a single scan direction requires just less than 7 minutes using a 50 MHz 80486 micro-computer. It is believed that this is the first application of an error functional of this type to the optimization of subreflector induced beam scanning in a dual reflector system.

The correcting subreflector surface fitting error functional of Section 5.1, after Kitsuregawa [4], was the second error functional used to find the optimum scanning motions of the subreflector. This error functional minimizes the far-field pattern degradation by fitting the unscanned subreflector to a phase correcting subreflector synthesized for the scan direction and a given path length through the system. Optimization of the test case system using this error functional was over six times slower at nearly 45 minutes per scan direction. This difference in optimization speed can be attributed to the additional optimization loop required to vary the path length. The 90% beam efficiency scan range of the test case when optimized using the correcting subreflector surface fitting error functional was found to be 9 HPBW for $D_M = 709\lambda$ and 1417λ and 10 HPBW for $D_M = 2835\lambda$.

The Foldes Type 6 reflector antenna system, discussed in Section 3.4, is the other subreflector scanned, high gain reflector system which was investigated. Althought the Type 6 system beam scans by subreflector tilt only it was found to be capable of a 90% beam efficiency scan range of 19 HPBW for $D_M = 833\lambda$, 21 HPBW for $D_M = 1667\lambda$, and 31 HPBW for $D_M = 3333\lambda$. This scan performance is significantly greater than the scan performance of the test case when optimized by either of the error functionals at the two smaller electrical aperture diameters. Because the Type 6 system has a higher subreflector eccentricity, one concern raised by its larger scan range is that the scan range of an offset Cassegrain reflector antenna may be highly affected by subreflector eccentricity. The transmit mode raytracing error functional does have a scan range which is comparable with that of the Type 6 system at the largest electrical aperture size. Also, the lower phase error observed for the transmit mode raytracing error functional promises better scan performance with increasing aperture size than for the Type 6 system. The scan characteristics of these three wide scanning reflector antenna system are summarized in Table 6.1-1.

The optimization approach presented in Chapter 5 should be applicable to any dual reflector antenna system. In general, the transmit mode raytracing error functional should be used to optimize systems with electrically large apertures. Also, the transmit mode raytracing error functional is more suitable for radiometric systems because the beam efficiency of the resulting scanned system is more constant as a function of frequency. The correcting subreflector surface fitting error functional is better suited to smaller aperture antennas. The transition between the applicable ranges of these two error functionals as implemented here occurs for systems of D_M from 800λ to 1000λ. The correcting subreflector surface fitting error functional is better suited for use in the optimization of systems using array feeds to compensate for aperture phase error because this error functional primarily maximizes illumination amplitude and spillover efficiency.

Other than the original geostationary radiometric mission, two possible uses for

Table 6.1-1. Scan characteristics of three high gain, wide scanning reflector antenna systems. (------ indicates unavailable information or incomplete information would be provided)

θ_o (deg)	ϕ_o (deg)	System	G (dBi)	SLL (dB)	XPOL (dB)	BE (%)	ε_{ap} (%)	ε_{sp} (%)	x_t (m)	z_t (m)	α_r (deg)
0.0	0	Type 6	79.27	-29.47	-44.5	94.61	77.08	96.21	------	------	0.00
		TMR	77.78	-29.45	-74.7	93.63	75.63	94.98	0.00	0.00	0.00
		CSSF	77.78	-29.43	-74.7	93.63	75.63	94.98	0.00	0.00	0.00
0.5	0	Type 6	76.26	-------	-42.0	77.76	39.12	95.87	------	------	-1.82
		TMR	76.90	-22.65	-55.3	87.04	61.76	90.37	0.12	0.06	-3.59
		CSSF	71.32	-------	-57.3	39.85	17.09	95.35	-0.08	-0.09	-0.42
0.5	45	Type 6	------	-------	------	------	------	------	------	------	------
		TMR	76.99	-22.69	-40.8	87.93	63.06	91.42	------	------	------
		CSSF	71.89	-------	-42.0	12.54	19.51	94.55	------	------	------
0.5	90	Type 6	------	-------	------	------	------	------	------	------	------
		TMR	77.05	-23.04	-37.8	89.80	63.93	92.40	------	------	------
		CSSF	71.58	-------	-39.1	6.12	18.14	93.71	------	------	------
0.5	135	Type 6	------	-------	------	------	------	------	------	------	------
		TMR	77.02	-23.29	-41.2	89.91	63.49	92.54	------	------	------
		CSSF	71.66	-------	-41.4	17.78	18.48	93.76	------	------	------
0.5	180	Type 6	77.18	-------	-48.1	82.72	47.86	94.28	------	------	1.79
		TMR	76.99	-23.66	-55.1	89.78	63.05	92.45	-0.07	-0.04	2.85
		CSSF	71.63	-------	-57.2	35.15	18.35	94.21	0.09	0.08	0.41
1.0	0	Type 6	69.67	-------	-38.7	37.31	8.51	92.75	------	------	3.69
		TMR	73.78	-18.13	-49.8	59.91	30.11	69.93	0.33	0.18	-8.47
		CSSF	67.33	-------	-51.2	19.10	6.82	95.14	-0.16	-0.19	-0.85
1.0	45	Type 6	------	-------	------	------	------	------	------	------	------
		TMR	74.77	-13.54	-34.8	68.96	37.86	79.04	------	------	------
		CSSF	67.87	-------	-35.9	0.89	7.72	93.30	------	------	------
1.0	90	Type 6	------	-------	------	------	------	------	------	------	------
		TMR	75.81	-24.11	-32.0	79.87	48.05	87.96	------	------	------
		CSSF	66.62	-------	-32.8	0.20	5.79	89.74	------	------	------
1.0	135	Type 6	------	-------	------	------	------	------	------	------	------
		TMR	75.98	-------	-35.3	77.83	49.97	88.95	------	------	------
		CSSF	67.86	-------	-35.4	4.82	7.70	90.42	------	------	------
1.0	180	Type 6	74.28	-------	-53.7	63.48	24.19	90.99	------	------	3.53
		TMR	75.97	-20.05	-49.8	79.68	49.85	88.98	-0.10	-0.07	5.18
		CSSF	67.78	-------	-50.3	5.95	7.56	92.47	0.19	0.16	0.82

subreflector induced beam scanning are tracking of geostationary satellites by large earth station antennas and reduction of the actuator demands imposed by over-zenith tracking in elevation over azimuth pedestals. A typical large earth station antenna in the 100' class has a half power beam width of about 0.06° at C-band. These earth stations must track geostationary satellites because most geostationary satellites have diurnal angular motions of greater than 0.06°. An antenna system capable of beam scanning over the limited tracking range required for this use would allow the use of smaller actuators for tracking by displacing the much smaller subreflector instead of the entire antenna. Over-zenith tracking in elevation over azimuth pedestals currently requires very rapid azimuth slew when the target passes through the zenith. A system capable of beam scanning by subreflector motion could reduce the maximum azimuth slew rate by using subreflector induced beam scanning to hold the beam on target near the zenith. This would allow the azimuth slew to occur more gradually during the time the target is near, rather than at, the zenith.

The characteristics of five scanning antenna configurations of increasing complexity are summarized in Table 6.1-2. The prime-focus paraboloid with scanning achieved by lateral or optimal feed movement is included for comparison purposes [1]. The Type 1 system is the test case system described here and is scanned by optimal subreflector positioning as determined with the transmit mode raytracing error functional. The Type 2 system is the Cassegrain II tri-reflector system of Werntz [1]. The spherical system is the two subreflector and one caustic mirror with feed tilt system of Shen [2]. As shown, the scan range of reflector antenna systems generally increases with increasing complexity. On the whole, the Type 1 system described here provides good overall scan range while remaining fairly simple. Also, the Type 1 system's areal and aperture efficiencies are significantly higher than those of the other two systems investigated here a Virginia Tech.

Table 6.1-2. Characteristics of five wide scanning reflector antenna systems

Parameter	Prime-focus Parab. Feed movement		Type 1 (LaPean)	Type 2 (Werntz)	Spherical (Shen)
	lateral	Optimal			
Main reflector diameter (D_M), λ	----------	700	2835	480	1200 × 1000
F/D_p	1.000	1.000	0.515	0.519	0.260
Areal efficiency $\left(\frac{D_M^2}{D_M^2 + \dots + D_{Sn}^2}\right)$	1.0000	1.0000	0.9817	0.8818	0.9218
Translational degrees of freedom	1	2	3	0	0
Rotational degrees of freedom	1	1	2	2	feed: 1 mirror: 2
Gain (G), dBi	----------	----------	77.78	62.44	63
Aperture efficiency (ε_{ap}), %	----------	----------	75.63	77.13	50
1 dB gain loss scan range, HPBW	8	34 × 0	50	30 × 60	82

6.2 Future Work

Future efforts to improve the scanning capabilities of offset canonical Cassegrain reflector antennas should focus on the following four main areas.

- Improving the transmit mode raytracing error functional.

  The basic form of the transmit mode raytracing error functional could be expanded to include illumination error effects as well as phase error effects. While this would necessarily cause the optimization to be performed for a given frequency of operation, many antenna systems, especially for civil communications, operate over only a narrow band of frequencies.

- Improving the correcting subreflector surface fitting error functional.

  The implementation of the error functional could be extended to allow the grid of points to be of variable size. This improvement would allow a portion of the actual subreflector to be fitted to the correcting subreflector. This will possibly allow a closer fit as the compound curved surface move relative to each other. One potential complication to this scheme is that the illuminated portion of the actual subreflector may shrink below the region where geometrical optics techniques apply.

- Investigating the possibility of using a simple array feed system to extend the scan range.

  A simple array feed could be used to reduce the aperture phase error. If the system was not limited by a low spillover or illumination amplitude efficiency this could significantly increase the scan range. As mentioned in Section 6.1, the correcting subreflector surface fitting error functional seems well suited for subreflector motion optimization for an array fed system because this error functional primarily optimizes the illumination amplitude and spillover efficiencies. Bailey [5] and Smith [6] have investigated the possibility of using array feed systems to improve the illumination phase efficiency of reflector antenna systems.

- Investigating the effects of the geometry of Cassegrain reflector antenna systems on scan range. The results of Section 3.2 indicate that the offset height of the equivalent paraboloid of an offset Cassegrain reflector antenna has little effect on its beam scanning behavior. However, the effects of main reflector focal length, subreflector eccentricity, and other parameters were not investigated due to the pre-existing geometry requirements. The potential importance of this line of investigation is hinted at by the scan range of the Foldes Type 6 system when scanned by subreflector tilt only.

References

[1] P. C. Werntz, *A High Gain Tri-reflector Antenna Configuration of Beam Scanning*, Ph.D. Dissertation, Virginia Polytechnic Institute and State University, 1993.

[2] B. Shen, *Multiple Reflector Scanning Antennas*, Ph.D. Dissertation, Virginia Polytechnic Institute and State University, 1993.

[3] K. Takamizawa, P. C. Werntz, and W. L. Stutzman, "Optimization of Multiple Reflector Antenna Configurations for Wide Angle Scan," *IEEE AP-S Symposium Digest (Chicago)*, pp. 359-362, July 1992.

[4] T. Kitsuregawa, "Section 2.6 Steerable Beam Antennas," *Advanced Technology in Satellite Communications Antennas*, pp. 177-188, Artech House, Boston, MA, 1990.

[5] M. C. Bailey, "Electronic Compensation for Reflector Surface Distortion to Improve Radiation Pattern Characteristics of Antenna," NASA Technical Memorandum 100652, July 1988.

[6] W. T. Smith and W. L. Stutzman, "A Pattern Synthesis Technique for Array Feeds to Improve Radiation Performance of Large Distorted Reflector Antennas," *IEEE Transactions on Antennas and Propagation*, Vol. AP-40, No. 1, pp. 57-62, January 1992.

Appendix 1

Program listing of the Correcting Subreflector Surface Fitting error functional optimization software

```
************************************************************************
*
*     Correcting Subreflector Surface Fitting Optimization Code
*
*     James W. LaPean, Jr.                       11/18/93
*
************************************************************************

      PROGRAM CSSF
      IMPLICIT NONE
      REAL*8 SRFMD(4),SRFM(25,25,6),SRFA(25,25,6),SCND(6),SCAN(2),FOC,
     C       FEED(3),X(4),SC(2),XP(4),PI,SRFS(25,25,6),SFOC(2,3)
      INTEGER*2 ICN,I,J,T,P,TINC,PINC
      CHARACTER*12 SUBFILE
      COMMON /REFL/ SRFMD,SRFA,FOC,FEED,SC,SRFM,SRFS
      PI=3.14158265358979323846D0
* Program inputs read from input file
      OPEN(3,FILE='KSFT1.INP',STATUS='OLD')
      READ(3,*)SRFMD(1),SRFMD(2),SRFMD(3),SRFMD(4)
      READ(3,*)FOC,FEED(1),FEED(2),FEED(3)
      READ(3,*)SCND(1),SCND(2),SCND(3),SCND(4),TINC,PINC
      READ(3,*)X(1),X(4)
      READ(3,*)ICN
      READ(3,'(A12)')SUBFILE
      X(3)=0.D0
      X(2)=0.D0
* Nominal subreflector data entry
      OPEN(4,FILE=SUBFILE,STATUS='OLD')
      READ(4,'(6F12.7)')SFOC(1,1),SFOC(1,2),SFOC(1,3),
     C                  SFOC(2,1),SFOC(2,2),SFOC(2,3)
      DO 1 I=1,25
        DO 1 J=1,25
 1        READ(4,'(6F12.7)')SRFA(I,J,1),SRFA(I,J,2),SRFA(I,J,3),
     C                      SRFA(I,J,4),SRFA(I,J,5),SRFA(I,J,6)
      CLOSE(4)
* Main reflector array setup
      CALL MNREF
* Perform scan optimized fitting for scan combinations
      WRITE(*,'(//,A1)')' '
      SCAN(2)=SCND(2)
      P=1
 2    SCAN(1)=SCND(1)
      T=1
 3    WRITE(*,'(A25,D8.3,A7,D8.3)')' Calculating for Theta = ',SCAN(1),
     C                             ' Phi = ',SCAN(2)
      SC(1)=SCAN(1)
      SC(2)=SCAN(2)
      XP(1)=X(1)
      XP(2)=X(2)
      XP(3)=X(3)
      XP(4)=X(4)
      CALL PATHOPT(ICN,XP,SFOC)
      ICN=ICN+1
      SCAN(1)=SCAN(1)+SCND(3)
      T=T+1
      IF (T.LE.TINC) GOTO 3
      SCAN(2)=SCAN(2)+SCND(4)
      P=P+1
      IF (P.LE.PINC) GOTO 2
      STOP
```

```
      END

************************************************************************
*
*     Main reflector array filling subroutine
*
************************************************************************

      SUBROUTINE MNREF
      IMPLICIT NONE
      REAL*8 SRFM(25,25,6),SRFMD(4),DEN,F,SRFA(25,25,6),FEED(3),SC(2),
     C       SRFS(25,25,6)
      INTEGER*2 I,J
      COMMON /REFL/ SRFMD,SRFA,F,FEED,SC,SRFM,SRFS
      DO 1 I=1,25
        DO 1 J=1,25
          SRFM(I,J,2)=(SRFMD(2)-SRFMD(1))*FLOAT(I-1)/24.D0+SRFMD(1)
          SRFM(I,J,3)=(SRFMD(4)-SRFMD(3))*FLOAT(J-1)/24.D0+SRFMD(3)
          SRFM(I,J,1)=2.5D-1*(SRFM(I,J,2)**2.D0+SRFM(I,J,3)**2.D0)/F
          DEN=SQRT((SRFM(I,J,2)/(2.D0*F))**2.D0
     C            +(SRFM(I,J,3)/(2.D0*F))**2.D0+1.D0)
          SRFM(I,J,4)=1.D0/DEN
          SRFM(I,J,5)=-SRFM(I,J,2)/(2.D0*F*DEN)
 1        SRFM(I,J,6)=-SRFM(I,J,3)/(2.D0*F*DEN)
      RETURN
      STOP
      END

************************************************************************
*
*     Path length optimization subroutine
*
************************************************************************

      SUBROUTINE PATHOPT(ICN,X,SFOC)
      IMPLICIT NONE
      REAL*8 SRFM(25,25,6),SRFS(25,25,6),FEED(3),SCAN(2),PI,FOC,PATH,
     C       SRFA(25,25,6),TRANS(6),R,C,TOL,X(4),EPS,F(2),SRFMD(4),
     C       SFOC(2,3),XI(5,5),DSCAN(2)
      INTEGER*2 ICN,I,J,N,ITER
      COMMON /REFL/ SRFMD,SRFA,FOC,FEED,SCAN,SRFM,SRFS
      PI=3.14159265358979323846D0
      R=0.61803399D0
      C=1.D0-R
      TOL=1.D-10
* Optimization initialization
      SCAN(1)=SCAN(1)*PI/1.8D2
      SCAN(2)=SCAN(2)*PI/1.8D2
      X(3)=(X(4)+X(1))/2.D0
      X(2)=R*X(3)+C*X(1)
      PATH=X(2)
      CALL RAYTRC(PATH)
      DO I=1,5
        TRANS(I)=0.D0
        DO J=1,5
          IF(I.EQ.J) THEN
            XI(I,J)=1.D0
           ELSE
```

```
            XI(I,J)=0.D0
           ENDIF
         ENDDO
       ENDDO
      N=5
      CALL POWELL(TRANS,XI,N,TOL,ITER,EPS)
      F(1)=EPS
      PATH=X(3)
      CALL RAYTRC(PATH)
      DO I=1,5
        TRANS(I)=0.D0
        DO J=1,5
          IF(I.EQ.J) THEN
            XI(I,J)=1.D0
           ELSE
            XI(I,J)=0.D0
           ENDIF
         ENDDO
       ENDDO
      N=5
      CALL POWELL(TRANS,XI,N,TOL,ITER,EPS)
      F(2)=EPS
* Optimization loop
 2    IF (ABS(X(4)-X(1)).GT.TOL*(ABS(X(2))+ABS(X(3)))) THEN
        IF (F(2).LT.F(1)) THEN
          X(1)=X(2)
          X(2)=X(3)
          X(3)=R*X(2)+C*X(4)
          F(1)=F(2)
          PATH=X(3)
          CALL RAYTRC(PATH)
          DO I=1,5
            TRANS(I)=0.D0
            DO J=1,5
              IF(I.EQ.J) THEN
                XI(I,J)=1.D0
               ELSE
                XI(I,J)=0.D0
               ENDIF
             ENDDO
           ENDDO
          N=5
          CALL POWELL(TRANS,XI,N,TOL,ITER,EPS)
          F(2)=EPS
         ELSE
          X(4)=X(3)
          X(3)=X(2)
          X(2)=R*X(3)+C*X(1)
          F(2)=F(1)
          PATH=X(2)
          CALL RAYTRC(PATH)
          DO I=1,5
            TRANS(I)=0.D0
            DO J=1,5
              IF(I.EQ.J) THEN
                XI(I,J)=1.D0
               ELSE
                XI(I,J)=0.D0
               ENDIF
             ENDDO
```

```
           ENDDO
          N=5
          CALL POWELL(TRANS,XI,N,TOL,ITER,EPS)
          F(1)=EPS
         ENDIF
        GOTO 2
       ENDIF
* Output of optimum subreflector translation and rotation and sys. info
      DSCAN(1)=SCAN(1)*1.8D2/PI
      DSCAN(2)=SCAN(2)*1.8D2/PI
      CALL OUT(FEED,TRANS,DSCAN,ICN,SFOC,PATH,EPS)
      RETURN
      STOP
      END


************************************************************************
*
*     Correcting subreflector generation subroutine
*
************************************************************************

      SUBROUTINE RAYTRC(PATH)
      IMPLICIT NONE
      REAL*8 SRFM(25,25,6),SRFS(25,25,6),FEED(3),SCAN(2),R1(3),R2(3),
     C       RDOTN,PATH,A,B,C,K,R3L,R3(3),R1L,PROD,DEN,SRFMD(4),FOC,
     C       SRFA(25,25,6)
      INTEGER*2 I,J
      COMMON /REFL/ SRFMD,SRFA,FOC,FEED,SCAN,SRFM,SRFS
* FIND COMPONENTS OF RAYS INCIDENT ON MAIN REFLECTOR
      R1(1)=-COS(SCAN(1))
      R1(2)=-SIN(SCAN(1))*COS(SCAN(2))
      R1(3)=-SIN(SCAN(1))*SIN(SCAN(2))
      DO 3 I=1,25
        DO 3 J=1,25
* FIND COMPONENTS OF RAY REFLECTED FROM MAIN REFLECTOR
          RDOTN=R1(2)*SRFM(I,J,5)+R1(3)*SRFM(I,J,6)+R1(1)*SRFM(I,J,4)
          R2(1)=R1(1)-2.*RDOTN*SRFM(I,J,4)
          R2(2)=R1(2)-2.*RDOTN*SRFM(I,J,5)
          R2(3)=R1(3)-2.*RDOTN*SRFM(I,J,6)
* FIND LENGTH OF INCIDENT RAY BETWEEN MAIN REFLECTOR AND A.P.
          R1L=COS(SCAN(1))*(1.D2+TAN(-SCAN(1))*COS(SCAN(2))*SRFM(I,J,2)+
     C              TAN(-SCAN(1))*SIN(SCAN(2))*SRFM(I,J,3)-SRFM(I,J,1))
* FIND SUBREFLECTOR POINTS BY SETTING TOTAL PATH LENGTH
          A=(R1(2)-2.D0*RDOTN*SRFM(I,J,5))/
     C      (R1(1)-2.D0*RDOTN*SRFM(I,J,4))
          C=R1(3)-2.D0*RDOTN*SRFM(I,J,6)
          B=C*SQRT(1+A**2.D0)/SQRT(1-C**2.D0)
          K=PATH-R1L
          PROD=2.D0*(K*SQRT(1+A**2.D0+B**2.D0)+A*(SRFM(I,J,2)-FEED(2))+
     C                 B*(SRFM(I,J,3)-FEED(3)))
          SRFS(I,J,1)=(K**2.D0+SRFM(I,J,1)*PROD
     C                 -(FEED(2)-SRFM(I,J,2))**2.D0
     C                 -(FEED(3)-SRFM(I,J,3))**2.D0+SRFM(I,J,1)**2.D0
     C            -FEED(1)**2.D0)/(PROD+2.D0*SRFM(I,J,1)-2.D0*FEED(1))
          SRFS(I,J,2)=A*(SRFS(I,J,1)-SRFM(I,J,1))+SRFM(I,J,2)
          SRFS(I,J,3)=B*(SRFS(I,J,1)-SRFM(I,J,1))+SRFM(I,J,3)
* FIND SUBREFLECTOR NORMAL
          R3L=SQRT((SRFS(I,J,1)-FEED(1))**2.D0
     C             +(SRFS(I,J,2)-FEED(2))**2.D0+
```

```
     C               (SRFS(I,J,3)-FEED(3))**2.D0)
          R3(1)=(FEED(1)-SRFS(I,J,1))/R3L
          R3(2)=(FEED(2)-SRFS(I,J,2))/R3L
          R3(3)=(FEED(3)-SRFS(I,J,3))/R3L
          SRFS(I,J,4)=R3(1)-R2(1)
          SRFS(I,J,5)=R3(2)-R2(2)
          SRFS(I,J,6)=R3(3)-R2(3)
         DEN=SQRT(SRFS(I,J,4)**2.D0+SRFS(I,J,5)**2.D0+SRFS(I,J,6)**2.D0)
          SRFS(I,J,4)=SRFS(I,J,4)/DEN
          SRFS(I,J,5)=SRFS(I,J,5)/DEN
 3        SRFS(I,J,6)=SRFS(I,J,6)/DEN
      RETURN
      STOP
      END


************************************************************************
*
*     Powell's Method Optimization
*
************************************************************************

      SUBROUTINE POWELL(P,XI,N,FTOL,ITER,FRET)
      IMPLICIT NONE
      REAL*8 P(5),XI(5,5),PT(5),PTT(5),XIT(5),FTOL,FPTT,FRET,FP,T,DEL,
     C       FUNC
      INTEGER*2 I,J,ITER,N,IBIG,ITMAX
      ITMAX=200
      FRET=FUNC(P)
      DO J=1,N
        PT(J)=P(J)
      END DO
      ITER=0
 1    ITER=ITER+1
      FP=FRET
      IBIG=0
      DEL=0.D0
      DO I=1,N
        DO J=1,N
          XIT(J)=XI(J,I)
        END DO
        FPTT=FRET
        CALL LINMIN(P,XIT,FRET)
        IF (ABS(FPTT-FRET).GT.DEL) THEN
          DEL=ABS(FPTT-FRET)
          IBIG=I
        END IF
      END DO
      IF (2.D0*DABS(FP-FRET).LE.FTOL*(DABS(FP)+DABS(FRET))) RETURN
      IF (ITER.EQ.ITMAX) PAUSE 'Powell exceeding maximum iteration'
      DO J=1,N
        PTT(J)=2.D0*P(J)-PT(J)
        XIT(J)=P(J)-PT(J)
        PT(J)=P(J)
      END DO
      FPTT=FUNC(PTT)
      IF (FPTT.GE.FP) GOTO 1
      T=2.D0*(FP-2.D0*FRET+FPTT)*(FP-FRET-DEL)**2.D0-DEL*(FP-FPTT)**2.D0
      IF (T.GT.0.) GOTO 1
      CALL LINMIN(P,XIT,FRET)
```

```
 DO J=1,N
   XI(J,IBIG)=XIT(J)
 END DO
 GOTO 1
 END

 SUBROUTINE LINMIN(P,XI,FRET)
 IMPLICIT NONE
 EXTERNAL F1DIM
 REAL*8 P(5),XI(5),AX,XX,FRET,TOL,PCOM(50),XICOM(50),BX,FA,FX,FB,
C       XMIN,BRENT
 INTEGER*2 J,NCOM
 COMMON /F1COM/ PCOM,XICOM,NCOM
 TOL=1.D-10
 NCOM=5
 DO J=1,5
   PCOM(J)=P(J)
   XICOM(J)=XI(J)
 END DO
 AX=0.
 XX=1.
 CALL MNBRAK(AX,XX,BX,FA,FX,FB,F1DIM)
 FRET=BRENT(AX,XX,BX,F1DIM,TOL,XMIN)
 DO J=1,5
   XI(J)=XMIN*XI(J)
   P(J)=P(J)+XI(J)
 END DO
 RETURN
 END

 REAL*8 FUNCTION F1DIM(X)
 IMPLICIT NONE
 REAL*8 PCOM(50),XICOM(50),XT(50),X,FUNC
 INTEGER*2 NCOM,J
 COMMON /F1COM/ PCOM,XICOM,NCOM
 DO J=1,NCOM
   XT(J)=PCOM(J)+X*XICOM(J)
 END DO
 F1DIM=FUNC(XT)
 RETURN
 END

 SUBROUTINE MNBRAK(AX,BX,CX,FA,FB,FC,FUNC)
 IMPLICIT NONE
 REAL*8 AX,BX,CX,FA,FB,FC,DUM,GLIMIT,GOLD,TINY,R,Q,U,ULIM,FU,
C       FUNC
 GOLD=1.618034D0
 GLIMIT=100.D0
 TINY=1.D-20
 FA=FUNC(AX)
 FB=FUNC(BX)
 IF(FB.GT.FA) THEN
   DUM=AX
   AX=BX
   BX=DUM
   DUM=FB
   FB=FA
   FA=DUM
 END IF
 CX=BX+GOLD*(BX-AX)
```

```
      FC=FUNC(CX)
1     IF (FB.GT.FC) THEN
        R=(BX-AX)*(FB-FC)
        Q=(BX-CX)*(FB-FA)
        U=BX-((BX-CX)*Q-(BX-AX)*R)/(2.*SIGN(MAX(ABS(Q-R),TINY),Q-R))
        ULIM=BX+GLIMIT*(CX-BX)
        IF ((BX-U)*(U-CX).GT.0.) THEN
          FU=FUNC(U)
          IF (FU.LT.FC) THEN
            AX=BX
            FA=FB
            BX=U
            FB=FU
            RETURN
          ELSE IF (FU.GT.FB) THEN
            CX=U
            FC=FU
            RETURN
          END IF
          U=CX+GOLD*(CX-BX)
          FU=FUNC(U)
        ELSE IF ((CX-U)*(U-ULIM).GT.0.) THEN
          U=ULIM
          FU=FUNC(U)
        ELSE
          U=CX+GOLD*(CX-BX)
          FU=FUNC(U)
        END IF
        AX=BX
        BX=CX
        CX=U
        FA=FB
        FB=FC
        FC=FU
        GOTO 1
      END IF
      RETURN
      END

      REAL*8 FUNCTION BRENT(AX,BX,CX,F,TOL,XMIN)
      IMPLICIT NONE
      REAL*8 AX,BX,CX,F,TOL,XMIN,CGOLD,ZEPS,A,B,V,W,X,E,FX,FV,FW,XM,
     C       TOL1,TOL2,R,Q,ETEMP,P,D,U,FU
      INTEGER*2 ITER,ITMAX
      ITMAX=100
      CGOLD=.3819660D0
      ZEPS=1.0D-10
      A=MIN(AX,CX)
      B=MAX(AX,CX)
      V=BX
      W=V
      X=V
      E=0.
      FX=F(X)
      FV=FX
      FW=FX
      DO ITER=1,ITMAX
        XM=0.5*(A+B)
        TOL1=TOL*ABS(X)+ZEPS
        TOL2=2.*TOL1
```

```
       IF (ABS(X-XM).LE.(TOL2-.5*(B-A))) GOTO 3
       IF (ABS(E).GT.TOL1) THEN
         R=(X-W)*(FX-FV)
         Q=(X-V)*(FX-FW)
         P=(X-V)*Q-(X-W)*R
         Q=2.*(Q-R)
         IF (Q.GT.0) P=-P
         Q=ABS(Q)
         ETEMP=E
         E=D
         IF(ABS(P).GE.ABS(.5*Q*ETEMP).OR.P.LE.Q*(A-X).OR.
    &         P.GE.Q*(B-X)) GOTO 1
         D=P/Q
         U=X+D
         IF(U-A.LT.TOL2.OR.B-U.LT.TOL2) D=SIGN(TOL1,XM-X)
         GOTO 2
       END IF
1      IF (X.GE.XM) THEN
         E=A-X
       ELSE
         E=B-X
       END IF
       D=CGOLD*E
2      IF(ABS(D).GE.TOL1) THEN
         U=X+D
       ELSE
         U=X+SIGN(TOL1,D)
       END IF
       FU=F(U)
       IF (FU.LE.FX) THEN
         IF (U.GE.X) THEN
           A=X
         ELSE
           B=X
         END IF
         V=W
         FV=FW
         W=X
         FW=FX
         X=U
         FX=FU
       ELSE
         IF (U.LT.X) THEN
           A=U
         ELSE
           B=U
         END IF
         IF (FU.LE.FW.OR.W.EQ.X) THEN
           V=W
           FV=FW
           W=U
           FW=FU
         ELSE IF (FU.LE.FV.OR.V.EQ.X.OR.V.EQ.W) THEN
           V=U
           FV=FU
         END IF
       END IF
     END DO
     PAUSE 'Brent exceed maximum iterations.'
3    XMIN=X
```

```
      BRENT=FX
      RETURN
      END


*************************************************************************
*
*     Powell's Method Optimization Error Function
*
*************************************************************************

      REAL*8 FUNCTION FUNC(TRANS)
      IMPLICIT NONE
      REAL*8 SRFA(25,25,6),SRFAT(25,25,6),TRANS(5),RMSERR,SRFS(25,25,6),
     C       SRFMD(4),FOC,FEED(3),SC(2),SRFM(25,25,6)
      INTEGER*2 I,J
      COMMON /REFL/ SRFMD,SRFA,FOC,FEED,SC,SRFM,SRFS
      CALL POSIT(SRFAT,TRANS)
      RMSERR=0.D0
      DO 1 I=1,25
        DO 1 J=1,25
          RMSERR=RMSERR+(((SRFAT(I,J,1)-SRFS(I,J,1))*SRFS(I,J,4))**2.D0
     C                 +((SRFAT(I,J,2)-SRFS(I,J,2))*SRFS(I,J,5))**2.D0
     C                 +((SRFAT(I,J,3)-SRFS(I,J,3))*SRFS(I,J,6))**2.D0)
 1       CONTINUE
      FUNC=DSQRT(RMSERR)
      RETURN
      STOP
      END


*************************************************************************
*
*     Type 1 Concept Subreflector Positioning Code
*
*************************************************************************

      SUBROUTINE POSIT(SRFAT,TRANS)
      IMPLICIT NONE
      REAL*8 SRFA(25,25,6),SRFAT(25,25,6),TRANS(5),SRFMD(4),FOC,FEED(3),
     C       SCAN(2),T(5),SRFM(25,25,6),SRFS(25,25,6)
      INTEGER*2 I,J
      COMMON /REFL/ SRFMD,SRFA,FOC,FEED,SCAN,SRFM,SRFS
      T(1)=TRANS(3)
      T(2)=TRANS(4)
      T(3)=TRANS(5)
      T(4)=TRANS(1)
      T(5)=TRANS(2)
      DO 1 I=1,25
        DO 1 J=1,25
          SRFAT(I,J,1)=T(1)+SRFA(13,13,1)-
     C                          SIN(T(4))*(SRFA(I,J,2)-SRFA(13,13,2))+
     C          COS(T(4))*SIN(T(5))*(SRFA(I,J,3)-SRFA(13,13,3))+
     C          COS(T(4))*COS(T(5))*(SRFA(I,J,1)-SRFA(13,13,1))
          SRFAT(I,J,2)=T(2)+SRFA(13,13,2)+
     C                          COS(T(4))*(SRFA(I,J,2)-SRFA(13,13,2))+
     C          SIN(T(4))*SIN(T(5))*(SRFA(I,J,3)-SRFA(13,13,3))+
     C          SIN(T(4))*COS(T(5))*(SRFA(I,J,1)-SRFA(13,13,1))
          SRFAT(I,J,3)=T(3)+SRFA(13,13,3)+
     C                          COS(T(5))*(SRFA(I,J,3)-SRFA(13,13,3))-
```

```
     C                   SIN(T(5))*(SRFA(I,J,1)-SRFA(13,13,1))
          SRFAT(I,J,4)=-SIN(T(4))*SRFA(I,J,5)+
     C        COS(T(4))*SIN(T(5))*SRFA(I,J,6)+
     C        COS(T(4))*COS(T(5))*SRFA(I,J,4)
          SRFAT(I,J,5)=COS(T(4))*SRFA(I,J,5)+
     C       SIN(T(4))*SIN(T(5))*SRFA(I,J,6)+
     C       SIN(T(4))*COS(T(5))*SRFA(I,J,4)
 1        SRFAT(I,J,6)=COS(T(5))*SRFA(I,J,6)-
     C                 SIN(T(5))*SRFA(I,J,4)
      RETURN
      STOP
      END


************************************************************************
*
*     Type 1 Concept Output Code
*
************************************************************************

      SUBROUTINE OUT(FEED,TRANS,SCAN,ICN,SFOC,PATH,RMSERR)
      IMPLICIT NONE
      REAL*8 FEED(3),TRANS(5),SCAN(2),SRFAT(25,25,6),PI,PATH,RMSERR,
     C       SFOC(2,3),GCOEF(10),U,V
      INTEGER*2 ICN,K(3)
      CHARACTER*12 OUTFILE
      PI=3.14159265358979323846D0
      U=SIN(SCAN(1)*PI/1.8D2)*COS(SCAN(2)*PI/1.8D2)
      V=SIN(SCAN(1)*PI/1.8D2)*SIN(SCAN(2)*PI/1.8D2)
      K(1)=48+ICN/100
      K(2)=48+(ICN-(K(1)-48)*100)/10
      K(3)=48+ICN-(K(1)-48)*100-(K(2)-48)*10
      CALL POSITF(SFOC,TRANS,GCOEF)
      CALL POSIT(SRFAT,TRANS)
      OUTFILE='KSFT1XXX.MOV'
      OUTFILE(6:6)=CHAR(K(1))
      OUTFILE(7:7)=CHAR(K(2))
      OUTFILE(8:8)=CHAR(K(3))
      OPEN(4,FILE=OUTFILE,STATUS='UNKNOWN')
      WRITE(4,'(A10,2F12.7)')'SCANNED TO ',SCAN(1),SCAN(2)
      WRITE(4,'(5F15.10)')TRANS(4),TRANS(5),TRANS(3),TRANS(1),TRANS(2)
      WRITE(4,'(2F15.10)')PATH,RMSERR
      ENDFILE(4)
      CLOSE(4)
* 20 GHz GRASP7 Input File
      OUTFILE='KSFT1XXX.INP'
      OUTFILE(6:6)=CHAR(K(1))
      OUTFILE(7:7)=CHAR(K(2))
      OUTFILE(8:8)=CHAR(K(3))
      OPEN(4,FILE=OUTFILE,STATUS='UNKNOWN')
      WRITE(4,'(A30)')'***** GRASP77 INPUT FILE *****'
      WRITE(4,'(A10,2F12.7)')'SCANNED TO ',SCAN(1),SCAN(2)
      WRITE(4,'(F12.7,4I2)')1.5D-2,2,1,0,0
      WRITE(4,'(A31)')'** MAIN REFLECTOR INPUT DATA **'
      WRITE(4,'(3F12.7)')0.,0.,0.
      WRITE(4,'(3F12.7)')1.,0.,0.
      WRITE(4,'(3F12.7)')0.,1.,0.
      WRITE(4,'(I2,2F12.7)')1,7.795,0.
      WRITE(4,'(3I2)')4,0,0
      WRITE(4,'(4F12.7)')0.,0.,0.,13.5
```

```
      WRITE(4,'(2F12.7)')5.315,5.315
      WRITE(4,'(A30)')'** SUB REFLECTOR INPUT DATA **'
      WRITE(4,'(3F12.7)')0.,0.,0.
      WRITE(4,'(3F12.7)')1.,0.,0.
      WRITE(4,'(3F12.7)')0.,1.,0.
      WRITE(4,'(I2,2F12.7)')1,(SRFAT(25,13,2)+SRFAT(1,13,2))/2.D0,
     C                        (SRFAT(13,25,3)+SRFAT(13,1,3))/2.D0
      WRITE(4,'(2I2)')3,0
      WRITE(4,'(5F14.7)')GCOEF(1),GCOEF(2),GCOEF(3),GCOEF(4),GCOEF(5)
      WRITE(4,'(5F14.7)')GCOEF(6),GCOEF(7),GCOEF(8),GCOEF(9),GCOEF(10)
      WRITE(4,'(5F12.7,I5)')0.,0.,0.,0.,0.,1
      WRITE(4,'(2F12.7)')(SRFAT(25,13,2)-SRFAT(1,13,2))/2.D0,
     C                   (SRFAT(13,25,3)-SRFAT(13,1,3))/2.D0
      WRITE(4,'(A21)')'** FEED INPUT DATA **'
      WRITE(4,'(3F12.7)')FEED(2),FEED(3),FEED(1)
      WRITE(4,'(3F12.7)').964483694,0.,-.264142395
      WRITE(4,'(3F12.7)')0.,1.,0.
      WRITE(4,'(I2)')1
      WRITE(4,'(6F12.7)')0.,0.,0.,0.,0.,0.
      WRITE(4,'(F12.7,I2)')0.,1
      WRITE(4,'(4F12.7,3I2)')0.,0.,1.,90.,0,0,3
      WRITE(4,'(I2)')6
      WRITE(4,'(5F12.7,I3)')-15.,-15.,7.1574,0.,0.,1
      WRITE(4,'(A40)')'** MAIN REFLECTOR FIELD SPECIFICATION **'
      WRITE(4,'(I2)')1
      WRITE(4,'(3F12.7)')7.795,0.,10.
      WRITE(4,'(3F12.7)')1.,0.,0.
      WRITE(4,'(3F12.7)')0.,1.,0.
      WRITE(4,'(2I6,F12.7,2I3)')60,144,0.,0,0
      WRITE(4,'(3I3)')0,-1,1
      WRITE(4,'(F12.7)')10.
      WRITE(4,'(2F12.7)')U,V
      WRITE(4,'(2I3)')0,1
      WRITE(4,'(2I3)')3,1
      WRITE(4,'(4F12.7,2I6)')-1.D-2,-1.D-2,1.D-2,1.D-2,25,25
      WRITE(4,'(4I6)')3,1
      OUTFILE='KSFT1XXX.P1'
      OUTFILE(6:6)=CHAR(K(1))
      OUTFILE(7:7)=CHAR(K(2))
      OUTFILE(8:8)=CHAR(K(3))
      WRITE(4,'(A12)')OUTFILE
      WRITE(4,'(A39)')'** SUB REFLECTOR FIELD SPECIFICATION **'
      WRITE(4,'(I2)')0
      WRITE(4,'(A30)')'** FEED FIELD SPECIFICATION **'
      WRITE(4,'(I2)')0
      ENDFILE(4)
      CLOSE(4)
      OUTFILE='KSFUVXXX.INP'
      OUTFILE(6:6)=CHAR(K(1))
      OUTFILE(7:7)=CHAR(K(2))
      OUTFILE(8:8)=CHAR(K(3))
      OPEN(4,FILE=OUTFILE,STATUS='UNKNOWN')
      WRITE(4,'(A25)')'UVPROC CONTROL INPUT FILE'
      OUTFILE='KSFT1XXX.P1'
      OUTFILE(6:6)=CHAR(K(1))
      OUTFILE(7:7)=CHAR(K(2))
      OUTFILE(8:8)=CHAR(K(3))
      WRITE(4,'(A12)')OUTFILE
      WRITE(4,'(6I2)')1,1,1,1,0,0
      WRITE(4,'(2I2)')1,1
```

```
      WRITE(4,'(6I2)')0,1,0,0,1,0
      WRITE(4,'(A12)')' TEMP.P2'
      WRITE(4,'(I2)')3
      WRITE(4,'(2I4)')101,101
      WRITE(4,'(7I2)')0,0,1,1,0,0,0
      WRITE(4,'(4I2)')3,0,2,0
      WRITE(4,'(F5.1)')3.
      WRITE(4,'(F5.1)')10.
      WRITE(4,'(5I2)')1,0,0,1,1
      WRITE(4,'(F7.4)')0.1213
      ENDFILE(4)
      CLOSE(4)
* 40 GHz GRASP7 Input File
      OUTFILE='KSFT1XXX.INP'
      OUTFILE(6:6)=CHAR(K(1)+1)
      OUTFILE(7:7)=CHAR(K(2))
      OUTFILE(8:8)=CHAR(K(3))
      OPEN(4,FILE=OUTFILE,STATUS='UNKNOWN')
      WRITE(4,'(A30)')'***** GRASP77 INPUT FILE *****'
      WRITE(4,'(A10,2F12.7)')'SCANNED TO ',SCAN(1),SCAN(2)
      WRITE(4,'(F12.7,4I2)')7.5D-3,2,1,0,0
      WRITE(4,'(A31)')'** MAIN REFLECTOR INPUT DATA **'
      WRITE(4,'(3F12.7)')0.,0.,0.
      WRITE(4,'(3F12.7)')1.,0.,0.
      WRITE(4,'(3F12.7)')0.,1.,0.
      WRITE(4,'(I2,2F12.7)')1,7.795,0.
      WRITE(4,'(3I2)')4,0,0
      WRITE(4,'(4F12.7)')0.,0.,0.,13.5
      WRITE(4,'(2F12.7)')5.315,5.315
      WRITE(4,'(A30)')'** SUB REFLECTOR INPUT DATA **'
      WRITE(4,'(3F12.7)')0.,0.,0.
      WRITE(4,'(3F12.7)')1.,0.,0.
      WRITE(4,'(3F12.7)')0.,1.,0.
      WRITE(4,'(I2,2F12.7)')1,(SRFAT(25,13,2)+SRFAT(1,13,2))/2.D0,
     C                        (SRFAT(13,25,3)+SRFAT(13,1,3))/2.D0
      WRITE(4,'(2I2)')3,0
      WRITE(4,'(5F14.7)')GCOEF(1),GCOEF(2),GCOEF(3),GCOEF(4),GCOEF(5)
      WRITE(4,'(5F14.7)')GCOEF(6),GCOEF(7),GCOEF(8),GCOEF(9),GCOEF(10)
      WRITE(4,'(5F12.7,I5)')0.,0.,0.,0.,0.,1
      WRITE(4,'(2F12.7)')(SRFAT(25,13,2)-SRFAT(1,13,2))/2.D0,
     C                   (SRFAT(13,25,3)-SRFAT(13,1,3))/2.D0
      WRITE(4,'(A21)')'** FEED INPUT DATA **'
      WRITE(4,'(3F12.7)')FEED(2),FEED(3),FEED(1)
      WRITE(4,'(3F12.7)').964483694,0.,-.264142395
      WRITE(4,'(3F12.7)')0.,1.,0.
      WRITE(4,'(I2)')1
      WRITE(4,'(6F12.7)')0.,0.,0.,0.,0.,0.
      WRITE(4,'(F12.7,I2)')0.,1
      WRITE(4,'(4F12.7,3I2)')0.,0.,1.,90.,0,0,3
      WRITE(4,'(I2)')6
      WRITE(4,'(5F12.7,I3)')-15.,-15.,7.1574,0.,0.,1
      WRITE(4,'(A40)')'** MAIN REFLECTOR FIELD SPECIFICATION **'
      WRITE(4,'(I2)')1
      WRITE(4,'(3F12.7)')7.795,0.,10.
      WRITE(4,'(3F12.7)')1.,0.,0.
      WRITE(4,'(3F12.7)')0.,1.,0.
      WRITE(4,'(2I6,F12.7,2I3)')60,144,0.,0,0
      WRITE(4,'(3I3)')0,-1,1
      WRITE(4,'(F12.7)')10.
      WRITE(4,'(2F12.7)')U,V
```

```
      WRITE(4,'(2I3)')0,1
      WRITE(4,'(2I3)')3,1
      WRITE(4,'(4F12.7,2I6)')-5.D-3,-5.D-3,5.D-3,5.D-3,25,25
      WRITE(4,'(4I6)')3,1
      OUTFILE='KSFT1XXX.P1'
      OUTFILE(6:6)=CHAR(K(1)+1)
      OUTFILE(7:7)=CHAR(K(2))
      OUTFILE(8:8)=CHAR(K(3))
      WRITE(4,'(A12)')OUTFILE
      WRITE(4,'(A39)')'** SUB REFLECTOR FIELD SPECIFICATION **'
      WRITE(4,'(I2)')0
      WRITE(4,'(A30)')'** FEED FIELD SPECIFICATION **'
      WRITE(4,'(I2)')0
      ENDFILE(4)
      CLOSE(4)
      OUTFILE='KSFUVXXX.INP'
      OUTFILE(6:6)=CHAR(K(1)+1)
      OUTFILE(7:7)=CHAR(K(2))
      OUTFILE(8:8)=CHAR(K(3))
      OPEN(4,FILE=OUTFILE,STATUS='UNKNOWN')
      WRITE(4,'(A25)')'UVPROC CONTROL INPUT FILE'
      OUTFILE='KSFT1XXX.P1'
      OUTFILE(6:6)=CHAR(K(1)+1)
      OUTFILE(7:7)=CHAR(K(2))
      OUTFILE(8:8)=CHAR(K(3))
      WRITE(4,'(A12)')OUTFILE
      WRITE(4,'(6I2)')1,1,1,1,0,0
      WRITE(4,'(2I2)')1,1
      WRITE(4,'(6I2)')0,1,0,0,1,0
      WRITE(4,'(A12)')' TEMP.P2'
      WRITE(4,'(I2)')3
      WRITE(4,'(2I4)')101,101
      WRITE(4,'(7I2)')0,0,1,1,0,0,0
      WRITE(4,'(4I2)')3,0,2,0
      WRITE(4,'(F5.1)')3.
      WRITE(4,'(F5.1)')10.
      WRITE(4,'(5I2)')1,0,0,1,1
      WRITE(4,'(F7.4)')0.0606
      ENDFILE(4)
      CLOSE(4)
* 80 GHz GRASP7 Input File
      OUTFILE='KSFT1XXX.INP'
      OUTFILE(6:6)=CHAR(K(1)+2)
      OUTFILE(7:7)=CHAR(K(2))
      OUTFILE(8:8)=CHAR(K(3))
      OPEN(4,FILE=OUTFILE,STATUS='UNKNOWN')
      WRITE(4,'(A30)')'***** GRASP77 INPUT FILE *****'
      WRITE(4,'(A10,2F12.7)')'SCANNED TO ',SCAN(1),SCAN(2)
      WRITE(4,'(F12.7,4I2)')3.75D-3,2,1,0,0
      WRITE(4,'(A31)')'** MAIN REFLECTOR INPUT DATA **'
      WRITE(4,'(3F12.7)')0.,0.,0.
      WRITE(4,'(3F12.7)')1.,0.,0.
      WRITE(4,'(3F12.7)')0.,1.,0.
      WRITE(4,'(I2,2F12.7)')1,7.795,0.
      WRITE(4,'(3I2)')4,0,0
      WRITE(4,'(4F12.7)')0.,0.,0.,13.5
      WRITE(4,'(2F12.7)')5.315,5.315
      WRITE(4,'(A30)')'** SUB REFLECTOR INPUT DATA **'
      WRITE(4,'(3F12.7)')0.,0.,0.
      WRITE(4,'(3F12.7)')1.,0.,0.
```

```
      WRITE(4,'(3F12.7)')0.,1.,0.
      WRITE(4,'(I2,2F12.7)')1,(SRFAT(25,13,2)+SRFAT(1,13,2))/2.D0,
     C                        (SRFAT(13,25,3)+SRFAT(13,1,3))/2.D0
      WRITE(4,'(2I2)')3,0
      WRITE(4,'(5F14.7)')GCOEF(1),GCOEF(2),GCOEF(3),GCOEF(4),GCOEF(5)
      WRITE(4,'(5F14.7)')GCOEF(6),GCOEF(7),GCOEF(8),GCOEF(9),GCOEF(10)
      WRITE(4,'(5F12.7,I5)')0.,0.,0.,0.,0.,1
      WRITE(4,'(2F12.7)')(SRFAT(25,13,2)-SRFAT(1,13,2))/2.D0,
     C                   (SRFAT(13,25,3)-SRFAT(13,1,3))/2.D0
      WRITE(4,'(A21)')'** FEED INPUT DATA **'
      WRITE(4,'(3F12.7)')FEED(2),FEED(3),FEED(1)
      WRITE(4,'(3F12.7)').964483694,0.,-.264142395
      WRITE(4,'(3F12.7)')0.,1.,0.
      WRITE(4,'(I2)')1
      WRITE(4,'(6F12.7)')0.,0.,0.,0.,0.,0.
      WRITE(4,'(F12.7,I2)')0.,1
      WRITE(4,'(4F12.7,3I2)')0.,0.,1.,90.,0,0,3
      WRITE(4,'(I2)')6
      WRITE(4,'(5F12.7,I3)')-15.,-15.,7.1574,0.,0.,1
      WRITE(4,'(A40)')'** MAIN REFLECTOR FIELD SPECIFICATION **'
      WRITE(4,'(I2)')1
      WRITE(4,'(3F12.7)')7.795,0.,10.
      WRITE(4,'(3F12.7)')1.,0.,0.
      WRITE(4,'(3F12.7)')0.,1.,0.
      WRITE(4,'(2I6,F12.7,2I3)')60,144,0.,0,0
      WRITE(4,'(3I3)')0,-1,1
      WRITE(4,'(F12.7)')10.
      WRITE(4,'(2F12.7)')U,V
      WRITE(4,'(2I3)')0,1
      WRITE(4,'(2I3)')3,1
      WRITE(4,'(4F12.7,2I6)')-2.5D-3,-2.5D-3,2.5D-3,2.5D-3,25,25
      WRITE(4,'(4I6)')3,1
      OUTFILE='KSFT1XXX.P1'
      OUTFILE(6:6)=CHAR(K(1)+2)
      OUTFILE(7:7)=CHAR(K(2))
      OUTFILE(8:8)=CHAR(K(3))
      WRITE(4,'(A12)')OUTFILE
      WRITE(4,'(A39)')'** SUB REFLECTOR FIELD SPECIFICATION **'
      WRITE(4,'(I2)')0
      WRITE(4,'(A30)')'** FEED FIELD SPECIFICATION **'
      WRITE(4,'(I2)')0
      ENDFILE(4)
      CLOSE(4)
      OUTFILE='KSFUVXXX.INP'
      OUTFILE(6:6)=CHAR(K(1)+2)
      OUTFILE(7:7)=CHAR(K(2))
      OUTFILE(8:8)=CHAR(K(3))
      OPEN(4,FILE=OUTFILE,STATUS='UNKNOWN')
      WRITE(4,'(A25)')'UVPROC CONTROL INPUT FILE'
      OUTFILE='KSFT1XXX.P1'
      OUTFILE(6:6)=CHAR(K(1)+2)
      OUTFILE(7:7)=CHAR(K(2))
      OUTFILE(8:8)=CHAR(K(3))
      WRITE(4,'(A12)')OUTFILE
      WRITE(4,'(6I2)')1,1,1,1,0,0
      WRITE(4,'(2I2)')1,1
      WRITE(4,'(6I2)')0,1,0,0,1,0
      WRITE(4,'(A7)')'TEMP.P2'
      WRITE(4,'(I2)')3
      WRITE(4,'(2I4)')101,101
```

```
      WRITE(4,'(7I2)')0,0,1,1,0,0,0
      WRITE(4,'(4I2)')3,0,2,0
      WRITE(4,'(F5.1)')3.
      WRITE(4,'(F5.1)')10.
      WRITE(4,'(5I2)')1,0,0,1,1
      WRITE(4,'(F7.4)')0.0303
      ENDFILE(4)
      CLOSE(4)
      RETURN
      STOP
      END


************************************************************************
*
*     Type 1 Concept Subreflector Focal Point Positioning Code
*
************************************************************************

      SUBROUTINE POSITF(SFOC,TRANS,GCOEF)
      IMPLICIT NONE
      REAL*8 SRFA(25,25,6),SFOC(2,3),TRANS(5),SRFMD(4),FOC,FEED(3),
     C       SCAN(2),T(5),GCOEF(10),SFOCT(2,3),ALPHA,BETA,GAMMA,
     C       DELTA,C,SRFM(25,25,6),SRFS(25,25,6)
      INTEGER*2 I
      COMMON /REFL/ SRFMD,SRFA,FOC,FEED,SCAN,SRFM,SRFS
      T(1)=TRANS(3)
      T(2)=TRANS(4)
      T(3)=TRANS(5)
      T(4)=TRANS(1)
      T(5)=TRANS(2)
      DO 1 I=1,2
          SFOCT(I,1)=T(1)+SRFA(13,13,1)-
     C                        SIN(T(4))*(SFOC(I,2)-SRFA(13,13,2))+
     C              COS(T(4))*SIN(T(5))*(SFOC(I,3)-SRFA(13,13,3))+
     C              COS(T(4))*COS(T(5))*(SFOC(I,1)-SRFA(13,13,1))
          SFOCT(I,2)=T(2)+SRFA(13,13,2)+
     C                        COS(T(4))*(SFOC(I,2)-SRFA(13,13,2))+
     C              SIN(T(4))*SIN(T(5))*(SFOC(I,3)-SRFA(13,13,3))+
     C              SIN(T(4))*COS(T(5))*(SFOC(I,1)-SRFA(13,13,1))
 1        SFOCT(I,3)=T(3)+SRFA(13,13,3)+
     C                        COS(T(5))*(SFOC(I,3)-SRFA(13,13,3))-
     C                        SIN(T(5))*(SFOC(I,1)-SRFA(13,13,1))
      C=DSQRT((SRFA(13,13,1)-SFOC(2,1))**2.D0+
     C        (SRFA(13,13,2)-SFOC(2,2))**2.D0+
     C        (SRFA(13,13,3)-SFOC(2,3))**2.D0)-
     C  DSQRT((SRFA(13,13,1)-SFOC(1,1))**2.D0+
     C        (SRFA(13,13,2)-SFOC(1,2))**2.D0+
     C        (SRFA(13,13,3)-SFOC(1,3))**2.D0)
      BETA=SFOCT(2,2)-SFOCT(1,2)
      GAMMA=SFOCT(2,3)-SFOCT(1,3)
      DELTA=SFOCT(2,1)-SFOCT(1,1)
      ALPHA=SFOCT(1,1)**2.D0+SFOCT(1,2)**2.D0+SFOCT(1,3)**2.D0-
     C      SFOCT(2,1)**2.D0-SFOCT(2,2)**2.D0-SFOCT(2,3)**2.D0-
     C      C**2.D0
      GCOEF(1) =4.D0*(BETA**2.D0-C**2.D0)
      GCOEF(2) =8.D0*BETA*GAMMA
      GCOEF(3) =4.D0*(GAMMA**2.D0-C**2.D0)
      GCOEF(4) =4.D0*(ALPHA*BETA+2.D0*C**2.D0*SFOCT(2,2))
      GCOEF(5) =4.D0*(ALPHA*GAMMA+2.D0*C**2.D0*SFOCT(2,3))
```

```
 GCOEF(6) =ALPHA**2.D0-4.D0*C**2.D0*(SFOCT(2,1)**2.D0+
C          SFOCT(2,2)**2.D0+SFOCT(2,3)**2.D0)
 GCOEF(7) =4.D0*(C**2.D0-DELTA**2.D0)
 GCOEF(8) =-4.D0*(ALPHA*DELTA+2.D0*C**2.D0*SFOCT(2,1))
 GCOEF(9) =-8.D0*BETA*DELTA
 GCOEF(10)=-8.D0*GAMMA*DELTA
 RETURN
 STOP
 END
```

Appendix 2

Program listing of the Transmit Mode Raytracing error functional optimization software

```
***********************************************************************
*
*     Transmit Mode Raytracing Optimization Code
*
*     James W. LaPean, Jr.                        11/18/93
*
***********************************************************************

      PROGRAM TMRT1
      IMPLICIT NONE
      REAL*8 SRFMD(4),SRFA(25,25,6),SCND(6),SCAN(2),FOC,RMSERR,TRANS(5),
     C       FEED(3),SC(2),PI,XI(5,5),TOL,SFOC(2,3)
      INTEGER*2 ICN,I,J,T,P,TINC,PINC,N,ITER
      CHARACTER*12 SUBFILE
      COMMON /REFL/ SRFMD,SRFA,FOC,FEED,SC
      PI=3.14159265358979323846D0
      TOL=1.D-10
* Program inputs read from input file
      OPEN(3,FILE='TMRT1.INP',STATUS='OLD')
      READ(3,*)SRFMD(1),SRFMD(2),SRFMD(3),SRFMD(4)
      READ(3,*)FOC,FEED(1),FEED(2),FEED(3)
      READ(3,*)SCND(1),SCND(2),SCND(3),SCND(4),TINC,PINC
      READ(3,*)ICN
      READ(3,'(A12)')SUBFILE
* Nominal subreflector data entry
      OPEN(4,FILE=SUBFILE,STATUS='OLD')
      READ(4,'(6F12.7)')SFOC(1,1),SFOC(1,2),SFOC(1,3),
     C                  SFOC(2,1),SFOC(2,2),SFOC(2,3)
      DO 1 I=1,25
        DO 1 J=1,25
 1        READ(4,'(6F12.7)')SRFA(I,J,1),SRFA(I,J,2),SRFA(I,J,3),
     C                      SRFA(I,J,4),SRFA(I,J,5),SRFA(I,J,6)
      CLOSE(4)
* Perform scan optimized fitting for scan combinations
      WRITE(*,'(//,A1)')' '
      SCAN(2)=SCND(2)
      P=1
 2    SCAN(1)=SCND(1)
      T=1
 3    WRITE(*,'(A25,D8.3,A7,D8.3)')' Calculating for Theta = ',SCAN(1),
     C                             ' Phi = ',SCAN(2)
      SC(1)=SCAN(1)*PI/1.8D2
      SC(2)=SCAN(2)*PI/1.8D2
      DO I=1,5
        TRANS(I)=0.d0
        DO J=1,5
          IF (I.EQ.J) THEN
            XI(I,J)=1.D0
           ELSE
            XI(I,J)=0.D0
          ENDIF
        ENDDO
      ENDDO
      N=5
      CALL POWELL(TRANS,XI,N,TOL,ITER,RMSERR)
      CALL OUT(FEED,TRANS,SCAN,ICN,SFOC)
      ICN=ICN+1
      SCAN(1)=SCAN(1)+SCND(3)
      T=T+1
      IF (T.LE.TINC) GOTO 3
```

```
      SCAN(2)=SCAN(2)+SCND(4)
      P=P+1
      IF (P.LE.PINC) GOTO 2
      STOP
      END


*************************************************************************
*
*     Powell's Method Optimization
*
*************************************************************************

      SUBROUTINE POWELL(P,XI,N,FTOL,ITER,FRET)
      IMPLICIT NONE
      REAL*8 P(5),XI(5,5),PT(5),PTT(5),XIT(5),FTOL,FPTT,FRET,FP,T,DEL,
     C       FUNC
      INTEGER*2 I,J,ITER,N,IBIG,ITMAX
      ITMAX=200
      FRET=FUNC(P)
      DO J=1,N
        PT(J)=P(J)
      END DO
      ITER=0
 1    ITER=ITER+1
      FP=FRET
      IBIG=0
      DEL=0.D0
      DO I=1,N
        DO J=1,N
          XIT(J)=XI(J,I)
        END DO
        FPTT=FRET
        CALL LINMIN(P,XIT,FRET)
        IF (ABS(FPTT-FRET).GT.DEL) THEN
          DEL=ABS(FPTT-FRET)
          IBIG=I
        END IF
      END DO
      IF (2.D0*DABS(FP-FRET).LE.FTOL*(DABS(FP)+DABS(FRET))) RETURN
      IF (ITER.EQ.ITMAX) PAUSE 'Powell exceeding maximum iteration'
      DO J=1,N
        PTT(J)=2.D0*P(J)-PT(J)
        XIT(J)=P(J)-PT(J)
        PT(J)=P(J)
      END DO
      FPTT=FUNC(PTT)
      IF (FPTT.GE.FP) GOTO 1
      T=2.D0*(FP-2.D0*FRET+FPTT)*(FP-FRET-DEL)**2.D0-DEL*(FP-FPTT)**2.D0
      IF (T.GT.0.) GOTO 1
      CALL LINMIN(P,XIT,FRET)
      DO J=1,N
        XI(J,IBIG)=XIT(J)
      END DO
      GOTO 1
      END

      SUBROUTINE LINMIN(P,XI,FRET)
      IMPLICIT NONE
      EXTERNAL F1DIM
```

```
      REAL*8 P(5),XI(5),AX,XX,FRET,TOL,PCOM(50),XICOM(50),BX,FA,FX,FB,
     C       XMIN,BRENT
      INTEGER*2 J,NCOM
      COMMON /F1COM/ PCOM,XICOM,NCOM
      TOL=1.D-10
      NCOM=5
      DO J=1,5
        PCOM(J)=P(J)
        XICOM(J)=XI(J)
      END DO
      AX=0.
      XX=1.
      CALL MNBRAK(AX,XX,BX,FA,FX,FB,F1DIM)
      FRET=BRENT(AX,XX,BX,F1DIM,TOL,XMIN)
      DO J=1,5
        XI(J)=XMIN*XI(J)
        P(J)=P(J)+XI(J)
      END DO
      RETURN
      END


      REAL*8 FUNCTION F1DIM(X)
      IMPLICIT NONE
      REAL*8 PCOM(50),XICOM(50),XT(50),X,FUNC
      INTEGER*2 NCOM,J
      COMMON /F1COM/ PCOM,XICOM,NCOM
      DO J=1,NCOM
        XT(J)=PCOM(J)+X*XICOM(J)
      END DO
      F1DIM=FUNC(XT)
      RETURN
      END


      SUBROUTINE MNBRAK(AX,BX,CX,FA,FB,FC,FUNC)
      IMPLICIT NONE
      REAL*8 AX,BX,CX,FA,FB,FC,DUM,GLIMIT,GOLD,TINY,R,Q,U,ULIM,FU,
     C       FUNC
      GOLD=1.618034D0
      GLIMIT=100.D0
      TINY=1.D-20
      FA=FUNC(AX)
      FB=FUNC(BX)
      IF(FB.GT.FA) THEN
        DUM=AX
        AX=BX
        BX=DUM
        DUM=FB
        FB=FA
        FA=DUM
      END IF
      CX=BX+GOLD*(BX-AX)
      FC=FUNC(CX)
1     IF (FB.GT.FC) THEN
        R=(BX-AX)*(FB-FC)
        Q=(BX-CX)*(FB-FA)
        U=BX-((BX-CX)*Q-(BX-AX)*R)/(2.*SIGN(MAX(ABS(Q-R),TINY),Q-R))
        ULIM=BX+GLIMIT*(CX-BX)
        IF ((BX-U)*(U-CX).GT.0.) THEN
```

```
          FU=FUNC(U)
          IF (FU.LT.FC) THEN
            AX=BX
            FA=FB
            BX=U
            FB=FU
            RETURN
          ELSE IF (FU.GT.FB) THEN
            CX=U
            FC=FU
            RETURN
          END IF
          U=CX+GOLD*(CX-BX)
          FU=FUNC(U)
        ELSE IF ((CX-U)*(U-ULIM).GT.0.) THEN
          U=ULIM
          FU=FUNC(U)
        ELSE
          U=CX+GOLD*(CX-BX)
          FU=FUNC(U)
        END IF
        AX=BX
        BX=CX
        CX=U
        FA=FB
        FB=FC
        FC=FU
        GOTO 1
      END IF
      RETURN
      END


      REAL*8 FUNCTION BRENT(AX,BX,CX,F,TOL,XMIN)
      IMPLICIT NONE
      REAL*8 AX,BX,CX,F,TOL,XMIN,CGOLD,ZEPS,A,B,V,W,X,E,FX,FV,FW,XM,
     C       TOL1,TOL2,R,Q,ETEMP,P,D,U,FU
      INTEGER*2 ITER,ITMAX
      ITMAX=100
      CGOLD=.3819660D0
      ZEPS=1.0D-10
      A=MIN(AX,CX)
      B=MAX(AX,CX)
      V=BX
      W=V
      X=V
      E=0.
      FX=F(X)
      FV=FX
      FW=FX
      DO ITER=1,ITMAX
        XM=0.5*(A+B)
        TOL1=TOL*ABS(X)+ZEPS
        TOL2=2.*TOL1
        IF (ABS(X-XM).LE.(TOL2-.5*(B-A))) GOTO 3
        IF (ABS(E).GT.TOL1) THEN
          R=(X-W)*(FX-FV)
          Q=(X-V)*(FX-FW)
          P=(X-V)*Q-(X-W)*R
          Q=2.*(Q-R)
```

```
          IF (Q.GT.0) P=-P
          Q=ABS(Q)
          ETEMP=E
          E=D
          IF(ABS(P).GE.ABS(.5*Q*ETEMP).OR.P.LE.Q*(A-X).OR.
     &         P.GE.Q*(B-X)) GOTO 1
          D=P/Q
          U=X+D
          IF(U-A.LT.TOL2.OR.B-U.LT.TOL2) D=SIGN(TOL1,XM-X)
          GOTO 2
        END IF
 1      IF (X.GE.XM) THEN
          E=A-X
        ELSE
          E=B-X
        END IF
        D=CGOLD*E
 2      IF(ABS(D).GE.TOL1) THEN
          U=X+D
        ELSE
          U=X+SIGN(TOL1,D)
        END IF
        FU=F(U)
        IF (FU.LE.FX) THEN
          IF (U.GE.X) THEN
            A=X
          ELSE
            B=X
          END IF
          V=W
          FV=FW
          W=X
          FW=FX
          X=U
          FX=FU
        ELSE
          IF (U.LT.X) THEN
            A=U
          ELSE
            B=U
          END IF
          IF (FU.LE.FW.OR.W.EQ.X) THEN
            V=W
            FV=FW
            W=U
            FW=FU
          ELSE IF (FU.LE.FV.OR.V.EQ.X.OR.V.EQ.W) THEN
            V=U
            FV=FU
          END IF
        END IF
      END DO
      PAUSE 'Brent exceed maximum iterations.'
 3    XMIN=X
      BRENT=FX
      RETURN
      END
```

****

```
*
*     Powell's Method Error Functional
*
************************************************************************

      REAL*8 FUNCTION FUNC(TRANS)
      IMPLICIT NONE
      REAL*8 SRFAT(25,25,6),TRANS(5),RMSERR
      CALL POSIT(SRFAT,TRANS)
      CALL XMTTRC(SRFAT,RMSERR)
      FUNC=RMSERR
      RETURN
      STOP
      END


************************************************************************
*
*     Type 1 Concept Subreflector Positioning Code
*
************************************************************************

      SUBROUTINE POSIT(SRFAT,TRANS)
      IMPLICIT NONE
      REAL*8 SRFA(25,25,6),SRFAT(25,25,6),TRANS(5),SRFMD(4),FOC,FEED(3),
     C       SCAN(2),T(5)
      INTEGER*2 I,J
      COMMON /REFL/ SRFMD,SRFA,FOC,FEED,SCAN
      T(1)=TRANS(3)
      T(2)=TRANS(4)
      T(3)=TRANS(5)
      T(4)=TRANS(1)
      T(5)=TRANS(2)
      DO 1 I=1,25
        DO 1 J=1,25
          SRFAT(I,J,1)=T(1)+SRFA(13,13,1)-
     C                    SIN(T(4))*(SRFA(I,J,2)-SRFA(13,13,2))+
     C          COS(T(4))*SIN(T(5))*(SRFA(I,J,3)-SRFA(13,13,3))+
     C          COS(T(4))*COS(T(5))*(SRFA(I,J,1)-SRFA(13,13,1))
          SRFAT(I,J,2)=T(2)+SRFA(13,13,2)+
     C                    COS(T(4))*(SRFA(I,J,2)-SRFA(13,13,2))+
     C          SIN(T(4))*SIN(T(5))*(SRFA(I,J,3)-SRFA(13,13,3))+
     C          SIN(T(4))*COS(T(5))*(SRFA(I,J,1)-SRFA(13,13,1))
          SRFAT(I,J,3)=T(3)+SRFA(13,13,3)+
     C                    COS(T(5))*(SRFA(I,J,3)-SRFA(13,13,3))-
     C                    SIN(T(5))*(SRFA(I,J,1)-SRFA(13,13,1))
          SRFAT(I,J,4)=-SIN(T(4))*SRFA(I,J,5)+
     C        COS(T(4))*SIN(T(5))*SRFA(I,J,6)+
     C        COS(T(4))*COS(T(5))*SRFA(I,J,4)
          SRFAT(I,J,5)=COS(T(4))*SRFA(I,J,5)+
     C       SIN(T(4))*SIN(T(5))*SRFA(I,J,6)+
     C       SIN(T(4))*COS(T(5))*SRFA(I,J,4)
 1        SRFAT(I,J,6)=COS(T(5))*SRFA(I,J,6)-
     C                 SIN(T(5))*SRFA(I,J,4)
      RETURN
      STOP
      END

************************************************************************
*
```

```
*     Type 1 Concept Transmit Mode Raytracing Error Functional
*
*************************************************************************

      SUBROUTINE XMTTRC(SRFAT,RMSERR)
      IMPLICIT NONE
      REAL*8 SRFM(6),SRFAT(25,25,6),FEED(3),R1(6),R2(6),R3(6),SCAN(2),
     C       RDOTN,A,B,C,FOC,R2L,PI,RMSERR,SRFMD(4),L,ANGLE(25,25),
     C       DEN,RA(3),SRFA(25,25,6)
      INTEGER*2 I,J,MISS(25,25),K
      COMMON /REFL/ SRFMD,SRFA,FOC,FEED,SCAN
      PI=3.14159265358979323846D0
* FIND IDEAL COMPONENTS OF REFLECTED RAY FROM MAIN REF. TO APERTURE PLANE
      RA(1)=COS(SCAN(1))
      RA(2)=SIN(SCAN(1))*COS(SCAN(2))
      RA(3)=SIN(SCAN(1))*SIN(SCAN(2))
      DO 1 I=1,25
        DO 1 J=1,25
          MISS(I,J)=1
* FIND RAY AND RAY COMPONENTS FROM FEED TO SUBREFLECTOR
          R3(1)=SRFAT(I,J,1)-FEED(1)
          R3(2)=SRFAT(I,J,2)-FEED(2)
          R3(3)=SRFAT(I,J,3)-FEED(3)
          L=DSQRT(R3(1)**2.D0+R3(2)**2.D0+R3(3)**2.D0)
          R3(4)=R3(1)/L
          R3(5)=R3(2)/L
          R3(6)=R3(3)/L
* FIND COMPONENTS OF RAY REFLECTED FROM SUBREFLECTOR
          RDOTN=R3(4)*SRFAT(I,J,4)+R3(5)*SRFAT(I,J,5)+R3(6)*SRFAT(I,J,6)
          R2(4)=R3(4)-2.*RDOTN*SRFAT(I,J,4)
          R2(5)=R3(5)-2.*RDOTN*SRFAT(I,J,5)
          R2(6)=R3(6)-2.*RDOTN*SRFAT(I,J,6)
* FIND INTERSECTION OF RAY FROM SUBREFLECTOR WITH MAIN REFLECTOR
          A=R2(5)**2.D0+R2(6)**2.D0
          B=2.D0*R2(5)*SRFAT(I,J,2)+2.D0*R2(6)*SRFAT(I,J,3)
     C            -4.D0*R2(4)*FOC
          C=SRFAT(I,J,2)**2.D0+SRFAT(I,J,3)**2.D0-4.D0*SRFAT(I,J,1)*FOC

          R2L=(DSQRT(B**2.D0-4.D0*A*C)-B)/(2.D0*A)
          SRFM(1)=SRFAT(I,J,1)+R2(4)*R2L
          SRFM(2)=SRFAT(I,J,2)+R2(5)*R2L
          SRFM(3)=SRFAT(I,J,3)+R2(6)*R2L
* FIND NORMAL OF MAIN REFLECTOR AT RAY INTERSECTION POINT
          DEN=DSQRT((SRFM(2)/(2.D0*FOC))**2.D0+
     C              (SRFM(3)/(2.D0*FOC))**2.D0+1.D0)
          SRFM(4)=1.D0/DEN
          SRFM(5)=-SRFM(2)/(2.D0*FOC*DEN)
          SRFM(6)=-SRFM(3)/(2.D0*FOC*DEN)
* INDICATE A MISS IF RAY HITS AN UNUSED PART OF THE PARABOLA
          IF (SRFM(2).GE.SRFMD(1)-(SRFMD(2)-SRFMD(1))/1.D2) THEN
            IF (SRFM(2).LE.SRFMD(2)+(SRFMD(2)-SRFMD(1))/1.D2) THEN
              IF (SRFM(3).GE.SRFMD(3)-(SRFMD(4)-SRFMD(3))/1.D2) THEN
                IF (SRFM(3).LE.SRFMD(4)+(SRFMD(4)-SRFMD(3))/1.D2) THEN
                  MISS(I,J)=0
                 ENDIF
               ENDIF
             ENDIF
           ENDIF
* FIND COMPONENTS OF RAY REFLECTED FROM MAIN REFLECTOR
          RDOTN=R2(4)*SRFM(4)+R2(5)*SRFM(5)+R2(6)*SRFM(6)
```

```
          R1(4)=R2(4)-2.*RDOTN*SRFM(4)
          R1(5)=R2(5)-2.*RDOTN*SRFM(5)
          R1(6)=R2(6)-2.*RDOTN*SRFM(6)
* FIND CROSS PRODUCT OF ACTUAL AND IDEAL REFLECTED RAYS TO THE APERTURE
 1        ANGLE(I,J)=(R1(5)*RA(3)-RA(2)*R1(6))**2.D0+
     C                (R1(4)*RA(3)-RA(1)*R1(6))**2.D0+
     C                (R1(4)*RA(2)-RA(1)*R1(5))**2.D0
* ERROR ANALYSIS
      K=0
      RMSERR=0.D0
      DO 2 I=1,25
        DO 2 J=1,25
          RMSERR=RMSERR+ANGLE(I,J)
 2        K=K+MISS(I,J)
      RMSERR=DSQRT(RMSERR)
      RETURN
      STOP
      END


*************************************************************************
*
*     Type 1 Concept Output Code
*
*************************************************************************

      SUBROUTINE OUT(FEED,TRANS,SCAN,ICN,SFOC)
      IMPLICIT NONE
      REAL*8 FEED(3),TRANS(5),SCAN(2),SRFAT(25,25,6),PI,
     C       SFOC(2,3),GCOEF(10),U,V
      INTEGER*2 ICN,K(3)
      CHARACTER*12 OUTFILE
      PI=3.14159265358979323846D0
      U=SIN(SCAN(1)*PI/1.8D2)*COS(SCAN(2)*PI/1.8D2)
      V=SIN(SCAN(1)*PI/1.8D2)*SIN(SCAN(2)*PI/1.8D2)
      K(1)=48+ICN/100
      K(2)=48+(ICN-(K(1)-48)*100)/10
      K(3)=48+ICN-(K(1)-48)*100-(K(2)-48)*10
      CALL POSITF(SFOC,TRANS,GCOEF)
      CALL POSIT(SRFAT,TRANS)
      OUTFILE='TMRT1XXX.MOV'
      OUTFILE(6:6)=CHAR(K(1))
      OUTFILE(7:7)=CHAR(K(2))
      OUTFILE(8:8)=CHAR(K(3))
      OPEN(4,FILE=OUTFILE,STATUS='UNKNOWN')
      WRITE(4,'(A10,2F12.7)')'SCANNED TO ',SCAN(1),SCAN(2)
      WRITE(4,'(5F15.10)')TRANS(4),TRANS(5),TRANS(3),TRANS(1),TRANS(2)
      ENDFILE(4)
      CLOSE(4)
* 20 GHz GRASP7 Input File
      OUTFILE='TMRT1XXX.INP'
      OUTFILE(6:6)=CHAR(K(1))
      OUTFILE(7:7)=CHAR(K(2))
      OUTFILE(8:8)=CHAR(K(3))
      OPEN(4,FILE=OUTFILE,STATUS='UNKNOWN')
      WRITE(4,'(A30)')'***** GRASP77 INPUT FILE *****'
      WRITE(4,'(A10,2F12.7)')'SCANNED TO ',SCAN(1),SCAN(2)
      WRITE(4,'(F12.7,4I2)')1.5D-2,2,1,0,0
      WRITE(4,'(A31)')'** MAIN REFLECTOR INPUT DATA **'
      WRITE(4,'(3F12.7)')0.,0.,0.
```

```
      WRITE(4,'(3F12.7)')1.,0.,0.
      WRITE(4,'(3F12.7)')0.,1.,0.
      WRITE(4,'(I2,2F12.7)')1,7.795,0.
      WRITE(4,'(3I2)')4,0,0
      WRITE(4,'(4F12.7)')0.,0.,0.,13.5
      WRITE(4,'(2F12.7)')5.315,5.315
      WRITE(4,'(A30)')'** SUB REFLECTOR INPUT DATA **'
      WRITE(4,'(3F12.7)')0.,0.,0.
      WRITE(4,'(3F12.7)')1.,0.,0.
      WRITE(4,'(3F12.7)')0.,1.,0.
      WRITE(4,'(I2,2F12.7)')1,(SRFAT(25,13,2)+SRFAT(1,13,2))/2.D0,
     C                         (SRFAT(13,25,3)+SRFAT(13,1,3))/2.D0
      WRITE(4,'(2I2)')3,0
      WRITE(4,'(5F14.7)')GCOEF(1),GCOEF(2),GCOEF(3),GCOEF(4),GCOEF(5)
      WRITE(4,'(5F14.7)')GCOEF(6),GCOEF(7),GCOEF(8),GCOEF(9),GCOEF(10)
      WRITE(4,'(5F12.7,I5)')0.,0.,0.,0.,0.,1
      WRITE(4,'(2F12.7)')(SRFAT(25,13,2)-SRFAT(1,13,2))/2.D0,
     C                    (SRFAT(13,25,3)-SRFAT(13,1,3))/2.D0
      WRITE(4,'(A21)')'** FEED INPUT DATA **'
      WRITE(4,'(3F12.7)')FEED(2),FEED(3),FEED(1)
      WRITE(4,'(3F12.7)').964483694,0.,-.264142395
      WRITE(4,'(3F12.7)')0.,1.,0.
      WRITE(4,'(I2)')1
      WRITE(4,'(6F12.7)')0.,0.,0.,0.,0.,0.
      WRITE(4,'(F12.7,I2)')0.,1
      WRITE(4,'(4F12.7,3I2)')0.,0.,1.,90.,0,0,3
      WRITE(4,'(I2)')6
      WRITE(4,'(5F12.7,I3)')-15.,-15.,7.1574,0.,0.,1
      WRITE(4,'(A40)')'** MAIN REFLECTOR FIELD SPECIFICATION **'
      WRITE(4,'(I2)')1
      WRITE(4,'(3F12.7)')7.795,0.,10.
      WRITE(4,'(3F12.7)')1.,0.,0.
      WRITE(4,'(3F12.7)')0.,1.,0.
      WRITE(4,'(2I6,F12.7,2I3)')60,144,0.,0,0
      WRITE(4,'(3I3)')0,-1,1
      WRITE(4,'(F12.7)')10.
      WRITE(4,'(2F12.7)')U,V
      WRITE(4,'(2I3)')0,1
      WRITE(4,'(2I3)')3,1
      WRITE(4,'(4F12.7,2I6)')-1.D-2,-1.D-2,1.D-2,1.D-2,25,25
      WRITE(4,'(4I6)')3,1
      OUTFILE='TMRT1XXX.P1'
      OUTFILE(6:6)=CHAR(K(1))
      OUTFILE(7:7)=CHAR(K(2))
      OUTFILE(8:8)=CHAR(K(3))
      WRITE(4,'(A12)')OUTFILE
      WRITE(4,'(A39)')'** SUB REFLECTOR FIELD SPECIFICATION **'
      WRITE(4,'(I2)')0
      WRITE(4,'(A30)')'** FEED FIELD SPECIFICATION **'
      WRITE(4,'(I2)')0
      ENDFILE(4)
      CLOSE(4)
      OUTFILE='TMRUVXXX.INP'
      OUTFILE(6:6)=CHAR(K(1))
      OUTFILE(7:7)=CHAR(K(2))
      OUTFILE(8:8)=CHAR(K(3))
      OPEN(4,FILE=OUTFILE,STATUS='UNKNOWN')
      WRITE(4,'(A25)')'UVPROC CONTROL INPUT FILE'
      OUTFILE='TMRT1XXX.P1'
      OUTFILE(6:6)=CHAR(K(1))
```

```
      OUTFILE(7:7)=CHAR(K(2))
      OUTFILE(8:8)=CHAR(K(3))
      WRITE(4,'(A12)')OUTFILE
      WRITE(4,'(6I2)')1,1,1,1,0,0
      WRITE(4,'(2I2)')1,1
      WRITE(4,'(6I2)')0,1,0,0,1,0
      WRITE(4,'(A7)')'TEMP.P2'
      WRITE(4,'(I2)')3
      WRITE(4,'(2I4)')101,101
      WRITE(4,'(7I2)')0,0,1,1,0,0,0
      WRITE(4,'(4I2)')3,0,2,0
      WRITE(4,'(F5.1)')3.
      WRITE(4,'(F5.1)')10.
      WRITE(4,'(5I2)')1,0,0,1,1
      WRITE(4,'(F7.4)')0.1213
      ENDFILE(4)
      CLOSE(4)
* 40 GHz GRASP7 Input File
      OUTFILE='TMRT1XXX.INP'
      OUTFILE(6:6)=CHAR(K(1)+1)
      OUTFILE(7:7)=CHAR(K(2))
      OUTFILE(8:8)=CHAR(K(3))
      OPEN(4,FILE=OUTFILE,STATUS='UNKNOWN')
      WRITE(4,'(A30)')'***** GRASP77 INPUT FILE *****'
      WRITE(4,'(A10,2F12.7)')'SCANNED TO ',SCAN(1),SCAN(2)
      WRITE(4,'(F12.7,4I2)')7.5D-3,2,1,0,0
      WRITE(4,'(A31)')'** MAIN REFLECTOR INPUT DATA **'
      WRITE(4,'(3F12.7)')0.,0.,0.
      WRITE(4,'(3F12.7)')1.,0.,0.
      WRITE(4,'(3F12.7)')0.,1.,0.
      WRITE(4,'(I2,2F12.7)')1,7.795,0.
      WRITE(4,'(3I2)')4,0,0
      WRITE(4,'(4F12.7)')0.,0.,0.,13.5
      WRITE(4,'(2F12.7)')5.315,5.315
      WRITE(4,'(A30)')'** SUB REFLECTOR INPUT DATA **'
      WRITE(4,'(3F12.7)')0.,0.,0.
      WRITE(4,'(3F12.7)')1.,0.,0.
      WRITE(4,'(3F12.7)')0.,1.,0.
      WRITE(4,'(I2,2F12.7)')1,(SRFAT(25,13,2)+SRFAT(1,13,2))/2.D0,
     C                         (SRFAT(13,25,3)+SRFAT(13,1,3))/2.D0
      WRITE(4,'(2I2)')3,0
      WRITE(4,'(5F14.7)')GCOEF(1),GCOEF(2),GCOEF(3),GCOEF(4),GCOEF(5)
      WRITE(4,'(5F14.7)')GCOEF(6),GCOEF(7),GCOEF(8),GCOEF(9),GCOEF(10)
      WRITE(4,'(5F12.7,I5)')0.,0.,0.,0.,0.,1
      WRITE(4,'(2F12.7)')(SRFAT(25,13,2)-SRFAT(1,13,2))/2.D0,
     C                   (SRFAT(13,25,3)-SRFAT(13,1,3))/2.D0
      WRITE(4,'(A21)')'** FEED INPUT DATA **'
      WRITE(4,'(3F12.7)')FEED(2),FEED(3),FEED(1)
      WRITE(4,'(3F12.7)').964483694,0.,-.264142395
      WRITE(4,'(3F12.7)')0.,1.,0.
      WRITE(4,'(I2)')1
      WRITE(4,'(6F12.7)')0.,0.,0.,0.,0.,0.
      WRITE(4,'(F12.7,I2)')0.,1
      WRITE(4,'(4F12.7,3I2)')0.,0.,1.,90.,0,0,3
      WRITE(4,'(I2)')6
      WRITE(4,'(5F12.7,I3)')-15.,-15.,7.1574,0.,0.,1
      WRITE(4,'(A40)')'** MAIN REFLECTOR FIELD SPECIFICATION **'
      WRITE(4,'(I2)')1
      WRITE(4,'(3F12.7)')7.795,0.,10.
      WRITE(4,'(3F12.7)')1.,0.,0.
```

```
      WRITE(4,'(3F12.7)')0.,1.,0.
      WRITE(4,'(2I6,F12.7,2I )')60,144,0.,0,0
      WRITE(4,'(3I3)')0,-1,1
      WRITE(4,'(F12.7)')10.
      WRITE(4,'(2F12.7)')U,V
      WRITE(4,'(2I3)')0,1
      WRITE(4,'(2I3)')3,1
      WRITE(4,'(4F12.7,2I6)')-5.D-3,-5.D-3,5.D-3,5.D-3,25,25
      WRITE(4,'(4I6)')3,1
      OUTFILE='TMRT1XXX.P1'
      OUTFILE(6:6)=CHAR(K(1)+1)
      OUTFILE(7:7)=CHAR(K(2))
      OUTFILE(8:8)=CHAR(K(3))
      WRITE(4,'(A12)')OUTFILE
      WRITE(4,'(A39)')'** SUB REFLECTOR FIELD SPECIFICATION **'
      WRITE(4,'(I2)')0
      WRITE(4,'(A30)')'** FEED FIELD SPECIFICATION **'
      WRITE(4,'(I2)')0
      ENDFILE(4)
      CLOSE(4)
      OUTFILE='TMRUVXXX.INP'
      OUTFILE(6:6)=CHAR(K(1)+1)
      OUTFILE(7:7)=CHAR(K(2))
      OUTFILE(8:8)=CHAR(K(3))
      OPEN(4,FILE=OUTFILE,STATUS='UNKNOWN')
      WRITE(4,'(A25)')'UVPROC CONTROL INPUT FILE'
      OUTFILE='TMRT1XXX.P1'
      OUTFILE(6:6)=CHAR(K(1)+1)
      OUTFILE(7:7)=CHAR(K(2))
      OUTFILE(8:8)=CHAR(K(3))
      WRITE(4,'(A12)')OUTFILE
      WRITE(4,'(6I2)')1,1,1,1,0,0
      WRITE(4,'(2I2)')1,1
      WRITE(4,'(6I2)')0,1,0,0,1,0
      WRITE(4,'(A7)')'TEMP.P2'
      WRITE(4,'(I2)')3
      WRITE(4,'(2I4)')101,101
      WRITE(4,'(7I2)')0,0,1,1,0,0,0
      WRITE(4,'(4I2)')3,0,2,0
      WRITE(4,'(F5.1)')3.
      WRITE(4,'(F5.1)')10.
      WRITE(4,'(5I2)')1,0,0,1,1
      WRITE(4,'(F7.4)')0.0606
      ENDFILE(4)
      CLOSE(4)
* 80 GHz GRASP7 Input File
      OUTFILE='TMRT1XXX.INP'
      OUTFILE(6:6)=CHAR(K(1)+2)
      OUTFILE(7:7)=CHAR(K(2))
      OUTFILE(8:8)=CHAR(K(3))
      OPEN(4,FILE=OUTFILE,STATUS='UNKNOWN')
      WRITE(4,'(A30)')'***** GRASP77 INPUT FILE *****'
      WRITE(4,'(A10,2F12.7)')'SCANNED TO ',SCAN(1),SCAN(2)
      WRITE(4,'(F12.7,4I2)')3.75D-3,2,1,0,0
      WRITE(4,'(A31)')'** MAIN REFLECTOR INPUT DATA **'
      WRITE(4,'(3F12.7)')0.,0.,0.
      WRITE(4,'(3F12.7)')1.,0.,0.
      WRITE(4,'(3F12.7)')0.,1.,0.
      WRITE(4,'(I2,2F12.7)')1,7.795,0.
      WRITE(4,'(3I2)')4,0,0
```

```
 WRITE(4,'(4F12.7)')0.,0.,0.,13.5
 WRITE(4,'(2F12.7)')5.315,5.315
 WRITE(4,'(A30)')'** SUB REFLECTOR INPUT DATA **'
 WRITE(4,'(3F12.7)')0.,0.,0.
 WRITE(4,'(3F12.7)')1.,0.,0.
 WRITE(4,'(3F12.7)')0.,1.,0.
 WRITE(4,'(I2,2F12.7)')1,(SRFAT(25,13,2)+SRFAT(1,13,2))/2.D0,
C                        (SRFAT(13,25,3)+SRFAT(13,1,3))/2.D0
 WRITE(4,'(2I2)')3,0
 WRITE(4,'(5F14.7)')GCOEF(1),GCOEF(2),GCOEF(3),GCOEF(4),GCOEF(5)
 WRITE(4,'(5F14.7)')GCOEF(6),GCOEF(7),GCOEF(8),GCOEF(9),GCOEF(10)
 WRITE(4,'(5F12.7,I5)')0.,0.,0.,0.,0.,1
 WRITE(4,'(2F12.7)')(SRFAT(25,13,2)-SRFAT(1,13,2))/2.D0,
C                   (SRFAT(13,25,3)-SRFAT(13,1,3))/2.D0
 WRITE(4,'(A21)')'** FEED INPUT DATA **'
 WRITE(4,'(3F12.7)')FEED(2),FEED(3),FEED(1)
 WRITE(4,'(3F12.7)').964483694,0.,-.264142395
 WRITE(4,'(3F12.7)')0.,1.,0.
 WRITE(4,'(I2)')1
 WRITE(4,'(6F12.7)')0.,0.,0.,0.,0.,0.
 WRITE(4,'(F12.7,I2)')0.,1
 WRITE(4,'(4F12.7,3I2)')0.,0.,1.,90.,0,0,3
 WRITE(4,'(I2)')6
 WRITE(4,'(5F12.7,I3)')-15.,-15.,7.1574,0.,0.,1
 WRITE(4,'(A40)')'** MAIN REFLECTOR FIELD SPECIFICATION **'
 WRITE(4,'(I2)')1
 WRITE(4,'(3F12.7)')7.795,0.,10.
 WRITE(4,'(3F12.7)')1.,0.,0.
 WRITE(4,'(3F12.7)')0.,1.,0.
 WRITE(4,'(2I6,F12.7,2I3)')60,144,0.,0,0
 WRITE(4,'(3I3)')0,-1,1
 WRITE(4,'(F12.7)')10.
 WRITE(4,'(2F12.7)')U,V
 WRITE(4,'(2I3)')0,1
 WRITE(4,'(2I3)')3,1
 WRITE(4,'(4F12.7,2I6)')-2.5D-3,-2.5D-3,2.5D-3,2.5D-3,25,25
 WRITE(4,'(4I6)')3,1
 OUTFILE='TMRT1XXX.P1'
 OUTFILE(6:6)=CHAR(K(1)+2)
 OUTFILE(7:7)=CHAR(K(2))
 OUTFILE(8:8)=CHAR(K(3))
 WRITE(4,'(A12)')OUTFILE
 WRITE(4,'(A39)')'** SUB REFLECTOR FIELD SPECIFICATION **'
 WRITE(4,'(I2)')0
 WRITE(4,'(A30)')'** FEED FIELD SPECIFICATION **'
 WRITE(4,'(I2)')0
 ENDFILE(4)
 CLOSE(4)
 OUTFILE='TMRUVXXX.INP'
 OUTFILE(6:6)=CHAR(K(1)+2)
 OUTFILE(7:7)=CHAR(K(2))
 OUTFILE(8:8)=CHAR(K(3))
 OPEN(4,FILE=OUTFILE,STATUS='UNKNOWN')
 WRITE(4,'(A25)')'UVPROC CONTROL INPUT FILE'
 OUTFILE='TMRT1XXX.P1'
 OUTFILE(6:6)=CHAR(K(1)+2)
 OUTFILE(7:7)=CHAR(K(2))
 OUTFILE(8:8)=CHAR(K(3))
 WRITE(4,'(A12)')OUTFILE
 WRITE(4,'(6I2)')1,1,1,1,0,0
```

```
      WRITE(4,'(2I2)')1,1
      WRITE(4,'(6I2)')0,1,0,0,1,0
      WRITE(4,'(A7)')'TEMP.P2'
      WRITE(4,'(I2)')3
      WRITE(4,'(2I4)')101,101
      WRITE(4,'(7I2)')0,0,1,1,0,0,0
      WRITE(4,'(4I2)')3,0,2,0
      WRITE(4,'(F5.1)')3.
      WRITE(4,'(F5.1)')10.
      WRITE(4,'(5I2)')1,0,0,1,1
      WRITE(4,'(F7.4)')0.0303
      ENDFILE(4)
      CLOSE(4)
      RETURN
      STOP
      END


*************************************************************************
*
*     Type 1 Concept Transmit Mode Raytracing Subreflector Focal Point
*     Positioning Code
*
*************************************************************************

      SUBROUTINE POSITF(SFOC,TRANS,GCOEF)
      IMPLICIT NONE
      REAL*8 SRFA(25,25,6),SFOC(2,3),TRANS(5),SRFMD(4),FOC,FEED(3),
     C       SCAN(2),T(5),GCOEF(10),SFOCT(2,3),ALPHA,BETA,GAMMA,
     C       DELTA,C
      INTEGER*2 I
      COMMON /REFL/ SRFMD,SRFA,FOC,FEED,SCAN
      T(1)=TRANS(3)
      T(2)=TRANS(4)
      T(3)=TRANS(5)
      T(4)=TRANS(1)
      T(5)=TRANS(2)
      DO 1 I=1,2
          SFOCT(I,1)=T(1)+SRFA(13,13,1)-
     C                    SIN(T(4))*(SFOC(I,2)-SRFA(13,13,2))+
     C          COS(T(4))*SIN(T(5))*(SFOC(I,3)-SRFA(13,13,3))+
     C          COS(T(4))*COS(T(5))*(SFOC(I,1)-SRFA(13,13,1))
          SFOCT(I,2)=T(2)+SRFA(13,13,2)+
     C                    COS(T(4))*(SFOC(I,2)-SRFA(13,13,2))+
     C          SIN(T(4))*SIN(T(5))*(SFOC(I,3)-SRFA(13,13,3))+
     C          SIN(T(4))*COS(T(5))*(SFOC(I,1)-SRFA(13,13,1))
 1        SFOCT(I,3)=T(3)+SRFA(13,13,3)+
     C                    COS(T(5))*(SFOC(I,3)-SRFA(13,13,3))-
     C                    SIN(T(5))*(SFOC(I,1)-SRFA(13,13,1))

      C=DSQRT((SRFA(13,13,1)-SFOC(2,1))**2.D0+
     C        (SRFA(13,13,2)-SFOC(2,2))**2.D0+
     C        (SRFA(13,13,3)-SFOC(2,3))**2.D0)-
     C  DSQRT((SRFA(13,13,1)-SFOC(1,1))**2.D0+
     C        (SRFA(13,13,2)-SFOC(1,2))**2.D0+
     C        (SRFA(13,13,3)-SFOC(1,3))**2.D0)
      BETA=SFOCT(2,2)-SFOCT(1,2)
      GAMMA=SFOCT(2,3)-SFOCT(1,3)
      DELTA=SFOCT(2,1)-SFOCT(1,1)
      ALPHA=SFOCT(1,1)**2.D0+SFOCT(1,2)**2.D0+SFOCT(1,3)**2.D0-
```

```
C       SFOCT(2,1)**2.D0-SFOCT(2,2)**2.D0-SFOCT(2,3)**2.D0-
C       C**2.D0
 GCOEF(1) =4.D0*(BETA**2.D0-C**2.D0)
 GCOEF(2) =8.D0*BETA*GAMMA
 GCOEF(3) =4.D0*(GAMMA**2.D0-C**2.D0)
 GCOEF(4) =4.D0*(ALPHA*BETA+2.D0*C**2.D0*SFOCT(2,2))
 GCOEF(5) =4.D0*(ALPHA*GAMMA+2.D0*C**2.D0*SFOCT(2,3))
 GCOEF(6) =ALPHA**2.D0-4.D0*C**2.D0*(SFOCT(2,1)**2.D0+
C           SFOCT(2,2)**2.D0+SFOCT(2,3)**2.D0)
 GCOEF(7) =4.D0*(C**2.D0-DELTA**2.D0)
 GCOEF(8) =-4.D0*(ALPHA*DELTA+2.D0*C**2.D0*SFOCT(2,1))
 GCOEF(9) =-8.D0*BETA*DELTA
 GCOEF(10)=-8.D0*GAMMA*DELTA
 RETURN
 STOP
 END
```

VITA

James William LaPean, Jr. was born in Norfolk, Virginia. He was admitted to Virginia Polytechnic Institute and State University in 1984 and received the Bachelor of Science degree in Electrical Engineering. He joined the Masters program at Virginia Polytechnic Institute and State University in 1989. He has worked on four projects as a member of the Satellite Communications Group starting in 1989: planning and satellite-ground link evaluation for the transition of the National Public Broadcasting Service from C-band to Ku-band distribution, construction of the Virginia Tech OLYMPUS propagation experiment receiver equipment, optimization of wide scanning, high gain reflector antenna systems for the NASA Mission to Planet Earth, and experiment design for an uplink power control experiment using the Advanced Communications Satellite.